

THESIS ON NATURAL AND EXACT SCIENCES B218

# **The Role of CD44 in the Control of Endothelial Cell Proliferation and Angiogenesis**

ANNE PINK

**TUT**  
PRESS

TALLINN UNIVERSITY OF TECHNOLOGY  
Faculty of Science  
Department of Gene Technology

**This dissertation was accepted for the defence of the degree of Doctor of Philosophy in Gene Technology on September 14, 2016.**

**Supervisors:**        **Docent Andres Valkna, PhD**  
Department of Gene Technology,  
Tallinn University of Technology, Estonia

**Lecturer Taavi Päll, PhD**  
Department of Gene Technology,  
Tallinn University of Technology, Estonia

**Opponents:**        **Prof. Elisabetta Dejana, PhD**  
Department of Biosciences,  
University of Milan, Italy

**Senior Researcher Viljar Jaks, PhD**  
Institute of Molecular and Cell Biology,  
University of Tartu, Estonia

Defence of the thesis: October 7, 2016

Declaration:

*Hereby I declare that this doctoral thesis, my original investigation and achievement, submitted for the doctoral degree at Tallinn University of Technology has not been submitted for any academic degree.*

/Anne Pink/



Copyright: Anne Pink, 2016  
ISSN 1406-4723  
ISBN 978-9949-83-016-9 (publication)  
ISBN 978-9949-83-017-6 (PDF)

LOODUS- JA TÄPPISTEADUSED B218

# **CD44 roll angiogeneesis ja endoteelirakkude jagunemises**

ANNE PINK



# CONTENTS

ORIGINAL PUBLICATIONS .....	7
INTRODUCTION.....	8
ABBREVIATIONS.....	9
LITERATURE REVIEW.....	11
1 Angiogenesis .....	11
1.1 Overview of the regulation of sprouting angiogenesis.....	12
1.2 Initiation of angiogenesis and tip/stalk cell specification.....	14
1.3 Tubule elongation.....	15
1.4 Vascular lumen formation and anastomosis.....	16
1.5 Vessel maturation.....	17
1.6 Vascular quiescence .....	18
1.7 Challenges in anti-angiogenesis treatment .....	21
1.8 Plasma half-life extension strategies of therapeutic proteins .....	23
2 CD44 .....	24
2.1 The structure of CD44.....	24
2.2 The physiological functions of CD44.....	27
2.3 The role of CD44 in inflammation .....	28
2.4 The functions of CD44 in cancer.....	29
2.5 The functions of CD44 in angiogenesis .....	31
2.6 CD44 as a co-receptor .....	33
2.7 Soluble CD44 .....	35
3 Vimentin and its functions in ECs.....	36
MATERIALS AND METHODS .....	39
AIMS OF THE STUDY .....	40
RESULTS AND DISCUSSION .....	41
1 Circulation half-life of CD44-3MUT and its modified versions.....	41
1.1 PEGylation of CD44-3MUT (Publication I).....	41
1.2 Half-life of PEGylated CD44-3MUT (Publication I).....	42
1.3 Plasma half-life of CD44-3MUT-Fc (Manuscript) .....	43
2 CD44 functions as an inhibitor of angiogenesis (Manuscript).....	45

2.1 CD44-3MUT-Fc inhibits <i>in vivo</i> neovascularization .....	45
2.2 <i>Cd44</i> -null mice display enhanced angiogenic response .....	46
3 CD44 as a negative regulator of EC proliferation .....	48
3.1 CD44-3MUT restrains EC growth (Publication I, Manuscript) .....	48
3.2 Knockdown of CD44 enhances EC proliferation and viability (Manuscript) .....	49
3.3 The molecular mechanism behind CD44 effects (Manuscript) .....	51
4 Vimentin is involved in the EC growth-inhibiting function of CD44 (Publications I-II, Manuscript, Patent, unpublished data) .....	52
CONCLUSIONS .....	55
REFERENCES .....	56
ACKNOWLEDGEMENTS .....	81
PUBLICATION I .....	83
PUBLICATION II .....	105
MANUSCRIPT .....	121
PATENT .....	155
ABSTRACT .....	183
KOKKUVÕTE .....	185
CURRICULUM VITAE .....	187
ELULOOKIRJELDUS .....	189

## ORIGINAL PUBLICATIONS

- I. **Pink, A**, Kallastu, A, Turkina, M, Školnaja, M, Kogerman, P, Päll, T, Valkna, A (2014). Purification, characterization and plasma half-life of PEGylated soluble recombinant non-HA-binding CD44. *BioDrugs*, 28, 4:393-402.
- II. Päll, T, **Pink, A**, Kasak, L, Turkina, M, Anderson, W, Valkna, A, Kogerman, P (2011). Soluble CD44 interacts with intermediate filament protein vimentin on endothelial cell surface. *PLoS ONE*, 6, 12:e29305.

## MANUSCRIPT

**Pink, A**, Školnaja, M, Päll, T, Valkna, A (2016). CD44 controls endothelial proliferation and functions as endogenous inhibitor of angiogenesis. *DOI*: <http://dx.doi.org/10.1101/049494>.

## PATENT

Päll, T, Anderson, W, Kasak, L, **Pink, A**, Kogerman, P, Allikas A, Valkna, A (2013). Methods of using vimentin to inhibit angiogenesis and endothelial cell proliferation. *US patent*: US 8524666 B2.

## INTRODUCTION

Blood vessels in our body supply the tissues with oxygen and nutrients. The inner surface of blood vessels is lined with endothelium, a special type of epithelium. In contrast to many other epithelial tissues, where constant regeneration is taking place, endothelial cells in an adult organism reside mostly in quiescence and formation of new blood vessels is initiated via sprouting from the pre-existing ones (angiogenesis) only on few occasions, such as wound healing or tissue regeneration. Sprouting angiogenesis is a tightly regulated pathophysiological process and its misregulation is involved in ischaemic diseases, inflammation, and tumour growth. In 1971 Judah Folkman, the pioneer of anti-angiogenesis therapy, proposed the idea that tumour growth depends on angiogenesis, and thus, reducing tumour blood supply would be beneficial for anti-tumour therapy (Folkman, 1971). Since 2004, a number of anti-angiogenesis drugs have been brought to market for use in cancer treatment. However, about dozen years of clinical use has also revealed that these drugs display only limited long-term benefit due to the intrinsic or acquired resistance mechanisms of tumours to anti-angiogenesis therapy. To overcome the difficulties in anti-angiogenesis therapy, a clearer insight into the mechanisms and factors regulating angiogenesis is needed.

CD44 is a highly glycosylated cell surface adhesion receptor that mediates its functions by binding to its principal ligand hyaluronan (HA) or other extracellular matrix (ECM) ligands. Although the functions of CD44 are foremost related to leukocyte homing and tumour metastasis, some studies describe CD44 also as an angiogenesis regulator. CD44 has been shown to be required for tumour vascularization (Cao et al., 2006), as well as for blood vessel invasion in response to HA oligomers (Lennon et al., 2014). Furthermore, studies by Päll et al. (2004) demonstrated that the recombinant soluble CD44 HA-binding domain (CD44-HABD) is able to inhibit angiogenesis and tumour xenograft growth independently of its HA binding function. To utilize CD44 in anti-angiogenic therapy, a better understanding of the role of CD44 in blood vessel formation would be beneficial.

The aim of this thesis was to elucidate the contribution of CD44 to endothelial cell proliferation and angiogenesis. To examine the role of CD44 in endothelial growth, three different approaches were used. The functions of CD44 in angiogenesis and endothelial proliferation were studied by the use of *Cd44*<sup>-/-</sup> mice, administration of the soluble non-HA-binding analogue of CD44 (CD44-3MUT), and CD44 silencing in human endothelial cells. As the *in vivo* use of CD44-3MUT was limited due to its rapid removal from circulation, we attempted to improve its pharmacokinetic properties as well.

## ABBREVIATIONS

aa – amino acid  
ADAM – a disintegrin and metalloproteinase  
ALK – activin receptor-like kinase  
ANG – angiopoietin  
BMDC – bone marrow derived cells  
BMP – bone morphogenetic protein  
CD44-3MUT – non-HA binding CD44-HABD (CD44-HABD21-132<sup>R41AR78SY79S</sup>)  
CD44s – standard (hematopoietic) CD44 isoform  
CD44v – variant CD44 isoforms  
CDK1 – cyclin dependent kinase 1  
CSC – cancer stem cells  
CXCL – C-X-C motif chemokine ligand  
CXCR – C-X-C motif chemokine receptor  
DIVAA – directed *in vivo* angiogenesis assay  
DLL4 – Delta-like ligand 4  
EC – endothelial cells  
ECIS – electrical cell-substrate impedance sensing  
ECM – extracellular matrix  
ELISA – enzyme-linked immunosorbent assay  
EMT – epithelial-to-mesenchymal transition  
ERM – ezrin, radixin and moesin  
FA – focal adhesion  
FAK – focal adhesion kinase  
Fc – Fragment crystallisable  
FGF – fibroblast growth factor  
FGFR – FGF receptor  
GDF-2 – growth differentiation factor-2  
GF – growth factor  
GPCR – G protein coupled receptor  
GST – glutathione S-transferase  
HA – hyaluronan  
HABD – HA binding domain  
HGF – hepatocyte growth factor  
HIF – hypoxia inducible factor  
HMW – high molecular weight  
HUVEC – human umbilical vein ECs  
ICAM-1 – intercellular cell adhesion molecule-1  
ICD – intracellular domain  
IF – intermediate filament  
Ig – immunoglobulin  
LMW – low molecular weight

LPS – lipopolysaccharide  
LRP6 – low-density lipoprotein receptor-related protein 6  
MDR1 – multidrug protein-1  
MLEC – mouse lung ECs  
MMP – matrix metalloprotease  
NF2 – neurofibromin 2 (merlin)  
NRARP – NOTCH-regulated ankyrin repeat protein  
NRP1 – Neuropilin-1  
PAI-1 – plasminogen activator inhibitor-1  
PDGF – platelet-derived growth factor  
PDGFR – PDGF receptor  
PECAM-1 – platelet/endothelial cell adhesion molecule-1  
PEG – polyethylene glycol  
PHD – prolyl-hydroxylase domain proteins  
PI3K – phosphoinositide 3-kinase  
PKC – protein kinase C  
PLGF – placental growth factor  
RHAMM – a receptor for hyaluronan-mediated motility  
ROS – reactive oxygen species  
RTK – receptor tyrosine kinase  
S1P – platelet derived sphingosine 1 phosphate  
sCD44 – soluble CD44  
SDF1 – stromal derived factor 1  
SIRT1 – NAD<sup>+</sup>-dependent sirtuin-1  
sVEGFR – soluble vascular endothelial growth factor receptor  
TAM – tumour associated macrophages  
TGF – transforming growth factor  
TGFBR – TGF- $\beta$  receptor  
TIMP – tissue inhibitor of metalloprotease  
TNF – tumour necrosis factor  
VASP – vasodilator stimulating phosphoprotein  
VCAM-1 – vascular cell adhesion molecule-1  
VEGFR – vascular endothelial growth factor receptor  
VEGF – vascular endothelial growth factor  
vSMC – vascular smooth muscle cells  
YAP1 – Yes-associated protein 1

# LITERATURE REVIEW

## 1 Angiogenesis

Blood circulation is essential to organisms for delivering oxygen and nutrients, removing metabolic waste products and providing gateways for immune surveillance (Potente et al., 2011). Blood vessels consist of an inner surface, lined with endothelial cells (ECs), a stabilising basement membrane underneath them, and an outer layer of mural cells that sheathe the vessels. The blood vessel network is formed mainly by vasculogenesis or angiogenesis (Risau, 1997). In a developing embryo blood vessels are formed *de novo* via vasculogenesis, where mesoderm-derived endothelial precursor cells differentiate into ECs and assemble a primitive vascular network (Swift and Weinstein, 2009). The subsequent angiogenesis is the formation of a functional blood vessel network by vessels sprouting from the pre-existing ones (Carmeliet and Jain, 2011). During embryogenesis, active angiogenesis occurs to guarantee normal organogenesis. In adults, ECs reside mostly in quiescence, and only a few physiological processes, like wound healing, tissue repair and growth of endometrium, induce angiogenesis. Proper blood supply is crucial for tissue homeostasis and the body's functioning, therefore, angiogenesis is tightly regulated and its misregulation may lead to several diseases (Goel et al., 2011). Insufficient angiogenesis can lead to several ischaemic diseases, such as myocardial infarction and neurodegenerative disorders, whereas excessive angiogenesis promotes tumour growth, inflammation and eye diseases (Carmeliet, 2003; Folkman, 2007).

Sprouting angiogenesis is a multistep process that relies on different behaviours and phenotypes of ECs (Figure 1A). The "tip/stalk" cell concept includes the activated endothelium with migratory tip cells that lead the vessel sprout and proliferative stalk cells trailing the tip cells (De Smet et al., 2009; Gerhardt et al., 2003). In quiescent vessels, ECs with more cobblestone morphology are called phalanx cells (Mazzone et al., 2009). Hypoxic, inflammatory or tumour cells can trigger the angiogenic switch from the quiescent to activated phenotype by releasing proangiogenic growth factors (GFs). Upon activation, pericytes detach from vessel walls, and EC cell-cell junctions are loosened, resulting in increased vessel permeability; then the basement membrane is degraded by activated proteases. All these processes together allow ECs to migrate towards angiogenic signals to initiate sprouting (Carmeliet and Jain, 2011). According to the "tip/stalk" cell concept, only few of the activated ECs are selected as tip cells (De Smet et al., 2009; Gerhardt et al., 2003). Tip cells extend filopodia and lead the newly established sprouts. Trailing stalk cells, in contrast, do not migrate, but instead proliferate to support sprout elongation and also to establish the vascular lumen. The tip and stalk cell phenotypes are dynamic, and neighbouring cells constantly compete for the tip cell position (Jakobsson et al., 2010). EC sprouting continues until tip cells from neighbouring sprouts meet and

anastomose, allowing vessel perfusion (Carmeliet and Jain, 2011). To become mature and functional, ECs restore their quiescent phalanx phenotype, recruit mural cells to cover and stabilise nascent vessels, and deposit a new basement membrane (Herbert and Stainier, 2011).

## 1.1 Overview of the regulation of sprouting angiogenesis

*The VEGF pathway.* The vascular endothelial growth factor (VEGF) signalling pathway, consisting of five largely non-redundant ligands and three receptors, is denoted as the predominant promoter of new blood vessel formation (Ferrara et al., 2003). In general, VEGFR1 is expressed in monocytes and macrophages, VEGFR2 in vascular ECs, and VEGFR3 in lymphatic ECs (Koch and Claesson-Welsh, 2012). VEGF-A, the most potent inducer of angiogenesis, drives angiogenesis mainly by binding to VEGFR2 (Ferrara et al., 2003). VEGF-A signalling in endothelial tip cells is enhanced by Neuropilin-1 (NRP1), an important co-receptor for VEGFR2. VEGF-A is also a ligand for VEGFR1 and its soluble isoform (sVEGFR1), which both bind VEGF with ten times higher affinity than VEGFR2. However, VEGFR1 is not directly required for signalling in ECs, but instead it serves as a decoy receptor for VEGF, and spatially controls VEGFR2 signalling and angiogenic sprouting (Kappas et al., 2008). VEGFR1-specific ligands, VEGF-B and placental growth factor (PLGF), are dispensable for normal vascular development, but they have functions in pathological angiogenesis (Fischer et al., 2008). VEGF-C/VEGFR3 signalling is important in embryogenesis (Dumont et al., 1998), lymphangiogenesis (Karkkainen et al., 2004) and in tumour angiogenesis (Tammela et al., 2008).

*The NOTCH pathway.* In vascular morphogenesis, the NOTCH pathway plays a crucial role in EC fate determination, being involved in the specification of angioblasts, arteriovenous identity and tip/stalk cell specification (Phng and Gerhardt, 2009). Although several members of the NOTCH pathway are expressed in vasculature, the specification of ECs into tip and stalk cells is mainly regulated by NOTCH1 and its ligand, Delta-like 4 (DLL4) (Hellström et al., 2007). NOTCH activity is also required for vessel stabilization and maintenance (Phng and Gerhardt, 2009). Overall, NOTCH signalling has been thought to serve as a negative regulator of VEGF-induced angiogenic sprouting (Blanco and Gerhardt, 2013).

*The HGF/MET pathway.* The hepatocyte growth factor (HGF) acts through its sole receptor MET (Naldini et al., 1991). The expression patterns of HGF and MET indicate that HGF is mainly a mesenchyme-derived factor that acts on MET-expressing epithelial cells (Zarnegar, 1995). However, MET is also expressed on ECs (Ding et al., 2003). Both HGF and MET are also upregulated in several tumours, whereas in many tumours, HGF activates MET in an autocrine loop (Ferracini et al., 1995). The HGF/MET pathway can promote angiogenesis directly, via inducing migration and motility of ECs (Bussolino et

al., 1992; Sengupta et al., 2003), indirectly, by regulating the expression of other GFs and angiogenic mediators (Nakamura et al., 2011; Zhang et al., 2003), or in synergy with the VEGF pathway, by activating common downstream signalling pathways (Sulpice et al., 2009).

*The ANG/TIE pathway* is an endothelial-specific binary signalling system that allows the blood vessels to switch between vascular quiescence and stimulation of angiogenic sprouting (Eklund and Saharinen, 2013). The main axis of this pathway is ANG1 and ANG2 signalling via TIE2. ANG2 is stored in the Weibel-Palade bodies of ECs (Fiedler et al., 2004) and is upregulated in the tip cells during hypoxia and tumourigenesis (del Toro et al., 2010). ANG1 is expressed by perivascular cells (Suri et al., 1996), and TIE2 is located on the surface of ECs (Dumont et al., 1992). Mural cell-derived ANG1 activates TIE2 on ECs and enhances vessel integrity (Jeansson et al., 2011; Suri et al., 1996). ANG2 is released from angiogenic tip cells by angiogenic stimuli. It promotes EC sprouting and tumour angiogenesis by counteracting ANG1/TIE2 signalling (Maisonpierre et al., 1997) and by recruiting tumour-associated macrophages (TAMs) (De Palma et al., 2005).

*The PDGF pathway.* The platelet derived growth factor (PDGF) family is structurally related to VEGF, but differently from VEGFs, PDGFs are the major mitogens for mesenchymal cells (Andrae et al., 2008). PDGF-BB and PDGFR- $\beta$  are the main components of the PDGF pathway involved in neovascularization. Endothelial-derived PDGF-BB promotes EC–mural cell interactions via recruiting PDGFR- $\beta$ -expressing mural cells and thereby increases vascular integrity (Bjarnegård et al., 2004; Hellström et al., 1999). PDGF-B is also an important player in tumour angiogenesis, as blocking of its signalling pathways causes pericyte detachment from tumour vessels, reduces tumour growth due to immature vessels and renders vessels more sensitive to anti-VEGF therapy (Bergers et al., 2003). On the other hand, lack of PDGF-B signalling can promote metastasis due to abnormal and leaky vessels in tumours (Xian et al., 2006).

*The FGF pathway.* The fibroblast growth factor (FGF) signalling occurs in many different cell types (Murakami and Simons, 2008). Acidic FGF (aFGF, FGF-1) and basic FGF (bFGF, FGF-2), the first angiogenic GFs discovered (Folkman et al., 1988; Thomas et al., 1984), regulate different phases of angiogenesis via the activation of FGFR1 or FGFR2. It is suggested that these FGFs do not exhibit a direct effect on ECs, but instead promote angiogenesis *in vivo* by acting as upstream organizers and coordinators of other GF systems and different angiogenic pathways (Murakami and Simons, 2008; Presta et al., 2005). Studies with *Fgfr1*<sup>-/-</sup> and *Vegfr2*<sup>-/-</sup> embryoid bodies show that the FGF pathway controls neovascularization upstream of the VEGF pathway (Magnusson et al., 2004). FGF also upregulates HGF (Onimaru et al., 2002) and PDGFR (Nissen et al., 2007), among others.

*The TGF- $\beta$  pathway.* The most important transforming growth factor beta (TGF- $\beta$ ) ligands involved in angiogenesis are TGF- $\beta$ 1 and BMP9, which mediate their effects on ECs via type I activin receptor-like kinase (ALK) receptors, ALK1 and ALK5 (David et al., 2007; Goumans et al., 2003). While ALK5 is expressed in different cell types, ALK1 expression is mainly restricted to the endothelium (Roelen et al., 1997; Seki et al., 2006). TGF- $\beta$  and BMP-9 signalling is highly context-dependent. TGF- $\beta$ 1 signalling through ALK5 or ALK1 causes opposing effects on EC proliferation (Goumans et al., 2003). TGF- $\beta$ 1/ALK5 signalling is also required for vessel maturation, as it promotes vascular smooth muscle cell (vSMC) differentiation and EC-vSMC interactions (Carvalho et al., 2007). BMP9 signalling via ALK1 leads to inhibition of EC proliferation and promotes EC quiescence (Scharpfenecker et al., 2007; Upton et al., 2009). However, in synergy with TGF- $\beta$ , BMP9 has been shown to promote angiogenesis (Cunha et al., 2010).

## **1.2 Initiation of angiogenesis and tip/stalk cell specification**

Angiogenesis is induced mainly due to deficiency of oxygen and nutrients. In normoxia, oxygen-sensing enzymes, the prolyl hydroxylase domain proteins (PHD1-3), regulate hypoxia-inducible transcription factors (HIFs) by hydroxylation; after which HIFs are constantly targeted for proteosomal degradation (Majmundar et al., 2010). In hypoxia, PHD proteins cannot hydroxylate HIF proteins, thus HIFs become stabilised and are able to induce angiogenesis by upregulating the transcription of proangiogenic proteins (Fraisl et al., 2009). Still, oncogenes and GFs can activate HIFs even in the absence of oxygen scarcity. HIF-1 $\alpha$  also stimulates angiogenesis indirectly by upregulating the chemoattractant SDF- $\alpha$ , which in turn recruits the pro-angiogenic bone marrow-derived cells (BMDCs) (Du et al., 2008). Nutrient deprivation can stimulate angiogenesis independently of HIFs via metabolic regulators (Arany et al., 2008). To enable sprouting, the ECM is proteolytically degraded by matrix metalloproteases (MMPs). In addition to remodelling the ECM and basement membrane, the activity of MMPs liberates matrix-bound proangiogenic GFs to further support sprouting (Deryugina and Quigley, 2010). To counter-balance proangiogenic signalling, proteolytic degradation of matrix components generates endogenous anti-angiogenic protein fragments (Nyberg et al., 2005). ANG2 mediates EC liberation by promoting pericyte detachment from the vessel surface (Augustin et al., 2009).

Although VEGF activates all targeted ECs through VEGFR2, the negative feedback loop between the NOTCH and VEGF pathways defines which of those ECs are selected as migratory tip cells (Hellström et al., 2007; Phng and Gerhardt, 2009). Activation of VEGFR2 upregulates DLL4 in tip cells, which in turn induces the NOTCH pathway in the neighbouring ECs. NOTCH activation inhibits tip cell behaviour by downregulating the receptors promoting tip cell function - VEGFR2, VEGFR3 and NRP1 (Fantin et al., 2013; Tammela et al.,

2008), while upregulating VEGFR1, which functions as a VEGF trap (Jakobsson et al., 2010; Krueger et al., 2011). Although all VEGF-activated ECs upregulate DLL4, stochastic differences in local VEGF or in transcription produce an imbalance in the expression of DLL4, and the quickest ECs to respond with the highest DLL4 levels have the advantage to acquire the tip cell phenotype (Blanco and Gerhardt, 2013). Thus, all VEGF-activated ECs that are not directly inhibited by neighbours expressing high levels of DLL4 are by default selected as tip cells and initiate a new sprout. Another NOTCH ligand, JAGGED1, is predominantly expressed in stalk cells and antagonises NOTCH activation through DLL4, thereby enhancing differential NOTCH activation in tip and stalk cells and providing robustness in tip/stalk cell selection (Benedito et al., 2009). Computational modelling suggests that such negative feedback loop between the VEGF and NOTCH pathways is sufficient for patterning of tip and stalk cells (Bentley et al., 2008). Additionally, the BMP/SMAD pathway adds some robustness into this model. It is proposed that the interplay between DLL4/NOTCH and BMP/SMAD signalling in ECs leads to nonsynchronous oscillatory fluctuations of NOTCH and BMP targets, which results in rapid and robust tip/stalk cell selection and at the same time, maintains a dynamic pool of permissive, but non-sprouting ECs (Beets et al., 2013; Moya et al., 2012).

### **1.3 Tubule elongation**

Tip cells start guiding the sprout towards the VEGF gradient (Gerhardt et al., 2003). VEGFR1 and its soluble variant (sVEGFR1) are predominantly expressed in stalk cells and function as VEGF traps in physiological angiogenesis. sVEGFR1 creates a VEGF gradient by depleting the VEGF adjacent to stalk cells, leaving higher VEGF levels ahead of the tip cells and thereby facilitating the migration of the sprout perpendicular to the mother vessel (Chappell et al., 2009). Dynamic shuffling of tip and stalk cells is based on their relative VEGFR1 and VEGFR2 expression levels. The constant competition for the tip cell position ensures that the most competent cells lead the sprout, and such collaborative behaviour of ECs enhances the capability of the migrating sprout to sense the direction of the VEGF gradient (Jakobsson et al., 2010). In parallel with the VEGF gradient, tip cells also use axonal guidance molecules for sprout guidance and are therefore, in a sense, reminiscent of axonal growth cones (Adams and Eichmann, 2010). There are several guidance receptors expressed in sprouting ECs, including ephrins and their EPH receptors; neuropilins and PlexinD1, which bind semaphorins, either alone or in complex with each other; ROBO4, which binds SLIT ligands; and UNC5B, which binds netrins (Adams and Eichmann, 2010; Carmeliet and Tessier-Lavigne, 2005).

While tip cells are migratory, stalk cells are more proliferative and are responsible for sprout elongation (Gerhardt et al., 2003). It is suggested that proliferating stalk cells do not push the sprout, but instead tip cells pull the sprout forward by interacting with the surrounding ECM (Geudens and

Gerhardt, 2011). However, the proliferation of stalk cells is required for the sustained growth of the sprout (Gerhardt et al., 2003; Phng et al., 2009). Tip cells have a high VEGF gradient, which, in combination with the high affinity receptor complex (VEGFR2 and NRP1), leads to tip cell migration. Stalk cells, on the other hand, express less VEGFR2, which, combined with the absence of NRP1 and lower local VEGF concentrations leads to EC proliferation (Gerhardt et al., 2003; Takahashi et al., 2001). Additionally, FGF and VEGF crosstalk is crucial for neovascularization and vessel integrity, as basal FGF stimulation maintains the VEGFR2 expression level and its ability to respond to VEGF stimulation by upregulating VEGFR2 (Murakami et al., 2011). Although NOTCH activation is important for tip/stalk cell specification, subsequent fine-tuning of the NOTCH activity in stalk cells is needed in order to allow vessel growth. Stalk cell proliferation is ensured by the negative feedback regulation of NOTCH signalling. NOTCH signalling in stalk cells upregulates the NOTCH-regulated ankyrin repeat protein (NRARP), which in turn limits NOTCH signalling and stimulates WNT signalling (Phng et al., 2009). NRARP-promoted WNT signalling induces EC proliferation and supports cell junctions and vessel stability. NOTCH activity is also regulated by an acetylation/deacetylation mechanism. Acetylation of NOTCH protects it from proteosomal degradation and enhances its signalling, whereas deacetylation by NAD<sup>+</sup>-dependent SIRTUIN1 opposes NOTCH stabilisation and leads to decreased signalling (Guarani et al., 2011).

#### **1.4 Vascular lumen formation and anastomosis**

Stalk cells are also responsible for vascular lumen formation. Different mechanisms have been proposed for this process. First, the cell hollowing model proposes that the lumen of intersegmental vessels in zebrafish form by the fusion of intracellular vacuoles in ECs (Kamei et al., 2006). This model was extended with the cord hollowing model, which suggests that the intercellular space of intersomitic vessels is formed by exocytosis of vacuoles instead (Blum et al., 2008; Wang et al., 2010). In the luminal repulsion model, which has been proposed for the formation of larger axial vessels, VE-cadherin localises negatively charged CD34-sialomucins to the EC-EC contacts, which then triggers the initial separation of apical cell surfaces due to electrostatic repulsion and relocalisation of VE-cadherin junctions to the lateral cell contacts. A recent computational modelling study suggests that vacuolation and the cell-cell repulsion mechanism are synergistic and rather work in parallel than in different vessel types (Boas and Merks, 2014). A different lumenisation mechanism, EC budding, has been proposed for larger capillaries in zebrafish brain vasculature, where, in constantly perfused vessels, stalk cells seem to maintain their apicobasal polarity and the lumen of the new sprout remains continuous with the mother vessel (Ellertsdóttir et al., 2010). Besides these, also unicellular tube formation by membrane invagination (Herwig et al., 2011) and lumen

ensheathment in common cardinal veins of zebrafish have been proposed (Helker et al., 2013).

VEGFR2 activity in stalk cells during EC lumen formation is regulated by phosphatase VE-PTP, which forms Tie2-dependent trimeric complex with VEGFR2 and VE-cadherin (Hayashi et al., 2013). VE-PTP dephosphorylates VEGFR2 at the cell junctions, and its absence, when tested in gene-targeted *Ve-ptp*<sup>-/-</sup> embryoid bodies, results in defective lumen formation in vessel sprouts.

Anastomosis occurs when tip cells of adjacent sprouts establish contact with each other via their filopodia (Carmeliet and Jain, 2011; Herbert and Stainier, 2011). VE-cadherin-mediated initial spot-like junctional contacts of filopodia later expand into ring-like structures as tip cells slide along each other and establish tight EC-EC junctions (Blum et al., 2008; Herwig et al., 2011). The fusion of tip cells causes the ECs to form a continuous endothelium and lumen, accompanied by the loss of angiogenic properties of tip cells due to filopodia disappearance, and allowing perfusion (Herbert and Stainier, 2011; Herwig et al., 2011). It has been suggested that macrophages may act as bridges between two tip cells to facilitate the fusion of adjacent tubules. A study by Fantin et al. (2010) indicated that macrophages interact with ECs during all phases of vessel anastomosis, whereas, in some cases, macrophages bridged the adjacent tip cells in order to align them to facilitate fusion, in other cases, macrophages migrated to vessel junction sites and surrounded the fusing tubules. Rymo et al. (2011), on the other hand, suggested that, rather than making direct contact, macrophages and ECs communicate with each other in two ways: vessels attract macrophages through the secretion of attractive cues, and macrophages, in turn, promote sprouting by secreting soluble pro-angiogenic factors. It should be noted, however, that macrophages are not an absolute requirement for anastomosis, as vessel fusion occurs also in their absence, although, in that case, a reduced number of sprout fusion events were observed (Fantin et al., 2010; Rymo et al., 2011).

## 1.5 Vessel maturation

The recruitment of mural cells and deposition of the ECM are required for the stabilisation and maturation of nascent vessels (Jain, 2003; Potente et al., 2011). The deposition of the basement membrane is mediated by the upregulation of protease inhibitors – tissue inhibitors of metalloproteases (TIMPs) and the plasminogen activator inhibitor-1 (PAI-1) (Carmeliet and Jain, 2011). The recruitment of pericytes is mainly controlled by the PDGF-B pathway: ECs release PDGF-B, which stimulates PDGFR- $\beta$ -expressing pericytes to migrate and establish direct cell–cell contacts with ECs (Gaengel et al., 2009; Jain, 2003). In addition, mural cell-released ANG1 signalling via its receptor, Tie2, has been suggested to promote EC survival, quiescence and pericyte attachment (Suri et al., 1996). However, despite being critical for regulating the number and

diameter of developing vessels, ANG1 is not required for pericyte recruitment (Jeansson et al., 2011). The vessel maturation process can be reversed by ANG2, which antagonises the ANG1/TIE2 signalling and causes mural cell detachment and vessel destabilisation (Maisonpierre et al., 1997). Activation of different TGF- $\beta$  family members can lead to both the stimulation as well as resolution of angiogenesis (Pardali et al., 2010). For instance, low concentrations of BMP9 have been shown to stimulate EC proliferation, whereas high concentrations inhibit this (Scharpfenecker et al., 2007; Suzuki et al., 2010). Likewise, the same concentration-dependent effects on EC proliferation and migration apply to TGF- $\beta$  (Goumans et al., 2002). TGF- $\beta$  signalling is also important in mural cell recruitment, as it induces differentiation, proliferation and migration of vSMCs (Carvalho et al., 2007; Seki et al., 2006). The NOTCH pathway is involved in vessel maturation through endothelial JAGGED1, which promotes recruitment and differentiation of vSMCs via activating NOTCH3 in mural cells (Domenga et al., 2004; High et al., 2008).

Quiescent ECs form barriers to regulate the exchange of solutes and fluids between blood and tissues (Potente et al., 2011). While tight junctions are responsible for maintaining barriers, adherens junctions mediate cell–cell adhesion (Dejana et al., 2009). VE-cadherin forms a complex with VEGFR2 at cell–cell junctions and prevents VEGF signalling by recruiting phosphatase DEP1/CD148, which dephosphorylates VEGFR2 and inhibits its internalization (Lampugnani et al., 2006). At the same time, VE-cadherin clustering promotes the formation of the TGF- $\beta$  receptor complex, thereby enhancing TGF- $\beta$  signalling and leading to decreased EC migration and proliferation (Rudini et al., 2008). ANG1/TIE2 signalling promotes vascular integrity by inducing accumulation of adhesion proteins at EC-EC junctions (Eklund and Saharinen, 2013; Gavard et al., 2008). Adherens junctions between ECs and pericytes are strengthened by EC- and platelet-derived sphingosine-1-phosphate (S1P), which by binding to its receptor, S1PR1, promotes N-cadherin trafficking to EC–pericyte contact sites (Paik et al., 2004). It has been proposed that upon vessel perfusion, blood flow delivers S1P to the areas of active angiogenesis, and subsequent S1P/S1PR1 signalling restricts angiogenic responsiveness of ECs via inhibiting VEGFR2 signalling and stabilisation of junctional VE-cadherin (Gaengel et al., 2012).

## **1.6 Vascular quiescence**

Active cellular signalling is required for maintaining vascular integrity and homeostasis (Murakami, 2012). Autocrine signalling of VEGF is required for EC survival and vascular homeostasis. It has been demonstrated that endothelial-specific deletion of VEGF leads to progressive endothelial degeneration, whereas paracrine VEGF is not able to compensate for the loss of endothelial VEGF (Lee et al., 2007). Furthermore, cell-autonomous activation of the VEGF pathway is dispensable for angiogenesis, but crucial for the maintenance of

blood vessels, as the intracrine action of VEGF protects ECs from stress-induced apoptosis in non-pathological conditions (Lee et al., 2007). In addition, basal levels of FGF signalling were shown to be critical for vessel integrity, as disrupting FGF signalling in the quiescent endothelium caused increased vessel leakiness and disintegration of vasculature (Murakami et al., 2008). The absence of FGF signalling leads to the VE-cadherin–p120-catenin complex dissociation and subsequent disassembly of adherens and tight junctions, and results in EC loss and increased vessel permeability (Murakami et al., 2008). ANG1/TIE2 signalling either promotes vascular quiescence or stimulates vessel sprouting, depending on whether it occurs in the presence or absence of cell–cell contacts. In the presence of cell–cell contacts, ANG1 induces quiescence by activating the PI3K-AKT pathway via TIE2 transdimer formation, whereas in isolated ECs, ANG1 stimulation leads to ERK1/2-mediated cell migration and proliferation (Fukuhara et al., 2008; Saharinen et al., 2008). Furthermore, ANG1/TIE2 signalling augments basal NOTCH activity by upregulating endothelial DLL4, which in turn stimulates the deposition of the basement membrane (Zhang et al., 2011). The NOTCH pathway contributes to the vascular stabilisation process by inhibiting vessel sprouting, upregulating NRARP and also by stimulating the deposition of the ECM (Hellström et al., 2007; Lobov et al., 2007; Phng et al., 2009; Suchting et al., 2007; Zhang et al., 2011). In addition to being important for vessel maturation, the NOTCH pathway seems to be required for further maintenance of vascular quiescence, as endothelial specific inactivation of RBPJ (a main downstream regulator of the NOTCH pathway) as well as the blockade of DLL4 in adult mice lead to reinitiation of abnormal vascular growth (Dou et al., 2008; Yan et al., 2010). Cooperation between NOTCH and ALK1 results in the inhibition of retinal angiogenesis: combined disruption of NOTCH and ALK1 functions during postnatal development in mice leads to exacerbated retinal hypervascularization, while ALK1/BMP9 signalling counteracts hypersprouting induced by NOTCH inhibition (Larrivéé et al., 2012). BMP9 has been described as a circulating quiescence factor, which is present in serum at concentrations of 2-12 ng/mL (David et al., 2008). The role of BMP9 in vascular quiescence has also been supported by studies showing that BMP9 hinders VEGF- and FGF-2-stimulated EC migration and proliferation (David et al., 2007; Scharpfenecker et al., 2007).

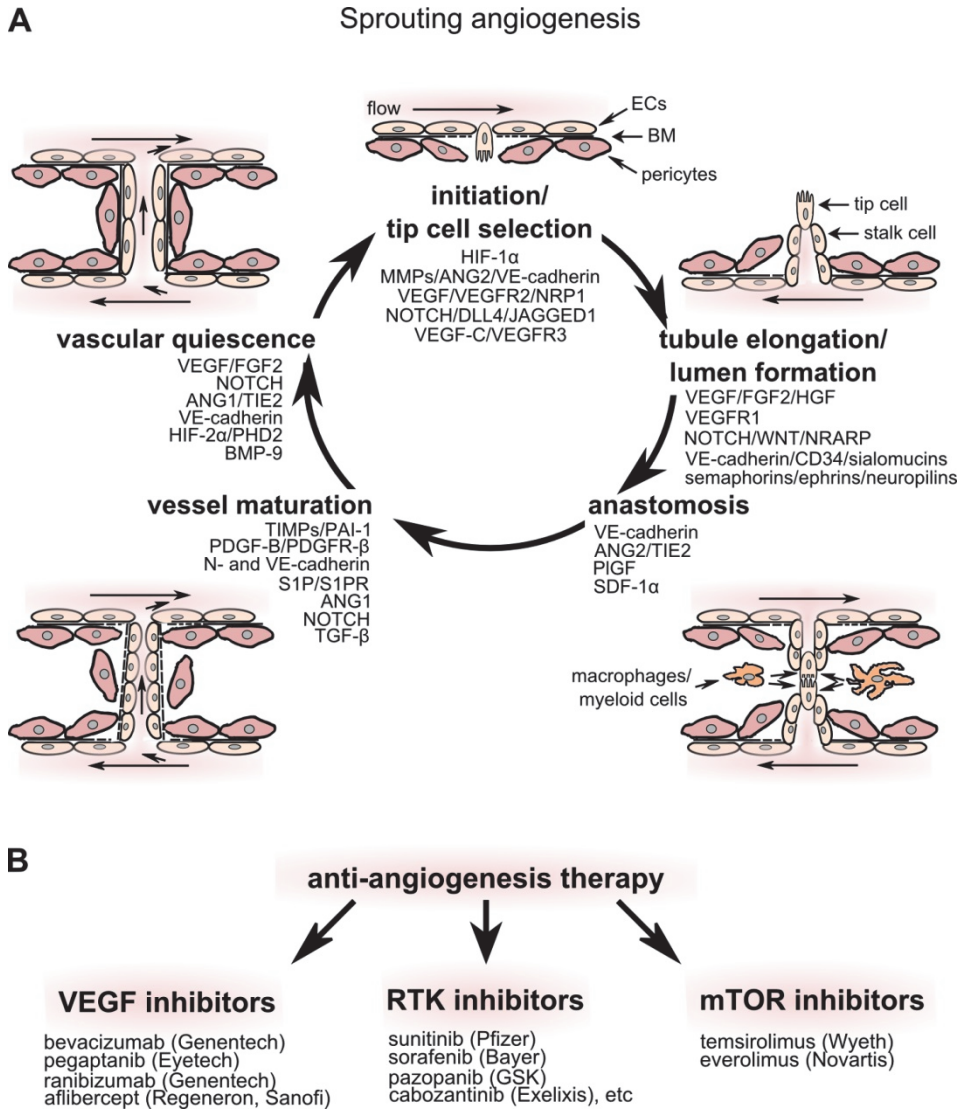


**Figure 1.** Overview of sprouting angiogenesis. **(A)** Different stages of sprouting angiogenesis (adapted from Herbert and Stainier, 2011). The most important mediators of each step are shown. Angiogenesis is initiated by hypoxia or inflammatory or tumor cells, which release proangiogenic GFs. Initiation process involves pericyte detachment, basement membrane (BM) degradation and selection of a tip cell, which leads and guides the new sprout. Stalk cells do not migrate, but proliferate and contribute to sprout elongation and vascular lumen formation. When tip cells of adjacent sprouts meet, 2 sprouts fuse (anastomosis) and allow initiation of blood flow. Also macrophages and myeloid cells are involved in anastomosis process. Recruitment of mural cells and deposition of new BM ensure the maturation of new vessels and restore the vascular quiescence. **(B)** Current anti-angiogenesis therapeutics used in clinic

## 1.7 Challenges in anti-angiogenesis treatment

While physiological angiogenesis is tightly regulated and results in a structured and hierarchically organised vascular network, in tumours, the highly unbalanced overexpression of proangiogenic GFs leads to the development of structurally abnormal vasculature with heterogeneous, leaky, tortuous and chaotically branching vessels (Jain, 2005). The aberrant vascular patterning in pathological angiogenesis is thought to be caused by high VEGF concentrations, leading to synchronous oscillations of the NOTCH pathway, which in turn cause the ECs to oscillate synchronously between tip and stalk cell phenotypes, instead of alternating them (Bentley et al., 2008). Hyperpermeability of vessels increases the interstitial fluid pressure, which, in combination with proliferating tumour mass, leads to heterogeneous tumour perfusion, hypoxia, acidosis and also compromised cytotoxic functions of infiltrating immune cells (Jain, 2005). Continuous hypoxia forces constant overproduction of proangiogenic GFs, which further exacerbates non-productive angiogenesis in a self-reinforcing manner and leads to disease progression by promoting the selection of more aggressive hypoxia-independent tumour cell clones and facilitating their escape through leaky vessels. Furthermore, uneven distribution of oxygen and chemotherapeutics due to irregular perfusion leads to limited efficacy of radiation therapy and resistance to conventional cancer therapeutics (Goel et al., 2011). There are at least 6 distinct types of vessels in tumours (Nagy et al., 2010). The “early“ vessels – unstable, leaky and pericyte-poor mother vessels and their more stable daughter vessels (glomeruloid microvascular proliferations, vascular malformations and capillaries) – develop via angiogenesis. The “late“ vessels – feeder arteries and draining veins – form via arteriovenogenesis from pre-existing vessels. Because “early“ vessels are dependent on exogenous VEGF, and “late“ vessels, due to their downregulated VEGFR2, are not, only VEGF-dependent “early“ vessels are susceptible to anti-VEGF therapy (Sitohy et al., 2011).

The concept of anti-angiogenesis therapy is based on the rationale that tumour growth is angiogenesis-dependent, and thus inhibition of blood vessel formation should result in vascular regression and render tumours dormant (Folkman, 1971). Given that VEGF is the key activator of angiogenesis, the present anti-angiogenic strategies (Figure 1B) have mainly focused on blocking the VEGF pathway. The first FDA-approved angiogenesis inhibitor was the humanized anti-VEGF monoclonal antibody, bevacizumab (Avastin; Genentech) (Presta et al., 1997), that is used for the treatment of several cancers, including metastatic colorectal cancer and metastatic renal cell carcinoma (Escudier et al., 2007; Hurwitz et al., 2004). Other therapeutics targeting VEGF include pegaptanib (Macugen; Eyetech) and ranibizumab (Lucentis; Genentech), used for the treatment of wet age-related macular degeneration, and aflibercept (Zaltrap; Regeneron, Sanofi-Aventis) for the treatment of refractory colorectal cancer. Multi-target receptor tyrosine kinase (RTK) inhibitors, which, among others,

include sunitinib (Sutent; Pfizer), sorafenib (Nexavar; Bayer), pazopanib (Votrient; GSK) and cabozantinib (Cometriq; Exelixis), act via blocking different receptors of angiogenic GFs. mTOR inhibitors, temsirolimus (Torisel; Wyeth) and everolimus (Afinitor; Novartis), target EC survival and proliferation via blocking the formation of the mTOR complex.

However, the majority of clinical trials concerning VEGF-targeted therapies fail due to limited long-term benefit caused by several intrinsic or acquired resistance mechanisms (Bergers and Hanahan, 2008; Welte et al., 2013). The refractoriness to anti-VEGF therapy may be caused by lost VEGF dependency (Sitohy et al., 2011) and a tight pericyte coat in mature “late“ vessels, which makes them less sensitive to drugs (Bergers et al., 2003), or by producing alternative pro-angiogenic GFs (e.g., FGF-2, PLGF, HGF and SDF1) in response to hypoxia (Casanovas et al., 2005; Kopetz et al., 2010). Besides, the use of VEGF-independent modes of vascularization in tumours may diminish the efficiency of the VEGF blockade (Carmeliet and Jain, 2011). For example, vessel co-option, hijacking of the pre-existing vasculature by tumour cells, has been reported to occur in well-vascularized tissues, such as brain (di Tomaso et al., 2011), and via vasculogenic mimicry highly aggressive tumour cells can generate vascular channels themselves (Maniotis et al., 1999). Tumour ECs that originate from differentiated CD133+ cancer stem-like cells are more resistant to the VEGF blockade (Wang et al., 2010). Furthermore, stromal cells contribute significantly to the anti-angiogenic resistance (Bergers and Hanahan, 2008). Anti-VEGF refractoriness is conferred in cancer-associated fibroblasts by releasing BMDC-mobilizing chemoattractants, such as PDGF-C and SDF1 (Crawford et al., 2009; Orimo et al., 2005), and in tumour-infiltrating CD11b+Gr1+ myeloid cells via the release of angiogenic factors, such as Bv8 (Shojaei et al., 2009). Finally, anti-angiogenesis therapy itself might cause enhanced tumour invasiveness and metastasis, foremost due to the aggravated hypoxic and inflammatory milieu (Ebos et al., 2009; Pàez-Ribes et al., 2009).

To enhance the efficacy of anti-angiogenesis therapy, several strategies have been proposed. First, there is an urgent need for predictive biomarkers, because to date, only few biomarker candidates (e.g., levels of circulating angiogenic GFs and hypertension) are available, whereas none have yet been validated for clinical use (Jain et al., 2009). Secondly, combination therapy that targets both the angiogenesis as well as resistance pathways could be beneficial, as exemplified by the successful treatment of pancreatic neuroendocrine tumours with concurrent inhibition of MET and VEGF pathways (Sennino et al., 2012). Another alternative anti-angiogenic approach, “sustained vessel normalization“, suggests that instead of destroying tumour blood vessels, anti-angiogenesis therapeutics should promote vessel maturation and stability (Goel et al., 2011). In addition, the emergence of evasive resistance can be blocked in proangiogenic TAMs by targeting the ANG2/TIE2 pathway (Mazzieri et al., 2011). Consistently, restoring the structure and function of tumour blood vessels has

been shown to reduce the interstitial pressure and hypoxia, and improve tumour responsiveness to chemotherapy (Koh et al., 2010; Mazzone et al., 2009). Finally, to facilitate the translation of new drug candidates into effective clinical therapies, more adequate and clinically relevant tumour models should be used in preclinical research (Ebos and Kerbel, 2011).

## 1.8 Plasma half-life extension strategies of therapeutic proteins

The *in vivo* potency of new therapeutic agents is also often limited due to their short plasma residence time, immunogenicity and susceptibility to protease degradation (Pasut and Veronese, 2012). Several strategies have been developed to overcome these limitations and improve the pharmacokinetic properties of therapeutics.

*PEGylation*, the chemical coupling of polyethylene glycol (PEG) (Abuchowski et al., 1977), is one of the most widely used and successful approaches for extending the half-life of biopharmaceuticals (Pasut and Veronese, 2012). By increasing the hydrodynamic radius and masking the surface of the therapeutic substance, PEGylation reduces the renal excretion rate, proteolytic degradation and immunogenicity, which all together result in improved *in vivo* plasma half-life. In addition to differently sized and structured PEG chains, a variety of non-selective and site-directed coupling methods have been established for PEGylation (Pasut and Veronese, 2012). Successful examples of selective site-specific PEGylation are N-terminally PEGylated PEG-G-CSF (Pegfilgrastim; Neulasta) (Kinstler et al., 2002) and C-terminally thiol-PEGylated PEG-anti-TNF Fab' (Certolizumab pegol; Cimzia) (Melmed et al., 2008). Furthermore, selective conjugation of branched 40 kDa PEG to the anti-VEGF aptamer resulted in clinical approval of pegaptanib (Macugen; Eyetech) for wet age-related macular degeneration (Ng et al., 2006). The major limitation that often seems to co-occur with PEGylation is decreased or abrogated protein bioactivity (Kontermann, 2011; Pasut and Veronese, 2012). For example, in the case of clinically approved PEG-interferon- $\alpha$ 2a (Pegasys), random PEGylation of interferon- $\alpha$ 2a with 40 kDa branched resulted in almost total loss of its *in vitro* activity (Bailon et al., 2001). Nevertheless, greatly prolonged *in vivo* residence time counterbalanced the reduced bioactivity of the PEG-interferon conjugate (Bailon et al., 2001).

*Fc-fusion protein technology* is another widely used approach for extending plasma half-life of protein based therapeutics. The aim of genetic linking of the constant fragment crystallisable (Fc) region of the human immunoglobulin (Ig) to therapeutic proteins is to provide the proteins with some of the beneficial antibody-like structural properties and thereby improve their pharmacological efficiency (Huang, 2009; Schmidt, 2009). The improved therapeutic effect is achieved mainly through utilizing the homodimeric nature of these fusion proteins. The dimeric nature considerably increases the molecular weight and

thereby prolongs *in vivo* plasma residence time. Furthermore, the bivalency of these dimeric drugs increases the ligand-binding affinity, which in turn results in enhanced therapeutic activity (Huang, 2009; Schmidt, 2009). The additional benefits of this technology include improved solubility and stability of the therapeutic proteins, and also a facilitated manufacturing process. Examples of Fc-fusion therapeutic proteins include a TNF- $\alpha$  antagonist, etanercept (Enbrel; Amgen), for the treatment of different forms of arthritis (Ducharme and Weinberg, 2008), and an angiogenesis inhibitor, aflibercept (Zaltrap; Regeneron, Sanofi), that functions as a VEGF trap (Holash et al., 2002).

## **2 CD44**

CD44 was first identified as a lymphocyte homing receptor (Gallatin et al., 1983). Later, it was also found to function as the principal receptor for hyaluronan (HA) (Aruffo et al., 1990). Although encoded by a single highly conserved gene (on chromosome 11 in humans and chromosome 2 in mice), the CD44 protein family represents a large and heterogeneous group of transmembrane glycoproteins (Screaton et al., 1992). Due to extensive post-translational modifications and alternative splicing, CD44 displays a great number of different, structurally diverse isoforms, with molecular size varying from 80 to 200 kDa. All CD44 isoforms are comprised of constant exons 1-5 in their N-terminal extracellular part, and exons 16-17 in the membrane proximal region, whereas up to 10 variant exons, exons 6-15 (v1-v10) can be inserted between them by alternative splicing (Screaton et al., 1992). The transmembrane domain is encoded by a constant exon 18 and the cytoplasmic domain either by a short variant exon 19 or, more commonly, by exon 20. The smallest, standard (hematopoietic) CD44 isoform (CD44s) lacks all variant exons and is ubiquitously expressed on the surface of most vertebrate cells (Naor et al., 1997). Variant CD44 isoforms (CD44v) are expressed mainly during development and T cell activation and maturation, otherwise CD44v expression is restricted only to a few epithelial cell types and a variety of advanced stage carcinomas (Naor et al., 2002).

### **2.1 The structure of CD44**

CD44 consists of the N-terminal extracellular domain (ectodomain), the transmembrane domain and the C-terminal cytoplasmic domain (Figure 2A). The ectodomain of CD44 regulates cell adhesion by associating with a variety of ECM components. Although HA has been denoted as the main ligand for CD44, it also provides a docking site for other ECM components, such as fibronectin, collagen, laminin and osteopontin (reviewed in Orian-Rousseau and Sleeman, 2014). The ectodomain of CD44 is composed of the N-terminal globular HA-binding domain (HABD) and the juxtamembrane stem region (Naor et al., 1997). CD44 HABD contains the evolutionary conserved Link module (aa 32-

120), shown to be critical for HA binding (Kohda et al., 1996), and a lobular extension flanking the Link module (Banerji et al., 1998). While two interchain disulphide bridges in the Link module stabilize the structure of the globular HA-binding domain (Kohda et al., 1996), an additional disulphide bridge in the flanking lobe is required for proper folding (Banerji et al., 2007; Teriete et al., 2004). Thus, the complete CD44-HABD is defined by residues 21-169 according to human CD44 (Figure 2B) (Banerji et al., 2007; Teriete et al., 2004). Four key residues (Arg41, Tyr42, Arg78 and Tyr78) in CD44-HABD have been identified as critical for HA binding (Bajorath et al., 1998).

The HA-binding ability of CD44 is strictly regulated. It has been proposed that CD44 occurs in 3 activation states on the cell surface: inactive, non-HA-binding CD44; active, constitutively HA-binding CD44; and inducible CD44, in which HA binding can be induced by external stimuli (Lesley et al., 1995). These states have been shown to correlate with the CD44 N-glycosylation pattern, where the inactive CD44 appears to be the most, and the constitutively active CD44 the least glycosylated (English et al., 1998; Lesley et al., 1995). Although CD44-HABD contains five N-glycosylation sites, only two (Asn25 and Asn125) have been shown to affect HA binding (English et al., 1998). The O-glycosylation sites are mostly located in the variable exons and stem region (Naor et al., 1997; Naor et al., 2002). Abundant O-glycosylation in the membrane proximal region gives the CD44 stem region a stalk-like structure (Ponta et al., 2003). The stem region contains also several putative proteolytic cleavage sites (Okamoto et al., 1999) and binding sites for GAGs, such as heparan sulphate on exon v3, which enable CD44 to interact with heparin binding GFs (Bennett et al., 1995). Inclusion of variant exons has been shown to promote clustering of CD44 and thereby enhance HA binding (Sleeman et al., 1996).

In addition to providing a binding site for HA, CD44 also mediates its metabolism in tissues. CD44 is one of the main receptors responsible for local HA uptake and turnover (Culty et al., 1992; reviewed in Knudson et al., 2002). Furthermore, lack of CD44 has been shown to cause HA accumulation in tissues and lead to different pathological conditions, thus indicating the physiological importance of CD44-mediated HA internalization (Kaya et al., 1997; Nedvetzki et al., 2004; Teder et al., 2002). This feature, HA uptake by CD44, has recently become the focus of cancer treatment. A growing body of research demonstrates that CD44-mediated HA endocytosis could be exploited for targeted delivery of siRNAs or chemotherapeutics (reviewed in Jordan et al., 2015).

The transmembrane domain of CD44 contains 23 hydrophobic amino acids (aa) and one cysteine residue. It is involved in CD44 oligomerisation and its association with the glycolipid-enriched microdomains (Liu and Sy, 1997; Neame et al., 1995). The cytoplasmic tail of CD44 (72 aa) binds to many intracellular cytoskeleton-linking proteins, which are important for CD44-mediated signal transduction and cytoskeleton reorganization. The contacts between CD44 and actin-based cytoskeleton, which are mediated by ankyrin and

ERM proteins (ezrin, radixin and moesin), are involved in HA-dependent cell motility and adhesion (Legg et al., 2002; Lokeshwar et al., 1994; Tsukita et al., 1994). Alternatively, the interaction of CD44 with the tumour suppressor NF2 mediate inhibition of cell growth and cell migration (Bai et al., 2007; Morrison et al., 2001). It has been demonstrated that the affinity of CD44 for its cytoplasmic interaction partners is regulated by phosphorylation. Upon PKC activation, Ser325 dephosphorylation and Ser291 phosphorylation in the cytoplasmic tail of CD44 enhance binding of ERM proteins to CD44, resulting in directional cell motility (Legg et al., 2002). On the other hand, NF2 has been found to associate with CD44 only when hypophosphorylated (Morrison et al., 2001).

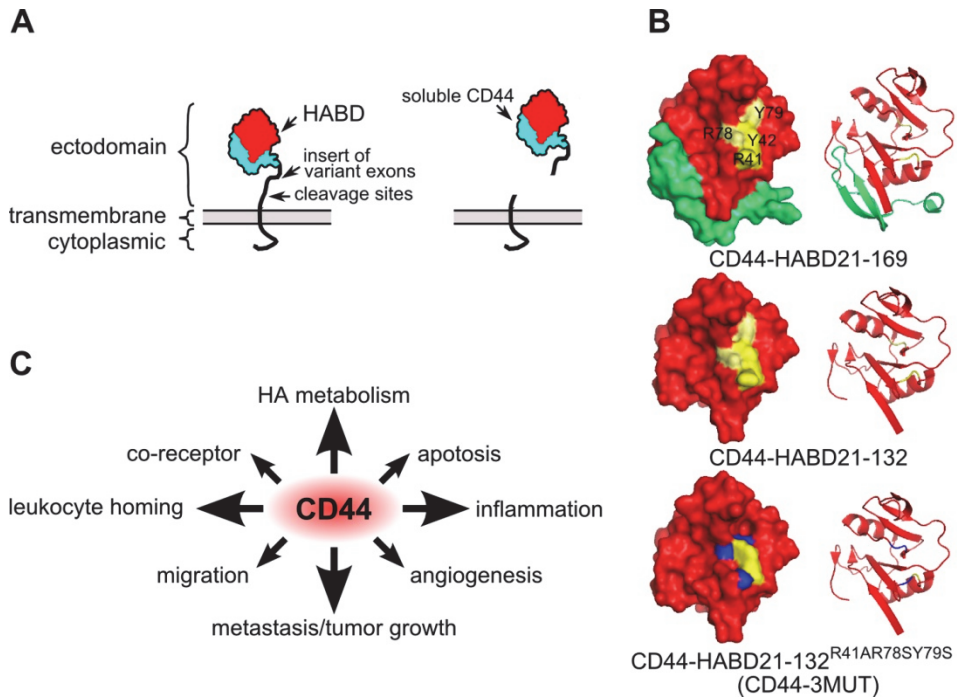


**Figure 2. The structure and functions of CD44.** (A) The schematic presentation of CD44 structure. CD44 is composed of 3 regions: the N-terminal extracellular ectodomain, the transmembrane domain and the C-terminal cytoplasmic domain. The ectodomain contains the evolutionarily conserved globular HA binding domain (HABD) in its N-terminus and the non-conserved stem region in its membrane proximal part. Up to 10 alternatively spliced exons can be inserted into the stem region. The membrane proximal part contains several proteolytic cleavage sites. The proteolytic cleavage of the CD44 ectodomain from cell surface results in release of soluble CD44 into circulation. (B) The structure of human CD44-HABD. The protein models are based on the crystal structure of CD44-HABD (PDB code: 1UUH) (Teriete et al., 2004). The complete human CD44-HABD required for HA binding is defined by residues 21-169 (upper panel). Two tyrosine-arginine clusters, R41-Y42 (yellow) and R78-Y79 (pale yellow) are critical for HA binding. The flanking structural lobe (green) stabilizes protein conformation. In CD44-HABD (middle panel) and CD44-3MUT (lower panel) the flanking region is removed and these proteins contain residues 21-132 (Päll et al., 2004). In CD44-3MUT the HA binding ability is abolished by substitutions of R41A, R78S and Y79S. (C) The functions of CD44

## 2.2 The physiological functions of CD44

CD44 protein family is described as the multidomain signalling platform that serves as the regulator of cell-cell and cell-ECM adhesion. By integrating the cues from the ECM with signals of GFs and cytokines, CD44 controls cell proliferation, migration, differentiation and survival (Orlan-Rousseau and

Sleeman, 2014). CD44 has been implicated in several physiological and pathological processes, such as HA metabolism, lymphocyte homing, leukocyte activation, inflammation and metastasis (Figure 2C). Therefore, it is surprising that, under normal physiological conditions, *Cd44*-null mice develop and reproduce normally (Protin et al., 1999; Schmits et al., 1997). Still, some mild aberrations were found in the immune system and haematopoiesis of *Cd44*<sup>-/-</sup> mice, showing CD44 as an important physiological receptor for immune and hematopoietic cell trafficking (Protin et al., 1999; Schmits et al., 1997). CD44 has been implicated in the homing of hematopoietic progenitor cells into their respective niche, as well as lymphocyte and leukocyte rolling on endothelium and their transendothelial migration during extravasation into inflammatory sites. For example, CD44 and HA were found to be crucial for SDF1-dependent transendothelial migration, as well as recruitment of hematopoietic progenitor cells into the bone marrow niche (Avigdor et al., 2004). Besides, CD44 deficiency caused altered distribution of myeloid progenitors between bone marrow and spleen due to defective egress of progenitors from bone marrow (Schmits et al., 1997). In regard to lymphocyte homing, CD44s has been shown to mediate T cell progenitor homing into thymus, whereas CD44v6 induces apoptosis resistance and expansion of thymocytes (Rajasagi et al., 2009). In line with this, *Cd44*-null mice display hindered lymphocyte trafficking into thymus, although the development of lymphoid organs was demonstrated to be normal (Protin et al., 1999). CD44 supports lymphocyte rolling on ECs by binding to different endothelial ligands. Under physiological flow conditions, CD44 has been found to mediate lymphocyte rolling and adhesion to ECs by binding to endothelial HA (DeGrendele et al., 1996). Efficient adhesion and rolling on HA is ensured by conformational transition of CD44-HABD between low and high HA-binding affinity states upon HA binding (Ogino et al., 2010). In addition to HA, T cells and neutrophils utilize CD44 binding to E-selectin for efficient trafficking into inflammatory sites (Katayama et al., 2005; N acher et al., 2011). Furthermore, the association of the CD44 intracellular domain (ICD) with  $\alpha 4\beta 1$  integrin in lymphocytes is required for firm adhesion and subsequent transendothelial migration (Nandi et al., 2004).

In contrast to mild changes in response to the total loss of CD44, conditional keratinocyte-specific ablation of CD44 in mice skin results in severely altered physiological responses, including delayed hair regrowth and impaired wound healing that result from reduced keratinocyte proliferation and impaired HA metabolism (Kaya et al., 1997).

## **2.3 The role of CD44 in inflammation**

Pathologically challenged *Cd44*<sup>-/-</sup> mice display more pronounced defects than their counterparts under normal physiological conditions, indicating that CD44 plays an important role in different inflammatory conditions. Genetic ablation of CD44 in *ApoE*<sup>-/-</sup> mice leads to significantly decreased atherosclerotic lesion

formation due to impaired macrophage recruitment and vSMC dedifferentiation (Cuff et al., 2001). Interestingly, CD44 was required for maximal upregulation of the adhesion protein VCAM-1 on vSMCs in atherosclerotic lesions, whereas on ECs, the levels of VCAM-1, ICAM-1 and PECAM-1 in wild-type mice were comparable to those in *Cd44*<sup>-/-</sup> mice (Cuff et al., 2001). On ECs, as well as macrophages and T cells, CD44 supports leukocyte rolling and transendothelial migration (Zhao et al., 2008). Decreased neutrophil infiltration was observed in the *Cd44*<sup>-/-</sup> mouse model of renal ischemia-reperfusion injury, indicating the inflammation-promoting function for CD44 in this model (Rouschop et al., 2005). The protective role of CD44 was discovered in bleomycin induced pneumonia, in which case CD44 was shown to be needed for the resolution of lung inflammation, as the ablation of CD44 resulted in the accumulation of apoptotic neutrophils and HA fragments (Teder et al., 2002). *Cd44*-null hTNF- $\alpha$  transgenic mice suffered from more pronounced inflammatory bone loss due to their enhanced sensitivity towards TNF- $\alpha$ , which was caused by increased activation of p38 mitogen-activated protein kinase (Hayer et al., 2005). Furthermore, exaggerated granuloma formation was observed in *Cd44*<sup>-/-</sup> mice in response to pathogen infection (Schmits et al., 1997). Together, these studies indicate a context specific role for CD44 in inflammation, being involved in both promoting as well as limiting excess inflammatory reactions.

Collectively, studies with *Cd44*<sup>-/-</sup> mice suggest that the loss of CD44 may be compensated by another protein during early embryogenesis. Indeed, it was found that RHAMM can replace functions of CD44 during embryogenesis. Nedvetzki et al. (2004) demonstrated that RHAMM substituted CD44 in a mouse model of collagen-induced arthritis, where it bound to HA, enhanced migration, and upregulated proinflammatory genes instead of CD44. Interestingly, the compensation of CD44 ablation by RHAMM did not occur due to its increased expression, but rather due to HA accumulation caused by CD44-deficiency, allowing enhanced RHAMM signalling and leading to aggravated inflammatory response (Nedvetzki et al., 2004). Furthermore, another CD44 compensatory protein, ICAM-1, was shown to take over the MET co-receptor function of CD44 in the liver of *Cd44*<sup>-/-</sup> mice (Olaku et al., 2011).

## 2.4 The functions of CD44 in cancer

The role of CD44 in malignant transformation is very complex. In many cancers, CD44 isoforms are overexpressed and correlate with tumour progression and metastasis, whereas in others, CD44 plays a protective role and acts as a tumour suppressor. For example, CD44 was implicated in primary tumour formation in the *Apc*<sup>Min/+</sup> mouse model of colon cancer, where genetic ablation of CD44 suppressed the incidence of intestinal adenoma formation, while the introduction of variant CD44 promoted this (Zeilstra et al., 2008; Zeilstra et al., 2014). Interestingly, CD44-deficiency did not affect the incidence of primary tumour formation in the p53<sup>+/-tm1</sup> mouse model of osteosarcoma, but instead, reduced

metastases were observed in these mice, suggesting that CD44 is involved in metastasis rather than in tumour initiation (Weber et al., 2002). The supportive role of CD44 in the metastatic cascade was further demonstrated by studies, where overexpression of CD44v in non-metastatic rat pancreatic carcinoma (Günthert et al., 1991) or CD44s in mouse fibrosarcoma cells (Kogerman et al., 1997) was sufficient for establishing metastatic behaviour. Furthermore, transplantation of CD44v-expressing breast cancer cells in mice leads to successful formation of lung metastases (Yae et al., 2012). In contrast, the loss of CD44 in a spontaneously metastasizing MMTV-PyVmT mouse model of breast cancer resulted in enhanced lung metastasis (Lopez et al., 2005), indicating a protective role for CD44 against metastasis. In support of this, reduced metastases in lungs were observed in case of CD44s overexpression in rat prostate cancer cells (Gao et al., 1997). The anti-tumourigenic role of CD44 was also demonstrated by a study, where SV40-transformed fibroblasts derived from CD44-deficient mice formed large subcutaneous tumours, whereas reintroduction of CD44s in these fibroblasts resulted in the formation of only very small tumours (Schmits et al., 1997). These data suggest that the roles of CD44 in tumourigenesis appear to vary in different stages and types of cancer.

Despite its ambiguous role in malignancy, CD44 has emerged as a widely used biomarker for the isolation of cancer stem cells (CSCs). CD44 has been used to identify and isolate CSCs from breast (Al-Hajj et al., 2003), colorectal (Dalerba et al., 2007), prostate (Collins et al., 2005), pancreatic (Li et al., 2007) and ovarian (Zhang et al., 2008) cancer, among others. Several clinical studies have also tried to correlate the CD44 expression level with cancer prognosis, but the results have been controversial. For example, both favourable and unfavourable correlation, as well as no significant correlation between CD44v6 expression and overall survival have been demonstrated in breast cancer (Bánkfalvi et al., 1999; Friedrichs et al., 1995; Kaufmann et al., 1995). Similarly, many studies indicate CD44s as a negative prognostic marker for overall survival in renal cell carcinoma (Lim et al., 2008; Mikami et al., 2015), whereas others claim that CD44 does not have individual prognostic significance (Tawfik et al., 2007). However, a recent meta-analysis by Li et al. (2015) still suggests that high CD44 expression correlates with the overall survival rate in renal cell carcinoma patients.

To acquire stem cell properties cancer cells frequently undergo epithelial-to-mesenchymal transition (EMT). CD44 contributes to EMT by forming a complex with HA and moesin upon TNF- $\alpha$  stimulation, which is required for actin remodelling and activation of TGF- $\beta$  signalling and results in the induction of EMT and cells acquiring mesenchymal phenotype (Takahashi et al., 2010). More importantly, CD44 isoform switching from a variant CD44v to the standard CD44s isoform has been demonstrated to be critical for cancer cells to complete EMT and promote breast and pancreatic cancer metastasis (Preca et al., 2015; Xu et al., 2014). By contrast, a study by Yae et al. (2012) demonstrated

that the opposite CD44 isoform switching, from CD44s to CD44v, is required for lung colonization of metastatic breast cancer cells. CD44 is also implicated in chemo- and apoptosis resistance. In this regard, CD44 has been shown to induce multidrug protein-1 (MDR1) (Bourguignon et al., 2009), attenuate the tumour-suppressive HIPPO pathway (Xu et al., 2010) and protect cells from reactive oxygen species (ROS)-induced stress signalling via upregulation of reduced glutathione, acting thereby as a ROS scavenger (Ishimoto et al., 2011). Consistently, p53 has been shown to inhibit CD44 expression, thus allowing cells to respond to p53-dependent apoptotic and stress signals (Godar et al., 2008).

Altogether, CD44 can be considered as a multifaceted molecule that takes part in different aspects of cancer progression and can promote as well as inhibit tumourigenesis.

## 2.5 The functions of CD44 in angiogenesis

CD44 plays a role in EC physiology. By using blocking antibodies, it has been shown that CD44 is required for promoting EC proliferation, HA-induced EC migration, EC adhesion to HA, and also *in vitro* endothelial tubule formation (Savani et al., 2001; Trochon et al., 1996). CD44 can mediate EC functions via different signalling pathways depending on its ligands and the origin of ECs. For example, in human microvascular cells, repression of CD44 expression disrupted the formation of a regular tubule network via upregulation of CXCL9/CXCR3 and CXCL12/CXCR4 signalling (Olofsson et al., 2014). In human umbilical vein cells (HUVECs) high molecular weight (HMW) HA enhanced angiogenic sprouting and cell motility via CXCL12/CXCR4 signalling (Fuchs et al., 2013). Furthermore, CD44 mediates low molecular weight (LMW) HA-induced endothelial tubule formation in HUVECs via activation of SRC, FAK and ERK1/2 (Wang et al., 2011), and in bovine aortic ECs via activation of PKC $\alpha$ ,  $\gamma$ -adducin and CDK1 (Matou-Nasri et al., 2009). EC proliferation was also enhanced by CD44-stimulated cyclooxygenase induction and accompanying VEGF upregulation (Murphy et al., 2005). Tsuneki and Madri (2014) proposed that CD44 mediates several of its endothelial functions by modulating the expression of cell junctional molecules. In regard to EC proliferation, they demonstrated that disruption of CD44 in microvascular ECs leads to reduced CD31 and VE-cadherin expression, increased survivin expression and YAP nuclear translocation, and results in enhanced cell growth and reduced apoptosis (Tsuneki and Madri, 2014).

Although CD44 is involved in different aspects of EC functions, only few studies describe the functions of CD44 in *in vivo* angiogenesis. Endothelial specific silencing of CD44 *in vivo* resulted in reduced blood vessel invasion into Matrigel plugs in response to HA oligomer stimulation (Lennon et al., 2014). In response to arterial injury, *Cd44*<sup>-/-</sup> mice displayed increased neointima formation

and vSMC proliferation (Kothapalli et al., 2007). CD44 was also suggested to be involved in tumour angiogenesis, as its expression was specifically upregulated in the tumour vasculature and in cultured ECs stimulated by FGF-2 (Griffioen et al., 1997). The role of CD44 in tumour angiogenesis was further supported by findings that neovascularization of melanoma cells containing Matrigel plugs, as well as tumour and wound-induced angiogenesis, were reduced in *Cd44*<sup>-/-</sup> mice (Cao et al., 2006). Blood vessels in Matrigel plugs from *Cd44*<sup>-/-</sup> mice displayed abrogated cellular ruffling, irregular surface and thin endothelium. The intact leukocyte recruitment during tumour and wound angiogenesis and the inability of wild-type bone marrow to restore the normal angiogenic response in *Cd44*<sup>-/-</sup> mice suggested that primarily endothelial CD44 was involved in *in vivo* angiogenesis. The proliferation, survival and migration of ECs derived from either *Cd44*-null or wild-type mice were comparable. However, the ability to form tubular networks *in vivo* was severely impaired in ECs from *Cd44*-null mice (Cao et al., 2006). These data suggest that endothelial CD44 plays a role in the assembly, organization and integrity of newly forming blood vessels (Cao et al., 2006).

CD44 has been shown to play a protective role in vascular barrier integrity. *Cd44*<sup>-/-</sup> mice display significantly enhanced microvascular permeability following vasoactive histamine or lipopolysaccharide (LPS) challenge (Flynn et al., 2013). The loss of CD44 caused also decreased EC barrier strength, accompanied by altered expression and localization of cell adhesion proteins, VE-cadherin, PECAM-1 and  $\beta$ -catenin, and increased the expression of MMPs, which all together resulted in abnormal EC morphology. These data suggest that CD44 plays a role in restoring vascular integrity after vasoactive challenge, as well as in maintaining the vascular barrier function in the quiescent state. The regulation of the EC barrier function by CD44 was suggested to occur through a PECAM-1-dependent mechanism, as reconstitution of PECAM-1 expression in CD44-deficient ECs restored the EC barrier strength to the normal level (Flynn et al., 2013).

However, CD44 can regulate the EC barrier function differentially, depending on its ligands and isoforms. While HMW-HA and HGF enhance the endothelial barrier integrity and protect against induced vascular leakiness in a murine model of LPS-induced lung vascular permeability (Singleton et al., 2007), LMW-HA, on the contrary induces EC barrier disruption in pulmonary microvascular EC monolayers (Singleton et al., 2006). It was shown that HMW-HA strengthens the EC barrier via binding to CD44s in caveolin-1-enriched plasma membrane microdomains (CEMs). This, in turn, leads to the transactivation of the barrier-promoting SIP1 receptor and results in RAC1 activation, cortical actin formation and enhanced EC-EC contacts. In contrast, LMW-HA binding to CD44v10 isoform transactivates the barrier-disrupting SIP3 receptor, which leads to RhoA activation and stress fibre formation and results in decreased vascular integrity (Singleton et al., 2006). Interestingly, both

CD44v10 as well as CD44s isoforms were shown to contribute to HGF-mediated EC barrier integrity by functioning as MET co-receptors (Singleton et al., 2007). HGF induces MET binding to CD44v10, which subsequently leads to MET translocation to CEMs, where it temporally associates with CD44s. The recruitment of MET to CEMs and binding to CD44 is required for RAC1 activation and cortical actin formation (Singleton et al., 2007).

## 2.6 CD44 as a co-receptor

CD44 can function as a signalling hub by binding GFs and regulating the activity and signalling of a variety of cell surface receptors. First, it was noted that the heparin sulphate-modified CD44v3 isoform is able to bind several heparin-binding GFs, such as FGF-2, VEGF, HGF and HB-EGF (Bennett et al., 1995). However, later studies demonstrated that HS modification is not an absolute requirement for binding GFs to CD44. Various CD44 isoforms have been shown to modulate signalling of different cell surface receptors, including several RTKs, GPCRs and members of the TGF- $\beta$  receptor family (Orian-Rousseau and Sleeman, 2014).

*MET.* CD44 functions as an important co-receptor for MET. The physiological relevance of this function of CD44 was revealed by a study showing the haploinsufficiency of MET in the *Cd44*<sup>-/-</sup> background (Matzke et al., 2007). HGF binding to CD44v10 promotes HGF/MET signalling and regulates the vascular barrier function of ECs (Singleton et al., 2007). CD44v6 isoform, however, is required and sufficient for the full activation of HGF-induced MET signalling in several primary and cancer cell lines (Olaku et al., 2011). Introduction of the v6 isoform into tumour cells lacking CD44v6 induced MET activation and downstream signalling, whereas inhibition of the HGF/MET/CD44v6 complex formation with v6-specific antibodies blocked MET activation (Orian-Rousseau et al., 2002). Both extra- and intracellular parts of CD44 were shown to be needed for its co-receptor function. While the CD44 ectodomain presents HGF to MET and is needed for its activation, CD44-ICD link to cytoskeleton is required for promoting downstream signalling (Orian-Rousseau et al., 2002) and MET internalization (Hasenauer et al., 2013). In addition, CD44v6 mediates MET activation in ECs (Tremmel et al., 2009).

*VEGFR2 and other RTKs.* Interestingly, in ECs CD44v6 has been shown to function also as a VEGFR2 co-receptor, whereas, in a similar manner to MET, the CD44 ectodomain is required for binding to VEGFR2, and CD44-ICD promotes downstream signalling of activated VEGFR2 (Tremmel et al., 2009). Differently from MET, which requires HGF to associate with CD44v6, VEGFR2 forms a constitutive complex with CD44v6. The function of CD44v6 as a MET and VEGFR2 co-receptor has been suggested to be important in several *in vitro* and *in vivo* angiogenic processes, as the CD44v6-blocking peptide was able to impair VEGF- and HGF-induced EC migration, sprouting

and tubule formation, as well as *in vivo* tumour angiogenesis in pancreatic carcinoma (Tremmel et al., 2009).

In regard to other RTKs, CD44 can associate with and regulate the activity of several members of the ErbB family (Meran et al., 2011; Sherman et al., 2000; Yu et al., 2002) and form a complex with FGFR in chondrosarcoma cells (Wakahara et al., 2005). In addition, CD44 associates with PDGFR $\beta$  in foreskin fibroblasts, where it negatively regulates fibroblast migration by mediating HA-dependent recruitment of tyrosine phosphatases thereby reducing PDGFR $\beta$  activity (Li et al., 2006).

*TGF- $\beta$  receptor family.* CD44 forms a ternary complex with PDGFR $\beta$  and TGFBR1 in dermal fibroblasts and by affecting the stability of the receptors, negatively modulates their signalling (Porsch et al., 2014). In accordance with this, HA engagement of CD44 attenuates TGF- $\beta$  signalling in renal proximal tubular cells by promoting redistribution of TGF $\beta$ -RI into CEMs and thus increasing receptor turnover (Ito et al., 2004). In contrast, CD44 has been suggested to stabilize TGFBR1 at the plasma membrane of T cells (Flynn et al., 2013). CD44 interaction with TGFBR2 is required for TGF- $\beta$ -dependent EMT. TNF- $\alpha$ -induced HA-CD44-moesin complex interacts with TGFBR2 in clathrin-coated pits and leads to downstream SMAD2/3 phosphorylation and EMT in retinal pigment epithelial cells (Takahashi et al., 2010). Furthermore, galectin9-stimulated CD44/BMPRII complex formation is required for SMAD1/5/8 activation in the osteoblast differentiation process (Tanikawa et al., 2010). In chondrocytes, CD44 provides a binding site for SMAD1 in its cytoplasmic domain, and thus mediates BMP7-induced signalling via facilitating SMAD1 phosphorylation and nuclear translocation (Peterson et al., 2004).

*GPCRs, WNT and MMPs.* CD44 is also involved in the activation of GPCRs, regulating WNT signalling and acting as a signalling platform for MMPs. The crosstalk between CD44 and a chemokine receptor, CXCR4, was demonstrated by a study, where CD44-blocking antibodies as well as soluble CD44 were able to impair SDF1-dependent CD34<sup>+</sup> stem/progenitor cell homing to bone marrow (Avigdor et al., 2004). Furthermore, the SDF1-induced CD44 complex with CXCR4 in ECs was shown to be crucial for angiogenesis (Fuchs et al., 2013). CD44 acts as a positive regulator of WNT signalling by modulating LRP6 membrane localization and its signalling (Schmitt et al., 2015). CD44 provides a docking site for several MMPs. It binds to MMP-7 (Yu et al., 2002), associates with MT1-MMP at the leading edge of migrating cells to promote tumour cell migration (Mori et al., 2002), and facilitates tumour invasion and angiogenesis by docking MMP-9 to the cell membrane (Yu and Stamenkovic, 2000). Nevertheless, the MMP-9-CD44 axis is not essential for blood vessel invasion into the collagen matrix (Chun et al., 2004).

## 2.7 Soluble CD44

Besides the membrane-anchored form, soluble CD44 has been found to circulate in the serum and lymph of different species (Nagano and Saya, 2004). Soluble CD44 is mainly generated by releasing the ectodomain from the cell membrane via proteolytic cleavage (Okamoto et al., 1999). Shedding of soluble CD44 is regulated by several signalling pathways, including the activation of PKC, the activity of oncogenic RAC and RAS, and extracellular  $Ca^{2+}$  influx (Okamoto et al., 1999). Although only a small fraction of membrane CD44 is subjected to shedding (Hartmann et al., 2015), the proteolytic cleavage can be triggered by multiple external stimuli, such as serum, HGF, PDGF, TGF- $\beta$  or fragments of HA and chondroitin sulphate E (Cichy and Puré, 2004; Hartmann et al., 2015; Sugahara et al., 2008). The main proteases responsible for CD44 shedding are the members of MMPs, such as MT1-MMP, ADAM10 and ADAM17 (Anderegge et al., 2009; Kajita et al., 2001; Nagano and Saya, 2004). A recent study revealed that CD44 shedding is regulated by an inside-out signalling mechanism, where CD44 dimerization is the prerequisite for transmitting the cleavage-inducing signal from CD44-ICD to the ectodomain (Hartmann et al., 2015). It was shown that CD44 is associated with ADAM10 at the cell surface prior to stimulation, and that a considerable amount of CD44 exists at the cell membrane as dimers, which are stabilized by putative ectodomain interactions and cysteine bridges in their transmembrane/intracellular domains. However, effective cleavage of CD44 occurs only when cells are stimulated, because stimulation triggers specific modifications in CD44-ICD, which in turn induce conformational change in the CD44 ectodomain, enabling MMPs to access the CD44 cleavage site (Hartmann et al., 2015).

The ectodomain shedding is followed by intramembranous cleavage of CD44 by  $\gamma$ -secretase, whereupon the released CD44-ICD translocates to the nucleus and upregulates the transcription of its target genes, including *CD44* itself among others (Okamoto et al., 2002). More interestingly, a study by Miletti-González et al. (2012) revealed, that by binding to a novel CD44-ICD-specific promoter response element (CCTGCG), CD44-ICD can regulate transcription of multiple genes involved in cell survival, metabolism, inflammation and also tumour cell invasion. Consistently, increased serum levels of soluble CD44 seem to correlate with inflammatory diseases and tumour progression. For example, aberrant levels of soluble CD44 indicated tumour burden and metastasis in gastric and colon carcinoma (Guo et al., 1994), differentiate malignant cervical carcinoma from premalignant cases (Dasari et al., 2014) and could be associated with lymph node metastasis in breast cancer patients (Mayer et al., 2008). CD44 shedding is also associated with immune cell activity. While immunodeficient mice displayed reduced levels of soluble CD44, autoimmune diseases and tumours led to significantly increased expression of soluble CD44 (Kato et al., 1994). Cleavage of CD44 regulates cell–ECM interactions during cell migration and is thus thought to be critical for enhanced cellular motility. For example,

shedding of CD44 facilitated cell detachment from the ECM and promoted CD44-mediated migration of lung and pancreatic cancer cells (Kajita et al., 2001; Okamoto et al., 1999).

Soluble CD44 may act as a dominant negative regulator of the functions of membrane-bound CD44. By serving as a decoy receptor, soluble CD44 can prevent ligand binding, as was shown in metastatic mammary carcinoma and melanoma cells, where overexpression of soluble CD44 blocked HA binding to cell surface and resulted in the inhibition of tumour growth (Ahrens et al., 2001; Yu et al., 1997). Furthermore, soluble CD44 and its non-HA-binding mutant inhibit cell growth in logarithmically growing schwannoma cells, whereas in confluent, non-dividing cells these effects are reversed (Morrison et al., 2001). In line with this, it has been demonstrated that recombinant soluble CD44-HABD and its modified non-HA-binding form inhibit EC proliferation, *in ovo* angiogenesis, and tumour growth (Päll et al., 2004).

### 3 Vimentin and its functions in ECs

Vimentin, a 57 kDa intermediate filament (IF) protein, is broadly expressed during development and also in several mesenchyme-derived cells of the adult organism, such as fibroblasts and ECs (Evans, 1998). Vimentin is responsible for the mechanical stability of the cell. It provides cells with the cytoskeletal structural framework and maintains cytoplasm integrity via linking the cell nucleus to the plasma membrane (Goldman et al., 1996). The vimentin monomer consists of non-helical N-terminal and C-terminal tail domains and the central  $\alpha$ -helical rod domain between them (Figure 3) (Fuchs and Weber, 1994). Vimentin IF assembly starts with lateral association of  $\alpha$ -helical coiled-coil vimentin dimers into more stable tetrameric subunits, which gradually elongate into unit-length-filaments and give rise to mature IFs (Strelkov et al., 2003). Vimentin IFs are highly dynamic and motile structures that constantly change their configuration and shape, which is regulated by phosphorylation (Yoon et al., 1998). Vimentin phosphorylation has generally been shown to increase IF disassembly and release soluble vimentin subunits, whereas dephosphorylation favours vimentin IF stabilization (Eriksson et al., 2004).

Although vimentin is the only IF protein expressed in a variety of mesenchymal cell types and its protein sequence is highly conserved in different species, *Vim*<sup>-/-</sup> mice develop and reproduce normally (Colucci-Guyon et al., 1994). However, *Vim*-null mice display several phenotypic changes under certain stress and pathological conditions. *Vim*<sup>-/-</sup> mice display impaired wound healing due to delayed granulation tissue formation and decreased fibroblast mobility, whereas reduced fibroblast migration results from aberrant organisation of actin cytoskeleton and focal adhesion (FA) proteins (Eckes et al., 2000). Furthermore, vimentin depletion has an effect on vascular functions. Lack of vimentin resulted in abnormal lymphocyte extravasation due to impaired endothelial integrity

(Nieminen et al., 2006), reduced corneal and hypoxia-induced retinal neovascularization (Bargagna-Mohan et al., 2007; Lundkvist et al., 2004), and also reduced flow-induced vasodilation of arteries (Henrion et al., 1997; Terzi et al., 1997). These altered phenotypes imply that vimentin may have important functions in cell adhesion and migration (Ivaska et al., 2007). Depletion of vimentin in ECs resulted in decreased invasion of ECs into the collagen matrix, indicating its involvement in angiogenic sprouting (Kwak et al., 2012). It has been shown that a soluble pool of vimentin, generated by proangiogenic GF-induced calpain cleavage, facilitates MT1-MMP membrane translocation and ECM degradation, and results in successful endothelial tubulogenesis. Furthermore, vimentin regulates FA architecture and cell motility. In rat heart vessels and ECs, vimentin acts as a mechanosensitive scaffold for vasodilator stimulating phosphoprotein (VASP), which is essential for VASP localization to FAs and its phosphorylation (Lund et al., 2010). Additionally, vimentin is upregulated in activated ECs, where it modulates EC-ECM adhesion and endothelial invasion by regulating focal adhesion kinase (FAK) expression and activation (Dave et al., 2013).

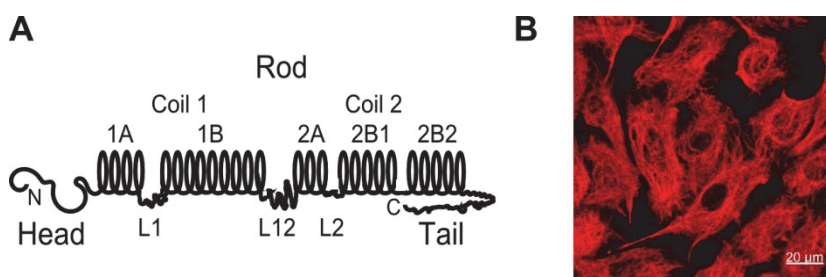


**Figure 3. Vimentin IFs.** (A) The schematic presentation of vimentin structure. Vimentin consists of N-terminal head, C-terminal tail and central rod domains. The rod domain contains alpha-helical coiled-coil subdomains (ellipses), connected with the linker regions (L1, L12 and L2). (B) An immunofluorescence image of anti-vimentin V9 antibody-stained HUVECs (T. Päll, unpublished, with permission of T. Päll)

Vimentin IFs regulate cell–matrix adhesions by associating with integrins, the core components of FAs. In most cases, vimentin is anchored to integrins via the cytoskeletal linker protein, plectin (Bhattacharya et al., 2009; Burgstaller et al., 2010). Disruption of the connection of vimentin or plectin with  $\beta 1$  integrin at FAs in fibroblasts results in reduced FA turnover and impaired directional migration (Gregor et al., 2014). Consistently, vimentin expression has been shown to correlate with enhanced FA dynamics (Mendez et al., 2010). Robust FAs and impaired motility were caused by attenuated FAK activity, which led the cells to try to compensate for the reduced tension by RhoA overactivation and upregulation of the activated (stretched) integrins (Gregor et al., 2014). Vimentin IFs associate also with collagen-binding  $\alpha 2\beta 1$  integrin in ECs, whereas

this interaction has been suggested to occur independently of plectin presence, and to be lost in confluent cells (Kreis et al., 2005). It has been demonstrated that vimentin mediates membrane traffic of  $\beta 1$  integrin (Ivaska et al., 2005) and EC adhesion molecules, ICAM-1 and VCAM-1, important mediators of lymphocyte homing, transmigration and vascular integrity (Nieminen et al., 2006). In addition, vimentin participates in endosomal trafficking by functioning as a reservoir for a synaptosome-associated tSNARE protein SNAP23 (Faigle et al., 2000), and by binding an adaptor protein complex, AP-3, which regulates sorting of late endosome/lysosome membrane proteins (Styers et al., 2004).

Besides its main subcellular location in the cytoplasm, vimentin can also be found at the cell surface. Cell-surface vimentin has been implicated in several functions, such as bacterial killing and ROS production on activated macrophages (Mor-Vaknin et al., 2003), activating latent TGF- $\beta$  on the EC surface (Nishida et al., 2009), rolling of circulating vascular cells across endothelium (Xu et al., 2004) and providing attachment sites for pathogens (Koudelka et al., 2009; Zou et al., 2008). More importantly, vimentin has been identified as a specific marker for tumour vasculature, whereas targeting of endothelial vimentin in *in vivo* mouse colorectal carcinoma tumour model resulted in effective inhibition of tumour growth and decreased microvessel density (van Beijnum et al., 2006). Furthermore, it has been suggested that cell surface vimentin could also serve as a common marker for metastatic cancers (Steinmetz et al., 2011).

## MATERIALS AND METHODS

The following methods were used in this thesis:

- DNA cloning (Publications I, II, Manuscript and Patent)
- Cell culture and DNA transfection (Publications I, II, Manuscript and Patent)
- siRNA transfection (Manuscript)
- Quantitative RT-PCR (Manuscript)
- GST-pulldown and co-immunoprecipitation (Publication II and Patent)
- ELISA (Publications I, II and Manuscript)
- Western blot analysis (Publications I, II, Manuscript and Patent)
- Immunofluorescence microscopy (Publications I, II and Manuscript)
- Endocytosis assay (Publications I and II)
- Electric cell-substrate impedance assay (Publication I and Manuscript)
- Apoptosis and cell viability assays (Manuscript)
- *In vivo* angiogenesis assay (Manuscript)
- Recombinant protein *in vivo* half-life studies (Publication I and Manuscript)
- Recombinant protein expression and purification (Publications I, II, Manuscript and Patent)
- PEGylation, Fc-fusion technology (Publication I and Manuscript)
- MALDI-TOF MS (Publications I and II)
- Statistical data analysis (Publications I, II, Manuscript and Patent)

## **AIMS OF THE STUDY**

The role of CD44 in lymphocyte homing and cancer progression has been extensively studied. At the same time, only scarce data demonstrate the involvement of CD44 in neovascularization and endothelial proliferation, and its many aspects are still unclear. The study by Päll et al. (2004) suggested that the recombinant soluble HA-binding domain of CD44 (CD44-HABD) and its non-HA-binding mutant CD44-3MUT could function as angiogenesis inhibitors. Nevertheless, CD44-3MUT displayed very short *in vivo* residence time, limiting its *in vivo* use. Together, these data provide the rationale for the present thesis.

The aims of this thesis were as follows:

1. Further elucidate the role of CD44 in angiogenesis and EC growth.
2. Improve the pharmacokinetic properties of CD44-3MUT by the use of two different half-life extension approaches (PEGylation and Fc-fusion).

## RESULTS AND DISCUSSION

The majority of the anti-angiogenic drugs in tumour therapy have been focused on targeting the VEGF signalling pathways. However, due to intrinsic and acquired resistance mechanisms, these therapeutics exhibit limited long-term benefits. Thus, there is a need for new anti-angiogenesis therapies that could be used in combination with anti-VEGF or as a second-line therapy. Moreover, to develop more effective therapies and new drugs, a better understanding of factors and mechanisms affecting EC proliferation and blood vessel formation is needed.

### 1 Circulation half-life of CD44-3MUT and its modified versions

We have shown that bacterially expressed recombinant unmodified CD44-3MUT is able to inhibit EC growth *in vitro* (Päll et al., 2004). However, our initial *in vivo* studies in mice showed that with only 0.04 h half-life this unmodified version of CD44-3MUT exhibits very short circulation residence time (Publication I). Such a short half-life can limit its *in vivo* efficacy. Consequently, we decided to improve the pharmacokinetic properties of CD44-3MUT. To this end, we used two different approaches: PEGylation and Fc-fusion technology. PEGylation is a well-known and FDA-approved strategy for extending the half-life of recombinant therapeutic proteins. Addition of the human IgG Fc region to a therapeutic protein in combination with the mammalian expression system, on the other hand, provides proteins with some beneficial antibody-like structural properties, facilitates their production process and maintains native post-translational modifications of proteins.

#### 1.1 PEGylation of CD44-3MUT (Publication I)

Having already established a large-scale purification protocol for bacterially expressed CD44-3MUT (Publication I), we first decided to PEGylate CD44-3MUT in order to improve its pharmacokinetic properties. We chose to PEGylate our protein with a 20 kDa methoxy-PEG-propionaldehyde, resulting in CD44-3MUT PEG-conjugate with the expected molecular weight of 31.6 kDa. 20 kDa aldehyde-functionalized PEG, which has been shown to preferentially couple to the N-terminal  $\alpha$ -amino group at pH 5-8 (Kinstler et al., 2002), was chosen for several reasons. First, in order to reduce the possibility that PEG would mask the CD44-3MUT surface and thereby interfere with its functional activity (Pasut and Veronese, 2012), we chose a PEG chain that would site-specifically react with the N-terminus of CD44-3MUT. Second, for minimizing the possibility of PEG-CD44-3MUT accumulating in the liver and causing the macromolecular syndrome, which is common for high molecular weight polymers, we used a PEG chain that was as small as possible. While 20 kDa PEG is relatively small, it would still most probably keep the PEG-CD44-3MUT

in the circulation and avoid rapid urinary excretion, as its molecular weight clearly exceeds the threshold of glomerular filtration, which has been demonstrated to be 30 kDa (Veronese and Pasut, 2005).

PEG-specific BaI<sub>2</sub> staining showed that PEGylation of CD44-3MUT resulted in the formation of predominantly mono-PEGylated form of CD44-3MUT. However, we were unable to purify the mono-PEG-CD44-3MUT to homogeneity and the presence of minor amounts of unmodified and di-PEGylated CD44-3MUT were still observed after all purification steps. Densitometric analysis showed that PEG-CD44-3MUT batches contained roughly 2/3 of mono-PEGylated, 1/10 of di-PEGylated and 1/4 of unmodified CD44-3MUT.

As we used methoxy-PEG-propionaldehyde for PEGylation, which should preferentially have attached to the N-terminus of CD44-3MUT in our reaction conditions, we analysed the PEG-attachment site using the MALDI-TOF MS fingerprinting of Glu-C protease-digestion peptides. The depletion of N-terminal peptides from the mass spectrum compared to non-PEGylated CD44-3MUT indicated that PEG indeed coupled to the N-terminal  $\alpha$ -amino group of PEGylated CD44-3MUT. No other peptides were missing or reduced in the mass spectrum, as could be expected because of the presence of the di-PEGylated form of CD44-3MUT in the analysed preparation. It is possible that the PEG dimer, instead of the PEG monomer, couples to the N-terminus of CD44-3MUT and this represents the di-PEGylated form of CD44-3MUT in the PEG-modified CD44-3MUT preparations. This suggestion was supported by the observation that besides the PEG monomer also the PEG dimer formed during PEGylation. Thus, it is most probable that instead of two PEG chains binding to different sites of CD44-3MUT, it is rather one PEG dimer that reacts with the N-terminus of CD44-3MUT.

PEGylated proteins commonly suffer from the complete or partial loss of their bioactivity due to the large hydrodynamic volume of PEG, which may limit the access to receptor/ligand binding sites (Kontermann, 2011; Pasut and Veronese, 2012). To exclude this possibility, we compared the *in vitro* activities of unmodified and PEGylated CD44-3MUT. The results of the cell proliferation assay confirmed the preserved bioactivity of PEGylated CD44-3MUT.

## **1.2 Half-life of PEGylated CD44-3MUT (Publication I)**

To determine the half-life of CD44-3MUT proteins we injected rats intravenously with untagged or PEGylated CD44-3MUT. After blood sampling, the half-life and other pharmacokinetic properties were calculated from the results of the ELISA assay. The calculated pharmacokinetic parameters (summarised in Table 1) showed that while untagged CD44-3MUT was eliminated from rat blood very rapidly, PEGylation of CD44-3MUT extended its blood residence time about 70-fold. In line with this, PEG-CD44-3MUT

displayed considerably enhanced systemic exposure (AUC) and diminished clearance (CL) when compared to its unmodified version. Both proteins displayed similar volume-of-distribution values (from 2% to 4% of total body weight), indicating that unmodified as well as PEGylated CD44-3MUT are confined to plasma water. In contrast, the initial pharmacokinetic studies in mice determined the volume of distribution for CD44-3MUT as 23% of total body weight, suggesting the distribution to extracellular water. Such discrepancy may have been caused by the different doses of injected proteins used in rats and mice (1 mg vs 50  $\mu$ g, respectively). It is plausible that the severalfold higher doses used in rats may have saturated the extracellular water compartment and therefore resulted in different volume-of-distribution values. When tissue protein binding is saturable, the dose of administered drug and the volume of distribution may be negatively correlated.

In conclusion, PEGylation improved the pharmacokinetic properties of CD44-3MUT while retaining its cell proliferation inhibitory activity. Nevertheless, the production process of PEG-CD44-3MUT was still quite complicated and resulted in a mixture of unmodified, di- and mono-PEGylated species of CD44-3MUT.

**Table 1:** Pharmacokinetic parameters of CD44-3MUT and its derivatives in rats, calculated from the ELISA data performed after intravenous administration of proteins.

Protein	C <sub>0</sub> , $\mu$ g/ml (95% CI)	AUC, $\mu$ g·h/ml	CL (ml/h)	V <sub>d</sub> (%TBW) <sup>1</sup>	T <sub>1/2</sub> , h (95% CI)
CD44-3MUT	315 (293- 337)	13.6	79.0	1.8	0.027 (0.023-0.032)
PEG-CD44-3MUT	142 (130-155)	803	1.2	3.9	1.84 (0.69-2.98)
CD44-3MUT-Fc	66 (53-87)	19.0	158	18	0.28 (0.13-0.40)

<sup>1</sup>, volume of distribution (V<sub>d</sub>) is expressed as % of total body weight (%TBW)

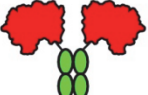
### 1.3 Plasma half-life of CD44-3MUT-Fc (Manuscript)

In order to simplify the manufacturing process of CD44-3MUT and produce a protein that is more akin to native CD44, we next sought to express the protein in a mammalian expression system. In addition, to improve pharmacokinetics, we decided to add human IgG Fc fragment to the C-terminus of CD44-3MUT. Producing CD44-3MUT-Fc in the mammalian expression system has several advantages (Figure 4). First, when compared to bacterially purified CD44-

3MUT, the mammalian expression of CD44-3MUT-Fc yields a roughly 8-fold increased amount of protein (unpublished data). Secondly, the production process of CD44-3MUT-Fc contains only two different stages instead of four as in the bacterial production of CD44-3MUT. Thirdly, the purity of CD44-3MUT-Fc is considerably higher, as it contains significantly less endotoxins than the bacterially expressed CD44-3MUT. Lastly, the production in a mammalian expression system provides CD44-3MUT-Fc with post-translational modifications similar to those of native CD44.

The pharmacokinetic parameters of CD44-3MUT-Fc in rats were calculated after intravenous administration of proteins and are shown in Table 1. The results show that the blood residence time of CD44-3MUT-Fc was increased more than 10-fold compared to untagged CD44-3MUT. However, it still remained nearly 7-fold shorter than the blood residency of PEGylated CD44-3MUT. Still, CD44-3MUT-Fc exhibited greater biodistribution when compared to untagged or PEGylated CD44-3MUT. The value of the volume of distribution – 18% of total body weight – indicates that CD44-3MUT-Fc is most probably distributed to extracellular water.

Due to considerably easier production, native structural properties and better biodistribution we decided to use the Fc-modified version of CD44-3MUT in our further functional studies.

	CD44-3MUT	PEG-CD44-3MUT	CD44-3MUT-Fc
schematic presentation			
MW	11.5 kDa	31.6 kDa	60 kDa (monomeric)
purification steps	4	6	2
yield	9-16 mg/L	< 9-16 mg/L	75-92 mg/L
endotoxins	22-93 EU/mg	NA	< 10 EU/mg
posttranslational modifications	unglycosylated	unglycosylated	glycosylated
protein form	monomer	monomer	dimer

**Figure 4. Comparison of CD44-3MUT and its derivatives.** CD44-3MUT (red globular domain) is produced in bacterial expression system. PEG-CD44-3MUT, a 20 kDa linear PEG (pale blue linear string) is added to the N-terminus of purified CD44-3MUT. CD44-3MUT-Fc, CD44-3MUT is provided with the human IgG-Fc region (green ellipses), genetically fused to its C-terminus. CD44-3MUT-Fc is produced in a mammalian expression system as a dimer

## **2 CD44 functions as an inhibitor of angiogenesis (Manuscript)**

### **2.1 CD44-3MUT-Fc inhibits *in vivo* neovascularization**

Previously it has been shown in our laboratory that bacterially expressed non-HA-binding CD44 (CD44-3MUT) reduces the angiogenic response in the chick chorioallantoic membrane and inhibits tumour xenograft growth in mice (Päll et al., 2004).

We asked whether the observed anti-angiogenic effects of bacterially expressed CD44-3MUT could be reproduced in a different model. For this, we performed *in vivo* angiogenesis assays in nude mice and used CD44-3MUT produced in a mammalian expression system as a therapeutic agent. To this end, we used a commercially available Matrigel plug assay (DIVAA), where angiogenesis was measured by blood vessel invasion into the tumour ECM-filled silicone tubes (angioreactors) (Guedez et al., 2003). In DIVAA, the angiogenic response is stimulated by FGF-2 and VEGF premixed into the matrix of angioreactors.

We treated nude mice carrying subcutaneously implanted angioreactors with human IgG1 Fc region-modified CD44-3MUT (CD44-3MUT-Fc). The results of the DIVAA showed that the intraperitoneal treatments with CD44-3MUT-Fc resulted in significantly reduced blood vessel ingrowth into angioreactors when compared to PBS- or rhIgG-Fc- treated control groups (Figure 5A). As PBS- and rhIgG-Fc-treated control groups displayed similar angiogenic response, it could be concluded that the anti-angiogenic effect of CD44-3MUT-Fc was not caused by the IgG Fc, but the CD44-3MUT portion of the protein.

The efficacy of CD44 non-HA-binding mutant in our studies demonstrates that the anti-angiogenic property of this molecule is independent of its HA-binding function. This suggests that a different mechanism than directly blocking HA binding to cells is responsible for the observed effects. Besides, the allosteric inhibitory effect of CD44-3MUT on CD44-HA interaction could be excluded, as Päll et al. (2004) had shown that CD44-3MUT had no effect on HMW HA-induced EC migration *in vitro*. Nevertheless, HA oligomers can induce angiogenesis and such angiogenesis can be blocked by EC-specific CD44 silencing (Lennon et al., 2014).

Together, by showing that systemic administration of mammalian CD44-3MUT-Fc is able to efficiently inhibit angiogenesis in a preclinical mouse model, this study validates Päll et al. (2004) results, which demonstrated anti-angiogenic activity of bacterially purified CD44-3MUT in an *in ovo* model. Furthermore, these results exclude the possibility that the anti-angiogenic effect of CD44-3MUT is solely the property of the bacterially expressed recombinant protein.

## 2.2 *Cd44*-null mice display enhanced angiogenic response

CD44 has been shown to be involved in tumour angiogenesis as an angiogenesis supporting molecule (Cao et al., 2006; Lennon et al., 2014), and thus, in this context, recombinant soluble CD44-3MUT appears to function as an antagonist to endogenous CD44.

To independently assess the pro-angiogenic role of CD44, we studied angiogenesis in *Cd44*<sup>-/-</sup> mice. We used the same *in vivo* angiogenesis assay as described in the Section 2.1 of this thesis to measure the angiogenesis induction in response to VEGF/FGF-2 stimulation. We found that the angiogenic response was significantly higher in *Cd44*-null mice than in wild-type mice (Figure 5A). It is important to note that our initial experiments were performed in *Cd44*<sup>-/-</sup> mice of mixed genetic backgrounds. Nevertheless, as shown by others, different genetic factors, besides CD44, may influence the angiogenic response in different inbred mouse strains (Rohan et al., 2000). Therefore, to reduce the possibility that confounding genetic factors cause the observed differences in angiogenesis induction, we used *Cd44*-null mice from homogenous inbred backgrounds for the next series of experiments. To this end, *Cd44*<sup>-/-</sup> mice were backcrossed six generations into the C57BL/6 background. The angiogenesis assay with the *Cd44*<sup>-/-</sup> mice of the C57BL/6 background corroborated our primary results, and showed that CD44<sup>-/-</sup> mice displayed significantly increased angiogenesis compared to their *Cd44*<sup>+/+</sup> or *Cd44*<sup>+/-</sup> littermates. Statistical analysis revealed that the induction of angiogenic response was associated with the *Cd44* genotype in VEGF/FGF-2-stimulated mice, but not in GF-unstimulated mice.

These results demonstrate that the absence of CD44 leads to elevated angiogenic response in mice, suggesting that CD44 functions as an angiogenesis inhibitory molecule. In the light of these findings, CD44-3MUT-Fc seems to mimic endogenous CD44 rather than antagonise its function. According to this model, systemic delivery of CD44-3MUT-Fc increased the dose of CD44 and enhanced the anti-angiogenic balance.

The differences between our study and previous studies showing CD44 as an angiogenesis promoting molecule may lie in the use of different models and different inducers of angiogenesis. Reduced blood vessel invasion into Matrigel plugs in *Cd44*<sup>-/-</sup> mice was observed in response to CD44-positive B16 melanoma cells (Cao et al., 2006), as well as in response to HA oligomers in mice with silenced endothelial CD44 expression (Lennon et al., 2014). In case of both of these models, CD44 was to some extent still present in the system and thus could function as a super inhibitor. This could also explain why wild-type bone marrow reconstitution in *Cd44*<sup>-/-</sup> mice did not restore the angiogenesis to normal levels (Cao et al., 2006). In contrast, we used a completely CD44-free system – *Cd44*-null mice and angiogenesis induction by VEGF and FGF-2.

Additionally, the duration of experiment to allow blood vessels to grow after induction can affect the results. It has been reported that CD44<sup>-/-</sup> ECs exhibit a lower growth rate in the early phase of proliferation, but increased secondary proliferation in dense cultures compared to wild-type ECs (Tsuneki and Madri, 2014). Therefore, while in Cao et al. (2006) study the blood vessels were allowed to invade the Matrigel plugs for 5 days, in our experiments, the ECs that had invaded the angioreactors were quantitated after 14 days. Still, *Cd44*<sup>-/-</sup> mice displayed inhibited tumour growth and vessel density in the melanoma and ovarian carcinoma xenograft models, where tumours were grown for two to nine weeks (Cao et al., 2006).

Given that soluble CD44-3MUT-Fc blocks *in vivo* angiogenesis and EC proliferation (see Sect. 2.1 and 3.1) and thereby mimics endogenous CD44, it is also possible that in Cao et al. (2006) study, CD44-deficient ECs were inhibited *in trans* by tumour cell expressed CD44. This hypothesis is also supported by our finding that the level of angiogenesis in *Cd44*-heterozygotes was similar to wild-type mice. This suggested that CD44 is not haploinsufficient and even reduced levels of CD44 are sufficient for the regulation of angiogenesis.

CD44 plays context specific roles in malignant transformation and metastasis, as well as in inflammatory reactions. The role of CD44 in tumourigenesis seems to be isoform-dependent, but it also depends on the stage and origin of the cancer (Gao et al., 1997; Kito et al., 2001; Kogerman et al., 1997; Lopez et al., 2005; Zeilstra et al., 2014). Regarding the context specific nature of CD44 in inflammatory reactions, blocking its functions by CD44-specific antibodies resulted in anti-inflammatory effects in experimental arthritis (Hutás et al., 2008), whereas aggravated inflammatory response was observed in *Cd44*-deficient mice (Nedvetzki et al., 2004). It has been demonstrated, that the loss of CD44 could be compensated by other molecules in early embryogenesis, but not at the later stages of development (Nedvetzki et al., 2004; Olaku et al., 2011). This suggests that the seemingly contradictory phenotypes in inflammatory responses of CD44-deficient mice versus CD44 targeting in wild-type mice could partly be explained by the molecular redundancy of CD44.

To conclude, our results together with Cao et al. (2006) and Lennon et al. (2014) studies fit into the context of and adds to the current paradigm about the context specific behaviour of CD44 in different pathophysiological processes. More specifically, we showed that CD44 can function as an endogeneous inhibitor of angiogenesis.

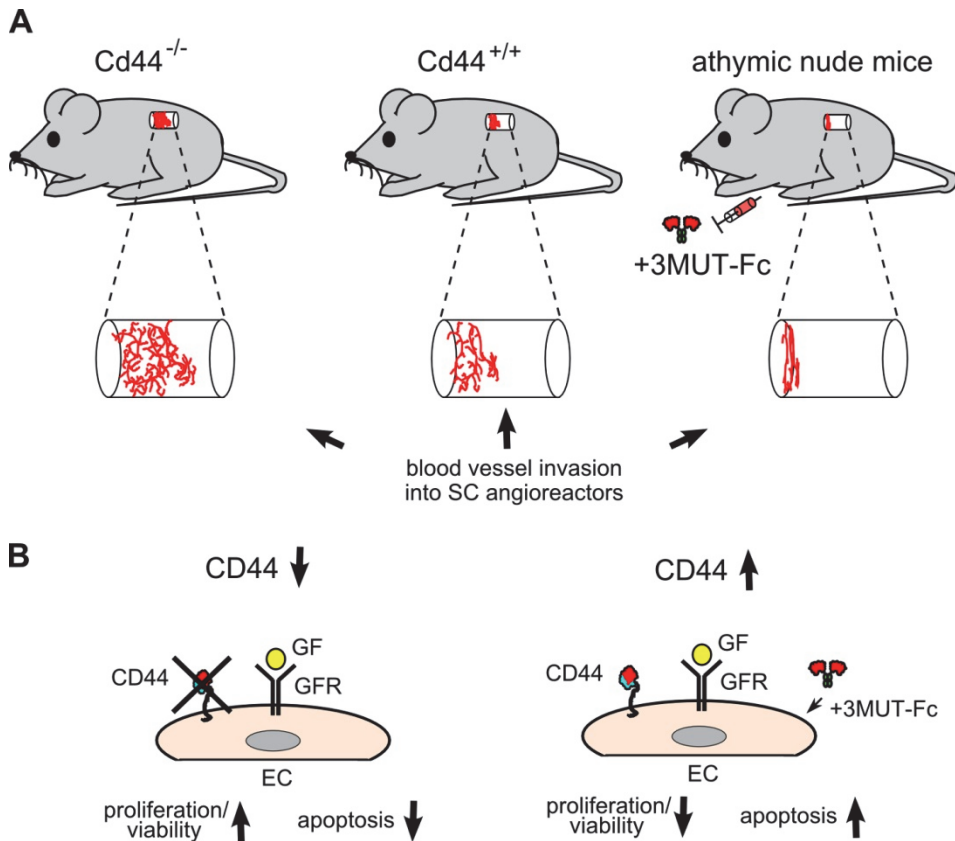


**Figure 5. CD44 is a negative regulator of angiogenesis.** (A) Blood vessel invasion into the subcutaneous (SC) angioreactors is enhanced in *Cd44*<sup>-/-</sup> mice and suppressed in CD44-3MUT-Fc (3MUT-Fc)-treated mice when compared to wild-type mice (*Cd44*<sup>+/+</sup>). (B) The reduction of CD44 level by siRNA transfection augments and the increase of CD44 dose by CD44-3MUT-Fc treatment inhibits endothelial cell (EC) growth. The effect of CD44 is independent of EC growth promoting effect of pro-angiogenic growth factors (GF; VEGF/bFGF/HGF). GFR, growth factor receptor (VEGFR2, FGFR1, MET)

### 3 CD44 as a negative regulator of EC proliferation

#### 3.1 CD44-3MUT restrains EC growth (Publication I, Manuscript)

Bacterially purified CD44-3MUT inhibits angiogenesis by inhibiting EC proliferation (Páll et al., 2004). Thus, we asked, whether the anti-angiogenic effect of CD44-3MUT-Fc might be similarly caused by its effects on ECs. To answer this question, we used a cell proliferation assay, which is based on real-time measurement of adherent cells using electrical cell-substrate impedance sensing (ECIS). Monitoring the growth of asynchronously growing mouse lung ECs (MLEC) treated with bacterially purified CD44-3MUT confirmed that

CD44-3MUT inhibits EC growth, as CD44-3MUT treatment resulted in reduced cell density, measured by the electrical resistance of the MLEC layer (Publication I). In the second series of experiments, we wanted to model the initial stages of angiogenesis induction by releasing the quiescent ECs from cell cycle block by angiogenic GF stimulation. Growth-arrested HUVECs were released from quiescence by stimulation with VEGF. As expected, the real-time monitoring of cell growth by ECIS revealed that VEGF stimulation resulted in HUVEC proliferation. At the same time, treatment of HUVECs with CD44-3MUT-Fc dose-dependently blocked VEGF-induced HUVEC proliferation (Manuscript; Figure 5B). The inhibitory effect of CD44-3MUT-Fc on EC growth was confirmed in cell viability assays, where we tested CD44-3MUT-Fc potency to inhibit cell proliferation stimulated by VEGF, FGF-2 or HGF. The results demonstrated that, while FGF-2 and VEGF proved to be strong inducers of cell proliferation, HGF induction, in contrast, showed only weak induction of proliferation. We found that the effect of CD44-3MUT-Fc on HUVEC growth was inversely related to the GF potency to induce cell growth. While CD44-3MUT-Fc caused relatively small inhibition of cell growth in HUVECs stimulated with strong inducers like VEGF and FGF-2, we observed much stronger inhibition of cell proliferation in HGF-stimulated cells. The same trend was also observed when the effect of CD44-3MUT-Fc was tested in HUVECs stimulated with the vascular quiescence factor GDF-2 (BMP-9). GDF-2 showed a strong anti-mitotic effect on HUVEC growth, and CD44-3MUT-Fc treatment further augmented this effect.

Further, we wanted to see, whether apoptosis is involved in the reduction of cell numbers in response to CD44-3MUT-Fc treatment. We found that the basal levels of apoptosis were expectedly in inverse correlation with the EC growth-inducing potency of the cytokine. The number of apoptotic cells was the lowest in FGF-2- and VEGF-stimulated cultures and the highest in GDF-2-stimulated cultures. Moreover, the effect of CD44-3MUT-Fc on apoptosis was found to be in correlation with its effects on cell proliferation. While VEGF- and FGF-2-induced ECs displayed a modest increase in apoptotic cell numbers in response to CD44-3MUT-Fc treatment, the increase was more noticeable in HGF-induced cells and GDF-2-induced ECs. Our results suggest that cells under stress are more sensitive to CD44-3MUT-Fc treatment, and therefore more prone to undergo apoptosis.

Together, our results indicate that CD44-3MUT affects angiogenesis primarily by inhibiting EC proliferation.

### **3.2 Knockdown of CD44 enhances EC proliferation and viability (Manuscript)**

CD44 is a coreceptor for receptor tyrosine kinases MET, VEGFR2, EGFR and ErbB2 (Meran et al., 2011; Tremmel et al., 2009; Yu et al., 2002). Accordingly,

its coreceptor function is involved in epithelial cell signaling, cancer, and angiogenesis. However, it is not clear, whether and how CD44 expression affects EC proliferation. Lung ECs derived from *Cd44*<sup>-/-</sup> mice displayed impaired *in vitro* ability of tube formation, but the proliferation and migration of those ECs remained unaltered (Cao et al., 2006). Another study showed a reduced initial proliferation rate of *Cd44*<sup>-/-</sup> mice-derived brain ECs compared to wild type-cells, whereas secondary proliferation in dense *Cd44*<sup>-/-</sup> EC cultures was increased (Tsuneki and Madri, 2014). This suggests that CD44 expression associates with reduced proliferation under certain conditions. We interrogated CD44 in ECs first by increasing CD44 dose by adding CD44-3MUT-Fc to the culture and, alternatively, by silencing its expression by siRNA transfection. We saw that treating ECs with soluble recombinant CD44-3MUT-Fc resulted in the inhibition of EC proliferation (see Sect. 3.1), which is in agreement with the findings of Tsuneki and Madri (2014) study.

Given that the *Cd44* gene deficiency resulted in augmented angiogenic response in our experiments and CD44-3MUT inhibited EC proliferation, we decided to study whether the knockdown of CD44 expression results in increased EC proliferation. We used CD44-siRNA transfected HUVECs in cell proliferation assays. CD44-silenced HUVECs were initially growth-arrested by serum starvation, and thereafter released from quiescence by stimulation with serum or different concentrations of VEGF, FGF-2, or GDF-2. The real-time tracking of cell culture impedance revealed that silencing of CD44 expression by transient siRNA transfection increased proliferation in ECs stimulated either by serum, VEGF, or FGF-2. At the end of the experiment, the increased cell numbers of siCD44-transfected ECs were confirmed by assessment of viable cells and also by modelling of the barrier formation. Consistent with the higher cell density, CD44-silenced ECs formed more robust barrier. Although the ECIS measurements showed that CD44 silencing could not rescue GDF-2-induced ECs, the cell viability assay showed more viable cells also in this group. Together, these results suggest that CD44 silencing results in augmented cell proliferation in response to different GFs (Figure 5B), further suggesting that CD44 is not involved with any specific GF pathway.

Consistently with our results, *Cd44*<sup>-/-</sup> mice displayed increased neointima formation and vSMC proliferation in response to arterial injury (Kothapalli et al., 2007). This suggests that CD44 expression regulates proliferation also in other cell types than ECs. In this case, HMW-HA binding to CD44 was shown to induce the growth suppression of vSMCs and other mesenchymal cell types (Kothapalli et al., 2007). As the previous studies demonstrated that CD44 is upregulated in tumour blood vessels as well as in FGF-2- and VEGF-stimulated ECs (Griffioen et al., 1997), it is plausible that CD44 controls EC proliferation via negative feedback signalling. Interestingly, we found that CD44-3MUT binding to ECs was increased in response to VEGF stimulation (Publication II). Taking into account that CD44 dimerizes partly via its ectodomain interactions

(Hartmann et al., 2015), and HMW-HA has been shown to increase CD44 clustering (Yang et al., 2012), it could be speculated that CD44-3MUT might enhance the EC growth-suppressive properties of endogenous CD44 by inducing CD44 clustering similarly to HMW-HA.

In summary, as silencing of CD44 in ECs resulted in elevated proliferation, *in vitro* data support the results of the *in vivo* angiogenesis assay, and indicate that enhanced angiogenic response in *Cd44*<sup>-/-</sup> mice might result from increased growth rates and survival of CD44-deficient ECs.

### **3.3 The molecular mechanism behind CD44 effects (Manuscript)**

We tested one of the possible molecular mechanisms behind the CD44-mediated control of cell proliferation on ECs. Our initial hypothesis was based on the fact that CD44 is extensively endocytosed and it is a co-receptor for several angiogenic GF receptors, such as MET (Orian-Rousseau et al., 2002) and VEGFR2 (Tremmel et al., 2009). We proposed that endocytosis of CD44 would decrease the level of GF receptors on the EC surface and thereby render ECs unresponsive to GF stimulation. To test this hypothesis, we used serum-starved HUVECs, treated them with CD44-3MUT-Fc, and then induced these cells with different CD44-related angiogenic GFs. However, we found no changes in activation or the level of GF receptors in response to CD44-3MUT-Fc. In addition, CD44-silenced HUVECs displayed no changes in basal VEGFR2 or FGFR1 levels. These results again indicate that CD44-3MUT-Fc does not target the signalling of these specific GF receptors directly, but rather causes EC growth inhibition downstream of GF receptor activation.

Another possible mechanism of CD44-mediated growth inhibition might be related to the employment of CD44 in TGF- $\beta$  signalling (Bourguignon et al., 2002; Peterson et al., 2004; Tanikawa et al., 2010). Our own results showed increased cell cycle block and apoptosis in response to CD44-3MUT-Fc treatment in GDF-2 induced HUVECs (see Sect. 3.1). This led us to the hypothesis that CD44 may exert its anti-angiogenic functions by enhancing GDF-2 signalling. Therefore, we tested whether GDF-2-mediated SMAD1/5 activation is affected by silencing of CD44 expression. As expected, we found that HUVEC stimulation with GDF-2 led to phosphorylation and nuclear localisation of SMAD1/5, and resulted in the activation of BMP-responsive element reporter and transcription of selected SMAD1/5 target genes. However, silencing of CD44 expression or CD44-3MUT-Fc treatment showed no effect on those GDF-2-mediated responses in HUVECs. In line with this, no changes in the expression levels of SMAD1/5 target genes in the lungs of CD44-3MUT-Fc-treated mice were observed. These results show that GDF-2 mediated SMAD1/5 signalling is not affected by CD44 or CD44-3MUT-Fc.

A study by Morrison et al. (2001) shows that CD44 is required for recruiting the tumour suppressor NF2 to the plasma membrane to mediate contact inhibition.

Based on this, it is possible that silencing of CD44 abolishes NF2 function and leads to defective contact inhibition and enhanced proliferation. However, embryonic fibroblasts derived from *Cd44*<sup>-/-</sup> mice displayed functional contact inhibition, yet faster growth rates compared to their wild-type counterparts (Lallemand et al., 2003). Moreover, we observed steadily increased growth rates, barrier formation, and unchanged cell adhesion in CD44-silenced ECs after they were released from quiescence by GF stimulation (see Sect. 3.2). Thus, it seems that mechanisms other than impaired contact inhibition are responsible for enhanced cell proliferation.

Taken together, our results suggest that the exertion of the effects of CD44 is independent of specific angiogenic GF signalling.

#### **4 Vimentin is involved in the EC growth-inhibiting function of CD44 (Publications I-II, Manuscript, Patent, unpublished data)**

We identified a CD44-binding protein on the EC surface. Surprisingly, we found that CD44-3MUT binds to the intermediate filament protein vimentin (Publication II and Patent). Vimentin is abundantly expressed in ECs and is also exposed to the cell surface. The pull-down assays with vimentin deletion mutants showed that vimentin N-terminal head domain was responsible for CD44-3MUT binding (Publication II and Patent). In order to locate the CD44 binding site in vimentin more precisely, we used synthetic peptides covering the vimentin N-terminal domain and CD44-3MUT in the MicroScale Thermoforesis binding assay (performed by NanoTemper Technologies). The analysis showed that CD44-3MUT binds to vimentin peptides that contain amino acids 14-37 (Kd  $461 \pm 45.8$  nM), 38-60 (Kd  $8.5 \pm 0.3$   $\mu$ M) and 50-72 (Kd  $9.4 \pm 0.9$   $\mu$ M), but does not bind to peptides containing amino acids 2-25, 62-85 and 75-97 (unpublished results). These data suggest that amino acids 26-62 in the vimentin head domain are sufficient for CD44 binding. The Surface Plasmon Resonance analysis revealed that there were two CD44-3MUT binding sites in vimentin (Publication II). The Kd values for high-affinity and low-affinity binding sites were 74 nM and 15  $\mu$ M, respectively. The results of the MicroScale Thermoforesis assay support the two-site ligand model of CD44-3MUT and suggest that aa residues 26-37 in the vimentin N-terminus mediate high-affinity binding and aa 38-62 mediate low-affinity binding.

Endogenous CD44 HABD contains five N-linked glycosylation sites (English et al., 1998). CD44-3MUT, on the other hand, is a bacterially purified recombinant protein without any post-translational modifications. Thus, we asked whether EC-endogenous CD44 and vimentin could also interact. By using co-immunoprecipitation with an anti-CD44 antibody, we demonstrated that full-length endogenous CD44 is able to form a complex with minor amounts of vimentin. However, the anti-vimentin antibody was not able to co-precipitate full-length CD44. This discrepancy may result from very high vimentin

expression in HUVECs, of which only a small population interacts with CD44. Vimentin is present in cells in different forms, most abundantly as long IFs, but also as short squiggles and particles (Prahlad et al., 1998). Filaments are concentrated around the nucleus, in the trailing edge and in the cell tail. Squiggles are located at the ends of filaments and non-filamentous particles are located in lamellipodia. It is plausible that CD44 interacts with the minor, non-filamentous vimentin fraction. Thus, the co-precipitated CD44 may just remain below the detection limit. Nevertheless, we confirmed the full-length CD44 and vimentin association by co-immunoprecipitation of over-expressed proteins. Together, these results show that vimentin can also form a complex with post-translationally modified CD44, indicating, therefore, that this interaction may have physiologically relevant functions in ECs.

The possible physiological importance of CD44–vimentin interaction is also supported by the studies where CD44 and vimentin were both found to form a complex with a (Na<sup>+</sup> K<sup>+</sup>)/H<sup>+</sup> exchanger at the membrane of breast cancer cells (Kagami et al., 2008). CD44 and vimentin colocalize during *E.coli*-induced neutrophil transmigration across brain microvascular ECs (Che et al., 2011), and direct MT1-MMP to the front of migrating cells to allow the ECM degradation (Kwak et al., 2012; Mori et al., 2002). CD44 and vimentin are also well-known EMT markers in cancer cells, whereas both proteins mutually regulate each other's expression in breast and colon cancer cells (Brown et al., 2011; Lehtinen et al., 2013). More importantly, CD44 and vimentin are upregulated on the activated tumour endothelium (Griffioen et al., 1997; van Beijnum et al., 2006), and disruption of the functions of either CD44 or vimentin results in compromised vascular integrity (Flynn et al., 2013; Nieminen et al., 2006).

In order to study the CD44–vimentin interaction, we first carried out the CD44-3MUT internalization assay. CD44 and vimentin were shown to associate with the vesicles of the clathrin-independent endocytic pathway (Howes et al., 2010). Our results demonstrated that CD44-3MUT was rapidly internalized by MLECs isolated from wild-type mice (Publication I and II), but not by MLECs derived from vimentin-deficient mice (Publication II). To test whether the EC growth-inhibiting function of CD44-3MUT might be dependent on vimentin, we used MLECs isolated from vimentin-deficient mice. The results showed that CD44-3MUT treatment inhibited the growth of wild-type MLECs, whereas this effect was not observed in vimentin-deficient MLECs. These data indicate that CD44-3MUT inhibits EC proliferation via a vimentin-dependent mechanism (Publication I). The ECIS cell growth assay showed that silencing of CD44 enhanced EC survival (see Sect 3.2). In case of CD44–vimentin signalling, we expected a similar effect in vimentin-silenced ECs. Indeed, the initial growth rate and barrier formation of vimentin-silenced ECs was increased after seeding and before serum starvation, and was comparable to CD44-silenced HUVECs (Manuscript). Nevertheless, after release from quiescence the impedance measured at high frequencies (e.g. 64000 Hz), which indicates the cell density

on the measuring electrode, was similar to controls. The similar-to-controls cell density of vimentin-silenced cells was confirmed by the quantitation of viable cells at the end of the experiment (Manuscript). Thus, it is possible that in vimentin-silenced ECs, the re-entry into the cell cycle after serum deprivation is not as efficient as in CD44-silenced cells. Low frequency impedance measurements of vimentin-silenced ECs ( $\leq 1000$  Hz; reporting mostly cell-cell and cell-matrix adhesions) suggested increased cell adhesion in these cells (Manuscript). Consistently, vimentin expression was shown to correlate with enhanced FA dynamics (Gregor et al., 2014; Mendez et al., 2010). Furthermore, vimentin-deficient fibroblasts display aberrant actin stress fibres lacking geodome structures (Eckes et al., 1998), along with more robust FAs and impaired motility (Eckes et al., 1998; Gregor et al., 2014). It was suggested that the enlarged FAs and FA reduced turnover in cells with disrupted vimentin IFs are caused by diminished cytoskeletal tension. Decreased cytoskeletal tension, in turn, leads to impaired integrin-mediated mechanotransduction. The absence of vimentin IFs at FAs resulted in attenuated FAK and ERK1/2 activity and RhoA overactivation. Via a compensatory positive feedback loop these alterations consequently result in the upregulation of activated, high-affinity, but functionally inefficient integrins (Gregor et al., 2014). Interestingly, the disruption of actin cytoskeleton was shown to restrict re-entry into the G1-phase from quiescence (G0), but not progression to the G1-phase from mitosis in cycling cells (Margadant et al., 2013). This observation may provide a plausible explanation for the differences in vimentin-silenced EC growth kinetics before and after cell cycle arrest.

In summary, our results indicate that vimentin might be involved in the EC growth-restraining properties of CD44. It remains to be elucidated, what the molecular mechanism behind this is, and whether vimentin is also required for CD44-mediated anti-angiogenic signalling *in vivo*.

## CONCLUSIONS

1. The pharmacokinetic properties of CD44-3MUT were improved by using two different approaches:
  - PEGylation increased the circulation half-life of CD44-3MUT.
  - Attachment of the human IgG Fc fragment to the C-terminus of CD44-3MUT resulted in increased half-life and improved biodistribution of the protein conjugate
2. CD44 is an endogenous inhibitor of angiogenesis.
  - *Cd44*<sup>-/-</sup> mice display enhanced angiogenesis.
  - Systemic administration of CD44-3MUT-Fc inhibits angiogenesis in mice.
3. CD44 controls EC proliferation.
  - CD44-silenced ECs display increased proliferation and survival.
  - CD44-3MUT-Fc inhibits EC growth and viability.
  - The EC growth inhibitory effects of CD44 are independent of specific pro-angiogenic GF signalling pathways.
4. Vimentin binds to CD44 via its N-terminal amino acids 26 to 62 and is involved in the growth inhibitory effect of CD44 in ECs.

## REFERENCES

- Abuchowski A, van Es T, Palczuk NC, Davis FF. 1977. Alteration of immunological properties of bovine serum albumin by covalent attachment of polyethylene glycol. *J Biol Chem.* 252:3578-81.
- Adams RH, Eichmann A. 2010. Axon guidance molecules in vascular patterning. *Cold Spring Harb Perspect Biol.* 2:a001875.
- Ahrens T, Sleeman JP, Schempp CM, Howells N, Hofmann M, Ponta H, Herrlich P, Simon JC. 2001. Soluble CD44 inhibits melanoma tumor growth by blocking cell surface CD44 binding to hyaluronic acid. *Oncogene.* 20:3399-408.
- Al-Hajj M, Wicha MS, Benito-Hernandez A, Morrison SJ, Clarke MF. 2003. Prospective identification of tumorigenic breast cancer cells. *Proc Natl Acad Sci U S A.* 100:3983-8.
- Andereg U, Eichenberg T, Parthaune T, Haiduk C, Saalbach A, Milkova L, Ludwig A, Grosche J, Averbeck M, Gebhardt C, Voelcker V, Sleeman JP, Simon JC. 2009. ADAM10 is the constitutive functional sheddase of CD44 in human melanoma cells. *J Invest Dermatol.* 129:1471-82.
- Andrae J, Gallini R, Betsholtz C. 2008. Role of platelet-derived growth factors in physiology and medicine. *Genes Dev.* 22:1276-312.
- Arany Z, Foo S, Ma Y, Ruas JL, Bommi-Reddy A, Girnun G, Cooper M, Laznik D, Chinsomboon J, Rangwala SM, Baek KH, Rosenzweig A, Spiegelman BM. 2008. HIF-independent regulation of VEGF and angiogenesis by the transcriptional coactivator PGC-1alpha. *Nature.* 451:1008-12.
- Aruffo A, Stamenkovic I, Melnick M, Underhill CB, Seed B. 1990. CD44 is the principal cell surface receptor for hyaluronate. *Cell.* 61:1303-13.
- Augustin HG, Koh GY, Thurston G, Alitalo K. 2009. Control of vascular morphogenesis and homeostasis through the angiopoietin-Tie system. *Nat Rev Mol Cell Biol.* 10:165-77.
- Avigdor A, Goichberg P, Shivtiel S, Dar A, Peled A, Samira S, Kollet O, Hershkovich R, Alon R, Hardan I, Ben-Hur H, Naor D, Nagler A, Lapidot T. 2004. CD44 and hyaluronic acid cooperate with SDF-1 in the trafficking of human CD34+ stem/progenitor cells to bone marrow. *Blood.* 103:2981-9.
- Bai Y, Liu Y, Wang H, Xu Y, Stamenkovic I, Yu Q. 2007. Inhibition of the hyaluronan-CD44 interaction by merlin contributes to the tumor-suppressor activity of merlin. *Oncogene.* 26:836-50.
- Bailon P, Palleroni A, Schaffer CA, Spence CL, Fung WJ, Porter JE, Ehrlich GK, Pan W, Xu ZX, Modi MW, Farid A, Berthold W, Graves M. 2001. Rational design of a potent, long-lasting form of interferon: a 40 kDa branched polyethylene glycol-conjugated interferon alpha-2a for the treatment of hepatitis C. *Bioconjug Chem.* 12:195-202.
- Bajorath J, Greenfield B, Munro SB, Day AJ, Aruffo A. 1998. Identification of CD44 residues important for hyaluronan binding and delineation of the binding site. *J Biol Chem.* 273:338-43.

- Banerji S, Day AJ, Kahmann JD, Jackson DG. 1998. Characterization of a functional hyaluronan-binding domain from the human CD44 molecule expressed in *Escherichia coli*. *Protein Expr Purif.* 14:371-81.
- Banerji S, Wright AJ, Noble M, Mahoney DJ, Campbell ID, Day AJ, Jackson DG. 2007. Structures of the Cd44-hyaluronan complex provide insight into a fundamental carbohydrate-protein interaction. *Nat Struct Mol Biol.* 14:234-9.
- Bargagna-Mohan P, Hamza A, Kim Y, Khuan Abby Ho Y, Mor-Vaknin N, Wendschlag N, Liu J, Evans RM, Markovitz DM, Zhan C, Kim KB, Mohan R. 2007. The tumor inhibitor and antiangiogenic agent withaferin A targets the intermediate filament protein vimentin. *Chem Biol.* 14:623-34.
- Beets K, Huylebroeck D, Moya IM, Umans L, Zwijsen A. 2013. Robustness in angiogenesis: notch and BMP shaping waves. *Trends Genet.* 29:140-9.
- Benedito R, Roca C, Sörensen I, Adams S, Gossler A, Fruttiger M, Adams RH. 2009. The notch ligands Dll4 and Jagged1 have opposing effects on angiogenesis. *Cell.* 137:1124-35.
- Bennett KL, Jackson DG, Simon JC, Tanczos E, Peach R, Modrell B, Stamenkovic I, Plowman G, Aruffo A. 1995. CD44 isoforms containing exon V3 are responsible for the presentation of heparin-binding growth factor. *J Cell Biol.* 128:687-98.
- Bentley K, Gerhardt H, Bates PA. 2008. Agent-based simulation of notch-mediated tip cell selection in angiogenic sprout initialisation. *J Theor Biol.* 250:25-36.
- Bergers G, Hanahan D. 2008. Modes of resistance to anti-angiogenic therapy. *Nat Rev Cancer.* 8:592-603.
- Bergers G, Song S, Meyer-Morse N, Bergsland E, Hanahan D. 2003. Benefits of targeting both pericytes and endothelial cells in the tumor vasculature with kinase inhibitors. *J Clin Invest.* 111:1287-95.
- Bhattacharya R, Gonzalez AM, Debiase PJ, Trejo HE, Goldman RD, Flitney FW, Jones JCR. 2009. Recruitment of vimentin to the cell surface by beta3 integrin and plectin mediates adhesion strength. *J Cell Sci.* 122:1390-400.
- Bjarnegård M, Enge M, Norlin J, Gustafsdottir S, Fredriksson S, Abramsson A, Takemoto M, Gustafsson E, Fässler R, Betsholtz C. 2004. Endothelium-specific ablation of PDGFB leads to pericyte loss and glomerular, cardiac and placental abnormalities. *Development.* 131:1847-57.
- Blanco R, Gerhardt H. 2013. VEGF and Notch in tip and stalk cell selection. *Cold Spring Harb Perspect Med.* 3:a006569.
- Blum Y, Belting H, Ellertsdottir E, Herwig L, Lüders F, Affolter M. 2008. Complex cell rearrangements during intersegmental vessel sprouting and vessel fusion in the zebrafish embryo. *Dev Biol.* 316:312-22.
- Boas SEM, Merks RMH. 2014. Synergy of cell-cell repulsion and vacuolation in a computational model of lumen formation. *J R Soc Interface.* 11:20131049.

- Bourguignon LYW, Singleton PA, Zhu H, Zhou B. 2002. Hyaluronan promotes signaling interaction between CD44 and the transforming growth factor beta receptor I in metastatic breast tumor cells. *J Biol Chem.* 277:39703-12.
- Bourguignon LYW, Spevak CC, Wong G, Xia W, Gilad E. 2009. Hyaluronan-CD44 interaction with protein kinase C(epsilon) promotes oncogenic signaling by the stem cell marker Nanog and the Production of microRNA-21, leading to down-regulation of the tumor suppressor protein PDCD4, anti-apoptosis, and chemotherapy resistance in breast tumor cells. *J Biol Chem.* 284:26533-46.
- Brown RL, Reinke LM, Damerow MS, Perez D, Chodosh LA, Yang J, Cheng C. 2011. CD44 splice isoform switching in human and mouse epithelium is essential for epithelial-mesenchymal transition and breast cancer progression. *J Clin Invest.* 121:1064-74.
- Burgstaller G, Gregor M, Winter L, Wiche G. 2010. Keeping the vimentin network under control: cell-matrix adhesion-associated plectin 1f affects cell shape and polarity of fibroblasts. *Mol Biol Cell.* 21:3362-75.
- Bussolino F, Di Renzo MF, Ziche M, Bocchietto E, Olivero M, Naldini L, Gaudino G, Tamagnone L, Coffler A, Comoglio PM. 1992. Hepatocyte growth factor is a potent angiogenic factor which stimulates endothelial cell motility and growth. *J Cell Biol.* 119:629-41.
- Bánkfalvi A, Terpe HJ, Breukelmann D, Bier B, Rempe D, Pschadka G, Krech R, Lellè RJ, Boecker W. 1999. Immunophenotypic and prognostic analysis of E-cadherin and beta-catenin expression during breast carcinogenesis and tumour progression: a comparative study with CD44. *Histopathology.* 34:25-34.
- Cao G, Savani RC, Fehrenbach M, Lyons C, Zhang L, Coukos G, Delisser HM. 2006. Involvement of endothelial CD44 during in vivo angiogenesis. *Am J Pathol.* 169:325-36.
- Carmeliet P. 2003. Angiogenesis in health and disease. *Nat Med.* 9:653-60.
- Carmeliet P, Jain RK. 2011. Molecular mechanisms and clinical applications of angiogenesis. *Nature.* 473:298-307.
- Carmeliet P, Tessier-Lavigne M. 2005. Common mechanisms of nerve and blood vessel wiring. *Nature.* 436:193-200.
- Carvalho RLC, Itoh F, Goumans M, Lebrin F, Kato M, Takahashi S, Ema M, Itoh S, van Rooijen M, Bertolino P, Ten Dijke P, Mummery CL. 2007. Compensatory signalling induced in the yolk sac vasculature by deletion of TGFbeta receptors in mice. *J Cell Sci.* 120:4269-77.
- Casanovas O, Hicklin DJ, Bergers G, Hanahan D. 2005. Drug resistance by evasion of antiangiogenic targeting of VEGF signaling in late-stage pancreatic islet tumors. *Cancer Cell.* 8:299-309.
- Chappell JC, Taylor SM, Ferrara N, Bautch VL. 2009. Local guidance of emerging vessel sprouts requires soluble Flt-1. *Dev Cell.* 17:377-86.
- Che X, Chi F, Wang L, Jong TD, Wu C, Wang X, Huang S. 2011. Involvement of IbeA in meningitic Escherichia coli K1-induced polymorphonuclear

- leukocyte transmigration across brain endothelial cells. *Brain Pathol.* 21:389-404.
- Chun T, Sabeh F, Ota I, Murphy H, McDonagh KT, Holmbeck K, Birkedal-Hansen H, Allen ED, Weiss SJ. 2004. MT1-MMP-dependent neovessel formation within the confines of the three-dimensional extracellular matrix. *J Cell Biol.* 167:757-67.
- Cichy J, Puré E. 2004. Cytokines regulate the affinity of soluble CD44 for hyaluronan. *FEBS Lett.* 556:69-74.
- Collins AT, Berry PA, Hyde C, Stower MJ, Maitland NJ. 2005. Prospective identification of tumorigenic prostate cancer stem cells. *Cancer Res.* 65:10946-51.
- Colucci-Guyon E, Portier MM, Dunia I, Paulin D, Pournin S, Babinet C. 1994. Mice lacking vimentin develop and reproduce without an obvious phenotype. *Cell.* 79:679-94.
- Crawford Y, Kasman I, Yu L, Zhong C, Wu X, Modrusan Z, Kaminker J, Ferrara N. 2009. PDGF-C mediates the angiogenic and tumorigenic properties of fibroblasts associated with tumors refractory to anti-VEGF treatment. *Cancer Cell.* 15:21-34.
- Cuff CA, Kothapalli D, Azonobi I, Chun S, Zhang Y, Belkin R, Yeh C, Secreto A, Assoian RK, Rader DJ, Puré E. 2001. The adhesion receptor CD44 promotes atherosclerosis by mediating inflammatory cell recruitment and vascular cell activation. *J Clin Invest.* 108:1031-40.
- Culty M, Nguyen HA, Underhill CB. 1992. The hyaluronan receptor (CD44) participates in the uptake and degradation of hyaluronan. *J Cell Biol.* 116:1055-62.
- Cunha SI, Pardali E, Thorikay M, Anderberg C, Hawinkels L, Goumans M, Seehra J, Heldin C, ten Dijke P, Pietras K. 2010. Genetic and pharmacological targeting of activin receptor-like kinase 1 impairs tumor growth and angiogenesis. *J Exp Med.* 207:85-100.
- Dalerba P, Dylla SJ, Park I, Liu R, Wang X, Cho RW, Hoey T, Gurney A, Huang EH, Simeone DM, Shelton AA, Parmiani G, Castelli C, Clarke MF. 2007. Phenotypic characterization of human colorectal cancer stem cells. *Proc Natl Acad Sci U S A.* 104:10158-63.
- Dasari S, Rajendra W, Valluru L. 2014. Evaluation of soluble CD44 protein marker to distinguish the premalignant and malignant carcinoma cases in cervical cancer patients. *Med Oncol.* 31:139.
- Dave JM, Kang H, Abbey CA, Maxwell SA, Bayless KJ. 2013. Proteomic profiling of endothelial invasion revealed receptor for activated C kinase 1 (RACK1) complexed with vimentin to regulate focal adhesion kinase (FAK). *J Biol Chem.* 288:30720-33.
- David L, Mallet C, Keramidas M, Lamandé N, Gasc J, Dupuis-Girod S, Plauchu H, Feige J, Bailly S. 2008. Bone morphogenetic protein-9 is a circulating vascular quiescence factor. *Circ Res.* 102:914-22.

- David L, Mallet C, Mazerbourg S, Feige J, Bailly S. 2007. Identification of BMP9 and BMP10 as functional activators of the orphan activin receptor-like kinase 1 (ALK1) in endothelial cells. *Blood*. 109:1953-61.
- De Palma M, Venneri MA, Galli R, Sergi L, Politi LS, Sampaolesi M, Naldini L. 2005. Tie2 identifies a hematopoietic lineage of proangiogenic monocytes required for tumor vessel formation and a mesenchymal population of pericyte progenitors. *Cancer Cell*. 8:211-26.
- De Smet F, Segura I, De Bock K, Hohensinner PJ, Carmeliet P. 2009. Mechanisms of vessel branching: filopodia on endothelial tip cells lead the way. *Arterioscler Thromb Vasc Biol*. 29:639-49.
- DeGrendele HC, Estess P, Picker LJ, Siegelman MH. 1996. CD44 and its ligand hyaluronate mediate rolling under physiologic flow: a novel lymphocyte-endothelial cell primary adhesion pathway. *J Exp Med*. 183:1119-30.
- Dejana E, Tournier-Lasserre E, Weinstein BM. 2009. The control of vascular integrity by endothelial cell junctions: molecular basis and pathological implications. *Dev Cell*. 16:209-21.
- Deryugina EI, Quigley JP. 2010. Pleiotropic roles of matrix metalloproteinases in tumor angiogenesis: contrasting, overlapping and compensatory functions. *Biochim Biophys Acta*. 1803:103-20.
- Ding S, Merkulova-Rainon T, Han ZC, Tobelem G. 2003. HGF receptor up-regulation contributes to the angiogenic phenotype of human endothelial cells and promotes angiogenesis in vitro. *Blood*. 101:4816-22.
- Domenga V, Fardoux P, Lacombe P, Monet M, Maciazek J, Krebs LT, Klonjowski B, Berrou E, Mericskay M, Li Z, Tournier-Lasserre E, Gridley T, Joutel A. 2004. Notch3 is required for arterial identity and maturation of vascular smooth muscle cells. *Genes Dev*. 18:2730-5.
- Dou G, Wang Y, Hu X, Hou L, Wang C, Xu J, Wang Y, Liang Y, Yao L, Yang A, Han H. 2008. RBP-J, the transcription factor downstream of Notch receptors, is essential for the maintenance of vascular homeostasis in adult mice. *FASEB J*. 22:1606-17.
- Du R, Lu KV, Petritsch C, Liu P, Ganss R, Passegué E, Song H, Vandenberg S, Johnson RS, Werb Z, Bergers G. 2008. HIF1alpha induces the recruitment of bone marrow-derived vascular modulatory cells to regulate tumor angiogenesis and invasion. *Cancer Cell*. 13:206-20.
- Ducharme E, Weinberg JM. 2008. Etanercept. *Expert Opin Biol Ther*. 8:491-502.
- Dumont DJ, Jussila L, Taipale J, Lymboussaki A, Mustonen T, Pajusola K, Breitman M, Alitalo K. 1998. Cardiovascular failure in mouse embryos deficient in VEGF receptor-3. *Science*. 282:946-9.
- Dumont DJ, Yamaguchi TP, Conlon RA, Rossant J, Breitman ML. 1992. tek, a novel tyrosine kinase gene located on mouse chromosome 4, is expressed in endothelial cells and their presumptive precursors. *Oncogene*. 7:1471-80.
- Ebos JML, Kerbel RS. 2011. Antiangiogenic therapy: impact on invasion, disease progression, and metastasis. *Nat Rev Clin Oncol*. 8:210-21.

- Ebos JML, Lee CR, Cruz-Munoz W, Bjarnason GA, Christensen JG, Kerbel RS. 2009. Accelerated metastasis after short-term treatment with a potent inhibitor of tumor angiogenesis. *Cancer Cell*. 15:232-9.
- Eckes B, Colucci-Guyon E, Smola H, Nodder S, Babinet C, Krieg T, Martin P. 2000. Impaired wound healing in embryonic and adult mice lacking vimentin. *J Cell Sci*. 113 ( Pt 13):2455-62.
- Eckes B, Dogic D, Colucci-Guyon E, Wang N, Maniotis A, Ingber D, Merckling A, Langa F, Aumailley M, Delouvé A, Koteliensky V, Babinet C, Krieg T. 1998. Impaired mechanical stability, migration and contractile capacity in vimentin-deficient fibroblasts. *J Cell Sci*. 111 ( Pt 13):1897-907.
- Eklund L, Saharinen P. 2013. Angiopoietin signaling in the vasculature. *Exp Cell Res*. 319:1271-80.
- Ellertsdóttir E, Lenard A, Blum Y, Krudewig A, Herwig L, Affolter M, Belting H. 2010. Vascular morphogenesis in the zebrafish embryo. *Dev Biol*. 341:56-65.
- English NM, Lesley JF, Hyman R. 1998. Site-specific de-N-glycosylation of CD44 can activate hyaluronan binding, and CD44 activation states show distinct threshold densities for hyaluronan binding. *Cancer Res*. 58:3736-42.
- Eriksson JE, He T, Trejo-Skalli AV, Härmälä-Braskén A, Hellman J, Chou Y, Goldman RD. 2004. Specific in vivo phosphorylation sites determine the assembly dynamics of vimentin intermediate filaments. *J Cell Sci*. 117:919-32.
- Escudier B, Pluzanska A, Koralewski P, Ravaud A, Bracarda S, Szczylik C, Chevreau C, Filipek M, Melichar B, Bajetta E, Gorbunova V, Bay J, Bodrogi I, Jagiello-Gruszfeld A, Moore N. 2007. Bevacizumab plus interferon alfa-2a for treatment of metastatic renal cell carcinoma: a randomised, double-blind phase III trial. *Lancet*. 370:2103-11.
- Evans RM. 1998. Vimentin: the conundrum of the intermediate filament gene family. *Bioessays*. 20:79-86.
- Faigle W, Colucci-Guyon E, Louvard D, Amigorena S, Galli T. 2000. Vimentin filaments in fibroblasts are a reservoir for SNAP23, a component of the membrane fusion machinery. *Mol Biol Cell*. 11:3485-94.
- Fantin A, Vieira JM, Gestri G, Denti L, Schwarz Q, Prykhodzhiy S, Peri F, Wilson SW, Ruhrberg C. 2010. Tissue macrophages act as cellular chaperones for vascular anastomosis downstream of VEGF-mediated endothelial tip cell induction. *Blood*. 116:829-40.
- Fantin A, Vieira JM, Plein A, Denti L, Fruttiger M, Pollard JW, Ruhrberg C. 2013. NR1 acts cell autonomously in endothelium to promote tip cell function during sprouting angiogenesis. *Blood*. 121:2352-62.
- Ferracini R, Di Renzo MF, Scotlandi K, Baldini N, Olivero M, Lollini P, Cremona O, Campanacci M, Comoglio PM. 1995. The Met/HGF receptor is over-expressed in human osteosarcomas and is activated by either a paracrine or an autocrine circuit. *Oncogene*. 10:739-49.

- Ferrara N, Gerber H, LeCouter J. 2003. The biology of VEGF and its receptors. *Nat Med.* 9:669-76.
- Fiedler U, Scharpfenecker M, Koidl S, Hegen A, Grunow V, Schmidt JM, Kriz W, Thurston G, Augustin HG. 2004. The Tie-2 ligand angiopoietin-2 is stored in and rapidly released upon stimulation from endothelial cell Weibel-Palade bodies. *Blood.* 103:4150-6.
- Fischer C, Mazzone M, Jonckx B, Carmeliet P. 2008. FLT1 and its ligands VEGFB and PlGF: drug targets for anti-angiogenic therapy?. *Nat Rev Cancer.* 8:942-56.
- Flynn KM, Michaud M, Canosa S, Madri JA. 2013. CD44 regulates vascular endothelial barrier integrity via a PECAM-1 dependent mechanism. *Angiogenesis.* 16:689-705.
- Flynn KM, Michaud M, Madri JA. 2013. CD44 deficiency contributes to enhanced experimental autoimmune encephalomyelitis: a role in immune cells and vascular cells of the blood-brain barrier. *Am J Pathol.* 182:1322-36.
- Folkman J. 1971. Tumor angiogenesis: therapeutic implications. *N Engl J Med.* 285:1182-6.
- Folkman J. 2007. Angiogenesis: an organizing principle for drug discovery?. *Nat Rev Drug Discov.* 6:273-86.
- Folkman J, Klagsbrun M, Sasse J, Wadzinski M, Ingber D, Vlodavsky I. 1988. A heparin-binding angiogenic protein--basic fibroblast growth factor--is stored within basement membrane. *Am J Pathol.* 130:393-400.
- Fraisl P, Mazzone M, Schmidt T, Carmeliet P. 2009. Regulation of angiogenesis by oxygen and metabolism. *Dev Cell.* 16:167-79.
- Friedrichs K, Franke F, Lisboa BW, Kügler G, Gille I, Terpe HJ, Hölzel F, Maass H, Günthert U. 1995. CD44 isoforms correlate with cellular differentiation but not with prognosis in human breast cancer. *Cancer Res.* 55:5424-33.
- Fuchs E, Weber K. 1994. Intermediate filaments: structure, dynamics, function, and disease. *Annu Rev Biochem.* 63:345-82.
- Fuchs K, Hippe A, Schmaus A, Homey B, Sleeman JP, Orian-Rousseau V. 2013. Opposing effects of high- and low-molecular weight hyaluronan on CXCL12-induced CXCR4 signaling depend on CD44. *Cell Death Dis.* 4:e819.
- Fukuhara S, Sako K, Minami T, Noda K, Kim HZ, Kodama T, Shibuya M, Takakura N, Koh GY, Mochizuki N. 2008. Differential function of Tie2 at cell-cell contacts and cell-substratum contacts regulated by angiopoietin-1. *Nat Cell Biol.* 10:513-26.
- Gaengel K, Genové G, Armulik A, Betsholtz C. 2009. Endothelial-mural cell signaling in vascular development and angiogenesis. *Arterioscler Thromb Vasc Biol.* 29:630-8.
- Gaengel K, Niaudet C, Hagikura K, Laviña B, Muhl L, Hofmann JJ, Ebarasi L, Nyström S, Rymo S, Chen LL, Pang M, Jin Y, Raschperger E, Roswall P,

- Schulte D, Benedito R, Larsson J, Hellström M, Fuxe J, Uhlén P, Adams R, Jakobsson L, Majumdar A, Vestweber D, Uv A, Betsholtz C. 2012. The sphingosine-1-phosphate receptor S1PR1 restricts sprouting angiogenesis by regulating the interplay between VE-cadherin and VEGFR2. *Dev Cell*. 23:587-99.
- Gallatin WM, Weissman IL, Butcher EC. 1983. A cell-surface molecule involved in organ-specific homing of lymphocytes. *Nature*. 304:30-4.
- Gao AC, Lou W, Dong JT, Isaacs JT. 1997. CD44 is a metastasis suppressor gene for prostatic cancer located on human chromosome 11p13. *Cancer Res*. 57:846-9.
- Gavard J, Patel V, Gutkind JS. 2008. Angiopoietin-1 prevents VEGF-induced endothelial permeability by sequestering Src through mDia. *Dev Cell*. 14:25-36.
- Gerhardt H, Golding M, Fruttiger M, Ruhrberg C, Lundkvist A, Abramsson A, Jeltsch M, Mitchell C, Alitalo K, Shima D, Betsholtz C. 2003. VEGF guides angiogenic sprouting utilizing endothelial tip cell filopodia. *J Cell Biol*. 161:1163-77.
- Geudens I, Gerhardt H. 2011. Coordinating cell behaviour during blood vessel formation. *Development*. 138:4569-83.
- Godar S, Ince TA, Bell GW, Feldser D, Donaher JL, Bergh J, Liu A, Miu K, Watnick RS, Reinhardt F, McAllister SS, Jacks T, Weinberg RA. 2008. Growth-inhibitory and tumor-suppressive functions of p53 depend on its repression of CD44 expression. *Cell*. 134:62-73.
- Goel S, Duda DG, Xu L, Munn LL, Boucher Y, Fukumura D, Jain RK. 2011. Normalization of the vasculature for treatment of cancer and other diseases. *Physiol Rev*. 91:1071-121.
- Goldman RD, Khuon S, Chou YH, Opal P, Steinert PM. 1996. The function of intermediate filaments in cell shape and cytoskeletal integrity. *J Cell Biol*. 134:971-83.
- Goumans M, Valdimarsdottir G, Itoh S, Rosendahl A, Sideras P, ten Dijke P. 2002. Balancing the activation state of the endothelium via two distinct TGF-beta type I receptors. *EMBO J*. 21:1743-53.
- Goumans MJ, Valdimarsdottir G, Itoh S, Lebrin F, Larsson J, Mummery C, Karlsson S, ten Dijke P. 2003. Activin receptor-like kinase (ALK)1 is an antagonistic mediator of lateral TGFbeta/ALK5 signaling. *Mol Cell*. 12:817-28.
- Gregor M, Osmanagic-Myers S, Burgstaller G, Wolfram M, Fischer I, Walko G, Resch GP, Jörgl A, Herrmann H, Wiche G. 2014. Mechanosensing through focal adhesion-anchored intermediate filaments. *FASEB J*. 28:715-29.
- Griffioen AW, Coenen MJ, Damen CA, Hellwig SM, van Weering DH, Vooy W, Blijham GH, Groenewegen G. 1997. CD44 is involved in tumor angiogenesis; an activation antigen on human endothelial cells. *Blood*. 90:1150-9.

- Guarani V, Deflorian G, Franco CA, Krüger M, Phng L, Bentley K, Toussaint L, Dequiedt F, Mostoslavsky R, Schmidt MHH, Zimmermann B, Brandes RP, Mione M, Westphal CH, Braun T, Zeiher AM, Gerhardt H, Dimmeler S, Potente M. 2011. Acetylation-dependent regulation of endothelial Notch signalling by the SIRT1 deacetylase. *Nature*. 473:234-8.
- Guedez L, Rivera AM, Salloum R, Miller ML, Diegmüller JJ, Bungay PM, Stetler-Stevenson WG. 2003. Quantitative assessment of angiogenic responses by the directed in vivo angiogenesis assay. *Am J Pathol*. 162:1431-9.
- Guo YJ, Liu G, Wang X, Jin D, Wu M, Ma J, Sy MS. 1994. Potential use of soluble CD44 in serum as indicator of tumor burden and metastasis in patients with gastric or colon cancer. *Cancer Res*. 54:422-6.
- Günthert U, Hofmann M, Rudy W, Reber S, Zöller M, Hausmann I, Matzku S, Wenzel A, Ponta H, Herrlich P. 1991. A new variant of glycoprotein CD44 confers metastatic potential to rat carcinoma cells. *Cell*. 65:13-24.
- Hartmann M, Parra LM, Ruschel A, Böhme S, Li Y, Morrison H, Herrlich A, Herrlich P. 2015. Tumor Suppressor NF2 Blocks Cellular Migration by Inhibiting Ectodomain Cleavage of CD44. *Mol Cancer Res*. 13:879-90.
- Hartmann M, Parra LM, Ruschel A, Lindner C, Morrison H, Herrlich A, Herrlich P. 2015. Inside-out Regulation of Ectodomain Cleavage of Cluster-of-Differentiation-44 (CD44) and of Neuregulin-1 Requires Substrate Dimerization. *J Biol Chem*. 290:17041-54.
- Hasenauer S, Malinger D, Koschut D, Pace G, Matzke A, von Au A, Orián-Rousseau V. 2013. Internalization of Met requires the co-receptor CD44v6 and its link to ERM proteins. *PLoS One*. 8:e62357.
- Hayashi M, Majumdar A, Li X, Adler J, Sun Z, Vertuani S, Hellberg C, Mellberg S, Koch S, Dimberg A, Koh GY, Dejana E, Belting H, Affolter M, Thurston G, Holmgren L, Vestweber D, Claesson-Welsh L. 2013. VE-PTP regulates VEGFR2 activity in stalk cells to establish endothelial cell polarity and lumen formation. *Nat Commun*. 4:1672.
- Hayer S, Steiner G, Görtz B, Reiter E, Tohidast-Akrad M, Amling M, Hoffmann O, Redlich K, Zwerina J, Skriner K, Hilberg F, Wagner EF, Smolen JS, Schett G. 2005. CD44 is a determinant of inflammatory bone loss. *J Exp Med*. 201:903-14.
- Helker CSM, Schuermann A, Karpanen T, Zeuschner D, Belting H, Affolter M, Schulte-Merker S, Herzog W. 2013. The zebrafish common cardinal veins develop by a novel mechanism: lumen ensheathment. *Development*. 140:2776-86.
- Hellström M, Kalén M, Lindahl P, Abramsson A, Betsholtz C. 1999. Role of PDGF-B and PDGFR-beta in recruitment of vascular smooth muscle cells and pericytes during embryonic blood vessel formation in the mouse. *Development*. 126:3047-55.
- Hellström M, Phng L, Hofmann JJ, Wallgard E, Coultas L, Lindblom P, Alva J, Nilsson A, Karlsson L, Gaiano N, Yoon K, Rossant J, Iruela-Arispe ML,

- Kalén M, Gerhardt H, Betsholtz C. 2007. Dll4 signalling through Notch1 regulates formation of tip cells during angiogenesis. *Nature*. 445:776-80.
- Henricson D, Terzi F, Matrougui K, Duriez M, Boulanger CM, Colucci-Guyon E, Babinet C, Briand P, Friedlander G, Poitevin P, Lévy BI. 1997. Impaired flow-induced dilation in mesenteric resistance arteries from mice lacking vimentin. *J Clin Invest*. 100:2909-14.
- Herbert SP, Stainier DYR. 2011. Molecular control of endothelial cell behaviour during blood vessel morphogenesis. *Nat Rev Mol Cell Biol*. 12:551-64.
- Herwig L, Blum Y, Krudewig A, Ellertsdottir E, Lenard A, Belting H, Affolter M. 2011. Distinct cellular mechanisms of blood vessel fusion in the zebrafish embryo. *Curr Biol*. 21:1942-8.
- High FA, Lu MM, Pear WS, Loomes KM, Kaestner KH, Epstein JA. 2008. Endothelial expression of the Notch ligand Jagged1 is required for vascular smooth muscle development. *Proc Natl Acad Sci U S A*. 105:1955-9.
- Holash J, Davis S, Papadopoulos N, Croll SD, Ho L, Russell M, Boland P, Leidich R, Hylton D, Burova E, Ioffe E, Huang T, Radziejewski C, Bailey K, Fandl JP, Daly T, Wiegand SJ, Yancopoulos GD, Rudge JS. 2002. VEGF-Trap: a VEGF blocker with potent antitumor effects. *Proc Natl Acad Sci U S A*. 99:11393-8.
- Howes MT, Kirkham M, Riches J, Cortese K, Walser PJ, Simpson F, Hill MM, Jones A, Lundmark R, Lindsay MR, Hernandez-Deviez DJ, Hadzic G, McCluskey A, Bashir R, Liu L, Pilch P, McMahon H, Robinson PJ, Hancock JF, Mayor S, Parton RG. 2010. Clathrin-independent carriers form a high capacity endocytic sorting system at the leading edge of migrating cells. *J Cell Biol*. 190:675-91.
- Huang C. 2009. Receptor-Fc fusion therapeutics, traps, and MIMETIBODY technology. *Curr Opin Biotechnol*. 20:692-9.
- Hurwitz H, Fehrenbacher L, Novotny W, Cartwright T, Hainsworth J, Heim W, Berlin J, Baron A, Griffing S, Holmgren E, Ferrara N, Fyfe G, Rogers B, Ross R, Kabbinavar F. 2004. Bevacizumab plus irinotecan, fluorouracil, and leucovorin for metastatic colorectal cancer. *N Engl J Med*. 350:2335-42.
- Hutás G, Bajnok E, Gál I, Finnegan A, Glant TT, Mikecz K. 2008. CD44-specific antibody treatment and CD44 deficiency exert distinct effects on leukocyte recruitment in experimental arthritis. *Blood*. 112:4999-5006.
- Ishimoto T, Nagano O, Yae T, Tamada M, Motohara T, Oshima H, Oshima M, Ikeda T, Asaba R, Yagi H, Masuko T, Shimizu T, Ishikawa T, Kai K, Takahashi E, Imamura Y, Baba Y, Ohmura M, Suematsu M, Baba H, Saya H. 2011. CD44 variant regulates redox status in cancer cells by stabilizing the xCT subunit of system xc(-) and thereby promotes tumor growth. *Cancer Cell*. 19:387-400.
- Ito T, Williams JD, Fraser DJ, Phillips AO. 2004. Hyaluronan regulates transforming growth factor-beta1 receptor compartmentalization. *J Biol Chem*. 279:25326-32.

- Ivaska J, Pallari H, Nevo J, Eriksson JE. 2007. Novel functions of vimentin in cell adhesion, migration, and signaling. *Exp Cell Res.* 313:2050-62.
- Ivaska J, Vuoriluoto K, Huovinen T, Izawa I, Inagaki M, Parker PJ. 2005. PKCepsilon-mediated phosphorylation of vimentin controls integrin recycling and motility. *EMBO J.* 24:3834-45.
- Jain RK. 2003. Molecular regulation of vessel maturation. *Nat Med.* 9:685-93.
- Jain RK. 2005. Normalization of tumor vasculature: an emerging concept in antiangiogenic therapy. *Science.* 307:58-62.
- Jain RK, Duda DG, Willett CG, Sahani DV, Zhu AX, Loeffler JS, Batchelor TT, Sorensen AG. 2009. Biomarkers of response and resistance to antiangiogenic therapy. *Nat Rev Clin Oncol.* 6:327-38.
- Jakobsson L, Franco CA, Bentley K, Collins RT, Ponsioen B, Aspalter IM, Rosewell I, Busse M, Thurston G, Medvinsky A, Schulte-Merker S, Gerhardt H. 2010. Endothelial cells dynamically compete for the tip cell position during angiogenic sprouting. *Nat Cell Biol.* 12:943-53.
- Jeansson M, Gawlik A, Anderson G, Li C, Kerjaschki D, Henkelman M, Quaggin SE. 2011. Angiopoietin-1 is essential in mouse vasculature during development and in response to injury. *J Clin Invest.* 121:2278-89.
- Jordan AR, Racine RR, Hennig MJP, Lokeshwar VB. 2015. The Role of CD44 in Disease Pathophysiology and Targeted Treatment. *Front Immunol.* 6:182.
- Kagami T, Chen S, Memar P, Choi M, Foster LJ, Numata M. 2008. Identification and biochemical characterization of the SLC9A7 interactome. *Mol Membr Biol.* 25:436-47.
- Kajita M, Itoh Y, Chiba T, Mori H, Okada A, Kinoh H, Seiki M. 2001. Membrane-type 1 matrix metalloproteinase cleaves CD44 and promotes cell migration. *J Cell Biol.* 153:893-904.
- Kamei M, Saunders WB, Bayless KJ, Dye L, Davis GE, Weinstein BM. 2006. Endothelial tubes assemble from intracellular vacuoles in vivo. *Nature.* 442:453-6.
- Kappas NC, Zeng G, Chappell JC, Kearney JB, Hazarika S, Kallianos KG, Patterson C, Annex BH, Bautch VL. 2008. The VEGF receptor Flt-1 spatially modulates Flk-1 signaling and blood vessel branching. *J Cell Biol.* 181:847-58.
- Karkkainen MJ, Haiko P, Sainio K, Partanen J, Taipale J, Petrova TV, Jeltsch M, Jackson DG, Talikka M, Rauvala H, Betsholtz C, Alitalo K. 2004. Vascular endothelial growth factor C is required for sprouting of the first lymphatic vessels from embryonic veins. *Nat Immunol.* 5:74-80.
- Katayama Y, Hidalgo A, Chang J, Peired A, Frenette PS. 2005. CD44 is a physiological E-selectin ligand on neutrophils. *J Exp Med.* 201:1183-9.
- Katoh S, McCarthy JB, Kincade PW. 1994. Characterization of soluble CD44 in the circulation of mice. Levels are affected by immune activity and tumor growth. *J Immunol.* 153:3440-9.

- Kaufmann M, Heider KH, Sinn HP, von Minckwitz G, Ponta H, Herrlich P. 1995. CD44 variant exon epitopes in primary breast cancer and length of survival. *Lancet*. 345:615-9.
- Kaya G, Rodriguez I, Jorcano JL, Vassalli P, Stamenkovic I. 1997. Selective suppression of CD44 in keratinocytes of mice bearing an antisense CD44 transgene driven by a tissue-specific promoter disrupts hyaluronate metabolism in the skin and impairs keratinocyte proliferation. *Genes Dev*. 11:996-1007.
- Kinstler O, Molineux G, Treuheit M, Ladd D, Gegg C. 2002. Mono-N-terminal poly(ethylene glycol)-protein conjugates. *Adv Drug Deliv Rev*. 54:477-85.
- Kito H, Suzuki H, Ichikawa T, Sekita N, Kamiya N, Akakura K, Igarashi T, Nakayama T, Watanabe M, Harigaya K, Ito H. 2001. Hypermethylation of the CD44 gene is associated with progression and metastasis of human prostate cancer. *Prostate*. 49:110-5.
- Knudson W, Chow G, Knudson CB. 2002. CD44-mediated uptake and degradation of hyaluronan. *Matrix Biol*. 21:15-23.
- Koch S, Claesson-Welsh L. 2012. Signal transduction by vascular endothelial growth factor receptors. *Cold Spring Harb Perspect Med*. 2:a006502.
- Kogerman P, Sy MS, Culp LA. 1997. Overexpressed human CD44s promotes lung colonization during micrometastasis of murine fibrosarcoma cells: facilitated retention in the lung vasculature. *Proc Natl Acad Sci U S A*. 94:13233-8.
- Koh YJ, Kim H, Hwang S, Lee JE, Oh N, Jung K, Kim M, Kim KE, Kim H, Lim N, Jeon C, Lee GM, Jeon BH, Nam D, Sung HK, Nagy A, Yoo OJ, Koh GY. 2010. Double antiangiogenic protein, DAAP, targeting VEGF-A and angiopoietins in tumor angiogenesis, metastasis, and vascular leakage. *Cancer Cell*. 18:171-84.
- Kohda D, Morton CJ, Parkar AA, Hatanaka H, Inagaki FM, Campbell ID, Day AJ. 1996. Solution structure of the link module: a hyaluronan-binding domain involved in extracellular matrix stability and cell migration. *Cell*. 86:767-75.
- Kontermann RE. 2011. Strategies for extended serum half-life of protein therapeutics. *Curr Opin Biotechnol*. 22:868-76.
- Kopetz S, Hoff PM, Morris JS, Wolff RA, Eng C, Glover KY, Adinin R, Overman MJ, Valero V, Wen S, Lieu C, Yan S, Tran HT, Ellis LM, Abbruzzese JL, Heymach JV. 2010. Phase II trial of infusional fluorouracil, irinotecan, and bevacizumab for metastatic colorectal cancer: efficacy and circulating angiogenic biomarkers associated with therapeutic resistance. *J Clin Oncol*. 28:453-9.
- Kothapalli D, Zhao L, Hawthorne EA, Cheng Y, Lee E, Puré E, Assoian RK. 2007. Hyaluronan and CD44 antagonize mitogen-dependent cyclin D1 expression in mesenchymal cells. *J Cell Biol*. 176:535-44.

- Koudelka KJ, Destito G, Plummer EM, Trauger SA, Siuzdak G, Manchester M. 2009. Endothelial targeting of cowpea mosaic virus (CPMV) via surface vimentin. *PLoS Pathog.* 5:e1000417.
- Kreis S, Schönfeld H, Melchior C, Steiner B, Kieffer N. 2005. The intermediate filament protein vimentin binds specifically to a recombinant integrin alpha2/beta1 cytoplasmic tail complex and co-localizes with native alpha2/beta1 in endothelial cell focal adhesions. *Exp Cell Res.* 305:110-21.
- Krueger J, Liu D, Scholz K, Zimmer A, Shi Y, Klein C, Siekmann A, Schulte-Merker S, Cudmore M, Ahmed A, le Noble F. 2011. Flt1 acts as a negative regulator of tip cell formation and branching morphogenesis in the zebrafish embryo. *Development.* 138:2111-20.
- Kwak H, Kang H, Dave JM, Mendoza EA, Su S, Maxwell SA, Bayless KJ. 2012. Calpain-mediated vimentin cleavage occurs upstream of MT1-MMP membrane translocation to facilitate endothelial sprout initiation. *Angiogenesis.* 15:287-303.
- Lallemant D, Curto M, Saotome I, Giovannini M, McClatchey AI. 2003. NF2 deficiency promotes tumorigenesis and metastasis by destabilizing adherens junctions. *Genes Dev.* 17:1090-100.
- Lampugnani MG, Orsenigo F, Gagliani MC, Tacchetti C, Dejana E. 2006. Vascular endothelial cadherin controls VEGFR-2 internalization and signaling from intracellular compartments. *J Cell Biol.* 174:593-604.
- Larrivée B, Prahst C, Gordon E, del Toro R, Mathivet T, Duarte A, Simons M, Eichmann A. 2012. ALK1 signaling inhibits angiogenesis by cooperating with the Notch pathway. *Dev Cell.* 22:489-500.
- Lee S, Chen TT, Barber CL, Jordan MC, Murdock J, Desai S, Ferrara N, Nagy A, Roos KP, Iruela-Arispe ML. 2007. Autocrine VEGF signaling is required for vascular homeostasis. *Cell.* 130:691-703.
- Legg JW, Lewis CA, Parsons M, Ng T, Isacke CM. 2002. A novel PKC-regulated mechanism controls CD44 ezrin association and directional cell motility. *Nat Cell Biol.* 4:399-407.
- Lehtinen L, Ketola K, Mäkelä R, Mpindi J, Viitala M, Kallioniemi O, Iljin K. 2013. High-throughput RNAi screening for novel modulators of vimentin expression identifies MTHFD2 as a regulator of breast cancer cell migration and invasion. *Oncotarget.* 4:48-63.
- Lennon FE, Mirzapooiazova T, Mambetsariev N, Mambetsariev B, Salgia R, Singleton PA. 2014. Transactivation of the receptor-tyrosine kinase ephrin receptor A2 is required for the low molecular weight hyaluronan-mediated angiogenesis that is implicated in tumor progression. *J Biol Chem.* 289:24043-58.
- Lesley J, English N, Perschl A, Gregoroff J, Hyman R. 1995. Variant cell lines selected for alterations in the function of the hyaluronan receptor CD44 show differences in glycosylation. *J Exp Med.* 182:431-7.

- Li C, Heidt DG, Dalerba P, Burant CF, Zhang L, Adsay V, Wicha M, Clarke MF, Simeone DM. 2007. Identification of pancreatic cancer stem cells. *Cancer Res.* 67:1030-7.
- Li L, Heldin C, Heldin P. 2006. Inhibition of platelet-derived growth factor-BB-induced receptor activation and fibroblast migration by hyaluronan activation of CD44. *J Biol Chem.* 281:26512-9.
- Li X, Ma X, Chen L, Gu L, Zhang Y, Zhang F, Ouyang Y, Gao Y, Huang Q, Zhang X. 2015. Prognostic value of CD44 expression in renal cell carcinoma: a systematic review and meta-analysis. *Sci Rep.* 5:13157.
- Lim SD, Young AN, Paner GP, Amin MB. 2008. Prognostic role of CD44 cell adhesion molecule expression in primary and metastatic renal cell carcinoma: a clinicopathologic study of 125 cases. *Virchows Arch.* 452:49-55.
- Liu D, Sy MS. 1997. Phorbol myristate acetate stimulates the dimerization of CD44 involving a cysteine in the transmembrane domain. *J Immunol.* 159:2702-11.
- Lobov IB, Renard RA, Papadopoulos N, Gale NW, Thurston G, Yancopoulos GD, Wiegand SJ. 2007. Delta-like ligand 4 (Dll4) is induced by VEGF as a negative regulator of angiogenic sprouting. *Proc Natl Acad Sci U S A.* 104:3219-24.
- Lokeshwar VB, Fregien N, Bourguignon LY. 1994. Ankyrin-binding domain of CD44(GP85) is required for the expression of hyaluronic acid-mediated adhesion function. *J Cell Biol.* 126:1099-109.
- Lopez JI, Camenisch TD, Stevens MV, Sands BJ, McDonald J, Schroeder JA. 2005. CD44 attenuates metastatic invasion during breast cancer progression. *Cancer Res.* 65:6755-63.
- Lund N, Henrion D, Tiede P, Ziche M, Schunkert H, Ito WD. 2010. Vimentin expression influences flow dependent VASP phosphorylation and regulates cell migration and proliferation. *Biochem Biophys Res Commun.* 395:401-6.
- Lundkvist A, Reichenbach A, Betsholtz C, Carmeliet P, Wolburg H, Pekny M. 2004. Under stress, the absence of intermediate filaments from Müller cells in the retina has structural and functional consequences. *J Cell Sci.* 117:3481-8.
- Magnusson P, Rolny C, Jakobsson L, Wikner C, Wu Y, Hicklin DJ, Claesson-Welsh L. 2004. Deregulation of Flk-1/vascular endothelial growth factor receptor-2 in fibroblast growth factor receptor-1-deficient vascular stem cell development. *J Cell Sci.* 117:1513-23.
- Maisonpierre PC, Suri C, Jones PF, Bartunkova S, Wiegand SJ, Radziejewski C, Compton D, McClain J, Aldrich TH, Papadopoulos N, Daly TJ, Davis S, Sato TN, Yancopoulos GD. 1997. Angiopoietin-2, a natural antagonist for Tie2 that disrupts in vivo angiogenesis. *Science.* 277:55-60.
- Majmundar AJ, Wong WJ, Simon MC. 2010. Hypoxia-inducible factors and the response to hypoxic stress. *Mol Cell.* 40:294-309.

- Maniotis AJ, Folberg R, Hess A, Seftor EA, Gardner LM, Pe'er J, Trent JM, Meltzer PS, Hendrix MJ. 1999. Vascular channel formation by human melanoma cells in vivo and in vitro: vasculogenic mimicry. *Am J Pathol.* 155:739-52.
- Margadant C, Cremers L, Sonnenberg A, Boonstra J. 2013. MAPK uncouples cell cycle progression from cell spreading and cytoskeletal organization in cycling cells. *Cell Mol Life Sci.* 70:293-307.
- Matou-Nasri S, Gaffney J, Kumar S, Slevin M. 2009. Oligosaccharides of hyaluronan induce angiogenesis through distinct CD44 and RHAMM-mediated signalling pathways involving Cdc2 and gamma-adducin. *Int J Oncol.* 35:761-73.
- Matzke A, Sargsyan V, Holtmann B, Aramuni G, Asan E, Sendtner M, Pace G, Howells N, Zhang W, Ponta H, Orian-Rousseau V. 2007. Haploinsufficiency of c-Met in cd44<sup>-/-</sup> mice identifies a collaboration of CD44 and c-Met in vivo. *Mol Cell Biol.* 27:8797-806.
- Mayer S, zur Hausen A, Watermann DO, Stamm S, Jäger M, Gitsch G, Stickeler E. 2008. Increased soluble CD44 concentrations are associated with larger tumor size and lymph node metastasis in breast cancer patients. *J Cancer Res Clin Oncol.* 134:1229-35.
- Mazzieri R, Pucci F, Moi D, Zonari E, Ranghetti A, Berti A, Politi LS, Gentner B, Brown JL, Naldini L, De Palma M. 2011. Targeting the ANG2/TIE2 axis inhibits tumor growth and metastasis by impairing angiogenesis and disabling rebounds of proangiogenic myeloid cells. *Cancer Cell.* 19:512-26.
- Mazzone M, Dettori D, Leite de Oliveira R, Loges S, Schmidt T, Jonckx B, Tian Y, Lanahan AA, Pollard P, Ruiz de Almodovar C, De Smet F, Vinckier S, Aragonés J, Debackere K, Luttun A, Wyns S, Jordan B, Pisacane A, Gallez B, Lampugnani MG, Dejana E, Simons M, Ratcliffe P, Maxwell P, Carmeliet P. 2009. Heterozygous deficiency of PHD2 restores tumor oxygenation and inhibits metastasis via endothelial normalization. *Cell.* 136:839-51.
- Melmed GY, Targan SR, Yasothan U, Hanicq D, Kirkpatrick P. 2008. Certolizumab pegol. *Nat Rev Drug Discov.* 7:641-2.
- Mendez MG, Kojima S, Goldman RD. 2010. Vimentin induces changes in cell shape, motility, and adhesion during the epithelial to mesenchymal transition. *FASEB J.* 24:1838-51.
- Meran S, Luo DD, Simpson R, Martin J, Wells A, Steadman R, Phillips AO. 2011. Hyaluronan facilitates transforming growth factor- $\beta$ 1-dependent proliferation via CD44 and epidermal growth factor receptor interaction. *J Biol Chem.* 286:17618-30.
- Mikami S, Mizuno R, Kosaka T, Saya H, Oya M, Okada Y. 2015. Expression of TNF- $\alpha$  and CD44 is implicated in poor prognosis, cancer cell invasion, metastasis and resistance to the sunitinib treatment in clear cell renal cell carcinomas. *Int J Cancer.* 136:1504-14.

- Miletti-González KE, Murphy K, Kumaran MN, Ravindranath AK, Wernyj RP, Kaur S, Miles GD, Lim E, Chan R, Chekmareva M, Heller DS, Foran D, Chen W, Reiss M, Bandera EV, Scotto K, Rodríguez-Rodríguez L. 2012. Identification of function for CD44 intracytoplasmic domain (CD44-ICD): modulation of matrix metalloproteinase 9 (MMP-9) transcription via novel promoter response element. *J Biol Chem.* 287:18995-9007.
- Mor-Vaknin N, Punturieri A, Sitwala K, Markovitz DM. 2003. Vimentin is secreted by activated macrophages. *Nat Cell Biol.* 5:59-63.
- Mori H, Tomari T, Koshikawa N, Kajita M, Itoh Y, Sato H, Tojo H, Yana I, Seiki M. 2002. CD44 directs membrane-type 1 matrix metalloproteinase to lamellipodia by associating with its hemopexin-like domain. *EMBO J.* 21:3949-59.
- Morrison H, Sherman LS, Legg J, Banine F, Isacke C, Haipek CA, Gutmann DH, Ponta H, Herrlich P. 2001. The NF2 tumor suppressor gene product, merlin, mediates contact inhibition of growth through interactions with CD44. *Genes Dev.* 15:968-80.
- Moya IM, Umans L, Maas E, Pereira PNG, Beets K, Francis A, Sents W, Robertson EJ, Mummery CL, Huylebroeck D, Zwijsen A. 2012. Stalk cell phenotype depends on integration of Notch and Smad1/5 signaling cascades. *Dev Cell.* 22:501-14.
- Murakami M. 2012. Signaling required for blood vessel maintenance: molecular basis and pathological manifestations. *Int J Vasc Med.* 2012:293641.
- Murakami M, Nguyen LT, Hatanaka K, Schachterle W, Chen P, Zhuang ZW, Black BL, Simons M. 2011. FGF-dependent regulation of VEGF receptor 2 expression in mice. *J Clin Invest.* 121:2668-78.
- Murakami M, Nguyen LT, Zhuang ZW, Moodie KL, Carmeliet P, Stan RV, Simons M. 2008. The FGF system has a key role in regulating vascular integrity. *J Clin Invest.* 118:3355-66.
- Murakami M, Simons M. 2008. Fibroblast growth factor regulation of neovascularization. *Curr Opin Hematol.* 15:215-20.
- Murphy JF, Lennon F, Steele C, Kelleher D, Fitzgerald D, Long AC. 2005. Engagement of CD44 modulates cyclooxygenase induction, VEGF generation, and proliferation in human vascular endothelial cells. *FASEB J.* 19:446-8.
- Nagano O, Saya H. 2004. Mechanism and biological significance of CD44 cleavage. *Cancer Sci.* 95:930-5.
- Nagy JA, Chang S, Shih S, Dvorak AM, Dvorak HF. 2010. Heterogeneity of the tumor vasculature. *Semin Thromb Hemost.* 36:321-31.
- Nakamura T, Sakai K, Nakamura T, Matsumoto K. 2011. Hepatocyte growth factor twenty years on: Much more than a growth factor. *J Gastroenterol Hepatol.* 26 Suppl 1:188-202.
- Naldini L, Weidner KM, Vigna E, Gaudino G, Bardelli A, Ponzetto C, Narsimhan RP, Hartmann G, Zarnegar R, Michalopoulos GK, et al.. 1991.

- Scatter factor and hepatocyte growth factor are indistinguishable ligands for the MET receptor. *EMBO J.* 10:2867-78.
- Nandi A, Estess P, Siegelman M. 2004. Bimolecular complex between rolling and firm adhesion receptors required for cell arrest; CD44 association with VLA-4 in T cell extravasation. *Immunity.* 20:455-65.
- Naor D, Nedvetzki S, Golan I, Melnik L, Faitelson Y. 2002. CD44 in cancer. *Crit Rev Clin Lab Sci.* 39:527-79.
- Naor D, Sionov RV, Ish-Shalom D. 1997. CD44: structure, function, and association with the malignant process. *Adv Cancer Res.* 71:241-319.
- Neame SJ, Uff CR, Sheikh H, Wheatley SC, Isacke CM. 1995. CD44 exhibits a cell type dependent interaction with triton X-100 insoluble, lipid rich, plasma membrane domains. *J Cell Sci.* 108 ( Pt 9):3127-35.
- Nedvetzki S, Gonen E, Assayag N, Reich R, Williams RO, Thurmond RL, Huang J, Neudecker BA, Wang F, Turley EA, Naor D. 2004. RHAMM, a receptor for hyaluronan-mediated motility, compensates for CD44 in inflamed CD44-knockout mice: a different interpretation of redundancy. *Proc Natl Acad Sci U S A.* 101:18081-6.
- Ng EWM, Shima DT, Calias P, Cunningham ETJ, Guyer DR, Adamis AP. 2006. Pegaptanib, a targeted anti-VEGF aptamer for ocular vascular disease. *Nat Rev Drug Discov.* 5:123-32.
- Nieminen M, Henttinen T, Merinen M, Marttila-Ichihara F, Eriksson JE, Jalkanen S. 2006. Vimentin function in lymphocyte adhesion and transcellular migration. *Nat Cell Biol.* 8:156-62.
- Nishida Y, Shibata K, Yamasaki M, Sato Y, Abe M. 2009. A possible role of vimentin on the cell surface for the activation of latent transforming growth factor-beta. *FEBS Lett.* 583:308-12.
- Nissen LJ, Cao R, Hedlund E, Wang Z, Zhao X, Wetterskog D, Funa K, Bråkenhielm E, Cao Y. 2007. Angiogenic factors FGF2 and PDGF-BB synergistically promote murine tumor neovascularization and metastasis. *J Clin Invest.* 117:2766-77.
- Nyberg P, Xie L, Kalluri R. 2005. Endogenous inhibitors of angiogenesis. *Cancer Res.* 65:3967-79.
- Nácher M, Blázquez AB, Shao B, Matesanz A, Prophete C, Berin MC, Frenette PS, Hidalgo A. 2011. Physiological contribution of CD44 as a ligand for E-Selectin during inflammatory T-cell recruitment. *Am J Pathol.* 178:2437-46.
- Ogino S, Nishida N, Umemoto R, Suzuki M, Takeda M, Terasawa H, Kitayama J, Matsumoto M, Hayasaka H, Miyasaka M, Shimada I. 2010. Two-state conformations in the hyaluronan-binding domain regulate CD44 adhesiveness under flow condition. *Structure.* 18:649-56.
- Okamoto I, Kawano Y, Tsuiki H, Sasaki J, Nakao M, Matsumoto M, Suga M, Ando M, Nakajima M, Saya H. 1999. CD44 cleavage induced by a membrane-associated metalloprotease plays a critical role in tumor cell migration. *Oncogene.* 18:1435-46.

- Okamoto I, Tsuiki H, Kenyon LC, Godwin AK, Emlet DR, Holgado-Madruga M, Lanham IS, Joynes CJ, Vo KT, Guha A, Matsumoto M, Ushio Y, Saya H, Wong AJ. 2002. Proteolytic cleavage of the CD44 adhesion molecule in multiple human tumors. *Am J Pathol.* 160:441-7.
- Olaku V, Matzke A, Mitchell C, Hasenauer S, Sakkaravarthi A, Pace G, Ponta H, Orian-Rousseau V. 2011. c-Met recruits ICAM-1 as a coreceptor to compensate for the loss of CD44 in Cd44 null mice. *Mol Biol Cell.* 22:2777-86.
- Olofsson B, Porsch H, Heldin P. 2014. Knock-down of CD44 regulates endothelial cell differentiation via NFκB-mediated chemokine production. *PLoS One.* 9:e90921.
- Onimaru M, Yonemitsu Y, Tanii M, Nakagawa K, Masaki I, Okano S, Ishibashi H, Shirasuna K, Hasegawa M, Sueishi K. 2002. Fibroblast growth factor-2 gene transfer can stimulate hepatocyte growth factor expression irrespective of hypoxia-mediated downregulation in ischemic limbs. *Circ Res.* 91:923-30.
- Orian-Rousseau V, Chen L, Sleeman JP, Herrlich P, Ponta H. 2002. CD44 is required for two consecutive steps in HGF/c-Met signaling. *Genes Dev.* 16:3074-86.
- Orian-Rousseau V, Sleeman J. 2014. CD44 is a multidomain signaling platform that integrates extracellular matrix cues with growth factor and cytokine signals. *Adv Cancer Res.* 123:231-54.
- Orimo A, Gupta PB, Sgroi DC, Arenzana-Seisdedos F, Delaunay T, Naeem R, Carey VJ, Richardson AL, Weinberg RA. 2005. Stromal fibroblasts present in invasive human breast carcinomas promote tumor growth and angiogenesis through elevated SDF-1/CXCL12 secretion. *Cell.* 121:335-48.
- Paik J, Skoura A, Chae S, Cowan AE, Han DK, Proia RL, Hla T. 2004. Sphingosine 1-phosphate receptor regulation of N-cadherin mediates vascular stabilization. *Genes Dev.* 18:2392-403.
- Pardali E, Goumans M, ten Dijke P. 2010. Signaling by members of the TGF-beta family in vascular morphogenesis and disease. *Trends Cell Biol.* 20:556-67.
- Pasut G, Veronese FM. 2012. State of the art in PEGylation: the great versatility achieved after forty years of research. *J Control Release.* 161:461-72.
- Peterson RS, Andhare RA, Rousche KT, Knudson W, Wang W, Grossfield JB, Thomas RO, Hollingsworth RE, Knudson CB. 2004. CD44 modulates Smad1 activation in the BMP-7 signaling pathway. *J Cell Biol.* 166:1081-91.
- Phng L, Gerhardt H. 2009. Angiogenesis: a team effort coordinated by notch. *Dev Cell.* 16:196-208.
- Phng L, Potente M, Leslie JD, Babbage J, Nyqvist D, Lobov I, Ondr JK, Rao S, Lang RA, Thurston G, Gerhardt H. 2009. Nrarp coordinates endothelial Notch and Wnt signaling to control vessel density in angiogenesis. *Dev Cell.* 16:70-82.

- Ponta H, Sherman L, Herrlich PA. 2003. CD44: from adhesion molecules to signalling regulators. *Nat Rev Mol Cell Biol.* 4:33-45.
- Porsch H, Mehić M, Olofsson B, Heldin P, Heldin C. 2014. Platelet-derived growth factor  $\beta$ -receptor, transforming growth factor  $\beta$  type I receptor, and CD44 protein modulate each other's signaling and stability. *J Biol Chem.* 289:19747-57.
- Potente M, Gerhardt H, Carmeliet P. 2011. Basic and therapeutic aspects of angiogenesis. *Cell.* 146:873-87.
- Prahlad V, Yoon M, Moir RD, Vale RD, Goldman RD. 1998. Rapid movements of vimentin on microtubule tracks: kinesin-dependent assembly of intermediate filament networks. *J Cell Biol.* 143:159-70.
- Preca B, Bajdak K, Mock K, Sundararajan V, Pfannstiel J, Maurer J, Wellner U, Hopt UT, Brummer T, Brabletz S, Brabletz T, Stemmler MP. 2015. A self-enforcing CD44s/ZEB1 feedback loop maintains EMT and stemness properties in cancer cells. *Int J Cancer.* 137:2566-77.
- Presta LG, Chen H, O'Connor SJ, Chisholm V, Meng YG, Krummen L, Winkler M, Ferrara N. 1997. Humanization of an anti-vascular endothelial growth factor monoclonal antibody for the therapy of solid tumors and other disorders. *Cancer Res.* 57:4593-9.
- Presta M, Dell'Era P, Mitola S, Moroni E, Ronca R, Rusnati M. 2005. Fibroblast growth factor/fibroblast growth factor receptor system in angiogenesis. *Cytokine Growth Factor Rev.* 16:159-78.
- Protin U, Schweighoffer T, Jochum W, Hilberg F. 1999. CD44-deficient mice develop normally with changes in subpopulations and recirculation of lymphocyte subsets. *J Immunol.* 163:4917-23.
- Pàez-Ribes M, Allen E, Hudock J, Takeda T, Okuyama H, Viñals F, Inoue M, Bergers G, Hanahan D, Casanovas O. 2009. Antiangiogenic therapy elicits malignant progression of tumors to increased local invasion and distant metastasis. *Cancer Cell.* 15:220-31.
- Päll T, Gad A, Kasak L, Drews M, Strömblad S, Kogerman P. 2004. Recombinant CD44-HABD is a novel and potent direct angiogenesis inhibitor enforcing endothelial cell-specific growth inhibition independently of hyaluronic acid binding. *Oncogene.* 23:7874-81.
- Rajasagi M, Vitacolonna M, Benjak B, Marhaba R, Zöller M. 2009. CD44 promotes progenitor homing into the thymus and T cell maturation. *J Leukoc Biol.* 85:251-61.
- Risau W. 1997. Mechanisms of angiogenesis. *Nature.* 386:671-4.
- Roelen BA, van Rooijen MA, Mummery CL. 1997. Expression of ALK-1, a type I serine/threonine kinase receptor, coincides with sites of vasculogenesis and angiogenesis in early mouse development. *Dev Dyn.* 209:418-30.
- Rohan RM, Fernandez A, Udagawa T, Yuan J, D'Amato RJ. 2000. Genetic heterogeneity of angiogenesis in mice. *FASEB J.* 14:871-6.

- Rouschop KMA, Roelofs JJTH, Claessen N, da Costa Martins P, Zwaginga J, Pals ST, Weening JJ, Florquin S. 2005. Protection against renal ischemia reperfusion injury by CD44 disruption. *J Am Soc Nephrol.* 16:2034-43.
- Rudini N, Felici A, Giampietro C, Lampugnani M, Corada M, Swirsding K, Garrè M, Liebner S, Letarte M, ten Dijke P, Dejana E. 2008. VE-cadherin is a critical endothelial regulator of TGF-beta signalling. *EMBO J.* 27:993-1004.
- Rymo SF, Gerhardt H, Wolfhagen Sand F, Lang R, Uv A, Betsholtz C. 2011. A two-way communication between microglial cells and angiogenic sprouts regulates angiogenesis in aortic ring cultures. *PLoS One.* 6:e15846.
- Saharinen P, Eklund L, Miettinen J, Wirkkala R, Anisimov A, Winderlich M, Nottebaum A, Vestweber D, Deutsch U, Koh GY, Olsen BR, Alitalo K. 2008. Angiopoietins assemble distinct Tie2 signalling complexes in endothelial cell-cell and cell-matrix contacts. *Nat Cell Biol.* 10:527-37.
- Savani RC, Cao G, Pooler PM, Zaman A, Zhou Z, DeLisser HM. 2001. Differential involvement of the hyaluronan (HA) receptors CD44 and receptor for HA-mediated motility in endothelial cell function and angiogenesis. *J Biol Chem.* 276:36770-8.
- Scharpfenecker M, van Dinther M, Liu Z, van Bezooijen RL, Zhao Q, Pukac L, Löwik CWGM, ten Dijke P. 2007. BMP-9 signals via ALK1 and inhibits bFGF-induced endothelial cell proliferation and VEGF-stimulated angiogenesis. *J Cell Sci.* 120:964-72.
- Schmidt SR. 2009. Fusion-proteins as biopharmaceuticals--applications and challenges. *Curr Opin Drug Discov Devel.* 12:284-95.
- Schmits R, Filmus J, Gerwin N, Senaldi G, Kiefer F, Kundig T, Wakeham A, Shahinian A, Catzavelos C, Rak J, Furlonger C, Zakarian A, Simard JJ, Ohashi PS, Paige CJ, Gutierrez-Ramos JC, Mak TW. 1997. CD44 regulates hematopoietic progenitor distribution, granuloma formation, and tumorigenicity. *Blood.* 90:2217-33.
- Schmitt M, Metzger M, Gradl D, Davidson G, Orian-Rousseau V. 2015. CD44 functions in Wnt signaling by regulating LRP6 localization and activation. *Cell Death Differ.* 22:677-89.
- Screaton GR, Bell MV, Jackson DG, Cornelis FB, Gerth U, Bell JI. 1992. Genomic structure of DNA encoding the lymphocyte homing receptor CD44 reveals at least 12 alternatively spliced exons. *Proc Natl Acad Sci U S A.* 89:12160-4.
- Seki T, Hong K, Oh SP. 2006. Nonoverlapping expression patterns of ALK1 and ALK5 reveal distinct roles of each receptor in vascular development. *Lab Invest.* 86:116-29.
- Sengupta S, Gherardi E, Sellers LA, Wood JM, Sasisekharan R, Fan TD. 2003. Hepatocyte growth factor/scatter factor can induce angiogenesis independently of vascular endothelial growth factor. *Arterioscler Thromb Vasc Biol.* 23:69-75.

- Sennino B, Ishiguro-Oonuma T, Wei Y, Naylor RM, Williamson CW, Bhagwandin V, Tabruyn SP, You W, Chapman HA, Christensen JG, Aftab DT, McDonald DM. 2012. Suppression of tumor invasion and metastasis by concurrent inhibition of c-Met and VEGF signaling in pancreatic neuroendocrine tumors. *Cancer Discov.* 2:270-87.
- Sherman LS, Rizvi TA, Karyala S, Ratner N. 2000. CD44 enhances neuregulin signaling by Schwann cells. *J Cell Biol.* 150:1071-84.
- Shojaei F, Wu X, Qu X, Kowanetz M, Yu L, Tan M, Meng YG, Ferrara N. 2009. G-CSF-initiated myeloid cell mobilization and angiogenesis mediate tumor refractoriness to anti-VEGF therapy in mouse models. *Proc Natl Acad Sci U S A.* 106:6742-7.
- Singleton PA, Dudek SM, Ma S, Garcia JGN. 2006. Transactivation of sphingosine 1-phosphate receptors is essential for vascular barrier regulation. Novel role for hyaluronan and CD44 receptor family. *J Biol Chem.* 281:34381-93.
- Singleton PA, Salgia R, Moreno-Vinasco L, Moitra J, Sammani S, Mirzapiozova T, Garcia JGN. 2007. CD44 regulates hepatocyte growth factor-mediated vascular integrity. Role of c-Met, Tiam1/Rac1, dynamin 2, and cortactin. *J Biol Chem.* 282:30643-57.
- Sitohy B, Nagy JA, Jaminet SS, Dvorak HF. 2011. Tumor-surrogate blood vessel subtypes exhibit differential susceptibility to anti-VEGF therapy. *Cancer Res.* 71:7021-8.
- Sleeman J, Rudy W, Hofmann M, Moll J, Herrlich P, Ponta H. 1996. Regulated clustering of variant CD44 proteins increases their hyaluronate binding capacity. *J Cell Biol.* 135:1139-50.
- Steinmetz NF, Maurer J, Sheng H, Bensussan A, Maricic I, Kumar V, Braciak TA. 2011. Two Domains of Vimentin Are Expressed on the Surface of Lymph Node, Bone and Brain Metastatic Prostate Cancer Lines along with the Putative Stem Cell Marker Proteins CD44 and CD133. *Cancers (Basel).* 3:2870-85.
- Strelkov SV, Herrmann H, Aebi U. 2003. Molecular architecture of intermediate filaments. *Bioessays.* 25:243-51.
- Styers ML, Salazar G, Love R, Peden AA, Kowalczyk AP, Faundez V. 2004. The endo-lysosomal sorting machinery interacts with the intermediate filament cytoskeleton. *Mol Biol Cell.* 15:5369-82.
- Suchting S, Freitas C, le Noble F, Benedito R, Bréant C, Duarte A, Eichmann A. 2007. The Notch ligand Delta-like 4 negatively regulates endothelial tip cell formation and vessel branching. *Proc Natl Acad Sci U S A.* 104:3225-30.
- Sugahara KN, Hirata T, Tanaka T, Ogino S, Takeda M, Terasawa H, Shimada I, Tamura J, ten Dam GB, van Kuppevelt TH, Miyasaka M. 2008. Chondroitin sulfate E fragments enhance CD44 cleavage and CD44-dependent motility in tumor cells. *Cancer Res.* 68:7191-9.

- Sulpice E, Ding S, Muscatelli-Groux B, Bergé M, Han ZC, Plouet J, Tobelem G, Merkulova-Rainon T. 2009. Cross-talk between the VEGF-A and HGF signalling pathways in endothelial cells. *Biol Cell*. 101:525-39.
- Suri C, Jones PF, Patan S, Bartunkova S, Maisonpierre PC, Davis S, Sato TN, Yancopoulos GD. 1996. Requisite role of angiopoietin-1, a ligand for the TIE2 receptor, during embryonic angiogenesis. *Cell*. 87:1171-80.
- Suzuki Y, Ohga N, Morishita Y, Hida K, Miyazono K, Watabe T. 2010. BMP-9 induces proliferation of multiple types of endothelial cells in vitro and in vivo. *J Cell Sci*. 123:1684-92.
- Swift MR, Weinstein BM. 2009. Arterial-venous specification during development. *Circ Res*. 104:576-88.
- Takahashi E, Nagano O, Ishimoto T, Yae T, Suzuki Y, Shinoda T, Nakamura S, Niwa S, Ikeda S, Koga H, Tanihara H, Saya H. 2010. Tumor necrosis factor-alpha regulates transforming growth factor-beta-dependent epithelial-mesenchymal transition by promoting hyaluronan-CD44-moesin interaction. *J Biol Chem*. 285:4060-73.
- Takahashi T, Yamaguchi S, Chida K, Shibuya M. 2001. A single autophosphorylation site on KDR/Flk-1 is essential for VEGF-A-dependent activation of PLC-gamma and DNA synthesis in vascular endothelial cells. *EMBO J*. 20:2768-78.
- Tammela T, Zarkada G, Wallgard E, Murtomäki A, Suchting S, Wirzenius M, Waltari M, Hellström M, Schomber T, Peltonen R, Freitas C, Duarte A, Isoniemi H, Laakkonen P, Christofori G, Ylä-Herttuala S, Shibuya M, Pytowski B, Eichmann A, Betsholtz C, Alitalo K. 2008. Blocking VEGFR-3 suppresses angiogenic sprouting and vascular network formation. *Nature*. 454:656-60.
- Tanikawa R, Tanikawa T, Hirashima M, Yamauchi A, Tanaka Y. 2010. Galectin-9 induces osteoblast differentiation through the CD44/Smad signaling pathway. *Biochem Biophys Res Commun*. 394:317-22.
- Tawfik OW, Kramer B, Shideler B, Danley M, Kimler BF, Holzbeierlein J. 2007. Prognostic significance of CD44, platelet-derived growth factor receptor alpha, and cyclooxygenase 2 expression in renal cell carcinoma. *Arch Pathol Lab Med*. 131:261-7.
- Teder P, Vandivier RW, Jiang D, Liang J, Cohn L, Puré E, Henson PM, Noble PW. 2002. Resolution of lung inflammation by CD44. *Science*. 296:155-8.
- Teriete P, Banerji S, Noble M, Blundell CD, Wright AJ, Pickford AR, Lowe E, Mahoney DJ, Tammi MI, Kahmann JD, Campbell ID, Day AJ, Jackson DG. 2004. Structure of the regulatory hyaluronan binding domain in the inflammatory leukocyte homing receptor CD44. *Mol Cell*. 13:483-96.
- Terzi F, Henrion D, Colucci-Guyon E, Federici P, Babinet C, Levy BI, Briand P, Friedlander G. 1997. Reduction of renal mass is lethal in mice lacking vimentin. Role of endothelin-nitric oxide imbalance. *J Clin Invest*. 100:1520-8.

- Thomas KA, Rios-Candelore M, Fitzpatrick S. 1984. Purification and characterization of acidic fibroblast growth factor from bovine brain. *Proc Natl Acad Sci U S A*. 81:357-61.
- Tremmel M, Matzke A, Albrecht I, Laib AM, Olaku V, Ballmer-Hofer K, Christofori G, Héroult M, Augustin HG, Ponta H, Orian-Rousseau V. 2009. A CD44v6 peptide reveals a role of CD44 in VEGFR-2 signaling and angiogenesis. *Blood*. 114:5236-44.
- Trochon V, Mabilat C, Bertrand P, Legrand Y, Smadja-Joffe F, Soria C, Delpech B, Lu H. 1996. Evidence of involvement of CD44 in endothelial cell proliferation, migration and angiogenesis in vitro. *Int J Cancer*. 66:664-8.
- Tsukita S, Oishi K, Sato N, Sagara J, Kawai A, Tsukita S. 1994. ERM family members as molecular linkers between the cell surface glycoprotein CD44 and actin-based cytoskeletons. *J Cell Biol*. 126:391-401.
- Tsuneki M, Madri JA. 2014. CD44 regulation of endothelial cell proliferation and apoptosis via modulation of CD31 and VE-cadherin expression. *J Biol Chem*. 289:5357-70.
- Upton PD, Davies RJ, Trembath RC, Morrell NW. 2009. Bone morphogenetic protein (BMP) and activin type II receptors balance BMP9 signals mediated by activin receptor-like kinase-1 in human pulmonary artery endothelial cells. *J Biol Chem*. 284:15794-804.
- Veronese FM, Pasut G. 2005. PEGylation, successful approach to drug delivery. *Drug Discov Today*. 10:1451-8.
- Wakahara K, Kobayashi H, Yagyu T, Matsuzaki H, Kondo T, Kurita N, Sekino H, Inagaki K, Suzuki M, Kanayama N, Terao T. 2005. Bikunin down-regulates heterodimerization between CD44 and growth factor receptors and subsequently suppresses agonist-mediated signaling. *J Cell Biochem*. 94:995-1009.
- Wang R, Chadalavada K, Wilshire J, Kowalik U, Hovinga KE, Geber A, Fligelman B, Leversha M, Brennan C, Tabar V. 2010. Glioblastoma stem-like cells give rise to tumour endothelium. *Nature*. 468:829-33.
- Wang Y, Kaiser MS, Larson JD, Nasevicius A, Clark KJ, Wadman SA, Roberg-Perez SE, Ekker SC, Hackett PB, McGrail M, Essner JJ. 2010. Moesin1 and Ve-cadherin are required in endothelial cells during in vivo tubulogenesis. *Development*. 137:3119-28.
- Wang YZ, Cao ML, Liu YW, He YQ, Yang CX, Gao F. 2011. CD44 mediates oligosaccharides of hyaluronan-induced proliferation, tube formation and signal transduction in endothelial cells. *Exp Biol Med (Maywood)*. 236:84-90.
- Weber GF, Bronson RT, Ilagan J, Cantor H, Schmits R, Mak TW. 2002. Absence of the CD44 gene prevents sarcoma metastasis. *Cancer Res*. 62:2281-6.

- Welti J, Loges S, Dimmeler S, Carmeliet P. 2013. Recent molecular discoveries in angiogenesis and antiangiogenic therapies in cancer. *J Clin Invest.* 123:3190-200.
- Xian X, Håkansson J, Ståhlberg A, Lindblom P, Betsholtz C, Gerhardt H, Semb H. 2006. Pericytes limit tumor cell metastasis. *J Clin Invest.* 116:642-51.
- Xu B, deWaal RM, Mor-Vaknin N, Hibbard C, Markovitz DM, Kahn ML. 2004. The endothelial cell-specific antibody PAL-E identifies a secreted form of vimentin in the blood vasculature. *Mol Cell Biol.* 24:9198-206.
- Xu Y, Gao XD, Lee J, Huang H, Tan H, Ahn J, Reinke LM, Peter ME, Feng Y, Gius D, Siziopikou KP, Peng J, Xiao X, Cheng C. 2014. Cell type-restricted activity of hnRNPM promotes breast cancer metastasis via regulating alternative splicing. *Genes Dev.* 28:1191-203.
- Xu Y, Stamenkovic I, Yu Q. 2010. CD44 attenuates activation of the hippo signaling pathway and is a prime therapeutic target for glioblastoma. *Cancer Res.* 70:2455-64.
- Yae T, Tsuchihashi K, Ishimoto T, Motohara T, Yoshikawa M, Yoshida GJ, Wada T, Masuko T, Mogushi K, Tanaka H, Osawa T, Kanki Y, Minami T, Aburatani H, Ohmura M, Kubo A, Suematsu M, Takahashi K, Saya H, Nagano O. 2012. Alternative splicing of CD44 mRNA by ESRP1 enhances lung colonization of metastatic cancer cell. *Nat Commun.* 3:883.
- Yan M, Callahan CA, Beyer JC, Allamneni KP, Zhang G, Ridgway JB, Niessen K, Plowman GD. 2010. Chronic DLL4 blockade induces vascular neoplasms. *Nature.* 463:E6-7.
- Yang C, Cao M, Liu H, He Y, Xu J, Du Y, Liu Y, Wang W, Cui L, Hu J, Gao F. 2012. The high and low molecular weight forms of hyaluronan have distinct effects on CD44 clustering. *J Biol Chem.* 287:43094-107.
- Yoon M, Moir RD, Prahlad V, Goldman RD. 1998. Motile properties of vimentin intermediate filament networks in living cells. *J Cell Biol.* 143:147-57.
- Yu Q, Stamenkovic I. 2000. Cell surface-localized matrix metalloproteinase-9 proteolytically activates TGF-beta and promotes tumor invasion and angiogenesis. *Genes Dev.* 14:163-76.
- Yu Q, Toole BP, Stamenkovic I. 1997. Induction of apoptosis of metastatic mammary carcinoma cells in vivo by disruption of tumor cell surface CD44 function. *J Exp Med.* 186:1985-96.
- Yu W, Woessner JFJ, McNeish JD, Stamenkovic I. 2002. CD44 anchors the assembly of matrilysin/MMP-7 with heparin-binding epidermal growth factor precursor and ErbB4 and regulates female reproductive organ remodeling. *Genes Dev.* 16:307-23.
- Zarnegar R. 1995. Regulation of HGF and HGFR gene expression. *EXS.* 74:33-49.
- Zeilstra J, Joosten SPJ, Dokter M, Verwiel E, Spaargaren M, Pals ST. 2008. Deletion of the WNT target and cancer stem cell marker CD44 in

- Apc(Min/+) mice attenuates intestinal tumorigenesis. *Cancer Res.* 68:3655-61.
- Zeilstra J, Joosten SPJ, van Andel H, Tolg C, Berns A, Snoek M, van de Wetering M, Spaargaren M, Clevers H, Pals ST. 2014. Stem cell CD44v isoforms promote intestinal cancer formation in Apc(min) mice downstream of Wnt signaling. *Oncogene.* 33:665-70.
- Zhang J, Fukuhara S, Sako K, Takenouchi T, Kitani H, Kume T, Koh GY, Mochizuki N. 2011. Angiopoietin-1/Tie2 signal augments basal Notch signal controlling vascular quiescence by inducing delta-like 4 expression through AKT-mediated activation of beta-catenin. *J Biol Chem.* 286:8055-66.
- Zhang S, Balch C, Chan MW, Lai H, Matei D, Schilder JM, Yan PS, Huang TH, Nephew KP. 2008. Identification and characterization of ovarian cancer-initiating cells from primary human tumors. *Cancer Res.* 68:4311-20.
- Zhang Y, Su Y, Volpert OV, Vande Woude GF. 2003. Hepatocyte growth factor/scatter factor mediates angiogenesis through positive VEGF and negative thrombospondin 1 regulation. *Proc Natl Acad Sci U S A.* 100:12718-23.
- Zhao L, Lee E, Zukas AM, Middleton MK, Kinder M, Acharya PS, Hall JA, Rader DJ, Puré E. 2008. CD44 expressed on both bone marrow-derived and non-bone marrow-derived cells promotes atherosclerosis in ApoE-deficient mice. *Arterioscler Thromb Vasc Biol.* 28:1283-9.
- Zou Y, He L, Chi F, Jong A, Huang S. 2008. Involvement of Escherichia coli K1 iibeT in bacterial adhesion that is associated with the entry into human brain microvascular endothelial cells. *Med Microbiol Immunol.* 197:337-44.
- del Toro R, Prahst C, Mathivet T, Siegfried G, Kaminker JS, Larrivee B, Breant C, Duarte A, Takakura N, Fukamizu A, Penninger J, Eichmann A. 2010. Identification and functional analysis of endothelial tip cell-enriched genes. *Blood.* 116:4025-33.
- di Tomaso E, Snuderl M, Kamoun WS, Duda DG, Auluck PK, Fazlollahi L, Andronesi OC, Frosch MP, Wen PY, Plotkin SR, Hedley-Whyte ET, Sorensen AG, Batchelor TT, Jain RK. 2011. Glioblastoma recurrence after cediranib therapy in patients: lack of "rebound" revascularization as mode of escape. *Cancer Res.* 71:19-28.
- van Beijnum JR, Dings RP, van der Linden E, Zwaans BMM, Ramaekers FCS, Mayo KH, Griffioen AW. 2006. Gene expression of tumor angiogenesis dissected: specific targeting of colon cancer angiogenic vasculature. *Blood.* 108:2339-48.

## ACKNOWLEDGEMENTS

This study was performed at the Department of Gene Technology, Tallinn University of Technology and the Competence Centre for Cancer Research.

First and foremost, I would like to thank my supervisor, Dr. Taavi Päll. He was the one who introduced me to experimental skills and the field of molecular and cell biology at the beginning of my bachelor studies and has guided and supported me ever since. I would like to express my gratitude to Dr. Andres Valkna for supervising me during the last years of my doctoral studies. I am grateful to Taavi and Andres for their endless enthusiasm and for encouraging me to finish my PhD studies.

I thank my former supervisor Dr. Priit Kogerman, who gave me the chance to work in his lab and be a part of the CD44 project team. I am very grateful to all my co-authors and former colleagues from Celecure and CCCR for their contribution to the CD44 project. My special thanks go to Aili – your friendly and supportive attitude is always appreciated. Your practical mind provided the control over the project and kept our feet on the ground when needed. Marianna and Marina, thank you for your contribution to the CD44 project, it was invaluable. The former colleagues from Priit Kogerman's lab – Lagle, Wally, Robi, Piret T, Piret M, Alla, Olja, Kristi L, Maarja L, Illar, Pille, Jaak, Lembi, Torben and Kersti – thank you all for providing the pleasant and friendly work environment! I also thank my former students Kristine and Kristiina for the opportunity to learn how to teach and supervise.

I want to express my deepest gratitude to Lagle – your help and presence during my studies cannot be overestimated. Your friendship, invaluable advice and moral support, but also constructive criticism, when needed, have kept me motivated and helped me to finish this thesis.

My sincerest thanks go to my family – my mother and father, Andres, Anu, Mann, Krista, Salme, Fredi, Margit and Merit – thank you all for your unlimited support. You are always around and inspire me to keep up the positive way of thinking. I am especially grateful to my mother, who has taken care that I would not strain myself too much and urged me to take some breakouts and visit her more often. My sisters and their children are my inspiration! They always keep up my spirit and bring much joy and fun to my life.

My warmest and deepest gratitude goes to my dearest Priit, who has put up with me all these years during my long-lasting doctoral studies. Thank you for your love and support!



## **PUBLICATION I**

**Pink, A**, Kallastu, A, Turkina, M, Školnaja, M, Kogerman, P, Päll, T, Valkna, A (2014). Purification, characterization and plasma half-life of PEGylated soluble recombinant non-HA-binding CD44. *BioDrugs*, 28, 4:393-402.



## Purification, Characterization and Plasma Half-Life of PEGylated Soluble Recombinant Non-HA-Binding CD44

Anne Pink · Aili Kallastu · Marina Turkina ·  
Marianna Skolnaja · Priit Kogerman ·  
Taavi Päll · Andres Valkna

Published online: 25 February 2014  
© Springer International Publishing Switzerland 2014

### Abstract

**Background and Objectives** The aim of this study was to increase the serum half-life of recombinant CD44 hyaluronan (HA) binding domain by PEGylation. We have previously found that recombinant soluble CD44 HA binding domain (CD44HABD) and its non-HA-binding triple mutant CD44HABD<sup>R41AY78SY79S</sup> (CD44-3MUT) inhibits angiogenesis and subcutaneous tumor growth. However, this ~12 kDa recombinant protein displays a high serum clearance rate.

**Methods** Here, we report the purification of monomeric CD44-3MUT from urea solubilized inclusion bodies using weak anion exchange chromatography and gel filtration. To increase the serum residence time of CD44-3MUT we PEGylated the resulting protein using 20 kDa methoxy-PEG-propionaldehyde.

**Results** PEGylation of CD44-3MUT prolonged its in vivo serum half-life about 70-fold from 0.03 to 1.8 hours. Along with extended plasma residence time, PEGylation also increased the systemic exposure. By cell impedance assay we confirmed that PEGylated CD44-3MUT maintained its in vitro function. The results from the impedance assay

additionally demonstrate that the CD44-3MUT effect on endothelial cells is mediated by vimentin.

**Conclusions** In summary, we have developed a purification protocol for large-scale production of CD44-3MUT and generated a PEGylated form of CD44-3MUT. HA binding domain of CD44(CD44HABD) and its modified non-HA binding form (CD44-3MUT) inhibit angiogenesis and tumor growth in vivo without disturbing HA-binding functions. CD44-3MUT has been PEGylated for use as a new type of anti-angiogenic human drug. PEGylation of CD44-3MUT improved pharmacokinetic properties but retains its functional activity.

### Abbreviations

AUC	Area under curve
C <sub>0</sub>	Initial plasma protein concentration
CD44HABD	CD44 hyaluronan binding domain
CD44-3MUT	Non-hyaluronan binding mutant of CD44HABD–CD44HABD <sup>R41AR78SY79S</sup>
CL	Total body clearance
CV	Column volumes
FT	Flow through fraction
GF	Gel filtration chromatography
GST-CD44-3MUT	CD44-3MUT GST-fusion protein
HA	Hyaluronan
IB	Inclusion bodies
ID	Initial dose of injected protein
IEC	Ion exchange chromatography
MLEC	Mouse lung endothelial cells
MS	Mass-spectrometric analysis
PEG	Polyethylene glycol
T <sub>1/2</sub>	Plasma half-life
%TBW	Percent of total body weight
V <sub>d</sub>	Volume of distribution

**Electronic supplementary material** The online version of this article (doi:10.1007/s40259-014-0089-y) contains supplementary material, which is available to authorized users.

A. Pink · M. Skolnaja · P. Kogerman · T. Päll · A. Valkna (✉)  
Department of Gene Technology, Tallinn University of  
Technology, Akadeemia tee 15, 12618 Tallinn, Estonia  
e-mail: andres.valkna@ttu.ee

A. Pink · A. Kallastu · M. Turkina · M. Skolnaja ·  
P. Kogerman · T. Päll · A. Valkna  
Competence Centre for Cancer Research, Akadeemia tee 15,  
12618 Tallinn, Estonia

## 1 Introduction

CD44 is an integral membrane glycoprotein, which functions as a hyaluronan (HA) receptor. Membrane CD44 mediates adhesion to HA and has physiological functions in lymphocyte homing and in cell–cell adhesions. Additionally, CD44 is present as a soluble circulating form in lymph and serum [1–5]. The soluble CD44 level is elevated in patients with several tumor types, and is mainly generated by ectodomain shedding by matrix metalloproteases [4, 6]. Overexpression of secreted CD44 extracellular domain in tumor cells inhibits proliferation and subcutaneous tumor growth [7]. We have previously found that recombinant CD44 HA binding domain (CD44HABD) functions as an angiogenesis inhibitor [8]. These effects were independent of HA binding, since the non-HA binding mutant of CD44HABD – CD44HABD<sup>R41AR78SY79S</sup> (CD44-3MUT) displayed similar effects. Successful large-scale purification of bacterially expressed recombinant CD44HABD has been reported by two groups [9, 10]. Both groups used the same purification method developed by Banerji et al. [9], where essentially all expressed protein resulted in inclusion bodies (IBs) and the bottleneck of CD44HABD purification was the refolding step.

PEGylation, a covalent conjugation of protein with polyethylene glycol (PEG), is commonly used to improve in vivo potency of protein-based therapeutics [11, 12]. Protein PEGylation increases its hydrodynamic radius resulting in reduced renal excretion rate and increased plasma half-life. Additionally, PEGylation masks protein surface, and reduces protease degradation and immunogenicity.

Recombinant bacterially expressed CD44-3MUT exhibits very short plasma half-life in vivo. Thus, the goal for this study was to improve the pharmacokinetic properties of recombinant CD44-3MUT.

## 2 Materials and Methods

### 2.1 Cell Culture, Antibodies and Reagents

Mouse lung endothelial cells (MLEC) were isolated and grown as previously described [13]. Anti-CD44-3MUT mouse mAb 1A2.H4 was produced by LabAS (Tartu, Estonia). Anti-CD44-3MUT rabbit pAb A148 was produced by Inbio AS (Tallinn, Estonia) [13]. Anti-PEG rabbit mAb PEG-B-47 (#2061-1) was from Epitomics (Burlingame, CA, USA). Anti-beta-catenin mouse mAb (E-5) (#sc-7963) was from Santa Cruz Biotechnology (Santa Cruz, CA, USA). All enzymes used for cloning were from Fermentas (Vilnius, Lithuania).

### 2.2 Protein Expression and Purification

Recombinant CD44-3MUT GST-fusion protein (GST-CD44-3MUT) was prepared as described [8]. A codon optimized CD44-3MUT gene was assembled from synthetic oligonucleotides and/or polymerase chain reaction (PCR) products, and was cloned into pGA14 vector. The codon optimization and gene synthesis was performed by GeneArt Gene Synthesis service (Life Technologies, Carlsbad, CA, USA). CD44-3MUT was further PCR amplified from pGA14 vector and the resulting PCR fragment was cloned into the NdeI/HindIII site of pET11c vector (Novagen, Darmstadt, Germany).

The detailed protocol for CD44-3MUT expression and purification is described in the Supplementary Methods (Online Resource 1). Briefly, CD44-3MUT was expressed in *BL21-CodonPlus(DE3)-RP strain* in autoinduction media [14] at 37° C for 20 hours. CD44-3MUT was purified from IBs by ion exchange chromatography (IEC) and subsequent gel filtration (GF). Refolding was performed by stepwise dialysis from 8 M urea solution into phosphate buffered saline (PBS). Purified proteins were sterile filtered using 0.22 µm low protein-binding filter (Millipore), concentrated using 10 kDa MW cut-off centrifugal filter devices (Millipore), lyophilized, and stored at 4 °C.

### 2.3 Analysis of Protein Purity

The purity and monomer content of PEGylated and non-PEGylated proteins were analyzed by GF, and by sodium dodecyl sulfate polyacrylamide gel electrophoresis (SDS-PAGE) in Tris-Tricine buffer system under reducing or nonreducing conditions. The purity and content of protein preparations was assessed by densitometric analysis of Coomassie brilliant blue stained SDS-PAGE gel. For densitometric analysis, ImageJ software (<http://imagej.nih.gov/ij/>) was used. For PEG detection, the gel was incubated with 5 % BaI<sub>2</sub> solution in H<sub>2</sub>O. After 10 minutes incubation, approximately 10 % of volume 0.1 M iodine solution in 50 % ethanol was added for color development. Matrix-assisted laser desorption/ionization–time of flight (MALDI-TOF) mass-spectrometric analysis (MS) was performed using Autoflex II TOF/TOF instrument and flexControl 3.0 software (Bruker Daltonics). 2,5-dihydroxybenzoic acid was used as MALDI matrix. Before spotting, samples were desalted using micro-ZipTip pipette tips with C18 resin (Millipore). For peptide mass fingerprinting proteins were digested with trypsin (sequencing grade porcine trypsin; Promega) or Glu-C endopeptidase (sequencing grade; Roche). Protein concentration was determined by bicinchoninic acid (BCA) assay (Thermo Scientific). Endotoxin level of purified proteins was measured using Endosafe-PTS (Charles River, L'Arbresle,

France). Endotoxin values of different protein batches were 22–93 EU/mg.

## 2.4 PEGylation of CD44-3MUT

Purified CD44-3MUT was conjugated with 20 kDa methoxy-PEG-propionaldehyde (Jenkem Technology USA, Allen, TX, USA) in the presence of 200-fold molar excess of NaBH<sub>3</sub>CN as reducing agent. The reaction was performed in PBS pH 7.4 for 24 hours. After 6 and 22 hours the reaction mixture was supplemented with an additional dose of reducer in 100- and 50-fold molar excess, respectively. The reaction mixture was dialyzed against 10 mM phosphate buffer by three consecutive steps and loaded to a strong anion exchange column Mono Q 4.6/100 PE (GE Healthcare) equilibrated with 10 mM phosphate buffer pH 7.4. After washing the column with five column volumes (CV) of 10 mM phosphate buffer, PEGylated CD44-3MUT was eluted by a linear gradient of 0–1 M NaCl in 10 mM phosphate buffer. Fractions containing the mono-PEGylated protein were pooled and dialyzed against PBS.

## 2.5 Pharmacokinetic Studies

The female Fisher 344/NHsd rats (body weight 170–178 g) were used for this study (Harlan Laboratories). The rats were injected intravenously with 1 mg of PEG-CD44-3MUT, 1 mg of CD44-3MUT, or 0.75 mg of GST-CD44-3MUT in 1 ml of PBS into the tail vein proximal site. Blood samples were collected from the cannula installed into the jugular vein. The plasma levels of test proteins were quantified by sandwich ELISA using 1A2.H4 antibody for GST-CD44-3MUT and CD44-3MUT capture, and PEG-B-47 antibody for PEG-CD44-3MUT capture. A148 and 1A2.H4 antibodies were used as detection antibodies, respectively. Vectastain<sup>®</sup> ABC kit (Vector Laboratories, Burlingame, CA, USA) and tetramethylbenzidine substrate were used for color development and absorbance was measured using ELISA plate reader (Tecan, Männedorf, Switzerland). Plasma concentrations of tested proteins were interpolated from the standard curves generated by using serums with known concentrations of proteins.

## 2.6 Internalization of PEGylated CD44-3MUT, Immunofluorescence Microscopy and Impedance Assay

Internalization assay and immunofluorescence microscopy were performed as previously described [13]. For the internalization assay, MLEC were seeded into 0.1 % gelatin-coated, 8-well microscopy slides at density 20,000 cells/well. Cell-bound CD44-3MUT was detected using 1A2.H4 mAb and anti-mouse-Alexa 488 conjugated secondary Ab

(Molecular Probes). Hoechst staining was used to identify nuclei and anti-beta-catenin staining was used to identify cell borders and cytoplasm. For automated image analysis, confocal image stacks were converted to maximum intensity projections using Fiji package (<http://pacific.mpi-cbg.de/wiki/index.php/Fiji>). CellProfiler 2.0 (r10415) [15] was used for image segmentation and quantitation. The measurement of cell layer resistance was performed using the ECIS Z-theta instrument, ECIS software and 96W10E + arrays (Applied Biophysics, Troy, NY, USA). The arrays were cysteine pretreated according to manufacturers instructions and coated with 1 µg/mL fibronectin in PBS. Cells were seeded at 10,000 cells/well, treatments were started 24 hours later.

## 2.7 Statistical Data Analysis

Data represent mean ± SE. Statistical analysis and non-linear fitting of data was performed using GraphPad Prism 5 software (GraphPad Software, San Diego, CA, USA), and R (version 2.15.1) [16]. Plasma half-life ( $T_{1/2}$ ), initial plasma protein concentration ( $C_0$ ) and the area under curve (AUC, µg·h/ml) were estimated by using non-linear regression. AUC was also expressed as %ID·h/mL (ID, initial dose of injected protein) and calculated as (AUC/ID) × 100 %. Other parameters were calculated as follows: total body clearance (CL) = dose/AUC, volume of distribution ( $V_d$ ) = dose/ $C_0$ .  $V_d$  was expressed as percent of total body weight (%TBW).

## 3 Results

### 3.1 CD44-3MUT Expressed in Inclusion Bodies

CD44-3MUT contains residues 27-132 according to human CD44 (Fig. 1a) and carries aa substitutions R41A, R78S and Y79S, which abolish CD44 HA binding property [8, 17]. We cloned CD44-3MUT into pET11c vector and expressed it in *BL21-CodonPlus(DE3)-RP* strain in autoinduction media. See Supplementary Table 1 (Online Resource 1) for a summary of the CD44-3MUT purification protocol. Typical yield of wet weight bacterial mass was 9–12 g/L culture. SDS-PAGE analysis showed that CD44-3MUT was expressed with an apparent molecular mass of ~12 kDa (Fig. 1b). CD44-3MUT was mostly expressed into insoluble protein fraction (Fig. 1b). Therefore, we purified CD44-3MUT from IBs. After dissolving isolated IBs in 8 M urea-buffer and removal of insoluble material, soluble IB lysate contained a considerable amount of CD44-3MUT (Fig. 1b). The yield of CD44-3MUT in soluble IB lysate was approximately 25 mg/g of wet bacterial mass, as calculated from densitometry analysis of Coomassie stained SDS-PAGE gel.

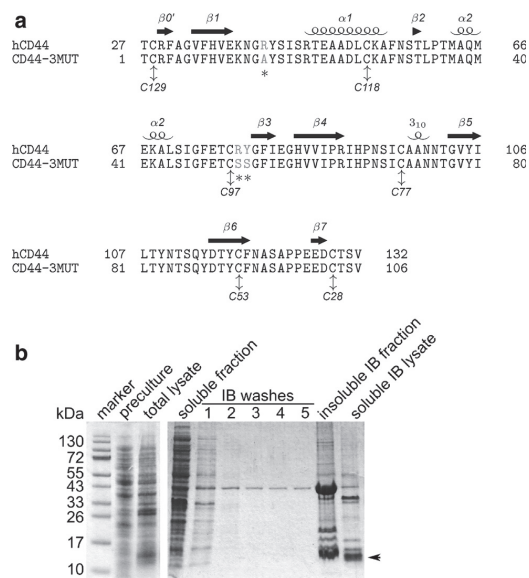


**Fig. 1** Expression of CD44-3MUT and isolation of inclusion bodies (IBs). **a** Sequence alignment of human CD44 (hCD44) and CD44-3MUT protein. The mutated residues in CD44-3MUT (R41A, R78S, and Y79S) are indicated by asterisks. The secondary structure elements are based on the Teriete et al. [19] study. Right arrows  $\beta$ -sheets, helices  $\alpha$ -helices and  $3_{10}$ -helix. Disulphide bonds between cysteine residues are indicated by up and down arrows. Note the absence of initial methionine residue in the CD44-3MUT sequence, which, according to MS analysis, is excised by aminopeptidase (see Supplementary Table 2 in Online Resource 1). **b** (left panel) SDS-PAGE analysis of CD44-3MUT expression. CD44-3MUT was expressed in autoinduction media for 20 h at 37 °C. CD44-3MUT (indicated by arrow) expression was estimated by analyzing samples from preculture and final culture (total lysate). **b** (right panel) SDS-PAGE analysis of IB purification course. CD44-3MUT expressing cells were lysed and soluble fraction was separated from IBs by centrifugation. After washing (IB washes), IBs were solubilized in 8 M urea containing buffer and centrifuged to separate insoluble IB fraction. CD44-3MUT containing soluble IB lysate was used for further CD44-3MUT purification

### 3.2 CD44-3MUT Purification by Ion Exchange and Subsequent Size-Exclusion Chromatography

We used weak anion exchange chromatography for the first CD44-3MUT purification step. The soluble IB fraction was applied onto a DEAE FF column and the proteins were eluted by stepwise and linear gradient of NaCl (Fig. 2a). In order to prevent protein carbamylation of urea-dissolved IBs, buffer B was supplemented with ethylenediamine (see Supplementary methods, Online Resource 1). Ethylenediamine addition resulted in a shift of CD44-3MUT into flow through fraction (FT), as shown by SDS-PAGE analysis of eluted IEC fractions (Fig. 2b). Most of the CD44-3MUT

protein was eluted in FT and peak 1 and peak 2 contained only a small amount of CD44-3MUT. In FT, CD44-3MUT appeared to be in its monomeric state, peak 1 and 2 contained mostly covalently aggregated or oligomeric CD44-3MUT as assessed by SDS-PAGE analysis under nonreducing conditions (Fig. 2b). For further purification, we pooled CD44-3MUT containing FT and termed it as IEC pool. To separate monomeric CD44-3MUT from oligomeric forms and other remaining *E. coli* contaminants we further purified CD44-3MUT containing IEC pool by GF on HiLoad 26/60 Superdex 200 column (Fig. 2c). Peak 3 contained a considerable amount of pure monomeric CD44-3MUT as found by SDS-PAGE under reducing and nonreducing conditions (Fig. 2d; data not shown for peak 1 and 2). We pooled fractions containing purified monomeric CD44-3MUT and used this pool in refolding steps.

### 3.3 Refolding and MALDI-TOF MS Characterization of Monomeric CD44-3MUT

We used seven dialysis steps for renaturation of CD44-3MUT from 8 M urea solution into PBS. The final yield of purified CD44-3MUT was 1–1.3 mg/g of wet bacterial mass. Analysis of refolded protein by SDS-PAGE showed that apparently all CD44-3MUT was in monomeric form (Fig. 2e). The monomeric form of CD44-3MUT was further confirmed by GF analysis (Fig. 2f).

SDS-PAGE analysis under nonreducing conditions showed that CD44-3MUT always migrated as two close bands, both close to the molecular size of monomeric CD44-3MUT (Fig. 2b, d, e). MALDI-TOF MS fingerprinting showed that these bands contained CD44-3MUT. Further, MALDI-TOF MS low resolution peptide fingerprinting of tryptic peptides suggested that these bands represent forms with different numbers of intramolecular disulphide bridges, whereas, under nonreducing conditions, the fastest migrating band corresponds to species with three disulphide bridges (data not shown). Cys-118 (see Fig. 1a), containing a disulphide bridge, was still present in the reduced sample. Densitometric quantization of three preparations shows that the upper band represents about  $30 \pm 4.7\%$  and lower band  $70 \pm 4.7\%$  material (Fig. 2e, nonreducing conditions). Therefore, we assumed that these bands represent conformational variants of CD44-3MUT. We were not able to separate these putative forms, either by IEC or GF.

Calculated average mass of CD44-3MUT is 11,497.8 Da, assuming that the N-terminal methionine of the protein is excised. MALDI-TOF MS analysis of CD44-3MUT showed that the average molecular mass of the protein was 11,500.4 Da (mass difference +2.6 Da; relative error 226 ppm; Fig. 2g). To confirm the identity of purified protein, we performed MALDI-TOF MS

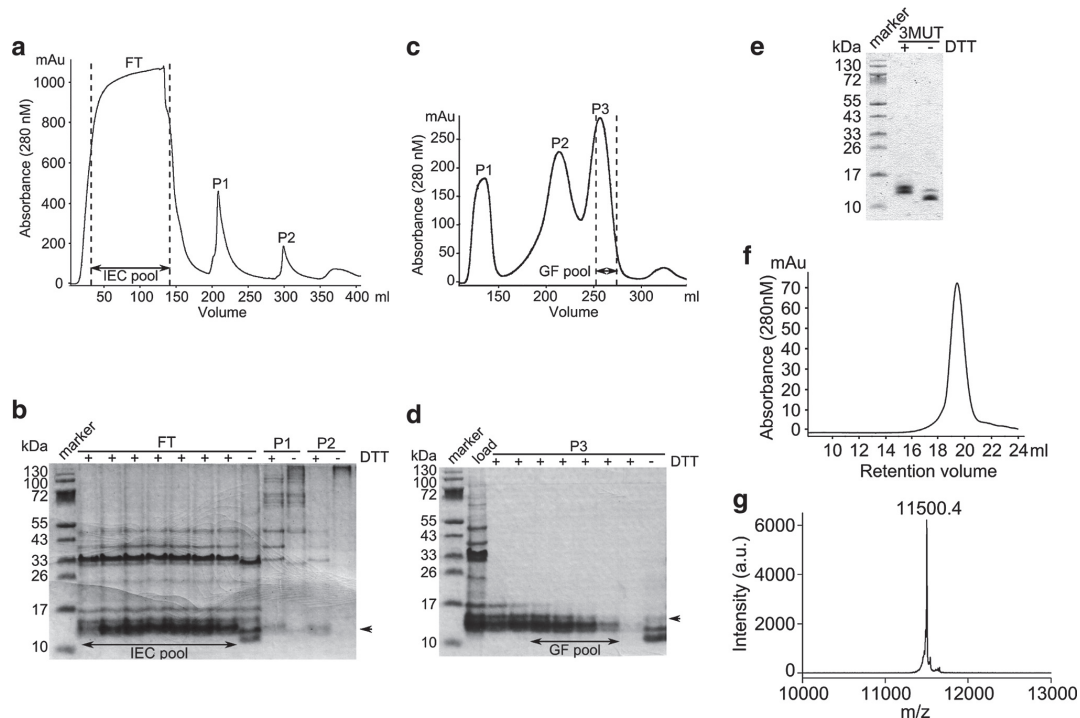


**Fig. 2** Purification of CD44-3MUT. **a** Ion exchange chromatogram of urea dissolved inclusion bodies (IBs). Soluble IB lysate was loaded onto HiPrep 16/10 diethylaminoethanol (DEAE) FF 20 ml column and bound proteins were eluted by stepwise and linear gradient of NaCl. Eluates from flow through fraction (FT) and from first and second peak (P1 and P2, respectively) were collected throughout ion exchange chromatography (IEC) and analyzed on sodium dodecyl sulfate polyacrylamide gel electrophoresis (SDS-PAGE). **b** Eluates containing monomeric CD44-3MUT (shown by arrow) were pooled (IEC pool). **c** Gel filtration (GF) chromatogram of IEC purified CD44-

3MUT. IEC pool containing CD44-3MUT (load) was applied onto HiLoad 26/60 Superdex 200 preparation grade column. Proteins eluted in 3 peaks (P1, P2, and P3). Fractions from P3 were analyzed on SDS-PAGE (**d**) and those containing monomeric CD44-3MUT were pooled (GF pool) for refolding. **e** SDS-PAGE analysis of refolded CD44-3MUT (3MUT). SDS-PAGE analysis was performed under reducing (+DTT) and nonreducing (-DTT) conditions. **f** GF analysis of purified CD44-3MUT (250 µg, Superdex 200 10/300 GL preparation grade column). **g** MALDI-TOF mass spectrum of purified CD44-3MUT

fingerprinting of Glu-C or trypsin digested CD44-3MUT. Fingerprinting results showed that Glu-C and trypsinolysis peptide spectra together covered 100 % of the CD44-3MUT sequence (see Supplementary Table 2 in Online Resource 1). Glu-C digestion of CD44-3MUT also confirmed the excision of N-terminal methionine.

### 3.4 Preparation of PEGylated CD44-3MUT

In order to improve pharmacokinetic properties of CD44-3MUT we decided to conjugate it with 20 kDa methoxy-PEG-propionaldehyde (see Sect. 2). Our PEGylation strategy involved the use of aldehyde functionalized PEG derivatives that predominantly react with N-terminal α-amino group at pH 5–8. We used SDS-PAGE staining with Coomassie brilliant blue or PEG-specific Ba<sub>2</sub> to

analyze the PEGylation reaction mixture. Expected molecular weight of monoPEG-CD44-3MUT is 31.6 kDa. However, we found that PEG and its conjugates moved about 18 kDa higher than expected on SDS-PAGE, as 20 kDa PEG migrated at ~38 kDa and PEG-CD44-3MUT at ~50 kDa on gel (Fig. 3a). This could be due to poor binding of SDS. MALDI-TOF MS analysis of PEG-CD44-3MUT showed that PEGylation reaction had produced ~33 and ~54 kDa products (Supplementary Fig. 1a in Online Resource 1). 33 kDa species corresponds to the calculated mass of mono-PEGylated and 54 kDa corresponds to di-PEGylated CD44-3MUT. Taken together, MS data confirms quite confidently that the ~50 kDa band on SDS-PAGE gel represents the mono-PEGylated form of CD44-3MUT. PEG attachment could significantly alter the mobility of conjugate in the gel matrix and therefore it is

difficult to use protein markers to identify the molecular mass of PEGylated conjugates.

Although SDS-PAGE showed that, preferentially, mono-PEGylated CD44-3MUT was formed during the reaction (Fig. 3a), we also detected bands with larger molecular weights on gel, and  $\sim 54$  kDa peak was also present in MS analysis, which indicates that, to some extent, di- and oligo-PEGylated products also formed during the reaction. Thus, we used IEC with a strong anion exchange column to isolate mono-PEGylated CD44-3MUT from the reaction mixture. We found that although mono-PEGylated CD44-3MUT was sufficiently separated from oligo-PEGylated products by IEC, we were unable to purify monoPEG-CD44-3MUT to homogeneity, as minor amounts of unmodified and di-PEGylated CD44-3MUT coeluted with the mono-PEGylated product in the same fraction (Fig. 3b). Immunoblotting and MS analysis also confirmed that a minor quantity of unmodified and di-PEGylated CD44-3MUT was present in IEC-purified PEG-CD44-3MUT preparation (Fig. 3c, Supplementary Fig. 1a in Online Resource 1). We evaluated the purity of PEG-CD44-3MUT preparation by densitometric analysis of Coomassie-stained SDS-PAGE gel. The analysis of three different PEG-CD44-3MUT batches showed that our preparations contain, on average,  $66.7 \pm 0.7$  % of mono-PEG-CD44-3MUT,  $10.5 \pm 3.0$  % of diPEG-CD44-3MUT and  $22.8 \pm 2.6$  % of unmodified CD44-3MUT. To map the PEG attachment site of PEG-CD44-3MUT, we performed MALDI-TOF MS fingerprinting. Analysis of GluC digested PEG-CD44-3MUT showed that its N-terminal peptides are depleted from mass spectrum compared with unmodified CD44-3MUT, which is consistent with N-terminal PEGylation (Supplementary Fig. 1b in Online Resource 1).

### 3.5 In Vivo Plasma Half-Life of PEGylated CD44-3MUT

Initial experiments using a mouse model to determine CD44-3MUT pharmacokinetic properties showed very short plasma half-life—0.038 hours (Supplementary Table 3 and Supplementary Fig. 3 in Online Resource 1). To test whether PEGylation improved the pharmacokinetics of CD44-3MUT we injected female Fisher 344/NHsd rats intravenously with unmodified or PEGylated CD44-3MUT. We also included GST-CD44-3MUT [8] to the study. GST-CD44-3MUT was purified from a soluble fraction of *E. coli* lysate by affinity chromatography [8] (Supplementary Fig. 2 in Online Resource 1). No signs of systemic toxicity were observed during experiments.

To determine the plasma concentration of test proteins following intravenous injection, we used a sandwich ELISA assay. The obtained protein plasma concentration time curves are shown in Fig. 4, and calculated pharmacokinetic properties are summarized in Table 1. Pharmacokinetic analysis showed that unmodified CD44-3MUT and GST-CD44-3MUT were rapidly cleared from rat circulation. In contrast, PEG coupling to CD44-3MUT extended its plasma half-life about 70-fold. In accordance with the increase in plasma residence time, PEGylation also considerably increased the systemic exposure (as measured by AUC) and respectively decreased the plasma clearance of CD44-3MUT when compared with unmodified proteins. Tested proteins displayed volume of distribution values from 2 to 6 % of TBW, which indicates that all these proteins were confined to plasma water. However, volume of distribution of unmodified CD44-3MUT in a mouse model was 23 % of TBW (Supplementary Table 3

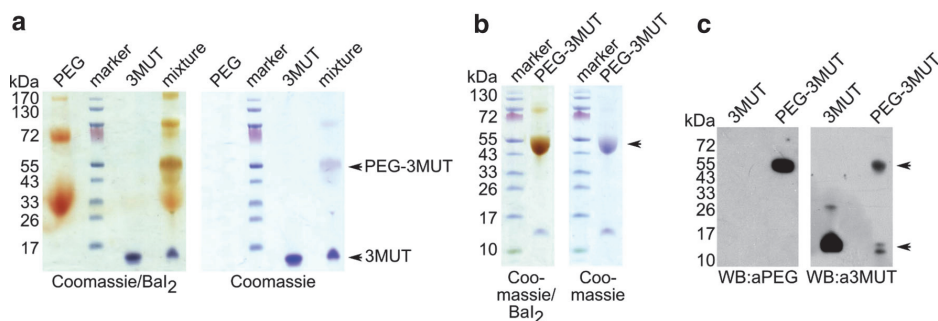


**Fig. 3** PEGylation of CD44-3MUT. **a** Sodium dodecyl sulfate polyacrylamide gel electrophoresis (SDS-PAGE) analysis of CD44-3MUT (3MUT) PEGylation reaction. CD44-3MUT was conjugated with 20 kDa methoxy-PEG-propionaldehyde. PEG, 3MUT and PEGylation reaction mixture (mixture) were analyzed by SDS-PAGE. **b** SDS-PAGE analysis of purified PEG-CD44-3MUT (PEG-3MUT). PEG-3MUT was purified from reaction mixture by ion exchange

chromatography (IEC) (Mono Q 4.6/100 PE column). SDS-PAGE gels were co-stained with Coomassie brilliant blue R-250 and PEG specific Bal<sub>2</sub> (**a**, **b** left panels) or Coomassie brilliant blue alone (**a**, **b** right panels). **c** Western blot analysis (WB) of 3MUT and PEG-3MUT detected with anti-PEG (aPEG, left panel) or anti-CD44-3MUT (a3MUT, right panel) antibodies. Unmodified and mono-PEGylated CD44-3MUT are indicated by arrows

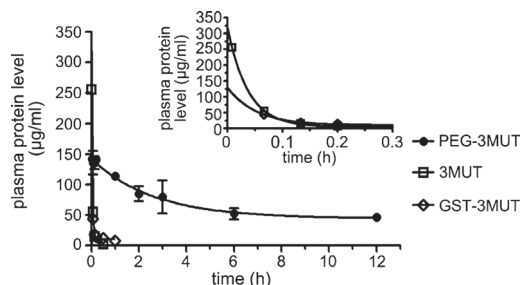


**Fig. 4** Plasma half-life of CD44-3MUT. Rats were injected intravenously with PEG-CD44-3MUT (PEG-3MUT;  $N = 2$ ), CD44-3MUT (3MUT;  $N = 1$ ) or GST-CD44-3MUT (GST-3MUT;  $N = 1$ ). Protein plasma levels were measured by ELISA assay. Data are represented as mean  $\pm$  SE. As non-PEGylated proteins display very short plasma half-life, these are also plotted on the graph with a shorter time scale (*inset*)

in Online Resource 1), consistent with distribution to extracellular water. Given the fact that we used several-fold higher doses in rats than in mice ( $C_0$  in rats 70–300 vs 10  $\mu\text{g/ml}$  in mice), this difference in  $V_d$ -s could result from saturation of the extracellular water compartment. Together, these data show that PEGylation clearly improves the pharmacokinetic properties of CD44-3MUT.

### 3.6 PEG-CD44-3MUT is Endocytosed and Suppresses Cell–Cell Adhesions Comparably to Unmodified CD44-3MUT

CD44HABD and CD44-3MUT bind to endothelial cells via vimentin and become endocytosed [13]. Therefore, to assess PEGylated CD44-3MUT *in vitro* activity, we investigated its cellular uptake similarly to the method described previously [13]. MLECs were incubated for 10 minutes with 0.11  $\mu\text{mol/L}$  CD44-3MUT or PEG-CD44-3MUT, followed by a 20-minute chase after change of media. Protein uptake was analyzed by immunofluorescence microscopy of anti-CD44-3MUT stained cells. Results showed that both proteins were endocytosed

(Fig. 5a). Quantization of internalization results confirmed that PEG-CD44-3MUT was endocytosed by MLEC comparably to unmodified CD44-3MUT (Fig. 5b). Immunofluorescence microscopy analysis of endothelial cells incubated for 18 hours with CD44-3MUT showed dose-dependent inhibition of beta-catenin (Supplementary Fig. 4 in Online Resource 1). The effect was mediated by vimentin, as vimentin-deficient MLECs did not respond to the treatment. Decreased beta-catenin levels result in release of intercellular contacts [18] and inhibition of cell proliferation which can be monitored by measuring the cell layer electrical impedance. Therefore, we used an impedance-based assay to compare unmodified CD44-3MUT with PEG-CD44-3MUT. We found that both CD44-3MUT and PEG-CD44-3MUT treatments resulted in reduced resistance of wild-type MLEC layer (Fig. 5c, left panel). In agreement with our beta-catenin immunofluorescence microscopy data, this effect was lost in vimentin-deficient endothelial cells (Fig. 5c, right panel). Together, we concluded that PEGylated CD44-3MUT has retained its *in vitro* activity.

## 4 Discussion

All reports of successful attempts to purify CD44HABD are based on the Banerji et al. [9] study, where they purified CD44HABD from refolded urea solubilized IBs by GF and sequential reverse phase chromatography [9]. Likewise, our initial approach to purify human CD44HABD proteins, which contain residues 27–132, was based on this protocol, however we were unable to refold the protein under these conditions (data not shown). In addition to a non-optimal purification-refolding protocol, the ineffective refolding could also result from lack of structurally important amino acids. Banerji et al. [9] reported unsuccessful refolding of the shorter version of CD44HABD, containing residues 20–120 (CD44HABD<sup>20–120</sup>). Lack of structurally important amino acids could also explain deficient refolding of the 27–132 variant. However, compared with the CD44HABD<sup>20–120</sup> version, the N-terminus of our construct

**Table 1** Summary of pharmacokinetic data, obtained after intravenous administration of CD44-3MUT variants

Sample	$C_0$ , $\mu\text{g/ml}$ (95 % CI)	AUC, $\mu\text{g}\cdot\text{h/ml}$ (95 % CI)	AUC (%ID·h/ml)	CL (ml/h)	$V_d$ (%TBW) <sup>a</sup>	$T_{1/2}$ , h (95 % CI)	$N^b$
PEG-CD44-3MUT	142 (130–155)	803 (554–1051)	82.3	1.2	3.9	1.84 (0.69–2.98)	2
CD44-3MUT	315 (293–337)	13.6 (NA)	1.3	79.0	1.8	0.027 (0.023–0.032)	1
GST-CD44-3MUT	74 (32–116)	12.2 (11.9–12.5)	1.6	61.6	5.96	0.08 (0.03–0.14)	1

<sup>a</sup>  $V_d$  is expressed as percentage of TBW

<sup>b</sup> Number of animals

AUC area under the curve,  $C_0$  initial plasma protein concentration, CL total body clearance, ID initial dose of injected protein, NA not available,  $T_{1/2}$  plasma half-life, TBW total body weight,  $V_d$  volume of distribution

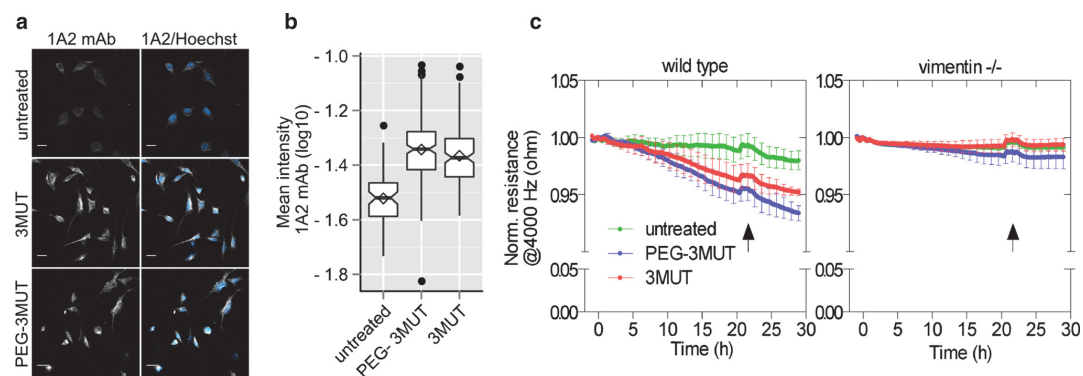


**Fig. 5** Comparison of CD44-3MUT and PEG-CD44-3MUT activity. **a** Immunofluorescence images of anti-CD44-3MUT mAb 1A2-stained mouse lung endothelial cells (MLEC), which were incubated with CD44-3MUT or PEG-CD44-3MUT for 10 min at 37 °C followed by 20-min chase in fresh media. Scale bars 20  $\mu$ m. **b** Quantification of cell-bound CD44-3MUT. Boxplot shows log-

transformed cell mean intensities. Filled circles represent outliers and empty diamonds represent mean. **c** Real-time measurement of electric cell-substrate impedance of wild type or vimentin deficient MLEC layers seeded to ECIS electrodes at confluence. Cells were treated with CD44-3MUT or PEG-CD44-3MUT. Arrow indicates media change and treatment replenishment. Error bars standard error

lacks the  $\beta$ -sheet in order to improve protein solubility. We removed the  $\beta$ -sheet, since according to a published CD44HABD model the  $\beta$ -sheet is solvent-exposed when the C-terminal lobe next to the Link module is absent [19, 20]. But more importantly, unlike the 27–132 variant, CD44HABD<sup>20–120</sup> lacks a disulphide bridge between Cys-28/Cys-129 which links the N- and C-terminal parts of CD44HABD and is critical for proper folding and HA binding. We have shown that the wild type CD44HABD<sup>21–132</sup> GST-fusion protein has retained its HA binding property [8], which confirms that these residues are sufficient for proper folding and structural integrity of CD44HABD.

In regard to purification and refolding conditions, Ouellette et al. [21] have reported that high molecular weight contaminants could decrease protein refolding efficiency and overall yield. To this end, they used IEC under denaturing conditions to remove contaminants before the refolding step [21]. Indeed, addition of a denaturing IEC step to our protocol before GF and refolding resulted in improved yield of the monomeric form of the protein after refolding. Thereby, we were able to reproducibly purify a large amount of monomeric CD44-3MUT. It is arguable whether the IEC step is essential for CD44-3MUT purification, as most of the CD44-3MUT protein is collected from FT fraction. FT fraction contains, beside CD44-3MUT, a considerable amount of other contaminating *E. coli* proteins, suggesting that the purity of CD44-3MUT does not increase in the IEC step. However, omitting the IEC step from the purification protocol resulted in a poor protein yield, mainly because of aggregation of CD44-3MUT. Thus, we suggest that although the IEC step

does not purify CD44-3MUT from bacterial contaminants, it still eliminates some of the high molecular weight contaminants appearing in peak 1 and 2. These contaminants are not separated by GF and, therefore, omitting IEC could interfere with CD44-3MUT proper refolding.

CD44-3MUT consistently migrated in two bands on SDS-PAGE. MS fingerprinting identified that both bands contain only CD44-3MUT peptides. We suggest that these distinct bands of CD44-3MUT represent forms with different numbers of disulphide bridges. Given that the species with three disulphide bridges shows fastest migration in SDS gel under nonreducing conditions, this is the predominant product of our purification protocol.

PEGylation is a common strategy to improve the plasma residence time of protein-based therapeutics. A 20 kDa PEG was chosen to modify our product as a result of several considerations. PEGylation of proteins is often accompanied by partial or total loss of biological activity. To minimize such a possibility we used a PEG with a relatively small molecular mass of 20 kDa. On the other hand, the resulting conjugate has total Mw clearly over 30 kDa, which would most probably avoid rapid urinary excretion. Urinary excretion is dependent on molecular mass and a glomerular filtration threshold has been calculated to be 30 kDa [22]. We also wanted to minimize the probability of accumulation of the PEGylated product in the liver that is common to PEG conjugates and other polymers with high molecular mass leading to macromolecular syndrome.

We used methoxy-PEG-propionaldehyde for CD44-3MUT N-terminal PEGylation to increase its serum half-life. Although the formation of monomeric PEG-conjugate

was apparent, we were unable to purify PEG-CD44-3MUT to complete homogeneity. We have not been able to completely separate mono-PEGylated CD44-3MUT from unmodified and di-PEGylated forms, although currently achieved purity is high. Therefore, the protocol could be further improved in order to fully eliminate possibilities that impurities could somehow compromise the pharmacokinetic properties and biological activity of PEG-CD44-3MUT. Nevertheless, pharmacokinetic studies showed that PEGylation significantly improved the pharmacokinetic properties of CD44-3MUT—its plasma residence time was prolonged about 70-fold when compared with unmodified CD44-3MUT. Interestingly, comparison of rat and mouse CD44-3MUT pharmacokinetic data brought out a discrepancy between volume of distribution values. In rats we used relatively higher doses and  $V_d$  corresponded to plasma water volume (4 % TBW); while in mice, lower CD44-3MUT doses yielded higher  $V_d$  values corresponding to extracellular water volume (~20 % TBW). Such negative correlation between dose and  $V_d$  has been observed in cases when drug binding to tissues is saturable.

The most common drawback of PEGylation is loss of protein bioactivity, since PEG, due to its high hydrodynamic volume, may mask the receptor/ligand binding sites. For example, Pegasys® has only retained 7 % in vitro activity of unmodified interferon, but this is greatly compensated by its improved in vivo residence time [23]. Functional assays demonstrated that PEG-CD44-3MUT has retained its in vitro activity. Cellular mechanism of antiangiogenic effect by CD44-3MUT is based on inhibition of endothelial cell proliferation. CD44-3MUT binds to endothelial cells via direct interaction with cell-surface exposed vimentin and undergoes endocytosis [13]. PEGylated CD44-3MUT is endocytosed by endothelial cells similarly to unmodified protein and causes a vimentin-dependent inhibition of endothelial cell growth. We propose that CD44-3MUT endocytosis reduces the number of growth factor receptors available in plasma membrane. This renders endothelial cells unresponsive to growth factor stimulation and results in inhibition of proliferation and angiogenesis.

## 5 Conclusions

HA binding domain of CD44 (CD44HABD) and its modified non-HA binding form (CD44-3MUT) are novel angiogenesis inhibitors that modulate tumor growth in vivo. In this article we demonstrate that PEGylation is a feasible strategy to improve the pharmacokinetic properties of CD44-3MUT. PEGylation of CD44-3MUT significantly increases serum half-life of the protein conjugate but retains its functional activity. We also presented a protocol

for large-scale production of PEG-CD44-3MUT. The resulting molecule may be a candidate for the development of new-generation angiogenesis modulating drugs.

**Acknowledgments and Disclosures** We are grateful to Anne Meikas for protein expression. This research was supported by the European Regional Development Fund via Enterprise Estonia grants (EU28138/EU28658, EU30013) to Competence Centre for Cancer Research and by Estonian Science Fund Grant 8116 to Prit Kogerman. The authors have no conflicts of interest that are directly relevant to the content of this article.

## References

- Cichy J, Bals R, Potempa J, Mani A, Puré E. Proteinase-mediated release of epithelial cell-associated CD44. Extracellular CD44 complexes with components of cellular matrices. *J Biol Chem.* 2002;277:44440–7.
- Guo YJ, Liu G, Wang X, Jin D, Wu M, Ma J, Sy MS. Potential use of soluble CD44 in serum as indicator of tumor burden and metastasis in patients with gastric or colon cancer. *Cancer Res.* 1994;54:422–6.
- Katoh S, McCarthy JB, Kincade PW. Characterization of soluble CD44 in the circulation of mice. Levels are affected by immune activity and tumor growth. *J Immunol.* 1994;153:3440–9.
- Nakamura H, Suenaga N, Taniwaki K, Matsuki H, Yonezawa K, Fujii M, Okada Y, Seiki M. Constitutive and induced CD44 shedding by ADAM-like proteases and membrane-type 1 matrix metalloproteinase. *Cancer Res.* 2004;64:876–82.
- Ristämäki R, Joensuu H, Grön-Virta K, Salmi M, Jalkanen S. Origin and function of circulating CD44 in non-Hodgkin's lymphoma. *J Immunol.* 1997;158:3000–8.
- Okamoto I, Kawano Y, Tsuiji H, Sasaki J, Nakao M, Matsumoto M, Suga M, Ando M, Nakajima M, Saya H. CD44 cleavage induced by a membrane-associated metalloprotease plays a critical role in tumor cell migration. *Oncogene.* 1999;18:1435–46.
- Ahrens T, Sleeman JP, Schempp CM, Howells N, Hofmann M, Ponta H, Herrlich P, Simon JC. Soluble CD44 inhibits melanoma tumor growth by blocking cell surface CD44 binding to hyaluronic acid. *Oncogene.* 2001;20:3399–408.
- Päll T, Gad A, Kasak L, Drews M, Strömblad S, Kogerman P. Recombinant CD44-HABD is a novel and potent direct angiogenesis inhibitor enforcing endothelial cell-specific growth inhibition independently of hyaluronic acid binding. *Oncogene.* 2004;23:7874–81.
- Banerji S, Day AJ, Kahmann JD, Jackson DG. Characterization of a functional hyaluronan-binding domain from the human CD44 molecule expressed in *Escherichia coli*. *Protein Expr Purif.* 1998;14:371–81.
- Takeda M, Terasawa H, Sakakura M, Yamaguchi Y, Kajiwaru M, Kawashima H, Miyasaka M, Shimada I. Hyaluronan recognition mode of CD44 revealed by cross-saturation and chemical shift perturbation experiments. *J Biol Chem.* 2003;278:43550–5.
- Psut G, Veronese FM. State of the art in PEGylation: the great versatility achieved after forty years of research. *J Control Release.* 2012;161:461–72.
- Kontermann RE. Strategies for extended serum half-life of protein therapeutics. *Curr Opin Biotechnol.* 2011;22:868–76.
- Päll T, Pink A, Kasak L, Turkina M, Anderson W, Valkna A, Kogerman P. Soluble CD44 interacts with intermediate filament protein vimentin on endothelial cell surface. *PLoS ONE.* 2011;6:e29305.

14. Studier FW. Protein production by auto-induction in high density shaking cultures. *Protein Expr Purif.* 2005;41:207–34.
15. Carpenter AE, Jones TR, Lamprecht MR, Clarke C, Kang IH, Friman O, Guertin DA, Chang JH, Lindquist RA, Moffat J, Golland P, Sabatini DM. Cell Profiler: image analysis software for identifying and quantifying cell phenotypes. *Genome Biol.* 2006;7:R100.
16. R Development Core Team. R: a language and environment for statistical computing. Vienna, Austria; 2012.
17. Bajorath J, Greenfield B, Munro SB, Day AJ, Aruffo A. Identification of CD44 residues important for hyaluronan binding and delineation of the binding site. *J Biol Chem.* 1998;273:338–43.
18. Cattelino A, Liebner S, Gallini R, Zanetti A, Balconi G, Corsi A, Bianco P, Wolburg H, Moore R, Oreda B, Kemler R, Dejana E. The conditional inactivation of the beta-catenin gene in endothelial cells causes a defective vascular pattern and increased vascular fragility. *J Cell Biol.* 2003;162:1111–22.
19. Teriete P, Banerji S, Noble M, Blundell CD, Wright AJ, Pickford AR, Lowe E, Mahoney DJ, Tammi MI, Kahmann JD, Campbell ID, Day AJ, Jackson DG. Structure of the regulatory hyaluronan binding domain in the inflammatory leukocyte homing receptor CD44. *Mol Cell.* 2004;13:483–96.
20. Banerji S, Wright AJ, Noble M, Mahoney DJ, Campbell ID, Day AJ, Jackson DG. Structures of the Cd44-hyaluronan complex provide insight into a fundamental carbohydrate-protein interaction. *Nat Struct Mol Biol.* 2007;14:234–9.
21. Ouellette T, Destrau S, Ouellette T, Zhu J, Roach JM, Coffman JD, Hecht T, Lynch JE, Giardina SL. Production and purification of refolded recombinant human IL-7 from inclusion bodies. *Protein Expr Purif.* 2003;30:156–66.
22. Pasut G, Veronese FM. PEGylation, successful approach to drug delivery. *Drug Discov Today.* 2005;10:1451–8.
23. Bailon P, Palleroni A, Schaffer CA, Spence CL, Fung WJ, Porter JE, Ehrlich GK, Pan W, Xu ZX, Modi MW, Farid A, Berthold W, Graves M. Rational design of a potent, long-lasting form of interferon: a 40 kDa branched polyethylene glycol-conjugated interferon alpha-2a for the treatment of hepatitis C. *Bioconjug Chem.* 2001;12:195–202.

*Electronic Supplementary Material*

**BioDrugs**

**Purification, characterization and plasma half-life of PEGylated soluble recombinant non-HA-binding CD44**

Anne Pink<sup>†,‡</sup>, Aili Kallastu<sup>‡</sup>, Marina Turkina<sup>‡</sup>, Marianna Skolnaja<sup>†,‡</sup>, Priit Kogerman<sup>†,‡</sup>, Taavi Päll<sup>†,‡</sup>  
and Andres Valkna<sup>†,‡,\*</sup>

<sup>†</sup>Tallinn University of Technology, Department of Gene Technology, Akadeemia tee 15, 12618  
Tallinn, Estonia;

<sup>‡</sup>Competence Centre for Cancer Research, Akadeemia tee 15, 12618 Tallinn, Estonia;

\* corresponding author. Estonia. E-mail: [andres.valkna@ttu.ee](mailto:andres.valkna@ttu.ee). Telephone: +372 6204335. Fax:  
+372 6204336

## ***Supplementary methods***

### **Expression of CD44-3MUT**

For protein expression, CD44-3MUT-vector was transformed into *E. coli* BL21-CodonPlus(DE3)-RP strain. For preculture, 3-4 colonies of transformants were inoculated into 20 ml of non-inducing media, 10 g/L tryptone, 5 g/L yeast extract, 1mM MgSO<sub>4</sub>, 3.3 g/L (NH<sub>4</sub>)<sub>2</sub>SO<sub>4</sub>, 6.8 g/L KH<sub>2</sub>PO<sub>4</sub>, 7.1 g/L Na<sub>2</sub>HPO<sub>4</sub> and 5 g/L glycerol, containing 100 µg/ml ampicillin and 34 µg/ml chloramphenicol. The preculture was grown at 37° C overnight at 200 rpm until OD600 reached ~10. For large scale protein production, 0.5 ml of starter culture was added to 500 ml of ampicillin-supplemented autoinduction media, 10 g/L tryptone, 5 g/L yeast extract, 1mM MgSO<sub>4</sub>, 3.3 g/L (NH<sub>4</sub>)<sub>2</sub>SO<sub>4</sub>, 6.8 g/L KH<sub>2</sub>PO<sub>4</sub>, 7.1 g/L Na<sub>2</sub>HPO<sub>4</sub>, 5 g/L glycerol, 0.5 g/L glycose and 2 g/L α-lactose, in 2 L baffled Erlenmeyer flask and grown at 37° C for 20 h at 220 rpm. After 20 h cells were harvested by centrifugation for 10 min at 5000 rpm at 4° C. Cells were washed once with ice-cold PBS and harvested again at 5000 rpm for 15 min at 4° C. Cell pellet was weighted, snap frozen in liquid nitrogen and stored at -80° C until protein purification. Average wet bulk yield of bacteria was 9–12 g/L. For protein purification the overnight thawed cell pellet was resuspended in Buffer A, 50 mM Tris-HCl, pH 8.0, 0.1% Triton X-100, 2 mM MgCl<sub>2</sub>, 150 mM NaCl, and 1 mM PMSF, by using a Dounce hand homogenizer. The buffer volume was 5 ml/g cells. Cell suspension was supplemented with 100 µg/ml lysozyme (Sigma) and 10 µg/ml DNase I (Sigma) and incubated with continuous stirring for 2 h at 4° C. Cells were lysed using French press 3 times at 18000 psi. After lysis, one volume of Buffer A was added to the lysate, and incubated for 2 h at 4° C on an end-over-end shaker. Inclusion bodies (IB) were isolated by centrifugation of the lysate at 46000xg for 30 min at 4° C. For removal of contaminating bacterial debris, IBs were washed 5 times. During each wash, IBs were fully homogenized in precooled wash buffers I-V by hand using Dounce homogenizer, incubated one hour at 4° C with continuous stirring and pelleted at 46000xg for 30 min at 4° C. Wash buffer I: 50 mM Tris-HCl pH 8.0, 2 M NaCl, 0.1% Triton X-100, 1 mM PMSF. Wash buffer II: 50 mM Tris-HCl pH 8.0, 150 mM NaCl, 0.1% Triton X-100, 1 M urea, 1 mM PMSF. Wash

buffer III, IV and V: 50 mM Tris-HCl pH 8.0, 150 mM NaCl, 1 M urea, 1 mM PMSF. The volume of IB wash and dissolving buffer was calculated as 12 ml per gram of starting cell mass. IBs were dissolved in Buffer B, 50 mM Tris-HCl, pH 8.0, 8 M urea, 25 mM ethylenediamine, 1 mM PMSF, overnight with continuous stirring at 4° C and insoluble debris was pelleted by centrifugation at 46000xg for 30 min at 4° C. Cleared lysate was sterilized by filtration 0.22 µm and left for 24 h at 4° C on the end-over-end shaker to equilibrate.

### **Purification and refolding of CD44-3MUT**

Ion exchange chromatography (IEC) was applied as first step of the purification protocol. Urea dissolved IBs (up to 150 ml) were loaded onto a HiPrep 16/10 DEAE FF 20 ml column (GE Healthcare) equilibrated with five column volumes (CV) of Start Buffer, 50 mM Tris-HCl pH 8.0, 8 M urea, 25 mM ethylenediamine, and connected to ÄKTA HPLC system (ÄKTA Explorer 10, GE Healthcare) at flow rate 1.5 ml/min. The column was further washed with five CVs of Start Buffer and bound proteins were eluted at flow rate 4 ml/min by stepwise and linear gradient of NaCl 40 mM, 80 mM and 80-500 mM NaCl respectively in Elution Buffer, 50 mM Tris-HCl pH 8.0, 8 M urea, 1 M NaCl and 25 mM ethylenediamine. During IEC the flow through fractions were collected and analyzed by SDS-PAGE. Fractions containing correct molecular weight protein were pooled for subsequent purification. Further separation of monomeric protein from oligomeric forms and other contaminating proteins was achieved by gel filtration (GF) on a HiLoad 26/60 Superdex 200 preparation grade column (GE Healthcare) using ÄKTA HPLC system. The column was pre-equilibrated with three CVs of Start Buffer. 20-23 ml of IEC-purified protein solution was loaded onto GF-column and eluted at flow rate 2.5-3 ml/min. Through the run, fractions were collected and analysed by SDS-PAGE. Monomeric protein containing fractions were pooled and diluted up to 0.1 mg/ml with GF buffer for subsequent refolding.

Refolding was performed by stepwise dialysis from 8 M urea solution into PBS. Each dialysis step was performed twice, except last PBS step which was performed six times, for 1 h on a magnetic stirrer at 4°C. The sequentially used dialysis solutions were I: 6 M urea, 50 mM Tris-HCl pH 8.0, 18

mM EN; II: 4 M urea, 50 mM Tris-HCl pH 8.0, 12 mM ethylenediamine; III: 2 M urea, 50 mM Tris-HCl pH 8.0, 150 mM NaCl, 6 mM ethylenediamine; IV: 1 M urea, 50 mM Tris-HCl pH 8.0, 150 mM NaCl, 3 mM ethylenediamine; V: 0.5 M urea, 50 mM Tris-HCl pH 8.0, 150 mM NaCl, 1.5 mM ethylenediamine; VI: 50 mM Tris-HCl pH 8.0, 150 mM NaCl; VIII PBS pH 7.4. All dialysis solutions were pre-cooled and pH was adjusted directly before use. Refolded protein solutions were centrifuged at 15000xg for 20 min at 4° C, sterile filtrated using 0.22 µm low protein-binding filter (Millipore) and concentrated using 10 kDa MW cut-off centrifugal filter devices (Millipore). The purified protein solutions were frozen at -80° C, lyophilized and stored at 4° C.

### **CD44-3MUT blood circulation half-life in mice**

BALB/c mice (Scanbur, Sweden) were injected with 50 µg CD44-3MUT into proximal site of tail vein. Blood sampling was performed using distal site of lateral tail vein. The time points of blood withdrawal were pre-serum, as soon as possible (0.5 min), every minute during first 10 minutes, every second minute during next 10 minutes. Three mice per time point was used. Clotted blood samples were centrifuged in a tabletop centrifuge for 10 min at 3200 rpm. Serums were collected and stored at -20°C until assayed. A sandwich ELISA format was used to detect and quantify CD44-3MUT titers in obtained samples. 1A2.H4 monoclonal antibody (Labas, Tartu, Estonia) was used as capture antibody and A148 polyclonal antibody (Inbio LTD, Tallinn, Estonia) as detection antibody (see Materials and methods). For colorimetric reaction, Vectastain® ABC kit (Vector Laboratories, Burlingame, CA, USA) and tetramethylbenzidine substrate were used. Absorbance was measured using ELISA plate reader (Tecan, Männedorf, Switzerland). Sample CD44-3MUT concentrations were derived by interpolation from a standard curve generated using mouse serums peaked with known concentrations of CD44-3MUT.

## Supplementary Tables

**Supplementary Table 1.** Summary of properties, expression and purification methods of CD44-3MUT

Protein	aa	MW	pI	Expression vector	Expression strain	Expression method	Purification method
CD44-3MUT	106	11497.8	5.15	pET11c	E.coli BL21-CodonPlus (DE3)-RP	Batch, MAI <sup>a</sup>	IB/IEC/GF/REF <sup>b</sup>

<sup>a</sup>, MAI, autoinduction media; <sup>b</sup>, REF, refolding

**Supplementary Table 2.** MALDI-TOF MS peptides of Glu-C or trypsin digested CD44-3MUT

Enzyme/peptide residues	Calculated mass	Measured mass	Difference	Relative error, ppm	Peptide sequence	Modification <sup>a</sup>
Glu-C digestion						
1-11	1322.631	1322.692	0.061	46	TCRFAGVFHVE	1xC
12-22	1225.617	1225.677	0.060	49	KNGAYSISRTE	
23-41	2098.961	2099.024	0.063	30	AADLCKAFNSTLPTMAQME	1xC
42-49	864.483	864.528	0.045	52	KALSIGFE	
50-57	900.377	900.402	0.025	28	TCSSGFIE	1xC
58-100	4825.277	NA			GHVVIPRIHPNSICAANNTGVYIL TYNTSQYDTYCFNASAPPE	2xC
Trypsin digestion						
4-12	1033.547	1033.572	0.025	24	FAGVFHVEK	
13-20	867.432	867.472	0.040	46	NGAYSISR	
21-28	850.398	850.393	-0.005	-6	TEAADLCK	
29-42	1568.745	1568.782	0.037	24	AFNSTLPTMAQMEK	
43-64	2376.202	2376.238	0.036	15	ALSIGFETCSSGFIEGHVVIPR	1xC
65-106	4704.048 <sup>b</sup>	4704.829	0.780	166	IHPNSICAANNTGVYILTYNTSQ YDTYCFNASAPPEEDCTSV	2xC
65-106	4761.100 <sup>b</sup>	4761.538	0.438	92	IHPNSICAANNTGVYILTYNTSQ YDTYCFNASAPPEEDCTSV	3xC

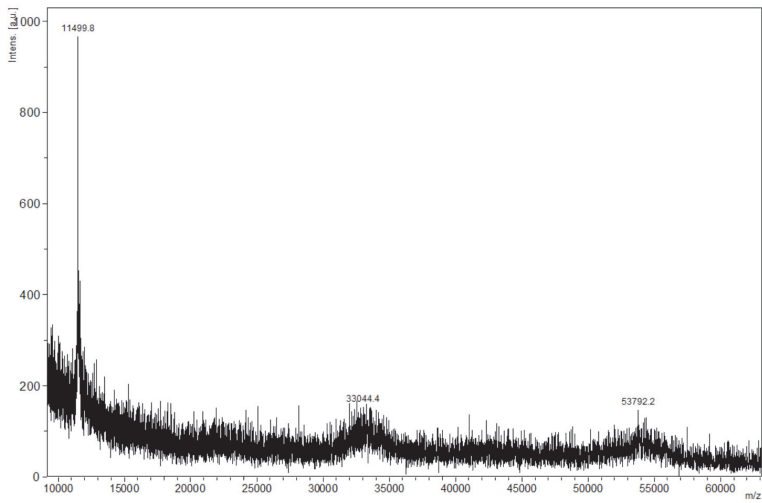
<sup>a</sup>, cysteine carbamidomethylation; <sup>b</sup>, average mass.

**Supplementary Table 3.** CD44-3MUT pharmacokinetic parameters in BALB/c mice, initial dose (ID) of 50 µg administered into tail vein, blood sampling via lateral tail vein.

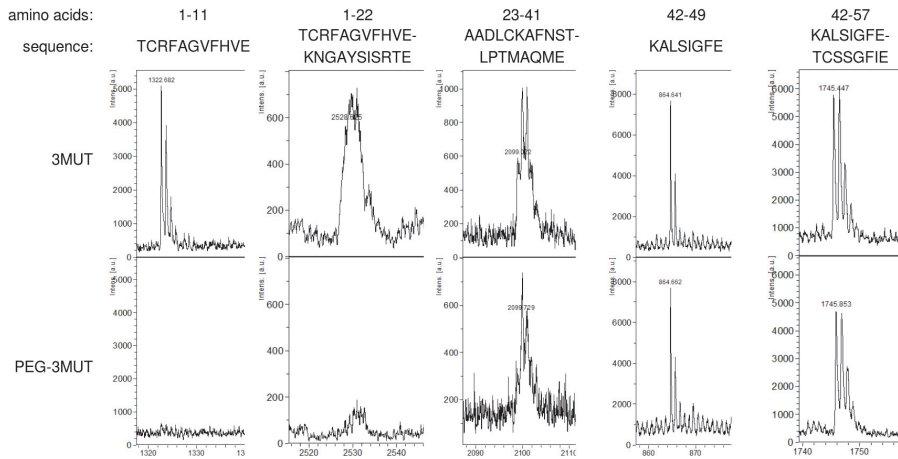
<b>Blood withdrawal site</b>	<b>C<sub>0</sub>, µg/ml (95% CI)</b>	<b>t<sub>1/2</sub>, hours (95% CI)</b>	<b>Vd, %TBW</b>	<b>AUC µg·h/L</b>	<b>CL, L/h</b>
Tail vein	11.2 (9.5, 12.9)	0.038 (0.025, 0.05)	23.1	0.82 (0.73, 0.90)	61.0

## Supplementary Figures

a

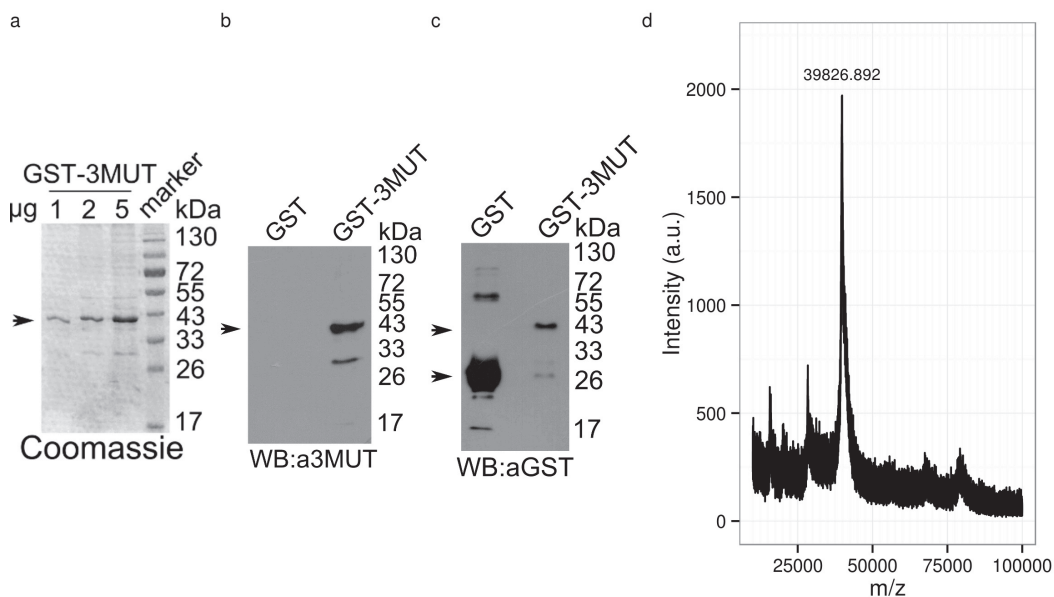


b

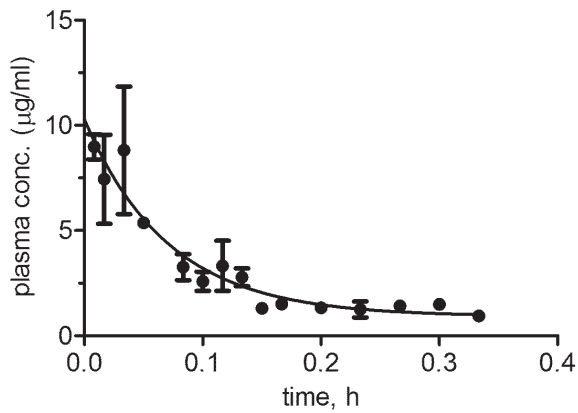


**Supplementary Fig. 1** Characterization of PEG-CD44-3MUT. (a) MALDI-TOF MS analysis of whole 20 kDa PEG modified CD44-3MUT sample. Nonpeglylated CD44-3MUT ions have m/z 11500, monopeglylated CD44-3MUT has m/z ~33000 and dipeglylated CD44-3MUT has m/z ~54000. (b) Characterization of PEG-CD44-3MUT pegylation site. MALDI-TOF MS analysis of Glu-C digested CD44-3MUT (3MUT) or PEG-CD44-3MUT (PEG-3MUT). Amino acid numbering is according to CD44-3MUT sequence. Cysteine

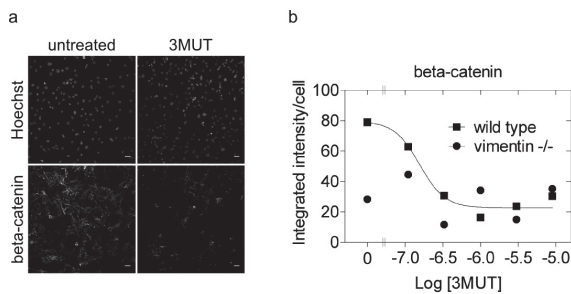
residues are carbamidomethylated. Calculated masses of peptides are shown in Supplementary Table 2. Peptides 1-22 (calculated mass 2529.2303) and 42-57 (calculated mass 1745.8414) contain one miscleavage.



**Supplementary Fig. 2** Characterization of GST-CD44-3MUT. (a) SDS-PAGE analysis of purified GST-CD44-3MUT (GST-3MUT). 1, 2 or 5 µg of GST-MUT was loaded onto gel. Gel was stained with Coomassie blue. (b and c) Western blot (WB) analysis of purified GST-3MUT and GST alone. Proteins were stained with anti-CD44-3MUT 1A2.H4 (b) or anti-GST antibody (c). The locations of GST (~26 kDa) or GST-3MUT (~40 kDa) are indicated by arrows. (d) MALDI-TOF mass spectrum of affinity purified whole GST-3MUT.



**Supplementary Fig. 3** Blood circulation half-life of CD44-3MUT in mice. Animals were injected with 50 µg CD44-3MUT into proximal site of tail vein. Blood sampling was performed using distal site of lateral tail vein. Three mice per time point were used. Error bars represent SE.



**Supplementary Fig. 4** CD44-3MUT inhibits beta-catenin in MLEC. (a) Immunofluorescence images of anti-beta-catenin stained wild type MLEC treated 18 hours with CD44-3MUT or left untreated. Scale bars, 20 µm. (b) Dose-response effect of CD44-3MUT treatment to cellular beta-catenin in wild type (squares) or vimentin knockout (circles) MLEC. Curve fitting using three-parameter logistic equation showed that CD44-3MUT inhibited beta-catenin in wild type MLECs with  $\log_{10}(\text{IC}_{50})$  -6.8 mol/L (95% CI -6.86 to -6.76, R-squared = 0.19, d.f. = 5227). Solid line represents

dose-response curve fitted to wild type MLEC data. Vimentin deficient MLECs did not show dose response to the treatment and curve could not be fitted.

## **PUBLICATION II**

Päll, T, **Pink, A**, Kasak, L, Turkina, M, Anderson, W, Valkna, A, Kogerman, P (2011). Soluble CD44 interacts with intermediate filament protein vimentin on endothelial cell surface. *PLoS ONE*, 6, 12:e29305.



# Soluble CD44 Interacts with Intermediate Filament Protein Vimentin on Endothelial Cell Surface

Taavi Päll<sup>1,2\*</sup>, Anne Pink<sup>1,2</sup>, Lagle Kasak<sup>1,2</sup>, Marina Turkina<sup>2</sup>, Wally Anderson<sup>2</sup>, Andres Valkna<sup>1,2</sup>, Priit Kogerman<sup>1,2</sup>

**1** Department of Gene Technology, Tallinn University of Technology, Tallinn, Estonia, **2** Competence Center for Cancer Research, Tallinn, Estonia

## Abstract

CD44 is a cell surface glycoprotein that functions as hyaluronan receptor. Mouse and human serum contain substantial amounts of soluble CD44, generated either by shedding or alternative splicing. During inflammation and in cancer patients serum levels of soluble CD44 are significantly increased. Experimentally, soluble CD44 overexpression blocks cancer cell adhesion to HA. We have previously found that recombinant CD44 hyaluronan binding domain (CD44HABD) and its non-HA-binding mutant inhibited tumor xenograft growth, angiogenesis, and endothelial cell proliferation. These data suggested an additional target other than HA for CD44HABD. By using non-HA-binding CD44HABD Arg41Ala, Arg78Ser, and Tyr79Ser-triple mutant (CD443MUT) we have identified intermediate filament protein vimentin as a novel interaction partner of CD44. We found that vimentin is expressed on the cell surface of human umbilical vein endothelial cells (HUVEC). Endogenous CD44 and vimentin coprecipitate from HUVECs, and when overexpressed in vimentin-negative MCF-7 cells. By using deletion mutants, we found that CD44HABD and CD443MUT bind vimentin N-terminal head domain. CD443MUT binds vimentin in solution with a K<sub>d</sub> in range of 12–37 nM, and immobilised vimentin with K<sub>d</sub> of 74 nM. CD443MUT binds to HUVEC and recombinant vimentin displaces CD443MUT from its binding sites. CD44HABD and CD443MUT were internalized by wild-type endothelial cells, but not by lung endothelial cells isolated from vimentin knock-out mice. Together, these data suggest that vimentin provides a specific binding site for soluble CD44 on endothelial cells.

**Citation:** Päll T, Pink A, Kasak L, Turkina M, Anderson W, et al. (2011) Soluble CD44 Interacts with Intermediate Filament Protein Vimentin on Endothelial Cell Surface. *PLoS ONE* 6(12): e29305. doi:10.1371/journal.pone.0029305

**Editor:** Valdur Saks, Université Joseph Fourier, France

**Received:** July 12, 2011; **Accepted:** November 24, 2011; **Published:** December 21, 2011

**Copyright:** © 2011 Päll et al. This is an open-access article distributed under the terms of the Creative Commons Attribution License, which permits unrestricted use, distribution, and reproduction in any medium, provided the original author and source are credited.

**Funding:** This work was supported by the European Regional Development Fund via Enterprise Estonia grants (EU28138/EU28658, EU30013) to Competence Center for Cancer Research and by Estonian Science Fund (grant 8116 to P.K.). The funders had no role in study design, data collection and analysis, decision to publish, or preparation of the manuscript.

**Competing Interests:** The authors have declared that no competing interests exist.

\* E-mail: taavi.pall@ttu.ee

## Introduction

CD44 transmembrane glycoprotein functions as hyaluronan (HA) receptor. CD44 has functions in a lymphocyte homing, mediates cell adhesion to HA and HA metabolism. CD44 is expressed on many cell types including endothelial cells (EC) and has multiple alternatively spliced isoforms. CD44 plays a significant role in tumor malignancy. High levels of CD44 expression on tumor cells is sufficient to establish metastatic behavior [1,2]. CD44 is involved in pathological angiogenesis, as its expression is elevated in tumor vasculature, and CD44 expression can be induced in cultured ECs by angiogenic growth factors [3]. Furthermore, CD44 knockout mice show reduced vascularisation of tumor xenografts and Matrigel plugs [4]. In addition to cell surface expression, CD44 is present in soluble form in lymph and serum [5] or bound to extracellular matrix [6]. Soluble CD44 is generated either by alternative splicing [7] or, more importantly, by ectodomain shedding by matrix metalloproteases [8,9]. The size of shed CD44 is highly heterogeneous because of glycosylations and variant exons [5,9–11]. The serum concentration of sCD44 in mice is known to range between 490 to 2100 ng/ml [5]. Studies of sCD44 in the sera of non-Hodgkin's lymphoma and breast cancer patients show that physiological sCD44 level in healthy persons is in the range of 250 to 500 ng/ml [12–14]. The serum concentration of sCD44 in healthy individuals is ~3 nM whereas it was shown to be significantly elevated in patients with advanced

gastric (24 nM) or colon cancer (31 nM) [11]. Elevated serum sCD44 or sCD44v6 is a predictor of poor therapeutic outcome in non-Hodgkin's lymphoma or breast cancer patients, respectively [12,15]. The source of sCD44 are lymphocytes, macrophages, ECs, and tumor cells [10,11,16]. In non-Hodgkin's lymphoma, the source of elevated sCD44 are lymphoma cells, and sCD44 levels decrease after treatment in patients with complete remission [10,17]. Endothelial and macrophage CD44 expression is increased in atherosclerosis and CD44 shedding from EC and macrophages is stimulated by proinflammatory cytokines [16].

Tumors are surrounded by HA-rich ECM. When overexpressed in tumor cells, soluble CD44 can function as an antagonist to cell membrane CD44 and block its binding to ECM HA. Overexpression of soluble forms of CD44 inhibits HA-adhesion of mouse mammary carcinoma or melanoma cells and caused inhibition of tumor cell proliferation, and reduced tumorigenicity [18–20]. CD44 knockout in mouse breast cancer model caused increased numbers of lung metastases, which correlated with reduced invasion of CD44-expressing metastatic breast cancer cell lines into HA-containing collagen matrices [21].

CD44 binds HA via the link module in its N-terminal domain. The link module is approximately 100 amino acids long and consists of two alpha helices and two triple-stranded antiparallel beta sheets, stabilized by two disulphide bridges [22]. The structure of CD44 HABD has an additional lobe consisting of

four beta strands formed by the residues flanking the core link module [23,24]. This enlarged structure is stabilized by an additional disulphide bridge between flanking regions. Together, the human CD44 HABD structure consists amino acids 21–169. The HA-binding surface of CD44 is exclusively covered by the link module and its flanking regions do not contribute to the HA binding [23]. The critical residues in CD44 HA-binding surface directly involved in binding are Arg41, Tyr42, Arg78, and Tyr79, according to studies of human CD44 [23,25]. Glycosylation of Asn25 and Asn125 within CD44 HABD is involved in regulation of HA binding [26]. Altogether, CD44 has five N-glycosylation sites (Asn25, Asn57, Asn100, Asn110, Asn120) within its HABD. Bacterially expressed recombinant human CD44 HABD containing amino acids 20–178 binds HA comparably to glycosylated CD44-Rg fusion protein [24]. HA binding function is also retained by a recombinant human CD44HABD containing amino acids 21–132, whereas HA binding was abolished by the mutations in Arg41, Arg78, and Tyr79 [27].

Vimentin intermediate filaments comprises supporting framework within cells. Vimentin functions in intracellular vesicular transport, including  $\beta$ 1-integrin trafficking [28], transport of lysosomal membrane proteins by binding AP-3 complex [29], and as a cytosolic reservoir for tSNARE SNAP23 [30]. Importantly, vimentin knockout cells apparently retain intact receptor-mediated endocytosis, as transferrin receptor level and distribution is normal [29,30]. Vimentin-deficient mice reproduce and develop normally [31], however, they show reduced elasticity of arteries, decreased nitric oxide production and elevated endothelin [32,33]. Vimentin is expressed on cell surface in several cell types, including TNF- $\alpha$  induced macrophages [34], cutaneous T-cell lymphoma [35], platelets [36], and brain microvascular endothelial cells [37]. Vimentin extracellular ligands include vitronectin/PAI-1 complex [36], and *E. coli* IbeA protein [37]. Vimentin is an antiangiogenesis target overexpressed on tumor endothelium *in vivo*. Anti-vimentin antibody treatment inhibited subcutaneous tumor xenograft growth and tumor blood vessel density in mice, suggesting that vimentin is localized to the cell surface in tumor endothelial cells [38].

CD44 and vimentin are both detectable from membrane lipid raft fractions [39–41] and from clathrin-independent pathway endocytic vesicles in fibroblasts [42]. CD44 and vimentin are upregulated during epithelial-mesenchymal transition (EMT) of cancer cells. Mammary epithelial cells undergoing EMT downregulate epithelial genes and upregulate mesenchymal genes, such as E-cadherin, N-cadherin and vimentin, respectively. Suppression of standard CD44 isoform in Snail- or TGF- $\beta$ -induced human mammary epithelial cells inhibits EMT, accompanied by vimentin downregulation [43].

We have previously found that recombinant CD44 HABD 21–132, as a model for soluble CD44, inhibited human subcutaneous tumor xenograft growth in mice, angiogenesis in chick chorio-allantoic membrane, and EC proliferation [27]. Surprisingly, these CD44HABD functions were independent of its HA-binding property, as non-HA-binding mutant was similarly effective. Therefore, we proposed that CD44HABD could bind additionally to a different ligand than HA. In this study, we used CD44HABD non-HA-binding mutant as a bait in GST pull-down assay and identified vimentin as a novel CD44 interacting protein.

## Results

### Identification of vimentin as CD44 HABD-binding protein

To identify EC target of CD44 HABD 21–132 (CD44HABD) and its non-HA-binding mutant CD44HABD<sup>R41AR78SY79S</sup> (CD443MUT), we used GST pull-down from HUVEC lysate. Silver staining of pull-down reactions separated by SDS-PAGE

revealed that GST-tagged CD443MUT precipitated a 60 kD protein (Figure 1A). This protein was identified by MALDI-TOF-MS protein fingerprinting as vimentin. To confirm that CD44HABD-proteins pull down vimentin, we used anti-vimentin (V9) immunoblotting. Immunoblotting confirmed that GST-tagged CD44HABD and CD443MUT pulled down endogenous vimentin from HUVEC lysates (Figure 1B, upper panel). To determine whether CD44HABD and CD443MUT bind vimentin directly, we used recombinant vimentin in the GST pull-down assay. We found that both CD44HABD and CD443MUT were able to pull down recombinant vimentin, suggesting that CD44 interacts with vimentin directly (Figure 1B, lower panel). We next used immunoprecipitation (IP) to determine whether endogenous CD44 and vimentin associate in EC. HUVEC lysate was immunoprecipitated using anti-CD44 (MEM-263) antibody and immunoprecipitates were subsequently analyzed by immunoblotting. We found that a minor population of vimentin coimmunoprecipitated with CD44 from HUVEC lysate (Figure 1C). We also tested whether anti-vimentin antibodies coimmunoprecipitate CD44. However, we were not able to detect CD44 from anti-vimentin IPs (A.P., unpublished data). To further confirm full-length CD44 and vimentin association we overexpressed C-terminally Flag-tagged CD44 standard isoform and Myc-tagged vimentin in vimentin nonexpressing MCF-7 cells. Overexpressed vimentin was exposed to the cell surface as detected by cell surface biotinylation (Figure S1). Immunoprecipitation results showed that anti-Flag immunoprecipitated a vimentin-Myc from CD44-Flag transfected cells (Figure 1D).

### Vimentin and CD443MUT *in vitro* binding affinity

CD443MUT interaction with recombinant full length human vimentin was further characterized by isothermal titration calorimetry (ITC) and by surface plasmon resonance (SPR). We used two different preparations of CD443MUT. ITC experiments showed that CD443MUT binds to recombinant vimentin with Kd in 12–37 nM range with stoichiometry (vimentin/CD443MUT) of  $\approx$ 7 mol/mol (Table 1). SPR experiments were carried out with vimentin immobilized into measuring cell. Kinetic analysis by SPR revealed that binding of CD443MUT to immobilized vimentin is described by a two-site ligand binding model. CD443MUT bound to a high-affinity site of immobilized vimentin with Kd 74 nM and Kd for low affinity site was 15  $\mu$ M (Table 2). Analysis of kinetic data using equilibrium response values resulted in  $15 \pm 2$   $\mu$ M Kd. The stoichiometry of vimentin/CD443MUT complex in SPR experiment was measured  $\approx$ 6 mol/mol.

### Mapping of vimentin CD44-binding region

To map CD44-binding region in vimentin, we generated truncated vimentin constructs (Figure 2A). Vimentin deletion mutant VIM1-96 contains only head domain, VIM1-245 contains head domain and alpha-helices 1A-B, and VIM97-466 mutant lacks the head domain (aa numbering according to human vimentin). VIM246-466 mutant contains C-terminal half of the protein starting from alpha-helices 2A-B. VIM407-466 contains the tail domain. Lysates of MCF-7 cells, expressing either full-length vimentin or its deletion mutants, were used in GST pull-down with CD44HABD or CD443MUT. Pull-downs were analyzed by immunoblotting using tag-specific antibodies. This analysis showed that CD44HABD and CD443MUT bound only vimentin deletion mutants containing the head domain (VIM1-96 and VIM1-245; Figure 2B). Deletion of the head domain was sufficient to abolish binding of vimentin to CD44HABD and CD443MUT (VIM97-477, VIM246-466 or VIM407-466).

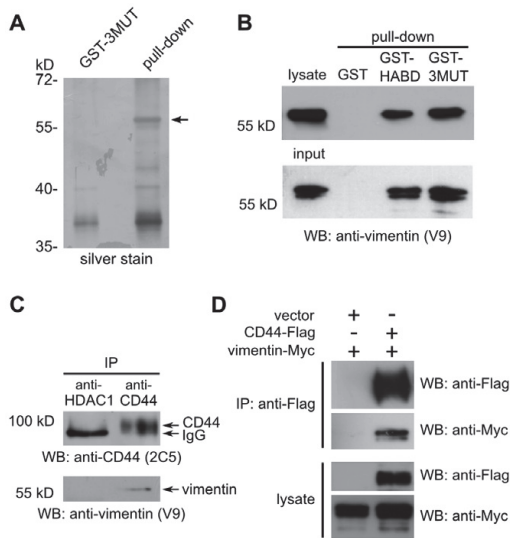


**Figure 1. Identification of vimentin as CD44HABD-binding protein.** (A) HUVEC lysate was used in GST pull-down to identify CD443MUT interacting proteins. Lysate was incubated with GST-CD443MUT (GST-3MUT) coated beads. Bound proteins were eluted using reduced glutathione and analyzed by SDS-PAGE and silver staining. GST-3MUT precipitated protein band (shown by arrow) was cut off from gel, trypsinolyzed and analyzed by MALDI-TOF MS. This protein was identified as vimentin. (B, upper panel) Vimentin pull-down by CD44HABD (GST-HABD) and GST-3MUT was confirmed by immunoblotting using anti-vimentin V9 antibody. (B, lower panel) GST-HABD and GST-3MUT pull-down recombinant vimentin. (C) Coimmunoprecipitation of vimentin with CD44 from HUVEC lysate. Anti-HDAC-1 antibody was used as a negative control (see Materials and methods). (D) Coimmunoprecipitation of over-expressed vimentin-Myc with CD44-Flag from MCF-7 lysates using tag-specific antibodies.  
doi:10.1371/journal.pone.0029305.g001

### Cell surface vimentin and CD443MUT-vimentin interaction is induced by VEGF

To detect cell surface vimentin, we performed biotinylation of cell surface proteins of adherent living HUVEC, followed by IP of vimentin from cell lysates. Biotinylated proteins were detected by immunoblotting using HRP-conjugated streptavidin. We found that anti-vimentin (V9) antibody immunoprecipitated from HUVEC lysate a 60 kD biotinylated protein. We used anti-CD44 (H4C4) antibody as positive control and found that it IPd a 100 kD biotinylated protein. These proteins correspond to expected sizes of vimentin and endothelial CD44, respectively

(Figure 3A upper panel). The identity of biotinylated proteins was confirmed by immunoblotting with vimentin- or CD44-specific antibodies (Figure 3A lower panel).

Next, we decided to test whether CD443MUT cellular binding can be induced with angiogenic growth factors. To determine the effect of angiogenic stimulus on CD443MUT cellular binding we induced 6 h serum starved HUVEC 30 min with VEGF165 at 37°C. Then we incubated cells with Alexa Fluor 488-labeled CD443MUT at 4°C. CD443MUT-A488 cellular binding was quantitated using flow cytometry. We found a significant binding of CD443MUT-A488 to HUVEC compared to GST-A488 control ( $P = 0.015$ ,  $n = 3$ , unpaired t-test). Under these conditions ~20% cells bound CD443MUT. VEGF treatment induced a further increase in CD443MUT cellular binding compared to non-induced cells, although this result was statistically marginally significant ( $P = 0.067$ ,  $n = 3$ ; Figure 3B). To confirm that VEGF induces cell surface vimentin binding sites for CD443MUT, we used cell surface biotinylation of HUVEC followed by GST pull-down with CD443MUT. For this, overnight serum starved HUVEC were induced 1 hour with VEGF or left non-induced, followed by cell surface biotinylation of live adherent cells. GST-CD443MUT or GST alone were used in pull-downs from cell-surface biotinylated HUVEC lysates. Subsequently, precipitated proteins were detected by western blotting either by streptavidin-HRP or anti-vimentin (V9) antibody. We found that CD443MUT pulled down a 60 kD biotinylated protein from VEGF-stimulated but not from serum starved cells. This protein turned out to be vimentin since it could be detected with a vimentin-specific antibody (Figure 3C).

### Vimentin displaces CD443MUT from HUVEC

To further characterize CD443MUT and vimentin interaction on HUVECs we measured the ability of vimentin to compete with  $^{125}$ I-labeled CD443MUT for cellular binding. The results of displacement binding experiments showed that CD443MUT displaced itself from HUVEC with  $\log EC_{50} -5.8 \pm 0.05$  M ( $EC_{50} = 1.57 \mu M$ ,  $n = 9$ ; Figure 3D). Vimentin displaced CD443MUT from HUVEC with  $\log EC_{50} -5.37 \pm 0.21$  M ( $EC_{50} = 4.26 \mu M$ ,  $n = 2$ ) which is not significantly different from displacement by CD443MUT itself (extra sum of squares F-test,  $P = 0.0711$ ;  $F = 3.298$  (1,171)). BSA did not displace CD443MUT effectively, with  $\log EC_{50} -3.93 \pm 0.06$  M ( $EC_{50} = 117 \mu M$ ,  $n = 4$ ).

### CD44HABD endocytosis by HUVEC

Given that vimentin provides specific binding site for CD443MUT on EC, we decided to test whether CD443MUT is endocytosed upon binding to cell surface vimentin. We incubated HUVEC with unlabeled CD443MUT for 30 min at 37°C to allow internalization. CD443MUT was detected by immunofluorescence confocal microscopy using CD443MUT specific mouse monoclonal antibody 1A2 (Figure S2). Recombinant GST uptake

**Table 1. Summary of Kd values for CD443MUT and vimentin interaction measured by ITC.**

CD443MUT preparation	CD443MUT ( $\mu M$ )	Vimentin ( $\mu M$ )	Kd (M)	$n^a$ (mol/mol)
A	4.2	1.8	$1.2 \cdot 10^{-8} \pm 10^{-9}$	$9.9 \pm 0.5$
	1.5	0.5	$3.7 \cdot 10^{-8} \pm 10^{-9}$	
B	4.2	1.8	$1.8 \cdot 10^{-8} \pm 10^{-9}$	$7.2 \pm 0.3$
	0.9	0.5	$2.3 \cdot 10^{-8} \pm 10^{-9}$	

<sup>a</sup>, stoichiometry (vimentin/CD443MUT).  
doi:10.1371/journal.pone.0029305.t001

**Table 2.** Kinetic parameters for binding of CD443MUT to vimentin measured by SPR.

Kass1 ( $M^{-1} s^{-1}$ ) $\times 10^3$	Kass2 ( $M^{-1} s^{-1}$ )	Kdiss1 ( $s^{-1}$ ) $\times 10^{-4}$	Kdiss2 ( $s^{-1}$ ) $\times 10^{-3}$	Kd ( $\mu M$ )	Kdiss1/Kass1	Kd ( $\mu M$ ) equation 1	n (mol/mol)
7.6 $\pm$ 0.1	183 $\pm$ 7	5.6 $\pm$ 0.1	1.9 $\pm$ 0.1	0.074		15 $\pm$ 2	6.2

doi:10.1371/journal.pone.0029305.t002

was used as a control. The results showed that CD443MUT was readily endocytosed by HUVEC and displayed a vesicular localization pattern (Figure 4A). Next, we used CD443MUT directly conjugated to Alexa Fluor 568 for internalization assay. CD443MUT-A568 was endocytosed and distributed in HUVEC cytoplasm similarly to unlabeled CD443MUT (Figure 4B). HUVECs express vimentin at high level, and endocytosed CD443MUT-containing vesicles were surrounded by a dense network of vimentin intermediate filaments, however, there was no direct colocalization of CD443MUT with vimentin filaments (Figure 4A and B).

Next, we used a generic endocytosis marker cholera toxin B conjugated to Alexa Fluor 555 (CTxB-A555) to trace CD443MUT following endocytosis. We found that after 30 min uptake Alexa Fluor 488-labeled CD44HABD as well as -3MUT colocalized with CTxB-A555 positive structures (Figure 5A). We quantitated colocalization of CTxB with CD44HABD and CD443MUT from single slices of confocal image stacks as described in Materials and Methods. Altogether,  $\sim 2.6 \cdot 10^4$  CTxB-positive vesicles were analyzed from CD44HABD- ( $n = 39$ ) or CD443MUT-incubated cells ( $n = 38$ ). As shown in Figure 5B, approximately 4–5% of CTxB-vesicles colocalized and showed positive correlation with CD44HABD (average Pearson's  $r = 0.469$ , 95% CI 0.438 to 0.498,  $df = 679$ ,  $P < 0.0001$ ) or CD443MUT ( $r = 0.532$ , 95% CI 0.503 to 0.531,  $df = 608$ ,  $P < 0.0001$ ). We next analyzed CD443MUT-A488 colocalization with early endosome marker EEA1 in HUVEC after 10 min

uptake followed by 20 min chase. We found that CD443MUT-A488 showed extensive colocalization with EEA1-positive vesicles after 10 min incubation (Figure 5C). Quantitation of CD443MUT and EEA1 colocalization in  $\sim 6.5 \cdot 10^3$  EEA1-endosomes showed that 32% of EEA1-endosomes colocalized with CD443MUT after 10 min incubation ( $r = 0.311$ , 95% CI 0.266 to 0.355,  $df = 407$ ,  $P < 0.0001$ ), whereas a fraction of EEA1-endosomes showing colocalization fell to 7% after 20 min chase ( $r = 0.321$ , 95% CI 0.251 to 0.388,  $df = 172$ ,  $P < 0.0001$ ) following the incubation (Figure 5D). The number of CD443MUT-vesicles in cells reduced during 20 min chase by  $\sim 7.5$  times (Figure 5D, rightmost panel) suggesting trafficking of CD44 to late endosomal-lysosomal degradation pathway. Therefore, we next analyzed whether CD443MUT is targeted to the CD63-positive late endosomal compartment after 20 min chase following a 10 min pulse with CD443MUT-A488. However, we found that CD443MUT-A488 showed no significant accumulation within anti-CD63 staining vesicles after 20 min (Figure 5E) or 50 min chase (data not shown). Together, these results indicate that recombinant CD44HABD and CD443MUT are endocytosed and reach early endosomal compartment.

#### CD443MUT endocytosis is inhibited in ECs derived from vimentin-null mice

To test directly whether vimentin mediates CD443MUT internalization, we isolated lung endothelial cells from wild-type

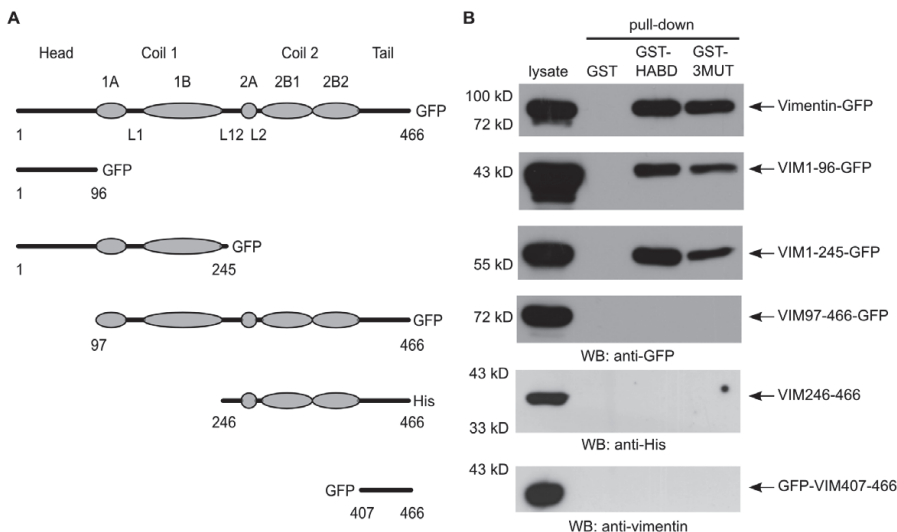


**Figure 2. CD443MUT binds vimentin N-terminal head domain.** (A) A diagram of vimentin sub-domains and deletion mutants used in pull-down reactions. Ellipses represent alpha-helices in coiled-coil domains and L1-L2 mark linker regions. GFP, green fluorescent protein. (B) GST pull-down reactions were performed from cell lysates transfected with full length vimentin or its deletion mutants (see Materials and methods). Eluates from pull-downs were analyzed by immunoblotting. doi:10.1371/journal.pone.0029305.g002

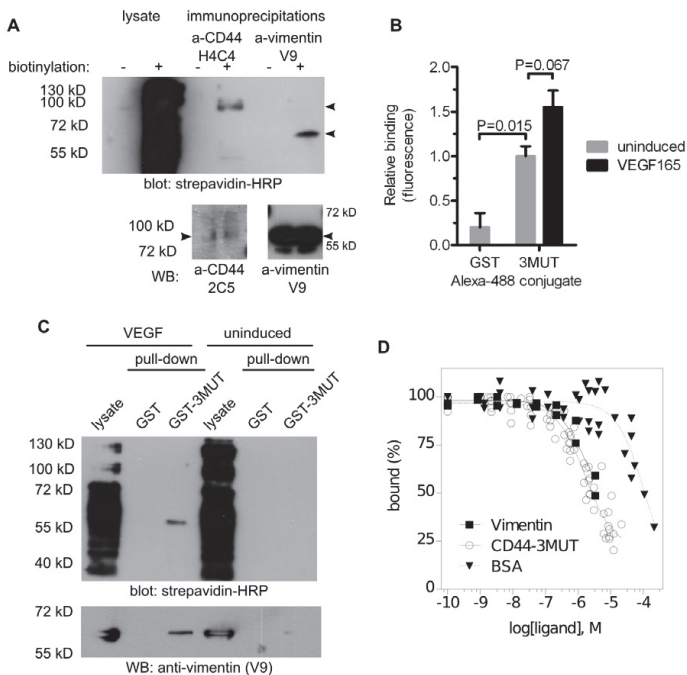


**Figure 3. VEGF induces cell surface vimentin and CD443MUT cellular binding.** (A) For detection of cell surface vimentin, asynchronously growing live adherent HUVEC were cell surface biotinylated and lysate was used for immunoprecipitation using anti-vimentin or anti-CD44 antibodies. Immunoprecipitated proteins were detected by immunoblotting using streptavidin-HRP (upper panel) or specific antibodies (lower panels). (B) 6 hour serum-starved HUVEC were induced for 30 min with VEGF165, followed by incubation on ice with Alexa Fluor 488-labeled CD443MUT (3MUT). GST Alexa Fluor 488 conjugate was used as negative control. Cellular binding of A488-conjugated proteins was analyzed by FACS. Bars represent average geometric mean of fluorescence from three experiments (mean  $\pm$  SE). (C) Overnight serum-starved HUVEC were induced for 1 hour with VEGF165, followed by cell surface biotinylation. Lysate from biotinylated cells was used in pull-down using GST-3MUT. Precipitated proteins were detected by immunoblotting using streptavidin-HRP (upper panel) or anti-vimentin antibody (lower panel). (D) For displacement assay, cells were resuspended in incubation buffer in 96-well plate. CD443MUT, vimentin or BSA at different concentrations was added to the wells along with  $^{125}$ I-labeled CD443MUT. Reactions were incubated overnight at 4°C. After incubation, reactions were stopped by filtration through glass fiber filters blocked with BSA. Filters were washed with PBS and bound radioactivity was measured using gamma counter. The curves represent global fitting of normalized radioligand binding data from two to nine experiments. doi:10.1371/journal.pone.0029305.g003

(WT) or vimentin-null mice (Figure 6A). We characterized isolated mouse lung endothelial cells (MLEC) for endothelial-specific cell surface markers by flow cytometry (Figure 6B). FACS staining showed that PECAM-1 and CD44 were expressed on vimentin-null MLEC at levels comparable to WT cells. However, ICAM-2 expression was reduced on vimentin-null MLEC compared to WT cells. We next tested the internalization of CD443MUT-A568 by MLEC. We found that WT MLEC endocytosed CD443MUT comparably to HUVEC after 30 min uptake, whereas CD443MUT uptake by MLECs isolated from vimentin-null mice was inhibited (Figure 6C).

## Discussion

We have identified vimentin as a novel CD44 binding protein. Our results – the fact that recombinant CD44HABD and CD443MUT pulled down both endogenous as well as recombinant vimentin, and the finding that vimentin displaces CD443MUT bound to HUVEC cells, suggest that CD44-vimentin interaction is a direct protein-protein interaction. To our knowledge, CD44-vimentin interaction is the first protein-protein interaction described

for CD44 HABD. CD44 HABD mediates low affinity interactions with its ECM ligand HA with an *in vitro* Kd of 50  $\mu$ M [23]. CD44 is a membrane glycoprotein and interacts via its glycosylated variant exons with various extracellular ligands, including fibronectin, collagen XIV, E-selectin and osteopontin [44–47]. CD44 HABD contains five N-linked glycosylation sites [48]. Our experiments, where glycosylated EC-endogenous or tumor cell over-expressed full-length CD44 immunoprecipitated vimentin correlate with our initial findings obtained with soluble recombinant CD44HABD or CD443MUT and strongly suggest that post-translationally modified CD44 can also form a complex with vimentin. However, we were not able to detect full-length CD44 in anti-vimentin antibody immunoprecipitates from HUVEC lysates, which can be explained by the fact that while HUVEC express high levels of vimentin, only a small fraction forms a complex with membrane bound CD44.

We found that CD44 HABD binds to vimentin within its head domain. Vimentin head-domain interactions include ankyrin binding at the plasma membrane [49], vimentin head-domain is also important in filament formation [50]. Our finding that CD44 binds to vimentin head domain is consistent with the proposed

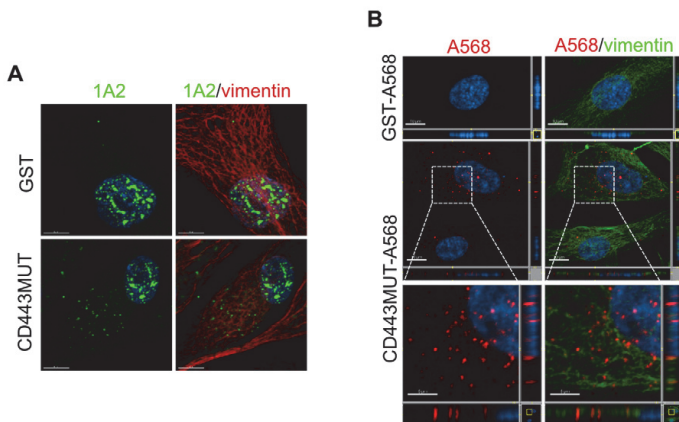


**Figure 4. CD443MUT endocytosis by HUVEC.** HUVEC were grown overnight on glass slides and incubated for 30 min at 37°C with 1  $\mu$ M unlabeled or Alexa Fluor 568-labeled CD443MUT or GST. Cells were analyzed by confocal microscopy. (A) Uptake of unlabeled CD443MUT by HUVEC was detected with anti-CD443MUT mouse mAb 1A2 (green). Vimentin intermediate filaments were detected with rabbit polyclonal antibody (red). Nuclei were stained with Hoechst (blue). Images are maximum intensity projections, generated along the z-axis of image stack. Scale bars, 10  $\mu$ m. (B) Internalization of directly Alexa Fluor 568-labeled CD443MUT by HUVEC (red). Vimentin (green) was detected with V9 mAb. Scale bars, upper and middle panels 10  $\mu$ m; insets 5  $\mu$ m.  
doi:10.1371/journal.pone.0029305.g004

vimentin structure. Parallely aligned dimers of vimentin assemble laterally into tetramers in a fashion whereby first halves of antiparallel coiled-coil domains overlap. Physiologically, vimentin forms a non-polar 32-meric unit-length filaments (ULF) consisting of 16 dimers or 8 tetramers [51]. The observed stoichiometries of 6–10 moles of vimentin per one mole CD443MUT probably reflects the number of head domains available on the ULF surface. The Kd values calculated from SPR data (12–37 nM) for the high affinity binding site are about 2–5 times higher than Kd-s resulting from ITC experiments (74 nM). Such experimental discrepancy can be explained either by limited dynamics of the immobilized vimentin or by sterical hindrances in the environment of the SPR chip. Currently the exact model of vimentin binding of CD44 or whether its binding site coincides with the HA binding surface, is not known. However, our data show that pharmacophores for HA-binding are not necessary for vimentin binding. Our data suggest a protein-protein interaction model which is constrained by the fact that CD44 is a type I membrane receptor and vimentin is a cytoplasmic intermediate filament protein. Nevertheless, several independent findings make this interaction spatiotemporally feasible. In addition to generation of CD44 intracellular domain resulting from shedding, full-length CD44 is also endocytosed and transported to the nucleus via NLS located in its intracellular domain [52,53]. In this process CD44 acts as scaffold for STAT3 and p300 [53]. Importantly, leptomycin B induces CD44 nuclear accumulation, suggesting a nuclear-cytoplasmic shuttling [52]. On the other hand, cell surface vimentin is a well-known phenomenon without any known function. We show that cell surface vimentin is readily detectable in primary human endothelial cells, in addition to its previously reported presence in malignant lymphocytes, activated macrophages and platelets [34–36]. Vimentin provides bacterial binding sites on the surface of human brain endothelial cells [37]. Our results suggest that vimentin might provide a binding site for soluble CD44 on EC. This is supported by our result that exogenously added vimentin can efficiently displace CD443MUT from ECs. In addition, we found that CD443MUT EC binding

was enhanced by VEGF. These results were confirmed by experiments of cell surface biotinylation of starved or VEGF-induced ECs showing that CD443MUT was able to pull-down biotinylated vimentin from VEGF-treated but not from serum starved ECs. The discrepancy between the binding of CD443MUT to starved EC in cellular binding experiment and lack of any detectable biotinylated vimentin in pull-downs from starved EC could be explained by the different length of serum starvation in these experiments (6 h v. over-night, respectively). We suggest that the physiological relevance of these results is supported by findings that vimentin and CD44 are up-regulated on tumor endothelial cells, whereas vimentin has been proposed as a potential anti-angiogenesis target [3,38].

Here we show that after binding CD44HABD and its non-HA-binding triple mutant are endocytosed by ECs. A fraction of CD44HABD-proteins colocalized with generic endocytosis tracer CTxB-positive vesicles and were targeted to early endosomal structures. Importantly, we found that CD443MUT uptake was lost in vimentin knock-out endothelial cells, suggesting further that such internalization is mediated by vimentin. The number of CD443MUT-positive vesicles and early-endosomal localization decreased rapidly, most probably suggesting its targeting to lysosomal degradation. However, we were not able to detect significant accumulation of fluorescently labeled CD443MUT within late endosomal compartment.

We propose that vimentin forms a complex with full-length CD44. In this model, soluble CD44 antagonizes binding of membrane CD44 to vimentin. However, the role for soluble CD44 in tumorigenesis still remains elusive, as highly elevated soluble CD44 associates with aggressive growth and bad prognosis in cancer patients, and yet our previous results suggest that recombinant CD44 administration can inhibit tumor xenograft growth and angiogenesis [27]. We can speculate, that in cancer patients with high sCD44, tumor cells have acquired resistance to its inhibitory effects, while shedding of cell-surface bound CD44 confers significant selective advantage in tumor microenvironment. In summary, given the facts that the expression of CD44

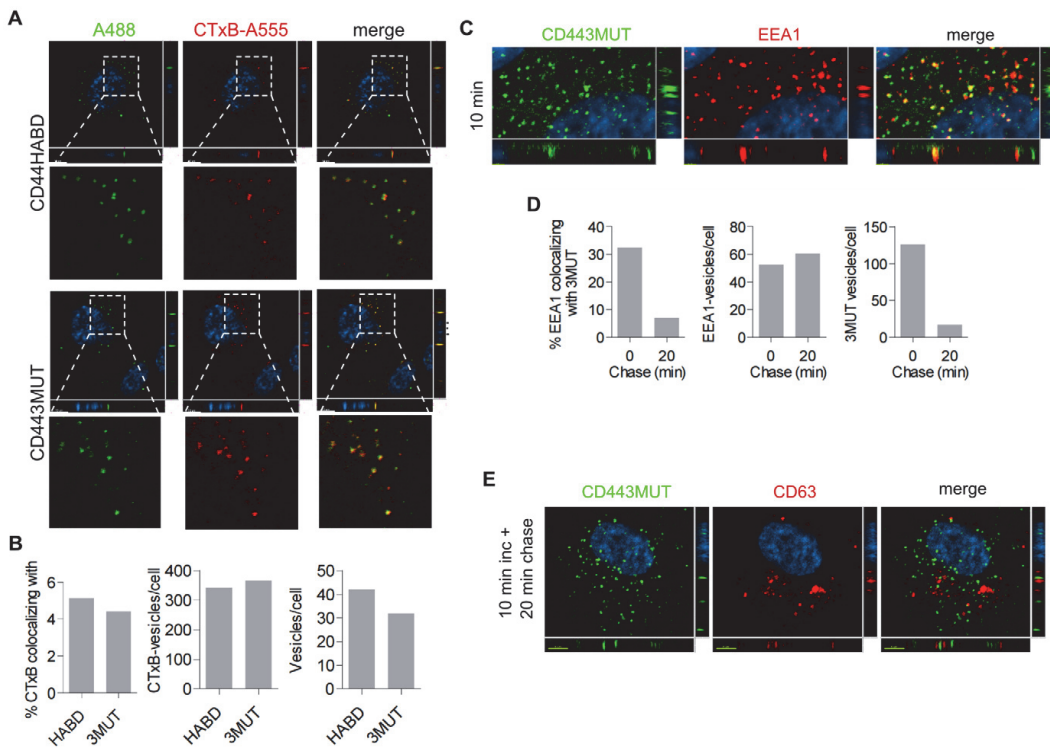


**Figure 5. Analysis of endocytosed CD443MUT localization.** (A) HUVEC were incubated with A488-labeled CD44HABD or CD443MUT (green) in the presence of CTxB-A555 (red) for 30 min. Nuclei were stained with Hoechst. Images show single confocal plane. Scale bars, 10  $\mu$ m. (B) Colocalization analysis of CD44HABD (HABD) and CD443MUT (3MUT) with CTxB. Left, the fraction of CTxB-vesicles colocalizing with HABD ( $n=39$  cells) or 3MUT ( $n=38$  cells). Middle, the number of CTxB-vesicles per cell; right, the number of HABD- or 3MUT-containing vesicles per cell. (C–E) HUVEC were incubated with CD443MUT-A488 for 10 min after which CD443MUT-containing media was changed to 10% FBS HUVEC growth media and cells were further incubated for 20 min. Then cells were fixed and stained with anti-EEA1 or anti-CD63 antibodies. (C) Localization of 3MUT- and early endosomal marker EEA1-positive vesicles after 10 min incubation in HUVEC. (D) Quantitation of EEA1-vesicles colocalizing with CD443MUT after 10 min incubation ( $n=26$  cells) and after 20 min chase ( $n=40$  cells; left). The number of EEA1- and 3MUT vesicles per cell (middle and left, respectively). (E) Localization of internalized 3MUT and late endosomal protein CD63-positive vesicles. Scale bars, 2  $\mu$ m (C) and 5  $\mu$ m (E). doi:10.1371/journal.pone.0029305.g005

and vimentin correlate with EMT in cancer cells, and with tumor angiogenesis, our findings provide rationale for further functional studies on the role of these proteins in EMT and angiogenesis.

## Materials and Methods

### Cell lines and antibodies

HUVEC and MLEC cells were grown in M199 medium supplemented with 20% FBS, 4 mM L-glutamine, 50  $\mu$ g/ml heparin and 30  $\mu$ g/ml EC growth supplement (ECGS, Upstate Biotechnology, Lake Placid, NY, USA). MCF-7 cells (ATCC, Manassas, VA, USA) were grown in RPMI, supplemented with 10% FBS and 2 mM L-glutamine. Anti-vimentin (V9), anti-Myc (A-14) and anti-HDAC1 (H-11) antibodies were from Santa Cruz Biotechnology (Santa Cruz, CA, USA). Anti-vimentin rabbit polyclonal (18-272-196311) was from Genway (San Diego, CA, USA). Anti human-CD44 (2C5) was from R&D Systems (Minneapolis, MN, USA). Mouse anti-human CD44 (H4C4) was from DSHB (University of Iowa, IA, USA). Anti CD443MUT mouse mAb 1A2 (Figure S2) was generated by LabAS Ltd (Tartu, Estonia).

Anti-CD44 (MEM-263) was from EXBIO Praha (Czech Republic). Anti-mouse PECAM-1 (MEC13.3), anti-mouse ICAM-2 (3C4) and anti-EEA1 mAb were from BD Pharmingen (Palo Alto, CA, USA). Rat anti-CD63/lamp-3 (R5G2) was from MBL International (Woburn, MA, USA). Anti-Flag-M2 antibody was from Sigma.

### Purification of recombinant proteins and fluorescence labeling

CD44HABD and CD443MUT GST fusion-proteins were purified as described [27]. CD44HABD and CD443MUT include aa 21–132 of human CD44 protein. CD44HABD and -3MUT were expressed using pET11c vector (Novagen). Urea dissolved inclusion bodies were purified by gel filtration in Superdex-200HR 16/60 column (GE Healthcare, Uppsala, Sweden). Refolding was performed by gradient dialysis into 50 mM Tris pH 8.0, 150 mM NaCl and final dialysis into PBS. Endotoxin level was measured using the Endosafe-PTS (Charles River, L'Arbresle, France). Endotoxin values of CD443MUT batches were 22–93 EU/mg. Human vimentin was expressed using pET15b vector (Novagen). His-tagged vimentin was purified using Ni-affinity resin (Sigma).

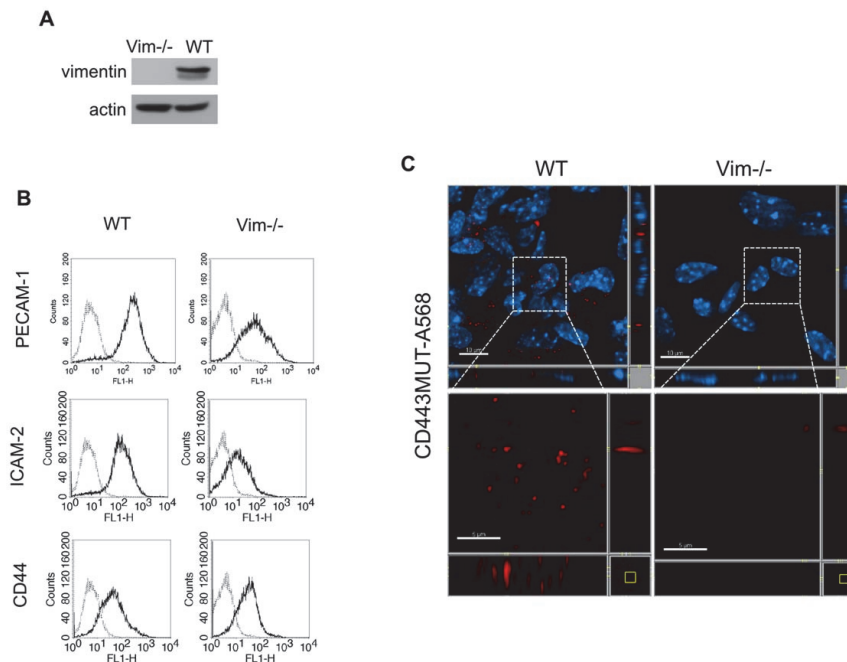


**Figure 6. Vimentin dependent endocytosis of CD443MUT.** MLEC were isolated either from wild-type (WT) or vimentin-null mice. (A) Immunoblot of WT or Vim<sup>-/-</sup> MLEC lysates with anti-vimentin rabbit polyclonal antibody. (B) FACS analysis of MLEC for cell surface markers with either anti-PECAM-1, anti-ICAM-2 or anti-CD44 antibodies (black lines). Gray lines, no primary antibody controls. (C) MLEC-s were incubated with CD443MUT-A568 (red) for 30 min and processed for immunofluorescence. Scale bars, upper panels 10 µm; insets 5 µm. doi:10.1371/journal.pone.0029305.g006

under denaturing conditions. Refolding was performed by gradient dialysis into 10 mM Tris pH 8.0 with final dialysis into 10 mM phosphate buffer pH 7.4. Proteins were fluorescence-labeled using sulfo-NHS-Alexa Fluor 488 or -568 protein labeling kit (Molecular Probes, Eugene, OR, USA).

#### GST pull-down, immunoprecipitation and cell surface biotinylation

Adherent cells were rinsed with ice-cold PBS and lysed on ice in 50 mM Tris pH 8.0, supplemented with protease inhibitor cocktail (PIC; Roche, Mannheim, Germany). Lysate was centrifuged at 14000 rpm for 30 min at 4°C. Pellet was solubilized in 2% CHAPS, 50 mM Tris pH 8.0, 50 mM NaCl, PIC buffer and centrifuged at 14000 rpm for 10 min at 4°C. Supernatant was precleared by incubation with GST-bound glutathione-sepharose 4FF beads (Amersham Biosciences, Uppsala, Sweden). Precleared lysate was incubated overnight at 4°C with 10 µg GST, GST-tagged CD44HABD or CD443MUT immobilized onto glutathione beads. After washes with 50 mM Tris pH 8.0, 150 mM NaCl, PIC buffer, beads were eluted with 20 mM reduced glutathione in 50 mM Tris pH 8.0. Eluates were precipitated with 20% TCA, precipitate was washed with cold acetone and aspirated dry. For MALDI-TOF MS analysis of tryptic peptides, protein samples were alkylated and visualized by silver staining on SDS-PAGE.

For biotinylation, adherent cells were incubated with 1 mM EZ-Link Sulfo-NHS-LC-biotin (Pierce, Rockford, IL, USA) in PBS-0.05% Na<sub>2</sub>S<sub>2</sub>O<sub>3</sub> for 30 min on ice, washed with 100 mM glycine-PBS

and lysed as described above. For IP of endogenous proteins, adherent cells were rinsed with cold PBS and lysed in 50 mM Tris pH 8.0, 50 mM NaCl, 1% CHAPS, PIC buffer. Lysate was centrifuged at 14000 rpm for 30 min at 4°C. Supernatant was precleared with anti-HDAC1 immobilized onto protein A/G sepharose beads (Amersham Biosciences) at 4°C. Precleared lysate was incubated with anti-HDAC1 or anti-CD44 (MEM-263) antibodies immobilized onto protein A/G beads overnight at 4°C. Beads were washed with lysis buffer and bound proteins were eluted with 0.5 M glycine (pH 2.5). Finally, pH of eluates was adjusted with 1 M Tris pH 8.0 and they were analyzed by immunoblotting using anti-CD44 (2C5) or rabbit anti-vimentin antibody. For IP of over-expressed proteins, adherent cells were rinsed in cold PBS, lysed in lysis buffer containing 40 mM Hepes pH 7.4, 120 mM NaCl, 1 mM EDTA, 0.6% CHAPS and PIC. Lysates were centrifuged at 14000 rpm for 30 min at 4°C. Supernatants were incubated with anti-Flag-M2 affinity gel (Sigma) overnight at 4°C, beads were washed with lysis buffer and bound proteins were eluted with 2× Laemmli sample buffer. Eluted protein complexes were analyzed by immunoblotting with anti-Flag-M2 or anti-Myc.

#### Isothermal titration calorimetry and surface plasmon resonance

ITC measurements were performed on a Nano-2G instrument (TA Instruments, New Castle, DE, USA). Experiments were performed in 50 mM Tris, 150 mM NaCl, pH 8.0 at 25°C. The

main experimental parameters were: sample cell volume – 1 ml, syringe size – 250  $\mu$ l, stirring rate – 250 rpm, injection volume – 10  $\mu$ l, time interval between injections – 300 s. Titration data were analyzed by non-linear fitting (SigmaPlot 10). SPR measurements were performed on Biacore3000 (GE Healthcare). Vimentin was covalently coupled to CM5 chip using amine coupling kit (GE Healthcare). In association phase, CD443MUT concentrations 0.46–123  $\mu$ M were injected over the chip surface. In the dissociation phase, the sensor chip surface was eluted with buffer 50 mM Tris, 150 mM NaCl, pH 8.0. The association rate constants and the dissociation rate constants were estimated using BLAevaluation software (GE Healthcare) using a parallel binding model, A+B1  $\leftrightarrow$  AB1, A+B2  $\leftrightarrow$  AB2.  $K_d$  values were also determined from analysis of the equilibrium data using equation 1:  $\Delta R = (\Delta R_{max} \cdot x) / (K_d + x) + (c \cdot x)$ , where  $x$  – concentration of the injected protein,  $\Delta R$  – the increase of the response value at equilibrium,  $\Delta R_{max}$  – capacity of the immobilised vimentin to bind a protein (the number of binding sites), and  $c$  describes weak or non-specific interaction.

### Displacement assays

Adherent cells were harvested from culture plates with 5 mM EDTA in PBS. Proteins were iodinated with  $^{125}$ I by using Iodo-beads (Pierce). Cells were resuspended in incubation buffer 20 mM Tris-HCl pH 7.5, 5 mM  $MgCl_2$ , 30 mM NaCl, 3 mM  $CaCl_2$  or DMEM, 25 mM HEPES, 0.1% BSA. Cell suspension was transferred into 96-well microtitre plate in 100  $\mu$ l volume. Unlabeled protein at different concentrations and  $^{125}$ I labeled protein in 20  $\mu$ l volume of incubation buffer was added into wells. Reactions were incubated overnight at 4°C and stopped by filtration through GF/B filters blocked with 0.1% BSA-PBS, followed by washes with cold PBS. Filters were transferred into 5 ml vials and bound radioactivity was measured using gamma counter (PerkinElmer).

### FACS analyses

For CD443MUT cellular binding, HUVEC were serum starved 6 h and then induced for 30 min at 37°C with 10 ng/ml VEGF-165 in media containing 0.5% FBS. Alexa Fluor 488-conjugated CD443MUT or GST was added into media at 25  $\mu$ g/ml and cells were incubated for 1 h on ice. Cells were harvested from culture plates by scraping. After washes with 0.1% BSA-PBS, cells were fixed in 4% formaldehyde-PBS and analyzed using FACSCalibur flow cytometer (BD Biosciences).

### DNA constructs and transfection

Full-length vimentin was PCR amplified from human vimentin cDNA and inserted into EcoRI/SacII site of pcDNA3.1/MycHisB vector (Invitrogen). Vimentin deletion mutants containing amino acids 1-96 (VIM1-96), 1-245 (VIM1-245), 246-466 (VIM246-466) and 97-466 (VIM97-466) were PCR amplified from human vimentin cDNA using oligonucleotide pairs containing EcoRI/NotI sites. PCR fragments were inserted into EcoRI/NotI site of pcDNA3.1/MycHisB vector. Vimentin-GFP (GFP, green fluorescent protein) constructs were created by inserting EcoRI/SacII fragment from respective vimentin-pcDNA3.1/MycHisB constructs into pEGFP-N1 vector. Vimentin deletion mutant containing aa 407-466 (VIM407-466) was PCR amplified from human vimentin cDNA and inserted into EcoRI/SacII site of pEGFP-C2 vector. For creating Flag-tagged CD44 DNA construct, full-length CD44 was PCR amplified from human standard CD44 isoform cDNA and inserted into EcoRI/NotI site of pCMV-Tag4a vector (Stratagene). MCF-7 cells were transfected using 1:2 DNA:PEI ratio. Transfected cells were

grown at 37°C for 24 h. GST pull-down was performed as described above.

### Mouse lung endothelial cells

Wild-type MLEC were isolated from C3H mouse strain (The Jackson Laboratory) and vimentin $^{-/-}$  from Vim1/Vim1 mice [31] obtained from EMMA (CNRS/CDTA, Orleans, France). Lungs from three 6–8 week old mice were dissected and finely minced with scissors on a dry culture dish. Lung pieces were put into 20 ml pre-warmed 0.2% collagenase-I (Sigma) in PBS and incubated with gentle agitation for 45 min at 37°C. Collagenase digested lung suspension was triturated through 100  $\mu$ m cell strainer (BD Biosciences). Cell suspension was centrifuged 8 min 400 g at 4°C. Cell pellet was resuspended in 2 ml 0.1% BSA-PBS. Cells were sorted by incubation for 15 min at RT with sheep anti-rat IgG Dynabeads (Dyna, Norway) coated with rat anti-mouse CD31 (MEC13.3) and rat anti-mouse ICAM-2 (3C4) antibodies. Bead-bound cells were separated using a magnetic rack and washed five times with M199 medium containing 10% FBS. After separation, cells were plated onto dish and grown in M199 containing 10 mM HEPES, 20% FBS, 4 mM L-glutamine and supplemented with 50  $\mu$ g/ml Heparin, 30  $\mu$ g/ml ECGS and penicillin-streptomycin.

### Internalization assay, immunofluorescence microscopy and image processing

For internalization assays, cells on 8-well slide (BD Falcon) were incubated at 37°C with CTxB-Alexa 555 (Invitrogen) and/or CD44HABD-proteins at 13  $\mu$ g/ml ( $\approx$ 1  $\mu$ M) in 0.5% FBS containing media for 10 or 30 min. After 10 min uptake, cells were washed with PBS two to three times and media was changed to 10% FBS containing M199 HUVEC growth media and slides were incubated for 20 or 50 min at 37°C. After incubations cells were washed and fixed with 4% formaldehyde-PBS on for 10 min on ice and for 10 min at RT. Cells were permeabilized using 0.1% Triton X-100 in 0.1% BSA-PBS. Antibodies were diluted in 0.1% BSA-PBS. Secondary antibody dilutions were supplemented with 10  $\mu$ g/ml Hoechst 33258 (Sigma). Slides were mounted in Mowiol 4–88 (Sigma-Aldrich, St Louis, MO, USA). Confocal fluorescent imaging was performed using Zeiss LSM510 microscope with  $\times$ 63/1.4 oil immersion objective in multi-channel mode (Carl Zeiss MicroImaging, Germany). Images were prepared using Imaris 6.4 software (Bitplane, Zurich, Switzerland). For quantitation of endocytosis and vesicular colocalization, single slices from the middle plane of the cell were semi-automatically selected from confocal image stacks using Fiji package (<http://pacific.mpi-cbg.de/wiki/index.php/Fiji>). Cell-profiler 2.0 (r10415) software was used for image segmentation and automated analysis [54]. Endosomal outlines were identified using Otsu global threshold, then endosomal marker/tracer object outlines were used to create a mask to identify colocalizing CD44HABD- or CD443MUT objects. Within these objects correlation was measured between endocytosis marker and CD44, and objects showing positive correlation were finally counted as colocalizing. For calculation of average correlation coefficient and 95% confidence interval, individual object coefficients were transformed to z scores.

### Statistical analysis of data

Data represent mean  $\pm$  SE. Statistical analysis and non-linear fitting of data was performed using GraphPad Prism 5 software (San Diego, CA, USA).

## Supporting Information

**Figure S1 Cell-surface expression of overexpressed vimentin in MCF-7 cells.** Vimentin- or empty vector transfected MCF-7 cells were subjected to cell surface biotinylation (see Materials and Methods). Lysates were immunoprecipitated with anti-vimentin antibody. Lysates and immunoprecipitates were analyzed by WB using streptavidin-HRP (upper panel) or anti-vimentin antibody (lower panel). Arrows indicate the location of full length vimentin. (TIF)

**Figure S2 Characterization of anti-CD443MUT mouse mAb 1A2.** (A) ELISA analysis of serially diluted 1A2 mAb (3.1 mg/ml) of rat serum-, rat serum+CD443MUT- or CD443MUT-coated wells. PBS, no primary antibody control. (B) Microplate wells were coated with different concentrations of CD443MUT mixed with rat serum and analyzed by ELISA using 1A2 mAb at 1:400 dilution. (C) Wells were coated with CD44 peptides and analyzed by ELISA using 1A2 mAb at 1:50000

## References

- Günther U, Hofmann M, Rudy W, Reber S, Zöller M, et al. (1991) A new variant of glycoprotein CD44 confers metastatic potential to rat carcinoma cells. *Cell* 65: 13–24.
- Kogerman P, Sy MS, Culp LA (1997) Counter-selection for over-expressed human CD44s in primary tumors versus lung metastases in a mouse fibrosarcoma model. *Oncogene* 15: 1407–1416.
- Griffioen AW, Coenen MJ, Damen CA, Hellwig SM, van Weering DH, et al. (1997) CD44 is involved in tumor angiogenesis; an activation antigen on human endothelial cells. *Blood* 90: 1150–1159.
- Cao G, Savani RC, Fehrenbach M, Lyons C, Zhang L, et al. (2006) Involvement of endothelial CD44 during in vivo angiogenesis. *Am J Pathol* 169: 325–336.
- Katoh S, McCarthy JB, Kincade PW (1994) Characterization of soluble CD44 in the circulation of mice. Levels are affected by immune activity and tumor growth. *J Immunol* 153: 3440–3449.
- Cichy J, Bals R, Potempa J, Mani A, Pure E (2002) Proteinase-mediated release of epithelial cell-associated CD44. Extracellular CD44 complexes with components of cellular matrices. *J Biol Chem* 277: 44440–44447.
- Yu Q, Toole BP (1996) A new alternatively spliced exon between v9 and v10 provides a molecular basis for synthesis of soluble CD44. *J Biol Chem* 271: 20603–20607.
- Okamoto I, Kawano Y, Tsuki H, Sasaki J, Nakao M, et al. (1999) CD44 cleavage induced by a membrane-associated metalloprotease plays a critical role in tumor cell migration. *Oncogene* 18: 1435–1446.
- Nakamura H, Suenaga N, Taniwaki K, Matsuki H, Yonezawa K, et al. (2004) Constitutive and induced CD44 shedding by ADAM-like proteases and membrane-type 1 matrix metalloproteinase. *Cancer Res* 64: 876–882.
- Ristimäki R, Joensuu H, Grön-Virta K, Salmi M, Jalkanen S (1997) Origin and function of circulating CD44 in non-Hodgkin's lymphoma. *J Immunol* 158: 3000–3008.
- Guo YJ, Liu G, Wang X, Jin D, Wu M, et al. (1994) Potential use of soluble CD44 in serum as indicator of tumor burden and metastasis in patients with gastric or colon cancer. *Cancer Res* 54: 422–426.
- Mayer S, zur Hausen A, Watermann DO, Stamm S, Jäger M, et al. (2008) Increased soluble CD44 concentrations are associated with larger tumor size and lymph node metastasis in breast cancer patients. *J Cancer Res Clin Oncol* 134: 1229–1235.
- Mäenpää H, Ristimäki R, Virtamo J, Franssila K, Albanes D, et al. (2000) Serum CD44 levels preceding the diagnosis of non-Hodgkin's lymphoma. *Leuk Lymphoma* 37: 585–592.
- Niitsu N, Iijima K (2002) High serum soluble CD44 is correlated with a poor outcome of aggressive non-Hodgkin's lymphoma. *Leuk Res* 26: 241–248.
- Ristimäki R, Joensuu H, Lappalainen K, Teerenhovi L, Jalkanen S (1997) Elevated serum CD44 level is associated with unfavorable outcome in non-Hodgkin's lymphoma. *Blood* 90: 4039–4045.
- Krettek A, Sukhova GK, Schönbeck U, Libby P (2004) Enhanced expression of CD44 variants in human atherosclerosis and abdominal aortic aneurysms: possible role for a feedback loop in endothelial cells. *Am J Pathol* 163: 1571–1581.
- Ristimäki R, Joensuu H, Salmi M, Jalkanen S (1994) Serum CD44 in malignant lymphoma: an association with treatment response. *Blood* 84: 238–243.
- Yu Q, Toole BP, Stamenkovic I (1997) Induction of apoptosis of metastatic mammary carcinoma cells in vivo by disruption of tumor cell surface CD44 function. *J Exp Med* 186: 1985–1996.
- Ahrens T, Sleeman JP, Schempp CM, Howells N, Hofmann M, et al. (2001) Soluble CD44 inhibits melanoma tumor growth by blocking cell surface CD44 binding to hyaluronic acid. *Oncogene* 20: 3399–3408.

dilution. (D) Amino acid alignment of CD44HABD, CD443MUT and peptides used for epitope mapping. Amino acid numbering is according to human CD44; mutated positions are indicated in green (wild-type amino acids) or red (mutant amino acids). Bars, mean  $\pm$  SD.

(TIF)

## Acknowledgments

We thank Dr. Ulf Hellmann for MS analyses, Miina Lillepruun and Dr. Aivar Lõökene for calorimetry and SPR, Aili Kallastu for protein purification, and Kersti Olsper for technical assistance. We thank Dr. Emma Colucci-Guyon for vimentin-deficient mice.

## Author Contributions

Conceived and designed the experiments: TP AP LK AV PK. Performed the experiments: TP AP LK MT WA. Analyzed the data: TP AP LK AV. Wrote the paper: TP AP AV.

- Peterson RM, Yu Q, Stamenkovic I, Toole BP (2000) Perturbation of hyaluronan interactions by soluble CD44 inhibits growth of murine mammary carcinoma cells in ascites. *Am J Pathol* 156: 2159–2167.
- Lopez JI, Camenisch TD, Stevens MV, Sands BJ, McDonald J, et al. (2005) CD44 Attenuates Metastatic Invasion during Breast Cancer Progression. *Cancer Research*. pp 6755–6763.
- Kohda D, Morton CJ, Parkar AA, Hatanaka H, Inagaki FM, et al. (1996) Solution structure of the link module: a hyaluronan-binding domain involved in extracellular matrix stability and cell migration. *Cell* 86: 767–775.
- Banerji S, Wright AJ, Noble M, Mahoney DJ, Campbell ID, et al. (2007) Structures of the Cd44-hyaluronan complex provide insight into a fundamental carbohydrate-protein interaction. *Nat Struct Mol Biol* 14: 234–239.
- Teriete P, Banerji S, Noble M, Blundell CD, Wright AJ, et al. (2004) Structure of the regulatory hyaluronan binding domain in the inflammatory leukocyte homing receptor CD44. *Molecular Cell* 13: 483–496.
- Bajorath J, Greenfield B, Munro SB, Day AJ, Aruffo A (1998) Identification of CD44 residues important for hyaluronan binding and delineation of the binding site. *J Biol Chem* 273: 338–343.
- English NM, Lesley JF, Hyman R (1998) Site-specific de-N-glycosylation of CD44 can activate hyaluronan binding, and CD44 activation states show distinct threshold densities for hyaluronan binding. *Cancer Res* 58: 3736–3742.
- Pall T, Gad A, Kasak L, Dreus M, Strömblad S, et al. (2004) Recombinant CD44-HABD is a novel and potent direct angiogenesis inhibitor enforcing endothelial cell-specific growth inhibition independently of hyaluronic acid binding. *Oncogene* 23: 7874–7881.
- Ivaska J, Vuoriluoto K, Huovinen T, Izawa I, Inagaki M, et al. (2005) PKCepsilon-mediated phosphorylation of vimentin controls integrin recycling and motility. *EMBO J* 24: 3834–3845.
- Styers ML, Salazar G, Love R, Peden AA, Kowalczyk AP, et al. (2004) The endo-lysosomal sorting machinery interacts with the intermediate filament cytoskeleton. *Mol Biol Cell* 15: 5369–5382.
- Faigle W, Colucci-Guyon E, Louvard D, Amigorena S, Galli T (2000) Vimentin filaments in fibroblasts are a reservoir for SNAP23, a component of the membrane fusion machinery. *Mol Biol Cell* 11: 3485–3494.
- Colucci-Guyon E, Portier MM, Dumia I, Paulin D, Pournin S, et al. (1994) Mice lacking vimentin develop and reproduce without an obvious phenotype. *Cell* 79: 679–694.
- Henrion D, Terzi F, Matrougui K, Duriez M, Boulanger CM, et al. (1997) Impaired flow-induced dilation in mesenteric resistance arteries from mice lacking vimentin. *J Clin Invest* 100: 2909–2914.
- Terzi F, Henrion D, Colucci-Guyon E, Federici P, Babinet C, et al. (1997) Reduction of renal mass is lethal in mice lacking vimentin. Role of endothelin-nitric oxide imbalance. *J Clin Invest* 100: 1520–1528.
- Mor-Vaknin N, Panturieri A, Sitvala K, Markovitz DM (2003) Vimentin is secreted by activated macrophages. *Nat Cell Biol* 5: 59–63.
- Huet D, Bagot M, Loyaux D, Capdevielle J, Conraux L, et al. (2006) SC5 mAb represents a unique tool for the detection of extracellular vimentin as a specific marker of Sezary cells. *J Immunol* 176: 652–659.
- Podor TJ, Singh D, Chindemi P, Foulon DM, McKelvie R, et al. (2002) Vimentin exposed on activated platelets and platelet microparticles localizes vitronectin and plasminogen activator inhibitor complexes on their surface. *J Biol Chem* 277: 7529–7539.
- Zou Y, He L, Huang S (2006) Identification of a surface protein on human brain microvascular endothelial cells as vimentin interacting with Escherichia coli invasion protein IbeA. *Biochem Biophys Res Commun* 351: 625–630.

38. van Beijnum JR, Dings RP, van der Linden E, Zwaans BMM, Ramaekers FCS, et al. (2006) Gene expression of tumor angiogenesis dissected: specific targeting of colon cancer angiogenic vasculature. *Blood* 108: 2339–2348.
39. Oliferenko S, Paiha K, Harder T, Gerke V, Schwärzler C, et al. (1999) Analysis of CD44-containing lipid rafts: Recruitment of annexin II and stabilization by the actin cytoskeleton. *J Cell Biol* 146: 843–854.
40. Runembert I, Queffeuilou G, Federici P, Vrtovnik F, Colucci-Guyon E, et al. (2002) Vimentin affects localization and activity of sodium-glucose cotransporter SGLT1 in membrane rafts. *J Cell Sci* 115: 713–724.
41. Lafourcade C, Sobo K, Kieffer-Jaquinod S, Garin J, van der Goot FG (2008) Regulation of the V-ATPase along the endocytic pathway occurs through reversible subunit association and membrane localization. *PLoS One* 3: e2758.
42. Howes MT, Kirkham M, Riches J, Cortese K, Walser PJ, et al. (2010) Clathrin-independent carriers form a high capacity endocytic sorting system at the leading edge of migrating cells. *J Cell Biol* 190: 675–691.
43. Brown RL, Reinke LM, Damerow MS, Perez D, Chodosh LA, et al. (2011) CD44 splice isoform switching in human and mouse epithelium is essential for epithelial-mesenchymal transition and breast cancer progression. *J Clin Invest* 121: 1064–1074.
44. Jalkanen S, Jalkanen M (1992) Lymphocyte CD44 binds the COOH-terminal heparin-binding domain of fibronectin. *J Cell Biol* 116: 817–825.
45. Elms T, Dieterich W, Bauer M, Lampe B, Schuppan D (1996) A chondroitin/dermatan sulfate form of CD44 is a receptor for collagen XIV (undulin). *Exp Cell Res* 229: 388–397.
46. Dimitroff CJ, Lee JY, Rafii S, Fuhlbrigge RC, Sackstein R (2001) CD44 is a major E-selectin ligand on human hematopoietic progenitor cells. *J Cell Biol* 153: 1277–1286.
47. Weber GF, Ashkar S, Glimcher MJ, Cantor H (1996) Receptor-ligand interaction between CD44 and osteopontin (Eta-1). *Science* 271: 509–512.
48. Bartolazzi A, Nocks A, Aruffo A, Spring F, Stamenkovic I (1996) Glycosylation of CD44 is implicated in CD44-mediated cell adhesion to hyaluronan. *J Cell Biol* 132: 1199–1208.
49. Georgatos SD, Weaver DC, Marchesi VT (1985) Site specificity in vimentin-membrane interactions: intermediate filament subunits associate with the plasma membrane via their head domains. *J Cell Biol* 100: 1962–1967.
50. Aziz A, Hess JF, Budamagunta MS, Voss JC, Fitzgerald PG (2010) Site-directed spin labeling and electron paramagnetic resonance determination of vimentin head domain structure. *J Biol Chem* 285: 15278–15285.
51. Sokolova AV, Kreplak L, Wedig T, Mücke N, Svergun DI, et al. (2006) Monitoring intermediate filament assembly by small-angle x-ray scattering reveals the molecular architecture of assembly intermediates. *Proc Natl Acad Sci U S A* 103: 16206–16211.
52. Janiszewska M, De Vito C, Le Bitoux M, Fusco C, Stamenkovic I (2010) Transportin regulates nuclear import of CD44. *J Biol Chem* 285: 30548–30557.
53. Lee J, Wang M, Chen J (2009) Acetylation and activation of STAT3 mediated by nuclear translocation of CD44. *J Cell Biol* 185: 949–957.
54. Carpenter AE, Jones TR, Lamprecht MR, Clarke C, Kang IH, et al. (2006) CellProfiler: image analysis software for identifying and quantifying cell phenotypes. *Genome Biol* 7: R100.

## Supporting information

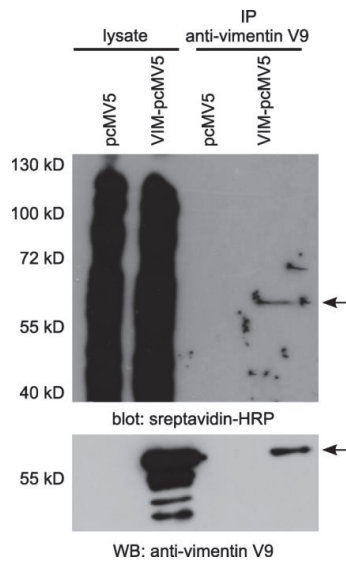


**Figure S1. Cell-surface expression of overexpressed vimentin in MCF-7 cells.** Vimentin- or empty vector transfected MCF-7 cells were subjected to cell surface biotinylation (see [Materials and Methods](#)). Lysates were immunoprecipitated with anti-vimentin antibody. Lysates and immunoprecipitates were analyzed by WB using streptavidin-HRP (upper panel) or anti-vimentin antibody (lower panel). Arrows indicate the location of full length vimentin.

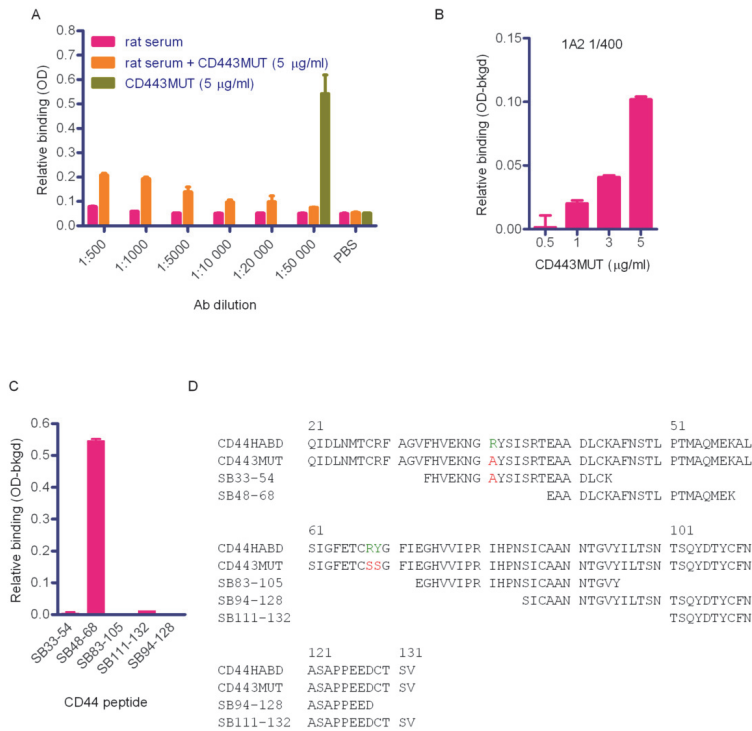


**Figure S2. Characterization of anti-CD443MUT mouse mAb 1A2.** (A) ELISA analysis of serially diluted 1A2 mAb (3.1 mg/ml) of rat serum-, rat serum+CD443MUT- or CD443MUT-coated wells. PBS, no primary antibody control. (B) Microplate wells were coated with different concentrations of CD443MUT mixed with rat serum and analyzed by ELISA using 1A2 mAb at 1:400 dilution. (C) Wells were coated with CD44 peptides and analyzed by ELISA using 1A2 mAb at 1:50000 dilution. (D) Amino acid alignment of CD44HABD, CD443MUT and peptides used for epitope mapping. Amino acid numbering is according to human CD44; mutated positions are indicated in green (wild-type amino acids) or red (mutant amino acids). Bars, mean  $\pm$  SD.



## MANUSCRIPT

**Pink, A, Školnaja, M, Päll, T, Valkna, A (2016).** CD44 controls endothelial proliferation and functions as endogenous inhibitor of angiogenesis. *DOI:* <http://dx.doi.org/10.1101/049494>.



# CD44 Controls Endothelial Proliferation and Functions as Endogenous Inhibitor of Angiogenesis

*Anne Pink, Marianna Školnaja, Taavi Päll, Andres Valkna*

Competence Centre for Cancer Research and Tallinn University of Technology, Akadeemia tee 15, 12618, Tallinn, Estonia

Corresponding author: Andres Valkna  
Email: andres.valkna@ttu.ee

## Abstract

CD44 transmembrane glycoprotein is involved in angiogenesis, but it is not clear whether CD44 functions as a pro- or antiangiogenic molecule. Here, we assess the role of CD44 in angiogenesis and endothelial proliferation by using *Cd44*-null mice and CD44 silencing in human endothelial cells. We demonstrate that angiogenesis is increased in *Cd44*-null mice compared to either wild-type or heterozygous animals. Silencing of CD44 expression in cultured endothelial cells results in their augmented proliferation and viability. The growth-suppressive effect of CD44 is mediated by its extracellular domain and is independent of its hyaluronan binding function. CD44-mediated effect on cell proliferation is independent of specific angiogenic growth factor stimulation. These results show that CD44 expression on endothelial cells constrains endothelial cell proliferation and angiogenesis. Thus, endothelial CD44 might serve as a therapeutic target both in the treatment of cardiovascular diseases, where endothelial protection is desired, as well as in cancer treatment, due to its antiangiogenic properties.

## Introduction

Angiogenesis is a pathophysiological process involved in wound healing as well as tumor growth and metastasis. The switch of normally quiescent blood vessels to angiogenesis is determined by the balance of proangiogenic and antiangiogenic factors in tissue microenvironment. In tumors, endothelial cell (EC) proliferation and survival is regulated by growth factors such as VEGF, FGF-2, or HGF, released either by tumor cells or normal cells in the tumor stroma. A survival benefit has been shown for blocking proangiogenic signaling by VEGF inhibitors in tumor therapy and continuation of such therapy beyond progression [1]. However, tumors can be intrinsically resistant to anti-VEGF therapy or acquire resistance through different mechanisms during the therapy [2]. Better understanding of microenvironmental or EC-specific factors involved in the regulation of EC proliferation and blood vessel formation is needed to develop new more effective antiangiogenic tumor therapies.

CD44 cell-surface glycoprotein has been shown to be necessary for efficient tumor vascularization [3] and to mediate induction of angiogenesis in response to hyaluronan (HA) oligomers [4]. CD44 mediates cell adhesion to its principal ligand HA via its N-terminal HA-binding domain (HABD) [5, 6]. CD44 and HA interaction is important in the immune

response where it mediates leukocyte rolling on HA during leukocyte recruitment into the inflammatory site [7–9]. CD44 also mediates HA-induced effects on vasculature. *In vivo* silencing of endothelial CD44 resulted in reduced vascular density of Matrigel plug implants in response to low molecular weight HA [4]. The interaction of CD44 with high molecular weight HA inhibits vascular smooth muscle cell proliferation, and CD44 deficiency has been shown to increase neointima formation after arterial injury [10]. *Cd44*-null mice display reduced vascularization of Matrigel plugs containing CD44-positive B16 melanoma cells, as well as reduced vessel density in B16 melanoma and ID8-VEGF ovarian carcinoma xenografts [3]. However, the contribution of CD44 to *in vivo* angiogenesis has not been studied in *Cd44*-null mice in less complex models using defined angiogenic growth factors instead of large numbers of tumor cells.

We have previously shown that administration of recombinant soluble CD44 hyaluronan binding domain (HABD) inhibits *in vivo* angiogenesis in both VEGF- and FGF2-stimulated chick chorioallantoic membranes and tumor xenograft growth, and that *in vitro*, sCD44 HABD controls EC proliferation [11]. Significant levels of soluble CD44 have been reported in normal human serum and even higher levels in mouse serum. Increased serum levels of soluble CD44 (sCD44) have been linked to different pathological conditions, including cancer and type 2 diabetes [12–14]. Soluble CD44 is mainly a shedding product of membrane CD44 [15, 16]. If the hypothesis of the proangiogenic role of CD44 holds, recombinant soluble CD44 HABD should function as a decoy receptor for HA, the principal ligand of CD44. Nevertheless, we have previously found that the non-HA binding mutant of CD44 HABD showed similar antiangiogenic and tumor growth inhibitory functions [11], suggesting that a mechanism other than HA binding might be involved.

The aim of the current study was to analyze the effects of *Cd44* gene deficiency and non-HA-binding CD44 HABD treatment on *in vivo* angiogenesis and *in vitro* EC proliferation to conclusively determine the role of CD44 in angiogenesis and in order to cast light upon the mode of action of the non-HA-binding CD44 HABD.

## Results

### ***Cd44*-null mice display increased angiogenic response**

We studied angiogenesis in mice lacking CD44 (*Cd44*<sup>-/-</sup>). In a preliminary experiment, we assessed the invasion of isolectin-B4- and CD105-positive cells into the Matrigel plug in response to 50 ng/ml VEGF. Surprisingly, results indicated that plugs from *Cd44*<sup>-/-</sup> mice contained more cells than plugs from wild-type mice (data not shown). We also tested capillary outgrowth in aortic fragments isolated from *Cd44*<sup>-/-</sup> mice. Aortic fragment assay indicated apparently more robust outgrowth of capillary-like structures from *CD44*<sup>-/-</sup> fragments compared to wild-types (Supplemental Fig. 1 in Online Resource 1). This finding is in agreement with Chun et al. 2004 study [17], showing no defect in capillary outgrowth and vessel morphogenesis in aortic fragments isolated from *Cd44*<sup>-/-</sup> mice. In the following series of experiments, we used the directed *in vivo* angiogenesis assay [18] to quantitatively test FGF-2/VEGF-induced angiogenic response in *Cd44*<sup>-/-</sup> and wild-type mice of C57BL/6, C3H or mixed genetic backgrounds (Fig. 1). We found a  $5.4 \pm 2.2$ -fold increase in blood vessel invasion in response to FGF-2/VEGF compared to unstimulated controls in *Cd44*<sup>-/-</sup> mice of mixed genetic background (t-test:  $P = 0.048$ ,  $N = 2$  experiments, effect size  $1.2 \pm 0.45$  [95% CI, 0.37-2.1]; Fig. 1A). Angiogenesis induction in wild-type mouse strains compared to unstimulated controls was in C3H  $1.4 \pm 0.5$ -fold (t-test:  $P = 0.41$ , effect size  $0.081 \pm 0.071$  [95% CI, -0.061-0.22]), C57BL/6  $1.5 \pm 0.62$ -fold ( $P = 0.38$ , effect size  $0.2 \pm 0.17$  [95% CI, -0.09-0.56]), and in wild-type mice of mixed genetic background  $4.2 \pm 1$ -fold (t-test:  $P = 0.13$ ,

effect size  $0.14 \pm 0.039$  [95% CI, 0.082-0.2]; Fig. 1A). The estimated effect size of growth factor stimulation was large in *Cd44*<sup>-/-</sup> mice with confidence interval ranging from small to very large, whereas in wild-type mouse strains growth factor stimulation displayed small effect size with confidence intervals including zero. When comparing growth factor-stimulated groups, *Cd44*<sup>-/-</sup> mice displayed apparently severalfold higher blood vessel invasion into angioreactors in response to FGF-2/VEGF than wild-type mice. These data suggest that *Cd44* deficiency results in augmented angiogenic response. However, factors other than CD44 might also affect the efficiency of angiogenesis induction in mice of different genetic backgrounds [19].

To confirm increased angiogenesis in the absence of CD44, and to study the contribution of CD44 to neoangiogenesis in an inbred, genetically homogeneous background, we backcrossed *Cd44*<sup>-/-</sup> mice for six generations to the C57BL/6 strain. Using littermate controls, we found that *Cd44* genotype had a significant effect on angiogenesis induction (ANOVA,  $F_{2,42} = 3.98$ ,  $P = 0.026$ ). Angiogenesis was increased in *Cd44*-null animals compared to wild-type or heterozygous mice. FGF-2/VEGF stimulation resulted in a  $2.1 \pm 0.5$ -fold increase of blood vessel invasion in C57BL/6 *Cd44*<sup>+/+</sup> mice (one-way ANOVA,  $P = 0.03$ ; effect size  $0.39 \pm 0.15$  [95% CI, 0.098-0.67]); in a  $1.4 \pm 0.24$ -fold increase in their *Cd44*<sup>+/-</sup> littermates (one-way ANOVA,  $P = 0.061$ ; effect size  $0.22 \pm 0.1$  [95% CI, 0.019-0.4]); and in a  $2.9 \pm 0.75$ -fold increase in their *Cd44*<sup>-/-</sup> littermates (one-way ANOVA,  $P = 0.0039$ ; effect size  $0.96 \pm 0.26$  [95% CI, 0.45-1.5]);  $N = 8$  mice per genotype from 2 independent experiments. Angiogenesis induction was associated with *Cd44* genotype in the growth factor-induced group of mice (ANOVA,  $F_{2,21} = 5.45$ ,  $P = 0.012$ ), whereas there was no difference in baseline vessel invasion between different *Cd44* genotypes in the unstimulated group. Post-hoc testing of pairwise differences indicated that *Cd44*<sup>-/-</sup> mice displayed increased angiogenesis compared to either their *Cd44*<sup>+/-</sup> or *Cd44*<sup>+/+</sup> littermates (Fig. 1B).

We conclude from these experiments that CD44 deficiency results in augmented angiogenesis induction; and thus CD44 functions as an endogenous angiogenesis inhibitor.

## **Recombinant CD44 non-HA-binding mutant Fc-fusion protein inhibits angiogenesis *in vivo***

We studied whether increasing the dose of CD44 by systemic administration of its soluble analog could suppress angiogenesis. We have previously shown that bacterially expressed GST-tagged non-HA-binding CD44 (CD44-3MUT) inhibits angiogenesis in chick chorioallantoic membrane and subcutaneous tumor xenograft growth in mice [11]. Untagged and GST-tagged CD44-3MUT display very short serum half-life limiting their potential *in vivo* use [20]. Thus, in order to improve *in vivo* efficacy, we generated CD44-3MUT with a C-terminal fusion of human IgG1 Fc region (CD44-3MUT-Fc). Regarding pharmacokinetic characterization of CD44-3MUT-Fc, its serum half-life after intravenous administration to rats was 17 min (Supplemental Fig. 2 in Online Resource 1). The volume of distribution of CD44-3MUT-Fc was 18% of total body weight (%TBW), suggesting improved biodistribution compared to untagged CD44-3MUT protein (1.8% TBW; [20]).

We tested the antiangiogenic effects of CD44-3MUT-Fc in athymic nude mice. The results showed that FGF-2/VEGF stimulation led to a  $4.5 \pm 1.1$ -fold increase of blood vessel invasion into angioreactors over the PBS treated control groups (t-test:  $P = 7.7e-07$ ; effect size  $0.8 \pm 0.15$  [95% CI, 0.5-1.1]; Fig. 2B, C). We observed that intraperitoneal treatment of mice with CD44-3MUT-Fc inhibited FGF-2/VEGF-induced angiogenesis. In the treatment group receiving 25 mg/kg CD44-3MUT-Fc, angiogenesis was inhibited to the unstimulated basal level compared to the growth factor-induced PBS treatment group (t-test:  $P = 1.6e-05$ ; effect size  $-0.8 \pm 0.16$  [95% CI, -1.1-0.5]). Administration of 0.5 or 5 mg/kg CD44-3MUT-Fc also

resulted in apparent angiogenesis inhibition, but the response was less robust (Fig. 2C). For recombinant protein control treatments, we used irrelevant rhIgG mAb or rhIgG-Fc. Both these molecules were purified identically to CD44-3MUT-Fc. The 0.5 mg/kg CD44-3MUT-Fc treatment showed significant inhibitory effect compared to pooled 0.5 mg/kg rhIgG/rhIgG-Fc control treatment group (t-test:  $P = 0.034$ ; effect size  $0.5 \pm 0.24$  [95% CI, 0-0.9]). Mice receiving intraperitoneally 5 or 15 mg/kg doses of rhIgG-Fc showed similar angiogenic response as PBS and 0.5 mg/kg rhIgG-Fc control treatment groups, suggesting that the IgG-Fc portion of CD44-3MUT-Fc is not responsible for the effects observed. Together, our results show that systemic administration of CD44-3MUT-Fc effectively inhibits *in vivo* angiogenesis.

## **Soluble CD44 levels are not affected by angiogenesis**

Serum levels of sCD44 are increased due to enhanced CD44 shedding in case of inflammation or tumor growth. Previous research suggests that serum sCD44 concentrations show substantial variability between different mouse strains, and are significantly reduced ( $< 1 \mu\text{g/ml}$ ) in severely immunodeficient mice [21]. To assess the significance of sCD44 in angiogenic response, we determined sCD44 concentrations in the sera of different wild-type mouse strains, in  $Cd44^{+/-}$  mice, and in athymic nude mice. Sera from  $Cd44^{-/-}$  mice were used as negative controls. We found that serum concentrations of sCD44 were similar in athymic nude mice and in wild-type mouse strains (Fig. 3A and Table 1). Soluble CD44 levels in  $Cd44^{+/-}$  animals were reduced on average by 35% (95% credible interval: 16-53%) compared to  $Cd44^{+/+}$  mice.

To analyse whether sCD44 concentrations correlate with angiogenesis induction, we excluded  $Cd44^{-/-}$  mice and nude mice from the dataset. We found no correlation between relative blood vessel invasion and post-experiment serum levels of sCD44 (Fig. 3B). Next, we evaluated whether the induction of angiogenesis, rhIgG-Fc or systemic treatments with CD44-3MUT-Fc that we used in the *in vivo* angiogenesis model lead to changes in the serum levels of sCD44 in nude mice. This analysis showed that neither angiogenesis induction nor treatments had any effect on the serum concentrations of sCD44 in nude mice (ANOVA,  $F_{11,32} = 0.975$ ,  $P = 0.49$ ; Fig. 3C). It also revealed that there was no correlation between post-experiment serum concentrations of sCD44 and vessel invasion into angioreactors irrespective of experimental intervention (Fig. 3D).

## **CD44-3MUT-Fc inhibits endothelial cell proliferation and viability**

To find out whether CD44-3MUT-Fc-mediated inhibition of angiogenesis is caused by its effects on ECs, we tested CD44-3MUT-Fc in a cell proliferation assay. We used cells synchronized by serum starvation to model the initial stages of stimulation of quiescent endothelial cells (Fig. 4A). We applied different concentrations of CD44-3MUT-Fc to growth arrested HUVECs and released cells from arrest by stimulation with 25 ng/ml VEGF. Real-time growth curves of untreated controls show that 25 ng/ml VEGF induces robust proliferation in HUVECs that is sustained for at least 72 h (Fig. 4B, leftmost panel). In contrast, CD44-3MUT-Fc treatment dose-dependently suppressed 25 ng/ml VEGF-stimulated HUVEC growth, compared to rhIgG-Fc control treatments (Fig. 4B). The difference in growth kinetics between CD44-3MUT-Fc and rhIgG-Fc treatments became apparent approximately 24 h after VEGF-induced release of cells from arrest. After this timepoint, rhIgG-Fc control-treated cells continued to proliferate, but in CD44-3MUT-Fc-treated wells cell density plateaued. Next, we used the same growth arrested HUVEC model in a cell proliferation and viability assay to compare CD44-3MUT-Fc efficacy in inhibiting cell proliferation stimulated by either FGF-2, VEGF or HGF (Fig. 4C to E). We used an

endothelial-specific inhibitor of cell proliferation, fumagillin, as a positive control to define the maximum response in our assay. FGF-2 and VEGF induced robust proliferation in growth-arrested HUVECs, whereas HGF-stimulation resulted in much lower cell proliferation (Fig. 4C to E, left panels). Compared to rhIgG-Fc, CD44-3MUT-Fc dose-dependently inhibited HGF-stimulated proliferation with the maximum inhibition of  $60\% \pm 12.6$  after 72 h incubation. FGF-2 or VEGF-stimulated EC growth was inhibited less efficiently by CD44-3MUT-Fc when compared to rhIgG-Fc, as the growth was reduced by a maximum of  $10.7\% \pm 2.4$  and  $13.9\% \pm 4.5$ , respectively (Fig. 4B to E, and G). These results are in agreement with respective growth factor potencies to stimulate HUVEC proliferation, CD44-3MUT-Fc was less efficient in inhibiting FGF-2- or VEGF-induced proliferation, and showed more efficacy in case of a weak inducer, HGF.

CD44v6 interacts with VEGFR2 and MET [22]. Therefore, we tested whether CD44-3MUT-Fc has any effect on the protein levels or activation of these receptors. Western blot analysis showed no change in either VEGFR2 or MET protein levels or receptor activation in response to CD44-3MUT-Fc (Supplemental Fig. 3 in Online Resource 1). This suggests that CD44-3MUT-Fc does not inhibit EC growth by direct targeting of growth factor receptor signaling pathways. Additionally, we tested the effect of CD44-3MUT-Fc on GDF-2-stimulated HUVECs (Fig. 4D). Vascular quiescence factor GDF-2 (BMP-9) belongs to the TGF- $\beta$  superfamily ligands and regulates angiogenesis via ALK1, a type 1 TGF- $\beta$  receptor [23, 24]. As shown in the left panel of Fig. 4F, in our model GDF-2 is strongly anti-mitotic and induces the cell cycle block. Compared to rhIgG-Fc control treatments, CD44-3MUT-Fc showed a dose-dependent inhibitory effect on cell numbers in GDF-2-treated HUVECs with  $79.6\% \pm 6.7$  of maximum response (Fig. 4F and G).

To ascertain whether apoptosis contributes to CD44-3MUT-Fc-induced growth inhibition, we used Annexin V-FITC staining. We found that upon release from serum starvation, the basal levels of apoptosis in the HUVEC population were inversely related to the growth factor potency to stimulate cell proliferation. In response to incubation with  $12.64 \mu\text{M}$  ( $-4.9 \log_{10} \text{M}$ ) CD44-3MUT-Fc, the number of apoptotic cells relative to pooled control treatments was increased by  $9\% \pm 5$  in VEGF,  $28\% \pm 14$  in 10%FBS,  $34\% \pm 6$  in FGF-2,  $45\% \pm 12$  in HGF, and  $46\% \pm 6$  in GDF-2-stimulated cells. However, VEGF- or FGF-2-induced cells were the most protected against apoptosis induced by CD44-3MUT-Fc-treatment (Fig. 4H). In contrast, GDF-2-mediated growth arrest enforced cells to undergo apoptosis and this trend was further increased by CD44-3MUT-Fc treatment. The observed increase in apoptosis from a relatively low basal level in response to CD44-3MUT-Fc treatment and its apparent correlation with growth factor potency to stimulate proliferation, suggest that apoptosis occurs secondary to CD44-3MUT-Fc-mediated inhibition of cell proliferation.

Collectively, our data show that CD44-3MUT-Fc inhibits EC proliferation.

### **CD44 is not involved in GDF-2/ALK1-dependent SMAD signaling**

Several studies suggest that CD44 is associated with TGF- $\beta$  signaling, since the cytoplasmic tail of CD44 directly interacts with SMAD1 [25], CD44 forms a galectin-9-mediated complex with BMPR2 [26], and HA induces CD44 to complex with TGFBR1 [27]. Given that CD44-3MUT-Fc treatment resulted in an enhanced growth inhibitory effect in GDF-2-arrested HUVECs, we wanted to test whether CD44 could be involved in GDF-2 mediated SMAD activation. We studied pSMAD1/5 nuclear localization and SMAD1/5 target gene activation in response to GDF-2 stimulation in CD44-silenced HUVECs. CD44-targeting siRNA (siCD44) transfection resulted in substantial CD44 protein or mRNA downregulation compared to non-targeting siRNA control (siNTP) (Supplemental Fig. 4 in Online Resource 1). Simultaneously, we detected a robust GDF-2-dependent pSMAD1/5 nuclear localization

(Supplemental Fig. 4A and B in Online Resource 1) and an induction or repression of selected known SMAD1/5 target genes ID1, SMAD6, SMAD7 or c-MYC, respectively (Supplemental Fig. 4C in Online Resource 1). Immunofluorescence analysis showed that the nuclear area or other size/shape parameters of cell nuclei did not differ between siCD44 or siNTP control-silenced cells (data not shown). We found that silencing of CD44 did not affect the nuclear localization of pSMAD1/5 or SMAD1/5 target gene expression in response to GDF-2 stimulation (Supplemental Fig. 4A to C in Online Resource 1).

Next, we studied the effect of CD44-3MUT-Fc on SMAD1/5 signaling by using a BMP-responsive element reporter (BRE). We found that BRE reporter activity in HUVECs was increased in response to GDF-2 stimulation, but this response was not sensitive to either CD44-silencing or CD44-3MUT-Fc treatment (Supplemental Fig. 5A in Online Resource 1). In line with this, Western blot analysis of GDF-2 stimulated HUVECs treated with CD44-3MUT-Fc showed no change in pSMAD1/5 levels (Supplemental Fig. 5B in Online Resource 1). To test whether prolonged CD44-3MUT-Fc exposure *in vivo* could trigger changes in SMAD1/5-mediated gene expression, we analysed lung tissue of nude mice from two angiogenesis experiments described in Fig. 2 for the expression of selected SMAD target genes. We found no changes in the expression levels of SMAD1/5 or NF- $\kappa$ B target genes (Supplemental Fig. 5C in Online Resource 1).

Together, these results suggest that neither CD44 nor CD44-3MUT-Fc are involved in GDF-2-ALK1-SMAD1/5 signaling in ECs.

### **CD44 silencing augments endothelial cell proliferation**

Since angiogenesis assay results showed increased blood vessel invasion in *Cd44*<sup>-/-</sup> mice and inhibition of this response by CD44-3MUT-Fc treatment, we wanted to test whether CD44 knockdown in ECs results in increased cell growth. To this end, we used siRNA transfected HUVECs that had been growth arrested by serum starvation. Growth-arrested cells were released by the addition of either 20% FBS or different concentrations of VEGF or FGF-2. Real-time impedance measurements showed that compared to 5% FBS stimulation (Fig. 5A, left), 20% FBS or growth factor supplementation released cells from the cell-cycle block and stimulated their growth sustainably over 72 h (Fig. 5A and C). We found that siCD44 transfected cells reached higher densities at 72 h than control siNTP-transfected cells. Augmented cell growth and higher cell density in siCD44-transfected ECs at the end of the experiment was independent of type and concentration of the growth factor used for stimulation (Fig. 5A, C and E). End-point quantitation of viable cells performed 72 h after release supported the impedance measurement results. siCD44-transfected HUVECs displayed increased cell numbers over all tested growth factors and concentrations (Fig. 5B and D). These data suggest that the effect of CD44 silencing on cell proliferation was additive to the stimulatory effect of growth factors. The additive effect of CD44 silencing on cell proliferation was further supported by the typical VEGF dose-dependent flattening of the growth curve that was observed in case of VEGF-stimulated HUVECs. In case of FGF-2, such suppression did not occur, and cell density increased linearly with growth factor concentration within the range (8 to 79 ng/ml) tested.

Western blot analysis showed that FGFR1, VEGFR2 or activated VEGFR2 levels were not affected in CD44-silenced HUVECs (Fig. 5G and Supplemental Fig. 3C in Online Resource 1). The initial proliferation rate of CD44-silenced HUVECs after seeding and before serum deprivation was increased compared to non-targeting siRNA or untransfected controls, and CD44-silenced cells reached higher cell density within this time frame (Supplemental Fig. 6A in Online Resource 1). Notably, vimentin-silenced (siVIM) HUVECs showed similar behavior to CD44-silenced cells before serum starvation (Supplemental Fig. 6A in Online

Resource 1). The observation that siCD44- or siVIM-transfected HUVECs reached higher cell density after seeding and before the start of serum starvation compared to siNTP-transfected or untransfected cells was confirmed by modeling impedance data for barrier formation (Supplemental Fig. 6B in Online Resource 1). The release of siCD44-transfected cells from serum starvation by VEGF or FGF-2 stimulation resulted in enhanced barrier reformation when compared to siNTP or siVIM-transfectants (Supplemental Fig. 6B in Online Resource 1).

We also assessed the effect of siCD44 by treating cells arrested in the cell cycle G1 phase with antimitogenic factor GDF-2. We found that GDF-2 induces cell cycle block and a subsequent decline in cell density, plausibly because cells undergo apoptosis (Fig. 4H). Impedance measurements showed that CD44-silencing did not rescue GDF-2-stimulated HUVECs from growth arrest and cell numbers declined over the course of the experiment (Fig. 5E). However, the cell viability assay performed after impedance measurements showed that CD44-silencing resulted in more surviving cells compared to controls and partially rescued the cells from GDF-2-induced cell cycle block (Fig. 5F). Nevertheless, the GDF-2 dose-dependent inhibitory trend persisted.

Together, these experiments show that CD44 knockdown results in enhanced EC proliferation, irrespective of the specific growth factor used for stimulation. Furthermore, CD44-silencing experiments are consistent with *Cd44*<sup>-/-</sup> mice data and suggest increased proliferation and survival of CD44-deficient ECs as a plausible cellular mechanism to enhance angiogenesis.

## Discussion

Here, we report that CD44 cell-surface glycoprotein is a negative regulator of angiogenesis. We show that CD44 constrains endothelial cell proliferation. Our results suggest that in the regulation of cell proliferation, CD44 functions independently of specific growth factor signaling pathways.

Based on our experiments, we extend the functions of CD44 to include the control of EC proliferation and angiogenesis. We found that blood vessel invasion into tumor extracellular matrix in response to FGF-2/VEGF stimulation was substantially increased in *Cd44*-null mice. This effect is likely to be cell-autonomous, as silencing of CD44 expression in cultured ECs also resulted in augmented cell proliferation. We suggest that CD44 functions downstream of mitogenic signaling. Griffioen et al. [28] have shown that CD44 is upregulated in response to FGF-2 or VEGF stimulation in cultured ECs, and in activated tumor blood vessels *in vivo*. Thus, enhanced angiogenesis and cell proliferation in case of CD44 deficiency or downregulation suggest that CD44 mediates negative feedback signaling that constrains cell proliferation. CD44 knockdown in dermal fibroblasts results in the stabilization of PDGF  $\beta$ -receptor and sustained ERK activation in response to PDGF-BB stimulation [29]. In our study, we show that intervening with CD44 function by silencing or CD44-3MUT-Fc has no effect on the activation of angiogenic growth factor receptors. However, we observed that the potency of CD44-3MUT-Fc to inhibit EC proliferation was inversely related to the potency of VEGF, FGF-2 or HGF to induce EC proliferation and survival. Several earlier reports have shown involvement of CD44 in TGF- $\beta$  signaling [25–27]. Therefore, we tested if CD44 functions in GDF-2 signaling. We saw enhanced growth arrest and apoptosis of ECs in response to CD44-3MUT-Fc treatment in GDF-2-stimulated ECs. Nevertheless, our different *in vitro* experiments showed that GDF-2-mediated signaling is not affected by disrupting CD44 expression or increasing CD44 dose via CD44-3MUT-Fc. We conclude from these

results that CD44 acts via a different mechanism than disrupting any specific growth factor pathways.

Plausibly, CD44-mediated negative feedback signaling on cell proliferation is activated by CD44-HA interaction. Binding of high molecular weight HA to CD44 controls proliferation of smooth muscle cells, and probably also other mesenchymal cell types, including ECs [10]. Kothapalli et al. [10] also showed that in *Cd44*-null mice the response to arterial injury resulted in increased neointima formation and smooth muscle cell proliferation during vessel regeneration. We have previously shown that the non-HA binding mutant of CD44 was as effective as its wild-type counterpart in angiogenesis inhibition in the chick chorioallantoic membrane angiogenesis model [11]. Here, we show that systemic administration of soluble mutant CD44 HABD (CD44-3MUT) has an antiangiogenic effect in a mouse model of angiogenesis, thus CD44-3MUT functions similarly to endogenous CD44. In this context, we were interested whether endogenous soluble CD44 levels correlate with angiogenesis. Soluble CD44 levels are reduced in immuno deficient BALB/c.Xid mice with defective B-cell maturation, and in SCID mice with absence of functional T cells and B cells, suggesting that immune cell-derived proteolytic activity is responsible for CD44 shedding [21]. In our angiogenesis assays, we observed that wild type mouse strains displayed much weaker angiogenic response than immuno deficient athymic nude mice. Given that nude mice carried normal *Cd44* gene dose, but their sCD44 levels were not known, we assumed that elevated angiogenesis in nude mice, compared to wild type strains, could be related to decreased sCD44 levels. We found serum sCD44 levels to be normal in athymic nude mice, suggesting that the induction of angiogenesis is not related to serum sCD44 levels. Furthermore, as athymic nude mice lack T cells, this result suggests that a large proportion of serum sCD44 is generated by B cell-dependent activity.

The signaling pathway downstream of CD44 is not well understood. CD44 has been implicated in cell–cell contact inhibition in schwannoma cells by recruiting the NF2 tumor suppressor protein to the plasma membrane [30]. Thus, it is possible that CD44 silencing abolishes the function of NF2, which leads to loss of contact inhibition and increased proliferation. However, embryonic fibroblasts isolated from *Cd44*-null mice still exhibit functional contact inhibition compared to cells from *Nf2*-null mice, but *Cd44*-null cells seem to display faster growth rates compared to wild-type cells [31]. Our impedance-based real-time monitoring of cell proliferation suggests steadily increased growth rates of CD44-silenced ECs after release from serum starvation. We found that barrier formation, which is directly related to cell density, is apparently more robust in CD44-silenced ECs after growth factor stimulation. This suggest that the mechanisms behind enhanced cell proliferation could be other than defective cell–cell adhesion.

Our *in vivo* findings contrast with previous works showing that CD44 absence or its downregulation *in vivo* results in reduced angiogenesis [3, 4]. Lennon et al. [4] studied the contribution of CD44 to HA oligomer-induced angiogenesis, and found that CD44 silencing *in vivo* resulted in inhibited angiogenesis in response to oligo HA. Cao et al. [3] used a relatively high number of rapidly growing B16 melanoma cells as a source of angiogenic growth factors in a Matrigel plug assay and allowed the blood vessels to grow for 5 days only. Nevertheless, tumor angiogenesis assays using two different cell lines with very different tumor growth kinetics, B16 melanoma and ID8-VEGF ovarian carcinoma, still suggested considerable inhibition of tumor formation and reduced vascular density at tumor margins in *Cd44*-null mice [3]. However, it is plausible that CD44-negative ECs were inhibited *in trans* by CD44 that was present on tumor cells [3]. Here, we show that administration of

exogenous soluble CD44 inhibited *in vivo* angiogenesis and EC proliferation. We found that *Cd44* heterozygous mice displayed angiogenesis at a similar level to wild-type animals, showing that *Cd44* is not haploinsufficient and lower than normal amounts are still sufficient for controlling angiogenesis. Tumor angiogenesis is dependent on interactions between tumor cells and host tissue stroma, and such interactions might be compromised in *Cd44*-null animals. Tumor cells recruit macrophages to promote angiogenesis. However, Cao et al. [3] showed that in case of *Cd44*-null mice bone marrow reconstitution with wild-type bone marrow did not rescue the angiogenesis defect, suggesting that endothelial CD44 expression is important.

*Cd44*-null mice develop normally and do not display apparent vascular abnormalities. We suggest that CD44 plays a non-redundant role in physiological angiogenesis. CD44-mediated interactions after its upregulation in endothelial cells in response to growth factor stimulation restrain cell proliferation. This control may contribute to the robust shutdown of angiogenesis during wound repair. In case of tumors, CD44-mediated control of angiogenesis might be overridden by a surplus of growth factors and increased shedding of CD44.

In summary, we conclude that CD44 functions as a negative regulator of angiogenesis. Therefore, systemic absence of CD44 expression in mice results in increased angiogenic response. Our results also demonstrate that soluble CD44 regulates angiogenesis by suppressing endothelial cell proliferation. Importantly, the antiangiogenic effect of CD44 is achieved independently of its HA-binding property. Together, our data suggest that CD44 is important in maintaining normal angiogenesis levels and targeting of CD44 can be utilized in antiangiogenesis treatment strategies for cancer or in other applications where angiogenesis modulation is desired.

## **Materials and Methods**

### **Cells, Reagents and Primary Antibodies**

HUVECs were obtained from Cell Applications, Inc., ECGS was from Millipore. VEGF-165 was from Serotec; GDF-2, HGF and FGF-2 were from Peprotech. Lipofectamine RNAiMAX (LF) was from Life Technologies. Non-targeting pool siRNA, #D-001810-10-05, human CD44 siRNA, #L-009999-00-0005, and human vimentin siRNA, #L-003551-00-0005 (ON-TARGETplus SMARTpool) were from Thermo Fisher Scientific. siRNA target sequences are listed in Supplemental Methods section in Online Resource 1. jetPEI-HUVEC transfection reagent was from Polyplus-transfection SA. Annexin V-FITC and annexin binding buffer were from BD Pharmingen. CellTiter-Glo reagent was from Promega. Primary antibodies, dilution and source used in this study: anti-CD44 (2C5) mouse mAb 1/1000 from R&D Systems, anti-VEGFR2 rabbit mAb (55B11) 1/1500 and anti-FGFR1 rabbit mAb (D8E4) from Cell Signaling Technology and anti-GAPDH mouse mAb 1/10000 from Millipore, IM7 rat anti-mouse CD44 (MCA4703; AbD Serotec), rat anti-mouse CD44 KM81-biotin (Abcam).

### **Production of CD44-3MUT-Fc**

CD44-3MUT with C-terminal human IgG1-Fc domain, recombinant human IgG1-Fc domain (rhIgG-Fc) and irrelevant human IgG1 mAb were produced by Icosagen Cell Factory

(Estonia). Cystatin S signal peptide sequence was added to the N-terminus of the CD44-3MUT-Fc cDNA and the gene was synthesized by Genewiz, Inc. The synthesized CD44-3MUT-Fc cDNA was cloned into RSV-LTR promoter containing pQMCF-5 expression vector (Icosagen Cell Factory). The resulting expression plasmids were transfected into CHOEBNALT85 cells (Icosagen Cell Factory) and the expressed Fc-fusion proteins were purified by Protein G sepharose, followed by Superdex 200 gel-filtration chromatography. The purified CD44-3MUT-Fc had a monomeric molecular weight of approximately 60 kDa. The endotoxin level of the purified CD44-3MUT-Fc was < 10 EU/mg as determined by chromogenic Limulus amoebocyte lysate test (Lonza).

### **CD44-3MUT-Fc serum half-life**

F344/NCrHsd male rats were from Harlan, Netherlands. The rats carried a polyurethane round tipped jugular vein catheter for blood sampling (Harlan Laboratories Surgical Services). After the pre-serum blood sample was taken, rats were injected intravenously via the tail vein with 3 mg of CD44-3MUT-Fc in 1 ml volume. Blood samples were collected using the jugular vein catheter at different time points. Blood samples were held at 37°C for 30 min to allow clot formation, and then centrifuged at 1300×g for 10 min at RT. The supernatants were collected and stored at -20°C until assayed. For sandwich ELISA microwell plates were coated with mouse anti-human IgG1 antibody clone G17-1 (BD Biosciences). Blocking was performed with 1.5% BSA/PBS. Standards were step-diluted (40 µg/ml – 0 µg/ml) in 0.5% BSA/PBS supplemented with 5%, 2% or 1% rat serum. Samples taken at different time points (pre-serum, from as soon as possible to 24 hours) were diluted 1:50 or 1:100 in 0.5% BSA/PBS solution and applied to wells. Biotin mouse anti-human IgG antibody clone G18-145 (BD Biosciences) and streptavidin-HRP were used for detection. Tetramethylbenzidine was used for color development. Concentration at time zero and half-life were estimated from two-parameter exponential decay model with the function  $f(x)=d(\exp(-x/e))$ , where  $d$  is the upper limit at  $x = 0$ , and  $e$  is the decay constant.

### ***In Vivo* Angiogenesis Assay**

Animal experiments were conducted under the license of the Project Authorization Committee for Animal Experiments of the Ministry of Rural Affairs of the Republic of Estonia. We used the Directed in Vivo Angiogenesis Assay kit (DIVAA; Trevigen, USA) according to manufacturers instructions. For the angiogenesis assay, 20 µl angioreactors were filled with growth factor-reduced basement membrane extract containing 1.4 ng/µl FGF-2, 0.47 ng/µl VEGF and heparin for the induction of angiogenic response or an equal volume of PBS for uninduced controls. Angioreactors were implanted subcutaneously into the dorsolateral flank of 9-week-old athymic Nude-Foxn1/nu female mice (Harlan, Netherlands). *Cd44*-null mice were of mixed inbred background (B6;129-Cd44tm1Hbg/J), termed “Cd44KO mix”. B6;129 hybrid mice “WT mix” were used as controls. C57BL/6 and C3H mice were obtained from Harlan, Netherlands. The experimental groups of wild-type and *Cd44*-null mice comprised 8-11-week-old female and male mice. In one experiment, the Cd44KO mix and the respective wild-type mice were 40-43 weeks old. For the angiogenesis assay in the C57BL/6 genetic background, the *Cd44*-null allele was backcrossed for six generations to C57BL/6 mice (Harlan, Netherlands); experimental groups contained an equal number of female and male littermates. Implantation was performed on both flanks and one or two angioreactors were inserted per flank into immune competent mice or nude mice, respectively. Nude mice were injected intraperitoneally every second day with CD44-3MUT-

Fc, irrelevant human IgG1 mAb, rhIgG-Fc or vehicle (PBS) during two weeks. Mice were sacrificed after 14 days from start of the experiment by carbon dioxide asphyxiation and angioreactors were dissected. The angioreactor contents were retrieved and the EC that had invaded the angioreactors were quantitated by FITC-Lectin (*Griffonia simplicifolia* lectin I) staining [32]. Cell-bound fluorescence was measured at 485 nm excitation and 535 nm emission wavelengths using a microtiter plate reader (Tecan, Switzerland). Data from irrelevant human IgG1 mAb and rhIgG1-Fc treatments were pooled for analysis. Raw fluorescence values from each experiment were scaled by dividing by their root mean square.

## **Mouse sCD44 ELISA**

For quantification of the serum levels of sCD44 in nude mice from the DIVAA experiments, wild-type mice of different backgrounds (C3H, C57BL/6, mixed), and their *Cd44*-null, heterozygous and wild-type littermates of the C57BL/6 background were used. For ELISA measurements 96-well plates were coated with 50 ng IM7 Ab/well overnight (ON) at 4°C and blocked with 5% non-fat dry milk for 2 h at 37°C. After blocking, samples and standards (Recombinant Mouse CD44 Fc Chimera; R&D Systems) were incubated in wells for 30 min at 37°C. Bound sCD44 was detected by incubating the plate with KM81-biotin Ab for 30 min at 37°C. For color development, Vectastain ABC (Vector Laboratories) and tetramethylbenzidine substrate were used. Absorbance was recorded at 450 nm using a microtiter plate reader (Tecan).

## **HUVEC Growth and Treatments**

HUVECs (passage 4-6) were cultured in 20% FBS containing M199 medium supplemented with 4 mM L-glutamine, 50 µg/ml heparin, 10 mM Hepes, and 30 µg/ml ECGS. For treatments, HUVECs were seeded into 0.1% gelatin-coated cell culture plates. After 24 h, the cells were starved ON in M199 media supplemented with 1% FBS, 25 mM Hepes and 4 mM L-glutamine. After starving, the cells were incubated with different concentrations of rhIgG-Fc or CD44-3MUT-Fc in the 5% FBS containing HUVEC growth media (5% FBS, M199, 4 mM L-glutamine, 12.5 µg/ml heparin, 10 mM Hepes, and 7.5 µg/ml ECGS) for 1 h at 37°C; and thereafter, stimulated with 25 ng/ml VEGF-165, 25 ng/ml FGF-2, 10 ng/ml GDF-2 or 63 ng/ml HGF. The cells were further grown for 48 or 72 h at 37°C.

## **Electric Cell-Substrate Impedance Sensing Assay**

Cell layer impedance was recorded by an ECIS Z0 instrument connected to a computer running an ECIS software version 1.2.169.0 (Applied Biophysics, USA). We used 96WE1+ PET plates, pretreated with 10 mM cysteine (Applied Biophysics, USA). HUVECs were seeded at a density of 5000 cells/well. The final media volume during treatments was 175 µl per well. Cell growth was monitored at seven frequencies in the range of 1000-64000 Hz. Each well was measured approximately four times per hour. To summarize different experiments, values for each experiment were binned by hours and hourly means were calculated. The release mark from serum starvation was set as time point zero. Hourly means of raw readings were normalized by dividing by the mean value of the first hour after time point zero.

## Apoptosis and Cell Viability Assays

For the apoptosis assay HUVECs were cultured in 0.1% gelatin-coated 24-well plates at a density of 25000 cells/well. Annexin V-FITC staining was performed according to manufacturer's protocol. Briefly, cells were incubated with 1:20 Annexin V-FITC in 50  $\mu$ l of annexin-binding buffer for 15 min at room temperature (RT) in the dark and analysed by FACS Calibur (BD Biosciences). For the cell viability assay, HUVECs were cultured in 0.1% gelatin-coated white 96-well cell culture plates (Greiner Bio-one) at a density of 5000 cells/well. After treatments, the cells were incubated with the CellTiter-Glo reagent (in a ratio of 1:1 of reagent volume to media) for 10 min at RT and luminescence was recorded using a microtiter plate reader. For analysis, raw luminescence values were min-max normalized. Curves were fitted using a five parameter logistic equation:  $f(x) = \text{Bottom} + \frac{\text{Top} - \text{Bottom}}{1 + \exp(\text{HillsSlope}(\log(x) - \log(\text{EC50})))}$ .

## HUVEC Transfection with siRNAs

siRNA transfections were performed using PEI or LF and 30 nM siRNAs. Transfection reagents and siRNAs were separately diluted in serum-free DMEM (4500 mg/l glucose). Diluted siRNA and transfection reagents were mixed and the transfection complex was incubated for 15-20 min at RT. The cells were transfected in 2% FBS and 4 mM L-glutamine containing DMEM (4500 mg/l glucose) for 3 h (PEI transfection) or 4 h (LF transfection) at 37°C. Then, the transfection media was replaced with 20% FBS HUVEC culture media and cells were further incubated for 24 h at 37°C. For impedance measurements, the transfected cells were plated out at a 5000 cells/well density into cysteine pretreated and gelatin coated 96WE1+ PET plates. After starving, cells were stimulated with different concentrations of GDF-2, VEGF or FGF-2 in 5% FBS containing HUVEC growth media. After 72 h of incubation, the CellTiterGlo reagent was added to cells for cell viability measurement.

## Western Blot Analysis

48 h after siRNA transfection, the cells were lysed in RIPA buffer (50 mM Tris pH 8.0, 150 mM NaCl, 1% NP-40, 0.5% sodium deoxycholate, 0.1% SDS) containing protease inhibitor cocktail (Roche). The proteins (5  $\mu$ g of total protein) were separated on 7.5-10% SDS-PAGE gradient gel and transferred to PDVF membrane at 350 mA for 1.5 h. The membranes were blocked in 5% whey in 0.1% Tween20-TBS (TBST) at RT for 1 h, followed by a primary Ab incubation ON at 4°C and subsequent HRP-conjugated secondary Ab (Jackson ImmunoResearch) incubation for 1 h at RT in 2% whey in TBST.

## Statistical Analysis

We used R version 3.3.1 (2016-06-21) for data analysis and graphs (for the complete list of packages see Supplemental Methods in Online Resource 1). The percentile confidence intervals were obtained using nonparametric bootstrap resampling on 1000 replications. Cohen's d effect sizes with bootstrap confidence intervals were calculated using the *bootES* 1.2 package. Bayesian credible intervals were obtained via the Markov chain Monte Carlo method using the *rjags* 4.6 package. Scaling was done by dividing raw data by their root mean square using the R function *scale*. The data are shown as mean  $\pm$  SEM.

## Supplementary Material

Supplemental Fig. 1 shows aortic fragment angiogenesis assay using aortic rings dissected from wild-type and *Cd44*<sup>-/-</sup> mice. Supplemental Fig. 2 shows the CD44-3MUT-Fc serum half-life curve. Supplemental Fig. 3 shows the effect of CD44-3MUT-Fc on angiogenic growth factor receptor activation. Supplemental Fig. 4 shows the immunofluorescence analysis of GDF-2-induced pSMAD1/5 nuclear localisation in CD44-silenced HUVECs and transcription of SMAD target genes in CD44-silenced HUVECs in response to GDF-2 stimulation. Supplemental Fig. 5 shows the BMP-responsive element reporter activity of 10 ng/ml GDF-2 stimulated HUVECs transfected with CD44 siRNA and treated with CD44-3MUT-Fc and *in vivo* expression of SMAD target genes in mice treated with CD44-3MUT-Fc. Supplemental Fig. 6 shows that CD44 silencing augments EC growth and EC barrier formation is functional. Supplemental Table 1 gives the list of primers used for real-time qPCR experiments. Supplemental Table 2 gives the list of siRNA target sequences. Supplemental Table 3 gives the list of loaded R packages to compile this document.

## Author Contributions

Conceptualization, A.P., T.P., and A.V.; Methodology, A.P., M.S., and T.P.; Investigation, A.P., M.S., and T.P.; Formal Analysis, and Visualization, T.P.; Writing – Original Draft, A.P. and T.P.; Writing – Review & Editing, A.P., M.S., T.P., and A.V.; Funding Acquisition, A.V.; Supervision, T.P., and A.V.

## Acknowledgments

We are grateful to Kati Mädo for her contribution to half-life studies and Aili Kallastu for her contribution to half-life and animal studies. We thank Richard Tamme and Alliki Lukk for proofreading the manuscript. This research was supported by the European Regional Development Fund via the Enterprise Estonia grants (EU28138/EU28658, EU30013) to the Competence Centre for Cancer Research and by the Estonian Science Fund Grant PUT698 to Andres Valkna. The authors declare no competing financial interests.

## Abbreviations List

CD44-3MUT – CD44-HABD non-HA-binding triple-mutant  
EC – endothelial cell  
ECIS – Electric Cell-substrate Impedance Sensing  
HA – hyaluronan  
HABD – hyaluronan-binding domain  
sCD44 – soluble CD44

# Figures

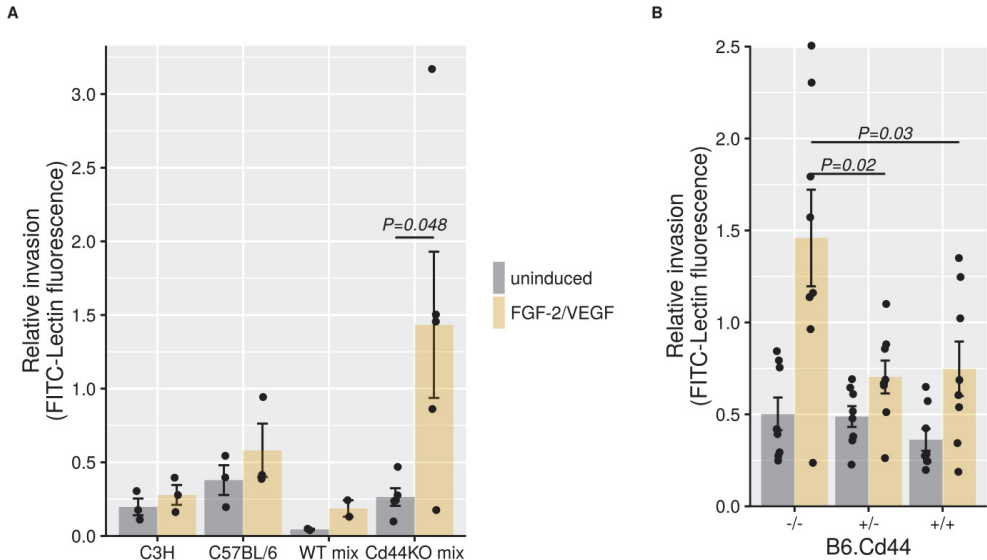


**Fig. 1** Increased angiogenesis in CD44-null mice. **(A)** Angiogenesis was analysed in C3H, C57BL/6, and in wild-type and *Cd44*<sup>-/-</sup> mice of mixed genetic backgrounds (WT mix and Cd44KO mix, respectively). Basement membrane extract-filled angioreactors containing premixed FGF-2, VEGF and heparin or PBS for uninduced controls were implanted SC into the flanks of mice. Each mouse received 2 angioreactors, 1 per flank. 14 days after implantation, angioreactors were resected and the population of ECs within the angioreactor matrix was assessed by FITC-lectin staining. The number of fluorescent cells was quantitated by microplate reader. Raw readings from independent experiments were scaled by dividing by their quadratic mean. N = 2–5 mice per condition from 2 independent experiments. P value is from Student's t-test. **(B)** Angiogenesis in *Cd44*<sup>-/-</sup> mice and their heterozygous (*Cd44*<sup>+/-</sup>) and wild-type (*Cd44*<sup>+/+</sup>) littermate that had been backcrossed six generations to the C57BL/6 background. The data are represented as the mean ± SEM. Each dot represents the mean of two angioreactors for an individual mouse. N = 8 mice per condition from 2 independent experiments. P values are from ANOVA post hoc comparisons using the Tukey HSD test.

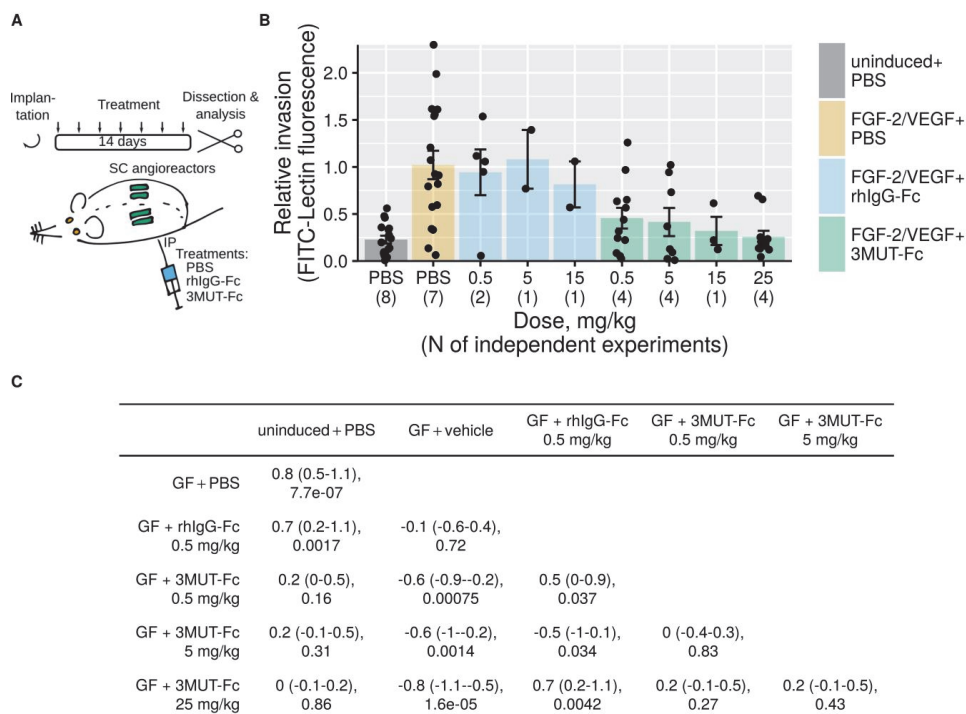


**Fig. 2** Recombinant CD44-3MUT Fc fusion protein inhibits angiogenesis *in vivo*. First, the assay and quantitation were performed similarly to those described in Fig. 1, except that each mouse received 4 angioreactors, 2 per flank. The day after implantation, the mice started to receive CD44-3MUT-Fc, control (rhIgG1-Fc) or vehicle (PBS) every second day via IP injections for 14 days. **(A)** Schematic presentation of experimental design. **(B)** Relative blood vessel invasion into matrix-filled angioreactors. The data are represented as the mean  $\pm$  SEM. Datapoints show the mean of 4 angioreactors for individual mice. N – the number of independent experiments. GF – growth factors (FGF-2/VEGF). **(C)** Effect size with 95% confidence intervals (upper row) and P values (lower row) of pairwise comparisons of the data shown in **(B)**. Effect sizes were calculated by Cohen's d formula. Confidence intervals were derived using bootstrap resampling. P values are from t tests using pooled SD.

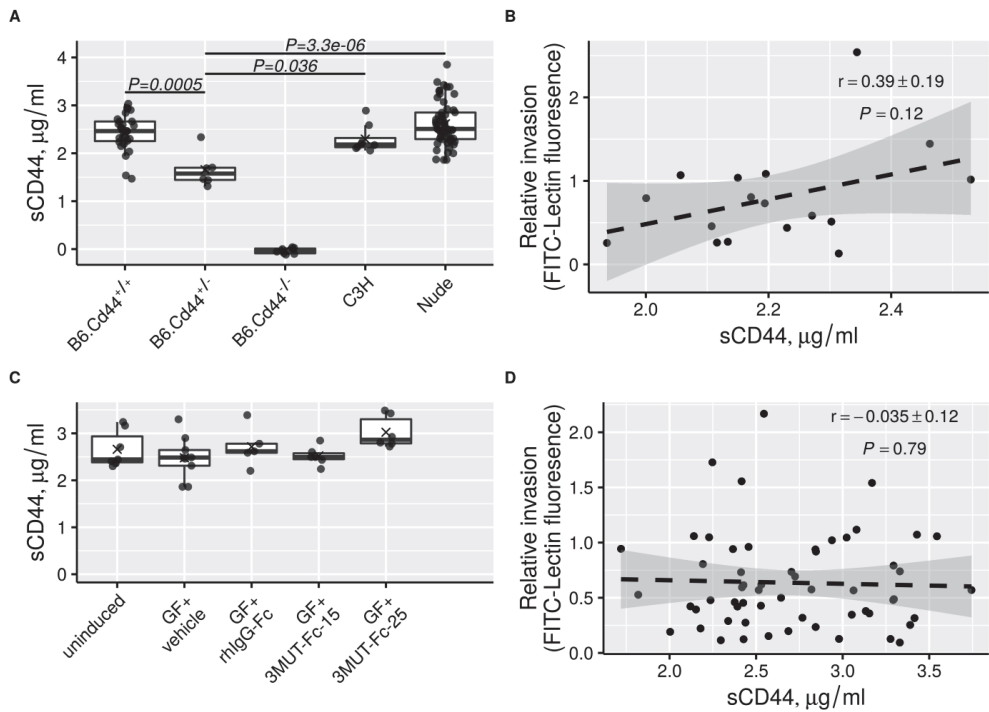


**Fig. 3** Soluble CD44 concentrations in mouse serum. Blood was collected from mice of different genetic backgrounds and the mice used in the angiogenesis experiments shown in Figs 1 and 2. **(A)** Serum levels of soluble CD44 in mice from different strains. Each dot represents an individual mouse. Cross indicates the mean. P values are from ANOVA post hoc comparisons using the Tukey HSD test. **(B)** The correlation between relative blood vessel invasion and post-experiment serum sCD44 in wild-type mice. *Cd44*-null mice and nude mice were excluded from the dataset. Pearson's *r* and the associated P values are shown. **(C)** Post-experiment serum levels of sCD44 in nude mice from different treatment groups. Treatments where more than five mice were analysed are shown. Each dot represents an individual mouse. Cross indicates the mean. GF – growth factors (FGF-2/VEGF). **(D)** The correlation between relative blood vessel invasion and post-experiment serum sCD44 in nude mice. Pearson's *r* and the associated P values are shown. In **(B and D)**, dashed line is the linear model fit, gray shading is the standard error interval of fitted values.

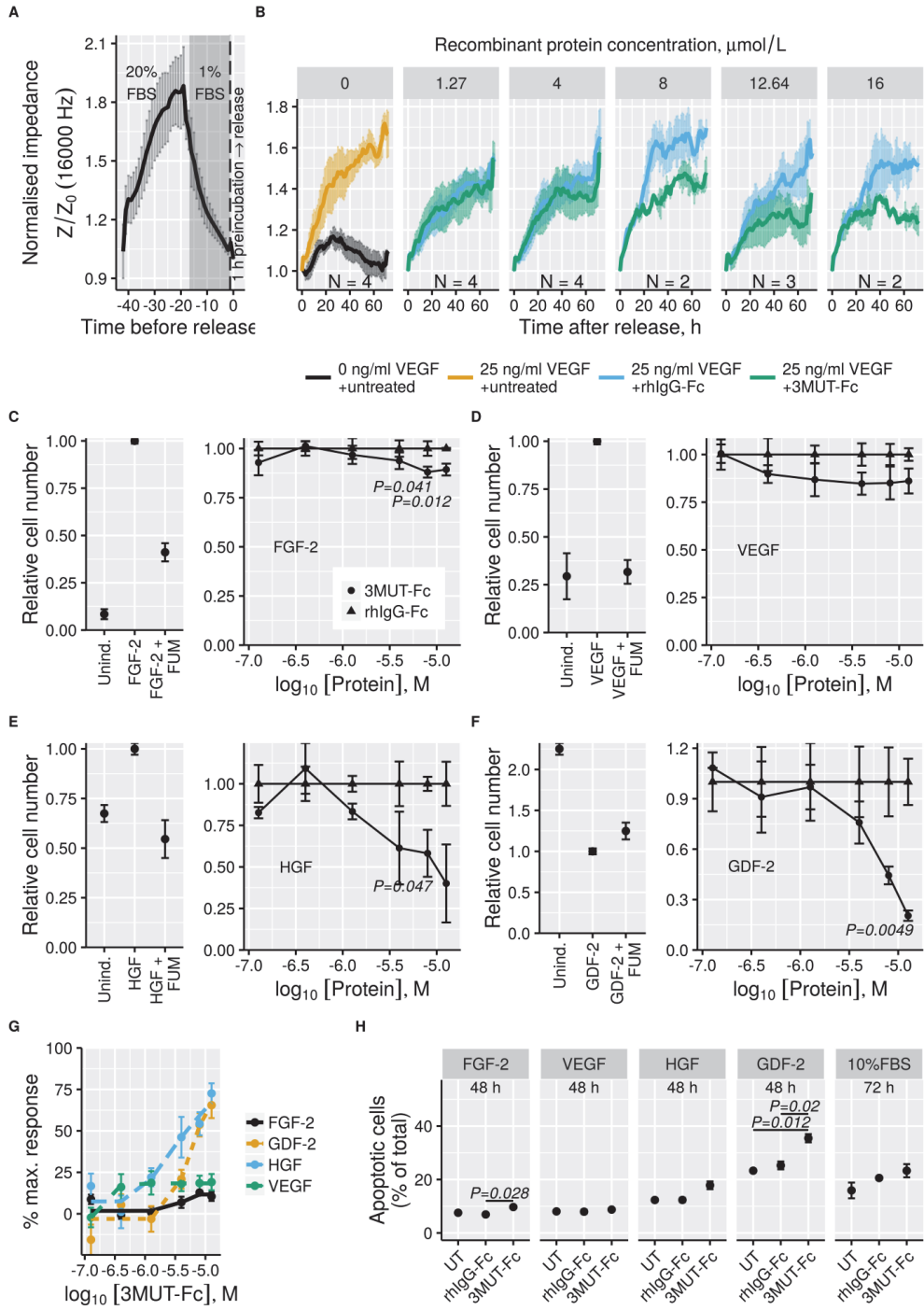


**Fig. 4** CD44-3MUT-Fc inhibits EC growth. **(A)** Real-time track of cell adhesion and synchronisation of HUVECs seeded onto 96-well electrode arrays. After seeding, the cells were grown for about 24 h. After that the cells were starved overnight in the media supplemented with 1% FBS (gray area). 1 h before the release from serum starvation (vertical dashed line) the cells were preincubated with different concentrations of rhIgG-Fc or CD44-3MUT-Fc in 5% FBS-containing media. **(B)** Growth curves of HUVECs released from serum starvation by supplementing preincubation media with 25 ng/ml VEGF. Facet labels show rhIgG-Fc or CD44-3MUT-Fc concentrations during preincubation. The data are represented as the mean  $\pm$  SEM. N – the number of independent experiments. **(C–F)** HUVECs were synchronised and pretreated as in panel A. After preincubation, the cells were stimulated either with 25 ng/ml FGF-2 **(C)**, 25 ng/ml VEGF **(D)**, 63 ng/ml HGF **(E)** or 10 ng/ml GDF-2 **(F)**. After 72 h, the number of viable cells was quantitated by measuring the ATP per well. Left: the effect of growth factor stimulation and the effect of 10 nM fumagillin (FUM) as a positive control for inhibition of cell proliferation. Right: the dose-response curves of rhIgG-Fc (filled triangles) and CD44-3MUT-Fc (filled circles). The data are represented as the mean  $\pm$  SEM. N = 3–4 independent experiments. **(G)** CD44-3MUT-Fc dose-response curves for FGF-2, GDF-2, HGF or VEGF stimulated HUVEC. The data are represented as the mean  $\pm$  SEM. **(H)** Apoptosis of HUVECs stimulated with different growth factors and treated with 12.64  $\mu$ M (  $-4.9 \log_{10}$  M) rhIgG-Fc, CD44-3MUT-Fc or left untreated. Apoptosis was quantitated by Annexin V staining. The data are represented as the mean  $\pm$  SEM. N = 2 independent experiments. P values are from the ANOVA post hoc comparisons using the Tukey HSD test.

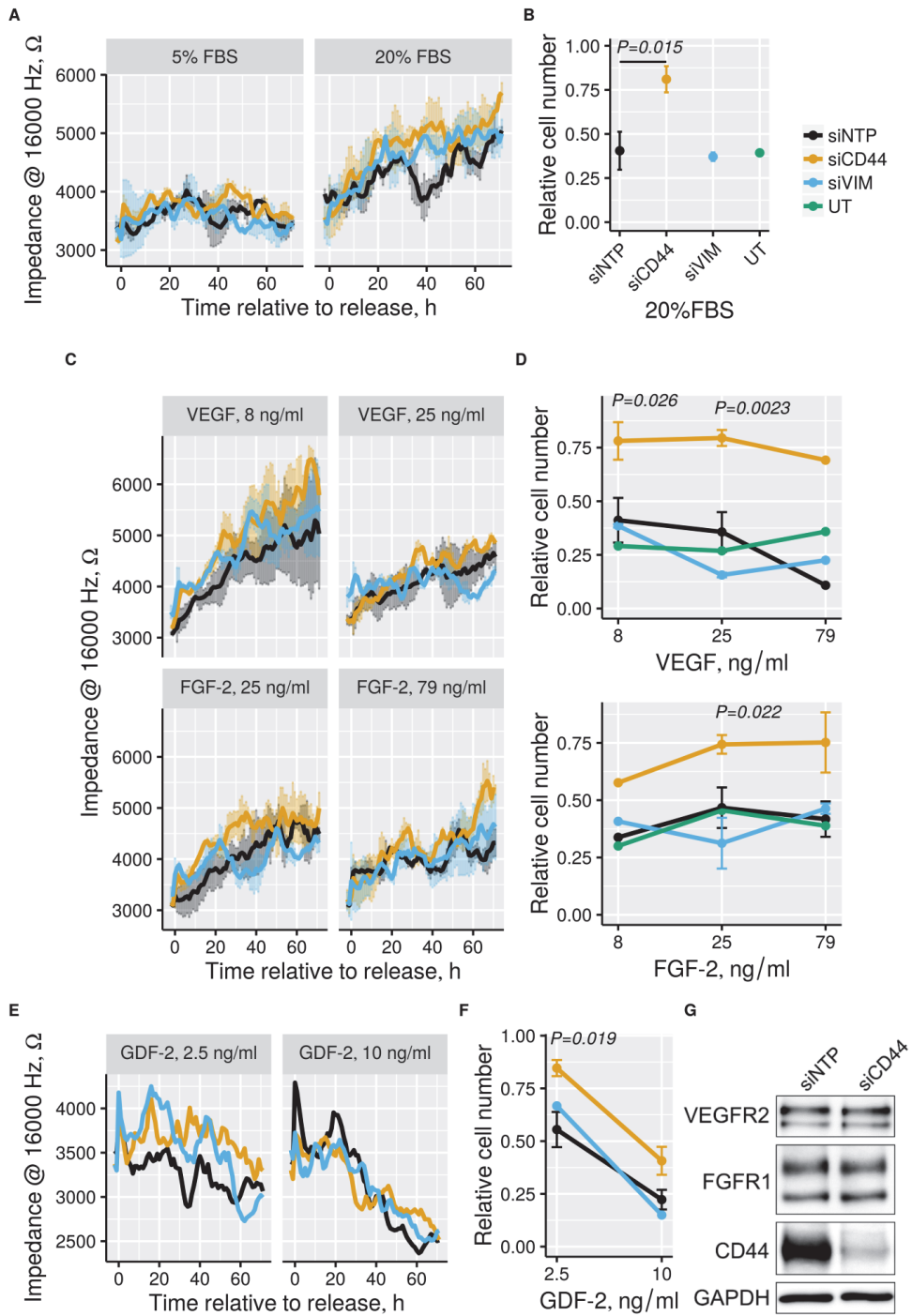


**Fig. 5** CD44 knockdown augments EC growth. siRNA transfected HUVECs were plated onto 96-well electrode arrays. After 24 h, the cells were starved in 1% FBS media overnight. After starving, the cells were released from cell cycle block by the addition of 20% FBS (**A**); 8 ng/ml, 25 ng/ml, or 79 ng/ml FGF-2 or VEGF (**C**); and 2.5 ng/ml or 10 ng/ml GDF-2 (**E**). Following stimulation, HUVEC growth was monitored by recording electrode impedance. Raw impedance readings are shown to allow direct comparison to endpoint measurements. N = 2 for 5% and 20% FBS, 25 ng/ml and 79 ng/ml FGF-2, and 8 ng/ml and 25 ng/ml VEGF. (**B, D, F**) 72 h after release from cell cycle block the viable cell numbers were determined by measuring the ATP per well. Treatments are labeled as shown in (**B**). The data are represented as the mean  $\pm$  SEM. P values are from the ANOVA post hoc comparisons using the Tukey HSD test. P values  $\leq$  0.05 of siCD44-siNTP comparisons are shown. siCD44-siNTP comparisons: N = 4 for 2.5 ng/ml and 10 ng/ml GDF-2, and N = 5 for 20% FBS, 25 ng/ml and 79 ng/ml FGF-2, and 8 ng/ml and 25 ng/ml VEGF. (**G**) Western blot analysis of CD44 silencing in HUVECs transfected with 30 nM siRNAs for 48 h. siNTP – non-targeting siRNA pool, siVIM – vimentin-targeting pool, siCD44 – CD44-targeting pool, UT – non-transfected cells.

## Tables

**Table 1.** Soluble CD44 level in mouse serum. Concentration is shown as mean  $\pm$  SEM.

Strain	sCD44, $\mu\text{g/ml}$	N	95% credible interval
B6	2.4 $\pm$ 0.07	28	2.3-2.6
B6.Cd44 <sup>+/-</sup>	1.7 $\pm$ 0.1	6	1.2-2.1
C3H	2.3 $\pm$ 0.1	8	2-2.6
Nude	2.6 $\pm$ 0.06	55	2.5-2.7

## Compliance with Ethical Standards

Ethical Approval: All procedures performed in studies involving animals were in accordance with the ethical standards of the institution or practice at which the studies were conducted.

Conflict of Interest: The authors declare that they have no conflict of interest.

## References

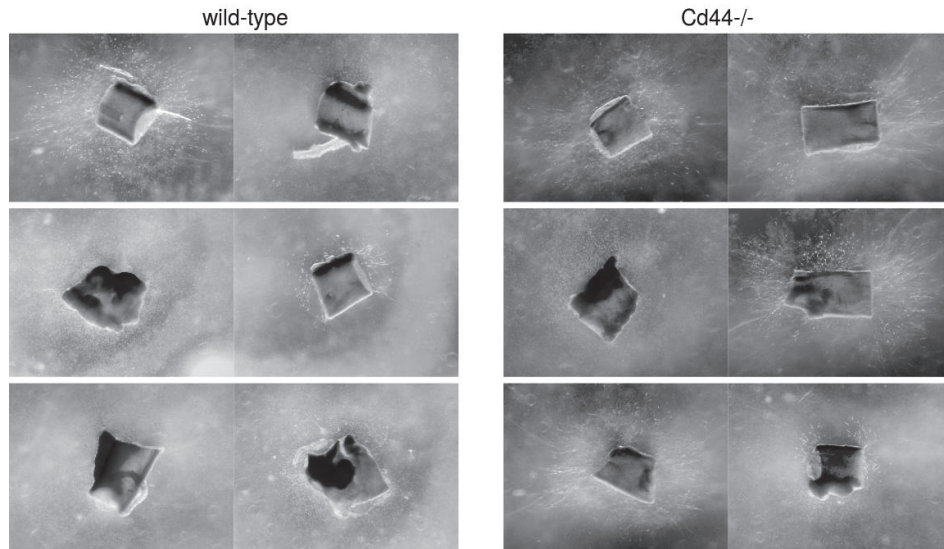
1. Mancuso MR, Davis R, Norberg SM, et al (2006) Rapid vascular regrowth in tumors after reversal of VEGF inhibition. *J Clin Invest* 116:2610–2621.
2. Loges S, Schmidt T, Carmeliet P (2010) Mechanisms of resistance to anti-angiogenic therapy and development of third-generation anti-angiogenic drug candidates. *Genes Cancer* 1:12–25.
3. Cao G, Savani RC, Fehrenbach M, et al (2006) Involvement of endothelial CD44 during in vivo angiogenesis. *Am J Pathol* 169:325–36.
4. Lennon FE, Mirzapooiazova T, Mambetsariev N, et al (2014) Transactivation of the receptor-tyrosine kinase ephrin receptor A2 is required for the low molecular weight hyaluronan-mediated angiogenesis that is implicated in tumor progression. *J Biol Chem* 289:24043–58.

5. Teriete P, Banerji S, Noble M, et al (2004) Structure of the regulatory hyaluronan binding domain in the inflammatory leukocyte homing receptor CD44. *Mol Cell* 13:483–96.
6. Banerji S, Wright AJ, Noble M, et al (2007) Structures of the CD44-hyaluronan complex provide insight into a fundamental carbohydrate-protein interaction. *Nat Struct Mol Biol* 14:234–9.
7. Protin U, Schweighoffer T, Jochum W, Hilberg F (1999) CD44-deficient mice develop normally with changes in subpopulations and recirculation of lymphocyte subsets. *J Immunol* 163:4917–23.
8. Cuff CA, Kothapalli D, Azonobi I, et al (2001) The adhesion receptor CD44 promotes atherosclerosis by mediating inflammatory cell recruitment and vascular cell activation. *J Clin Invest* 108:1031–40.
9. Rouschop KMA, Roelofs JJTH, Claessen N, et al (2005) Protection against renal ischemia reperfusion injury by CD44 disruption. *J Am Soc Nephrol* 16:2034–43.
10. Kothapalli D, Zhao L, Hawthorne EA, et al (2007) Hyaluronan and CD44 antagonize mitogen-dependent cyclin D1 expression in mesenchymal cells. *J Cell Biol* 176:535–544.
11. Päll T, Gad A, Kasak L, et al (2004) Recombinant CD44-HABD is a novel and potent direct angiogenesis inhibitor enforcing endothelial cell-specific growth inhibition independently of hyaluronic acid binding. *Oncogene* 23:7874–7881. doi: 10.1038/sj.onc.1208083
12. Mayer S, Hausen A zur, Watermann DO, et al (2008) Increased soluble CD44 concentrations are associated with larger tumor size and lymph node metastasis in breast cancer patients. *J Cancer Res Clin Oncol* 134:1229–35.
13. Ristamäki R, Joensuu H, Salmi M, Jalkanen S (1994) Serum CD44 in malignant lymphoma: An association with treatment response. *Blood* 84:238–43.
14. Kodama K, Horikoshi M, Toda K, et al (2012) Expression-based genome-wide association study links the receptor CD44 in adipose tissue with type 2 diabetes. *Proc Natl Acad Sci USA* 109:7049–7054.
15. Murakami D, Okamoto I, Nagano O, et al (2003) Presenilin-dependent  $\gamma$ -secretase activity mediates the intramembranous cleavage of CD44. *Oncogene* 22:1511–6.
16. Okamoto I, Kawano Y, Tsuiki H, et al (1999) CD44 cleavage induced by a membrane-associated metalloprotease plays a critical role in tumor cell migration. *Oncogene* 18:1435–46.
17. Chun TH, Sabeh F, Ota I, et al (2004) MT1-MMP-dependent neovessel formation within the confines of the three-dimensional extracellular matrix. *J Cell Biol* 167:757–767.
18. Guedez L, Rivera AM, Salloum R, et al (2003) Quantitative assessment of angiogenic responses by the directed in vivo angiogenesis assay. *The American Journal of Pathology* 162:1431–1439. doi: 10.1016/S0002-9440(10)64276-9
19. Rohan RM, Fernandez A, Udagawa T, et al (2000) Genetic heterogeneity of angiogenesis in mice. *The FASEB Journal* 14:871–876.
20. Pink A, Kallastu A, Turkina M, et al (2014) Purification, characterization and plasma half-life of pegylated soluble recombinant non-HA-binding CD44. *Biodrugs* 28:393–402. doi: 10.1007/s40259-014-0089-y
21. Katoh S, McCarthy JB, Kincade PW (1994) Characterization of soluble CD44 in the circulation of mice. Levels are affected by immune activity and tumor growth. *J Immunol* 153:3440–3449.
22. Tremmel M, Matzke A, Albrecht I, et al (2009) A CD44v6 peptide reveals a role of CD44 in VEGFR-2 signaling and angiogenesis. *Blood* 114:5236–5244.
23. Scharpfenecker M, Dinther M van, Liu Z, et al (2007) BMP-9 signals via ALK1 and inhibits bFGF-induced endothelial cell proliferation and VEGF-stimulated angiogenesis. *J Cell Sci* 120:964–972.

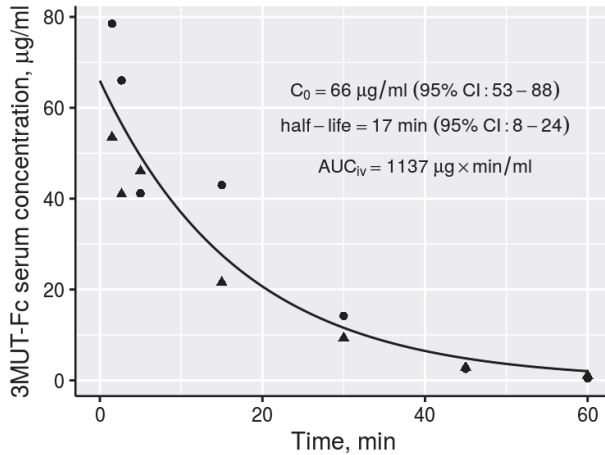
24. David L, Mallet C, Keramidas M, et al (2008) Bone morphogenetic protein-9 is a circulating vascular quiescence factor. *Circ Res* 102:914–922.
25. Peterson RS, Andhare RA, Rousche KT, et al (2004) CD44 modulates Smad1 activation in the BMP-7 signaling pathway. *J Cell Biol* 166:1081–1091.
26. Tanikawa R, Tanikawa T, Hirashima M, et al (2010) Galectin-9 induces osteoblast differentiation through the CD44/Smad signaling pathway. *Biochem Biophys Res Commun* 394:317–322.
27. Bourguignon LY, Singleton PA, Zhu H, Zhou B (2002) Hyaluronan promotes signaling interaction between CD44 and the transforming growth factor beta receptor I in metastatic breast tumor cells. *J Biol Chem* 277:39703–39712.
28. Griffioen AW, Coenen MJ, Damen CA, et al (1997) CD44 is involved in tumor angiogenesis; an activation antigen on human endothelial cells. *Blood* 90:1150–9.
29. Porsch H, Mehić M, Olofsson B, et al (2014) Platelet-derived growth factor  $\beta$ -receptor, transforming growth factor  $\beta$  type I receptor, and CD44 protein modulate each other's signaling and stability. *J Biol Chem* 289:19747–19757.
30. Morrison H, Sherman LS, Legg J, et al (2001) The NF2 tumor suppressor gene product, merlin, mediates contact inhibition of growth through interactions with CD44. *Genes Dev* 15:968–80.
31. Lallemand D, Curto M, Saotome I, et al (2003) NF2 deficiency promotes tumorigenesis and metastasis by destabilizing adherens junctions. *Genes Dev* 17:1090–1100.
32. Laitinen L (1987) Griffonia simplicifolia lectins bind specifically to endothelial cells and some epithelial cells in mouse tissues. *Histochem J* 19:225–234.

# Supplementary Material

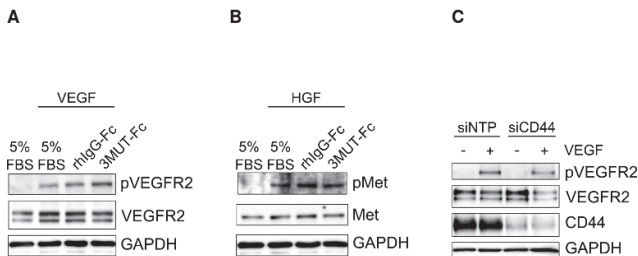
## Supplemental Figures



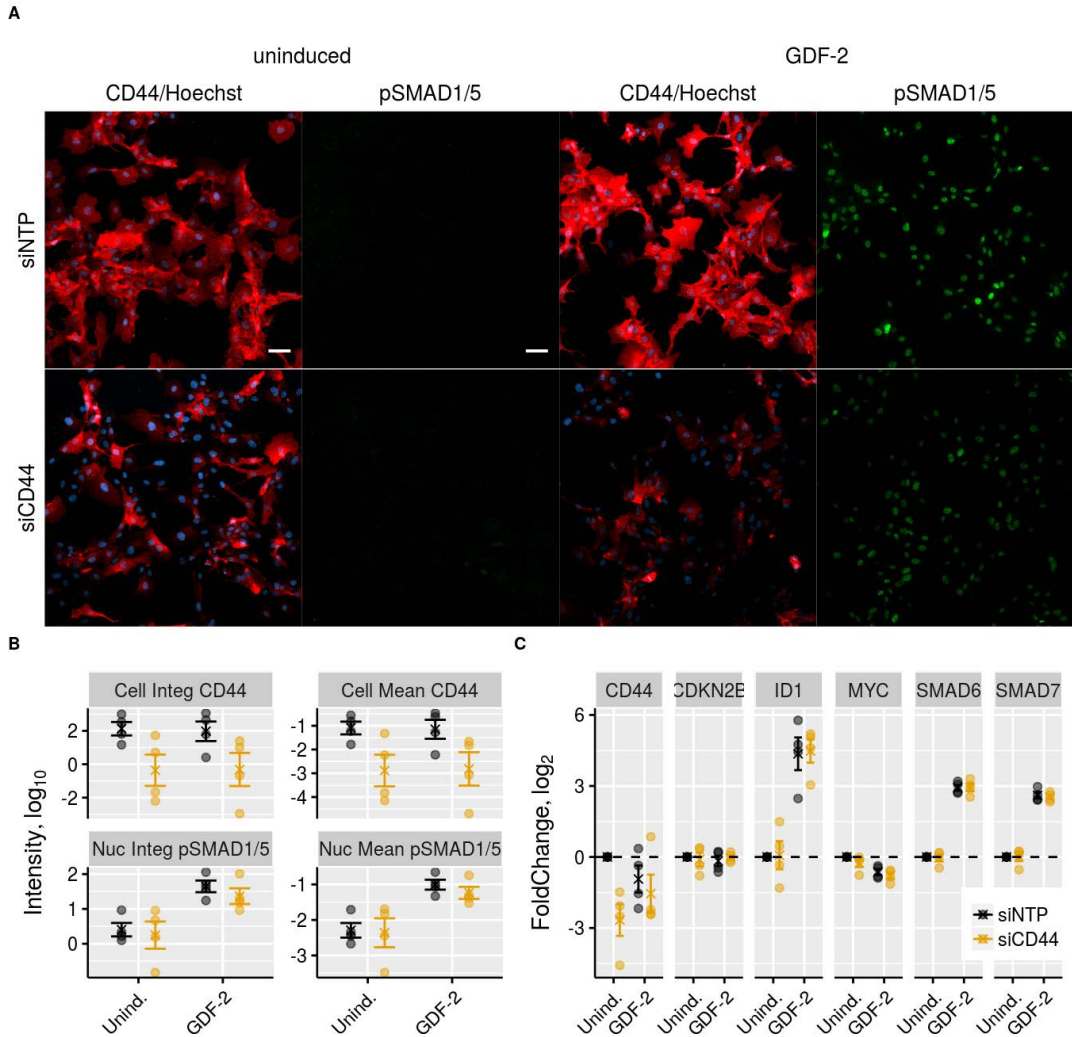
**Supplemental Fig. 1** Aortic fragment angiogenesis assay. 10-12 weeks old male and female wild-type and Cd44<sup>-/-</sup> mice were anaesthetized and thoracic aortae were dissected. Aortas were transferred to a Petri dish containing ice cold 1x MEM immediately after dissection and held on ice. Periaortic fibroadipose tissue and small lateral vessels were removed and aortas were cut into fragments. Collagen gel (7.5 vol of type 1 collagen 2 mg/ml, 0.02N acetic acid was used for concentration adjustment, 1 vol of 10x MEM and 1.5 vol of 1.4% NaHCO<sub>3</sub>; prepared on ice, gently mixed to avoid bubble formation, pH = 7.4) was pipetted into 8-well flexiPERM silicone chamber attached to Petri dish, 150  $\mu$ l per well. Rat tail collagen type-1 was from BD Biosciences. Wells were filled with the first layer of collagen and were left at 37°C for 10 min to allow the collagen to polymerize. Then aortic rings were placed onto first collagen gel layer and embedded into collagen. Collagen gel embedded aortic fragments were grown in M199 media supplemented with 2.5% autologous mouse serum, 4 mM GlutaMAX and penicillin-streptomycin. Aortic fragment cultures were incubated at 37°C for 14 days. Images were acquired with Zeiss Stereo Discovery V8 microscope.



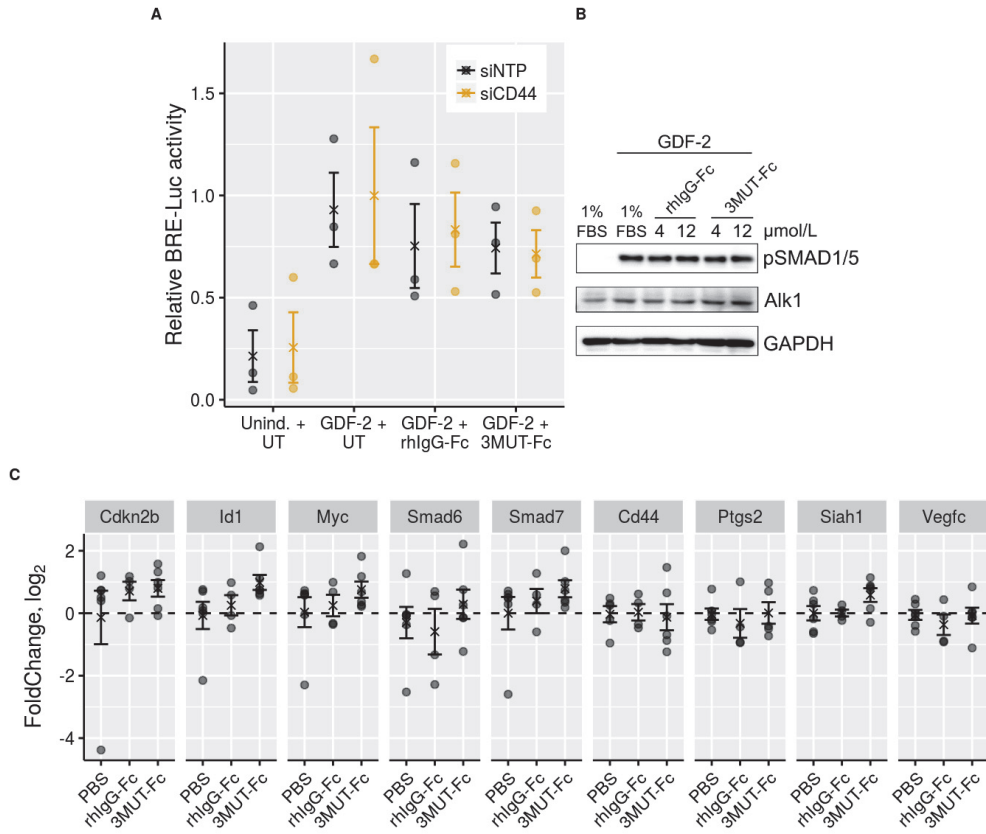
**Supplemental Fig. 2** CD44-3MUT-Fc serum half-life. CD44-3MUT-Fc showed 158 mL/h clearance and 17 min serum half-life in rats after intravenous administration. Volume of distribution was 45 ml or 18% TBW. Dots or triangles represent CD44-3MUT-Fc concentrations predicted from 100- or 50-fold sample dilutions respectively.



**Supplemental Fig. 3** The effect of CD44-3MUT-Fc and CD44 silencing on angiogenic growth factor receptor activation. Western blot analysis of synchronized HUVEC pretreated with CD44-3MUT-Fc in 5% FBS media for 1 h and subsequently released from cell-cycle block by stimulation with 25 ng/ml VEGF (A) or 63 ng/ml HGF (B). After growth factor stimulation, cells were further grown for 72 h before western blot analysis was performed. (C) siCD44 or control (siNTP) transfected HUVECs were synchronized by serum starvation for 6 h and released from cell-cycle block by stimulation with 25 ng/ml VEGF for 10 min. siNTP – non-targeting siRNA pool, siCD44 – CD44-targeting pool. pVEGFR2, pY1175 VEGFR2. pMET, pY1234/1235 MET.

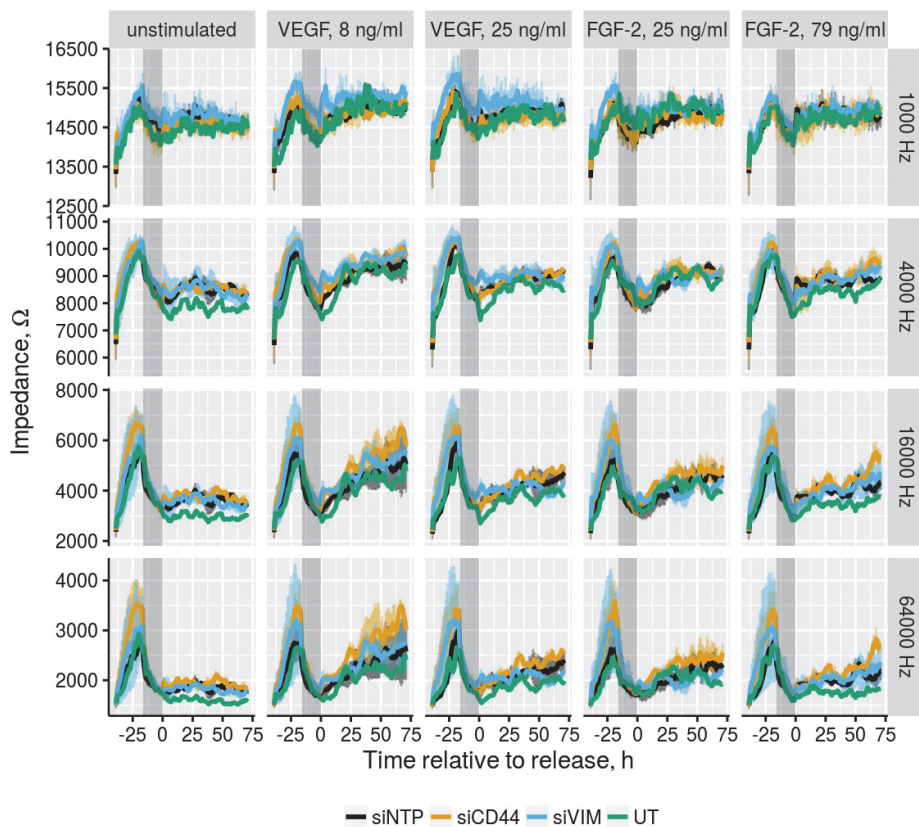


**Supplemental Fig. 4** CD44 is not critical for GDF-2/ALK1-dependent SMAD signaling. **(A to C)** siRNA transfected HUVECs were starved in 1% FBS media for overnight. After starving, cells were stimulated 2 h with 2.5 ng/ml GDF-2. **(A)** Fluorescent confocal microscopy analysis of pSMAD1/5 nuclear location in CD44-silenced HUVEC in response to GDF-2 stimulation. Cells were stained with anti-CD44 antibody (red), anti-pSMAD1/5(pS463/465) antibody (green) and Hoechst (blue). Maximum intensity projections of confocal image stacks are shown. Bars, 50  $\mu$ m. **(B)** Quantitation of anti-CD44 and anti-pSMAD1/5 staining. Integrated and mean intensities per cell or in nuclei of anti-CD44 or anti-pSMAD1/5 stainings are shown, respectively. Legend key is shown in panel C. **(C)** Transcription of SMAD target genes in CD44-silenced HUVEC in response to GDF-2 stimulation. Gene expression is shown relative to uninduced siNTP-transfected cells. Cross is mean and errorbar shows  $\pm$  SEM. N = 4 independent experiments. Dots are means from independent experiments. siNTP – non-targeting siRNA pool, siCD44 – CD44-targeting pool. See also Supplemental Methods.

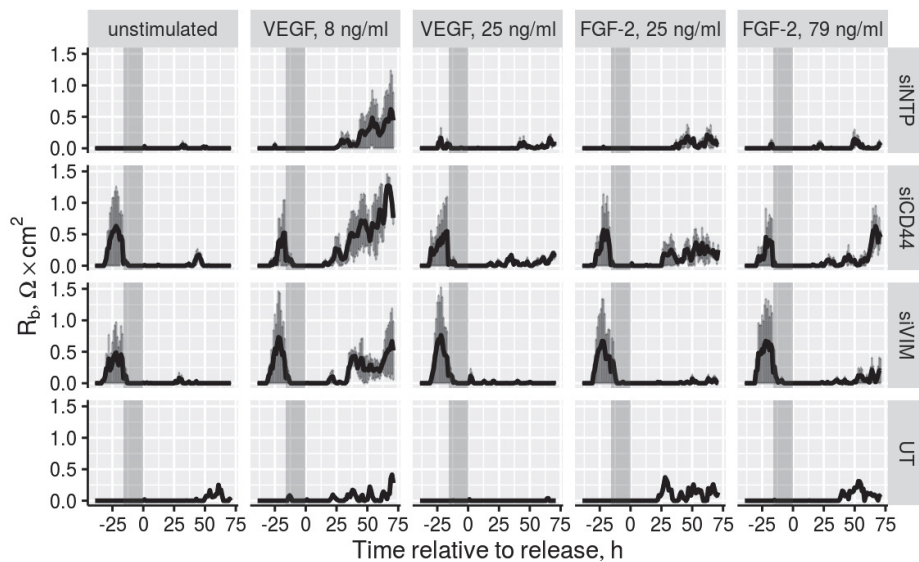


**Supplemental Fig. 5** CD44 is not involved in GDF-2/ALK1-dependent SMAD signaling. **(A)** BMP-responsive element reporter activity of 10 ng/ml GDF-2 stimulated HUVECs transfected with CD44 siRNA and treated with CD44-3MUT-Fc. **(B)** Western blot analysis of HUVEC treated with CD44-3MUT-Fc in 1% FBS starvation media for 6 h and subsequently stimulated with 10 ng/ml GDF-2 for 30 min. pSMAD1/5, pS463/465 SMAD1/5. **(C)** In vivo expression of SMAD target genes in mice treated with CD44-3MUT-Fc. RNA was isolated from lungs of mice treated with 15 mg/kg CD44-3MUT-Fc or hIgG-Fc in angiogenesis experiments described in Fig 2. Dots are individual mice, cross is mean and errorbar shows  $\pm$  SEM. N = 6 mice from two independent experiments. siNTP - non-targeting siRNA pool, siCD44 - CD44-targeting pool. See also Supplemental Methods.

A



B



**Supplemental Fig. 6** CD44 silencing augments EC growth, barrier formation is functional. siRNA transfected HUVECs were plated onto 96-well electrode arrays. After 24 h, cells were starved in 1% FBS media for overnight (gray area). After starving, cells were released from cell cycle block by addition of different concentrations of FGF-2 or VEGF. Following stimulation, HUVEC growth was monitored by measuring electrode impedance at different AC frequencies (A). Measurements recorded at 16000 Hz are shown in Fig. 5C. (B) After experiment, barrier function ( $R_b$ ) of cell layer was modeled using ECIS software [1]. Data are represented as mean  $\pm$  SEM. UT – non-transfected, siNTP – non-targeting siRNA pool, siCD44 – CD44-targeting pool, siVIM – vimentin-targeting pool.

## Supplemental Methods

### CD44-3MUT-Fc serum half-life

F344/NCrHsd male rats were from Harlan, Netherlands. Rats carried polyurethane round tipped jugular vein catheter for blood sampling (Harlan Laboratories Surgical Services). After pre-serum blood sample was taken, rats were injected intravenously via tail vein with 3 mg of CD44-3MUT-Fc in 1ml volume. Blood samples were collected using jugular vein catheter at different time points. Blood samples were held at +37°C for 30 min to allow clot formation and then centrifuged at 1300·g for 10 min at RT. The supernatants were collected and stored at -20°C until assayed. For sandwich ELISA microwell plates were coated with mouse anti-human IgG1 antibody clone G17-1 (BD Biosciences). Blocking was performed with 1.5% BSA/PBS. Standards were step-diluted (40  $\mu$ g/ml – 0  $\mu$ g/ml) in 0.5% BSA/PBS supplemented with 5%, 2% or 1% rat serum. Samples taken at different time points: pre-serum, asap to 24 hours were diluted 1:50 or 1:100 in 0.5% BSA/PBS solution and applied to wells. Biotin mouse anti-human IgG antibody clone G18-145 (BD Biosciences) and streptavidin-HRP was used for detection. Tetramethylbenzidine was used for color development. Concentration at time zero and half-life was estimated from two-parameter exponential decay model with function  $f(x)=d(\exp(-x/e))$ , where  $d$  is upper limit at  $x = 0$ , and  $e$  is decay constant.

### Bre-Luc Reporter Assay

For reporter assay siRNA transfected HUVECs were seeded in 24-well plates 25000 cells/well. The next day cells were co-transfected with Id1-promoter derived reporter construct BRE-Luc and pLacZ. BRE-Luc reporter plasmid was a gift from Martine Roussel & Peter ten Dijke [2](Addgene plasmid #45126). pLacZ was used for normalization of internal transfection efficiency. Transfection was carried out using jetPEI-HUVEC transfection reagent according to manufacturer's protocol. For transfection 900 ng BRE-Luc, 100 ng pLacZ and 2  $\mu$ l jetPEI-HUVEC per well was used. Cells were incubated with transfection complex in 2% FBS-DMEM (4500 mg/l glucose) for 3 h. Then, transfection media was changed to 0.1% FBS containing starvation media and cells were further incubated with 4  $\mu$ M hIgG-Fc or CD44-3MUT-Fc in the presence of 10 ng/ml GDF-2 for ON at 37°C. Cells were lysed and luciferase and  $\beta$ -galactosidase activity was determined using TECAN microtiter plate reader.

## Fluorescence Confocal Microscopy

siRNA transfected HUVECs were seeded into 0.1% gelatin-coated 8-well microscopy slides 24000 cells/well. After 24 h cells were switched to 0.1% FBS containing starvation media (M199, 0.1% FBS, 4 mM L-glutamine, 25 mM Hepes pH 7.4) for 6 h and then induced with 2.5 ng/ml GDF-2 for 2 h at 37°C. For immunofluorescence staining cells were fixed in freshly made 4% formaldehyde in PBS 10 min on ice followed by 10 min at RT. Primary Ab (mouse anti-human CD44 antibody MEM-263 from Exbio; anti phospho-SMAD1/5/8 rabbit mAb from Cell Signaling Technology) and fluorescently labelled secondary Ab (Alexa Fluor 488 or -568 conjugated secondary antibodies from Molecular Probes) stainings were performed sequentially in PBS/0.1% BSA buffer containing 0.1% saponin for 1 h at RT or ON at 4°C. Nuclei were stained with Hoechst 33285 (Sigma). Slides were mounted using Mowiol 4-88 (Sigma). Images were acquired using a Zeiss LSM 510 microscope with Plan-Apochromat 20x/0.8 M27 objective (Carl Zeiss). For each independent experiment, three random fields per well were acquired from two wells per condition. Confocal image stacks were converted to maximum intensity projections using Fiji software [3]. Maximum intensity projections of image channels were segmented and quantitated using CellProfiler software [4].

## Quantitative RT-PCR

For quantitative RT-PCR cells were seeded in 6-cm cell culture dish at density 320000 cells/plate. Treatments were performed as in immunofluorescence experiments (see the Fluorescence confocal microscopy section). Total RNA was isolated from cells or snap-frozen tissues using RNeasy Plus Mini kit (Qiagen). cDNA was synthesized using SuperScript VILO Kit (Invitrogen). Quantitative RT-PCR was performed using Hot Firepol Evagreen qPCR Mix Plus reagent (no ROX; Solis Biodyne) in LightCycler 480 II instrument (Roche). Relative gene expression was determined by ddCt method using GAPDH and ACTB as reference genes.

**Supplemental Table 1** List of primers used for real-time qPCR experiments.

Gene	Forward primer (5'-3')	Reverse primer (5'-3')
Cdkn2b	CCCTGCCACCCTTACCAGA	CAGATACCTCGCAATGTCACG
Id1	ACCCTGAACGGCGAGATCA	TCGTCCGGCTGGAACACATG
Myc	ATGCCCCCTCAACGTGAACTTC	GTCGCAGATGAAATAGGGCTG
Smad6	TTCTCGGCTGTCTCCTCCTGA	GTGGCCTCGGTTTCAGTGTAAGA
Smad7	GGCCTATCCACAGGCTTCTGA	GTGACAGGCGGCAGTAAGACA
Gapdh	AGGTCGGTGTGAACGGATTTG	GGGGTCGTTGATGGCAACA
Ptgs2	AGATTGCTGGCCGGTTGCTG	CAGGGAGAAGCGTTTGCGGT
Actb	GCCCTAGGCACCAGGGTGTG	GGGGCCACACGCAGCTCATT
Vegfc	GGGGGCGAGGTCAAGGCTTTT	GCCTTTCCGCAGCTGGCACT
Cd44	TGCCTCAGCCCCTCCTGAAGA	TGGAGCCGCTGCTGACATCG
Siah1a	AGGAATTCCAGAAAGGCAAGGT	AGAGACAAGAGCATCCTGCAC
CDKN2B	AAGCTGAGCCCAGGTCTCCTA	CCACCGTTGGCCGTAAACT
ID1	GGCTGTTACTCACGCCTCAAG	CCAAGTGAAGGTCCCTGATGTAG
MYC	CGTCTCCACACATCAGCACA	CACTGTCCAAGTCCCTGACTCTTG

**Supplemental Table 1** List of primers used for real-time qPCR experiments.

Gene	Forward primer (5'-3')	Reverse primer (5'-3')
SMAD6	TCTCCTCGCGACGAGTACAAG	GGAGCAGTGATGAGGGAGTTG
SMAD7	AGAGGCTGTGTTGCTGTGAATC	GCAGAGTCGGCTAAGGTGATG
GAPDH	TGCACCACCAACTGCTTAGC	GGCATGGACTGTGGTCATGAG

## Western Blot Analysis of Activation of Angiogenic Growth Factor Receptors

CD44 silencing was performed as described in Materials and methods (see HUVEC transfection with siRNAs section). 42 h after transfection, cells were switched to 0.1% FBS-containing starvation media (M199, 0.1% FBS, 4 mM L-glutamine, 25 mM Hepes pH 7.4) for 6 h and then induced with 25 ng/ml VEGF for 10 min at 37°C. After VEGF induction cells were lysed and subjected to Western blot analysis (see Materials and methods, Western blot analysis section). To evaluate whether CD44-3MUT-Fc affects VEGF, HGF or GDF-2 mediated receptor activation, HUVEC were seeded in 0.1% gelatin-coated 6-well plates 80000 cells/well. VEGF and HGF stimulated cells were grown and treated as described in Materials and methods (see HUVEC growth and treatments section). Briefly, serum-starved HUVEC were treated for 72 h with 4 µM rhIgG-Fc or CD44-3MUT-Fc in the presence of 25 ng/ml VEGF or 63 ng/ml HGF. After treatments cells were lysed in RIPA buffer (50 mM Tris pH 8.0, 150 mM NaCl, 1% NP-40, 0.5% sodium deoxycholate, 0.1% SDS) supplemented with 1 mM Na<sub>3</sub>VO<sub>4</sub>, 10 mM NaF and protease inhibitor cocktail. For analyzing GDF-2 mediated SMAD1/5 activation in response to CD44-3MUT-Fc treatment, 24 h after seeding cells were treated with 4 and 12 µM rhIgG-Fc or CD44-3MUT-Fc in 1% FBS containing starvation media (M199, 1% FBS, 4 mM L-glutamine, 25 mM Hepes pH 7.4) for 6 h and then stimulated with 10 ng/ml GDF-2 for 30 min at 37°C. Subsequently cells were lysed in 70 µl of 1x Laemmli's sample buffer. 10 µg of VEGF and HGF or 20 µl of GDF-2 stimulated samples were subjected to western blot analysis, which was carried out essentially as described in Materials and methods (see Western blot analysis section). Except, 5% BSA-TBST was used for primary Ab incubation and 5% or 2% skimmed milk-TBST respectively for blocking and secondary Ab incubation. Following Abs were used for western blot: anti-GAPDH mouse mAb 1/10000 from Millipore; anti phospho-SMAD1/5/8(Ser463/465) rabbit mAb (D5B10) 1/1000, anti-phospho-VEGFR2(Tyr1175) rabbit mAb (D5B11) 1/1000, anti-phospho-Met(Tyr1234/1235) rabbit mAb (D26) 1/1000 and anti-VEGFR2 rabbit mAb (55B11) 1/1500 from Cell Signaling Technology; anti-Met rabbit pAb (C-28) 1/1000 and anti-ALK-1 goat pAb (D-20) 1/1000 from Santa Cruz Biotechnology.

**Supplemental Table 2** List of siRNA target sequences.

Gene	Entrez gene id	Catalog #	Target sequence
CD44	960	J-009999-06	GAAUAUAACCGCCGCUUU
CD44	960	J-009999-07	CAAGUGGACUCAACGGAGA
CD44	960	J-009999-08	CGAAGAAGGUGUGGGCAGA
CD44	960	J-009999-09	GAUCAACAGUGGCAAUGGA
VIM	7431	L-003551-06	UCACGAUGACCUUGAAUAA
VIM	7431	L-003551-07	GAGGGAAACUAAUCUGGAU
VIM	7431	L-003551-08	UUAAGACGGUUGAAACUAG
VIM	7431	L-003551-09	GGAAAUGGCUCGUCACCUU

**Supplemental Table 2** List of siRNA target sequences.

<b>Gene</b>	<b>Entrez gene id</b>	<b>Catalog #</b>	<b>Target sequence</b>
NTP	NA	D-001810-10-05	UGGUUUACAUGUCGACUAA
NTP	NA	D-001810-10-05	UGGUUUACAUGUUGUGUGA
NTP	NA	D-001810-10-05	UGGUUUACAUGUUUUCUGA
NTP	NA	D-001810-10-05	UGGUUUACAUGUUUCCUA

## Reproducibility

This article and supplemental information is written in knitr [5], an R package for reproducible research. For reproducibility, all graphs, computations and statistics were computed at the same time that the text was typeset. The source code of the article and supplemental information is available upon request. The data files are available upon request.

**Supplemental Table 3.** List of loaded R packages.

<b>Package</b>	<b>Version</b>	<b>Date</b>	<b>Source</b>
boot	1.3-18	2016-02-23	CRAN (R 3.3.0)
bootES	1.2	2015-08-14	CRAN (R 3.3.0)
broom	0.4.1	2016-06-24	CRAN (R 3.3.1)
coda	0.18-1	2015-10-16	CRAN (R 3.3.0)
DBI	0.4-1	2016-05-08	CRAN (R 3.3.0)
dplyr	0.5.0	2016-06-24	CRAN (R 3.3.1)
drc	2.5-12	2015-04-14	CRAN (R 3.3.0)
Formula	1.2-1	2015-04-07	CRAN (R 3.3.0)
geepack	1.2-0.2	2016-07-05	CRAN (R 3.3.1)
ggplot2	2.1.0	2016-03-01	CRAN (R 3.3.0)
ggthemes	3.2.0	2016-07-11	CRAN (R 3.3.1)
gridExtra	2.2.1	2016-02-29	CRAN (R 3.3.0)
gtable	0.2.0	2016-02-26	CRAN (R 3.3.0)
Hmisc	3.17-4	2016-05-02	CRAN (R 3.3.0)
imager	0.20	2016-04-28	CRAN (R 3.3.1)
knitr	1.13	2016-05-09	CRAN (R 3.3.1)
lattice	0.20-33	2015-07-14	CRAN (R 3.2.1)
lubridate	1.5.6	2016-04-06	CRAN (R 3.3.0)
magrittr	1.5	2014-11-22	CRAN (R 3.3.1)
MASS	7.3-45	2015-11-10	CRAN (R 3.3.0)
MESS	0.4-3	2016-06-21	CRAN (R 3.3.1)
plyr	1.8.4	2016-06-08	CRAN (R 3.3.1)
png	0.1-7	2013-12-03	CRAN (R 3.3.0)

**Supplemental Table 3.** List of loaded R packages.

<b>Package</b>	<b>Version</b>	<b>Date</b>	<b>Source</b>
ProjectTemplate	0.6	2014-10-06	CRAN (R 3.3.0)
reshape2	1.4.1	2014-12-06	CRAN (R 3.3.0)
rjags	4-6	2016-02-19	CRAN (R 3.3.0)
rmarkdown	1.0	2016-07-08	CRAN (R 3.3.1)
RSQLite	1.0.0	2014-10-25	CRAN (R 3.3.0)
runjags	2.0.4-2	2016-07-25	CRAN (R 3.3.1)
scales	0.4.0	2016-02-26	CRAN (R 3.3.0)
survival	2.39-5	2016-06-26	CRAN (R 3.3.1)
tidyr	0.6.0	2016-08-12	CRAN (R 3.3.1)

## References

1. Giaever I, Keese CR (1991) Micromotion of mammalian cells measured electrically. *Proc Natl Acad Sci USA* 88:7896–7900.
2. Korchynskiy O, Dijke P ten (2002) Identification and functional characterization of distinct critically important bone morphogenetic protein-specific response elements in the Id1 promoter. *J Biol Chem* 277:4883–4891.
3. Schindelin J, Arganda-Carreras I, Frise E, et al (2012) Fiji: an open-source platform for biological-image analysis. *Nat Methods* 9:676–682.
4. Kametsky L, Jones TR, Fraser A, et al (2011) Improved structure, function and compatibility for CellProfiler: modular high-throughput image analysis software. *Bioinformatics* 27:1179–1180.
5. Xie Y (2016) Knitr: A general-purpose package for dynamic report generation in r.

## **PATENT**

Päll, T, Anderson, W, Kasak, L, **Pink, A**, Kogerman, P, Allikas A, Valkna, A (2013). Methods of using vimentin to inhibit angiogenesis and endothelial cell proliferation. *US patent*: US 8524666 B2.





US008524666B2

(12) **United States Patent**  
**Pall et al.**

(10) **Patent No.:** **US 8,524,666 B2**  
(45) **Date of Patent:** **Sep. 3, 2013**

(54) **METHODS OF USING VIMENTIN TO INHIBIT ANGIOGENESIS AND ENDOTHELIAL CELL PROLIFERATION**

(75) Inventors: **Taavi Pall**, Tiskre Kula (EE); **Wally Anderson**, Tallinn (EE); **Lagle Kasak**, Tallinn (EE); **Anne Pink**, Tallinn (EE); **Priit Kogerman**, Tabasalu (EE); **Aire Allikas**, Tallinn (EE); **Andres Valkna**, Viimsi (EE)

(73) Assignee: **IBCC Holding AS**, Tallinn (EE)

(\* ) Notice: Subject to any disclaimer, the term of this patent is extended or adjusted under 35 U.S.C. 154(b) by 202 days.

(21) Appl. No.: **13/142,541**

(22) PCT Filed: **Jul. 4, 2008**

(86) PCT No.: **PCT/EP2008/058697**  
§ 371 (c)(1),  
(2), (4) Date: **Oct. 6, 2011**

(87) PCT Pub. No.: **WO2009/010409**  
PCT Pub. Date: **Jan. 22, 2009**

(65) **Prior Publication Data**  
US 2012/0021974 A1 Jan. 26, 2012

**Related U.S. Application Data**  
(60) Provisional application No. 60/949,518, filed on Jul. 13, 2007.

(51) **Int. Cl.**  
**A61K 38/00** (2006.01)  
**A61P 35/00** (2006.01)  
**A61P 17/00** (2006.01)  
**A61P 29/00** (2006.01)  
**A61P 35/04** (2006.01)  
**C07K 14/515** (2006.01)

**C07K 5/00** (2006.01)  
**C07K 7/00** (2006.01)  
**C07K 16/00** (2006.01)  
**C07K 17/00** (2006.01)  
**C07K 1/00** (2006.01)  
**C07K 14/00** (2006.01)

(52) **U.S. Cl.**  
USPC ..... **514/13.3**; 514/18.7; 514/19.2; 514/19.3;  
514/19.8; 530/324; 530/350

(58) **Field of Classification Search**  
None  
See application file for complete search history.

(56) **References Cited**

**U.S. PATENT DOCUMENTS**

7,485,414 B2\* 2/2009 Lorens et al. .... 435/4  
2010/0260667 A1\* 10/2010 Georges et al. .... 424/1.49

**FOREIGN PATENT DOCUMENTS**

WO WO2004/030615 4/2004  
WO WO2007/039255 4/2007  
WO WO2007/072221 6/2007

\* cited by examiner

*Primary Examiner* — Robert Landsman

(74) *Attorney, Agent, or Firm* — Gearhart Law, LLC

(57) **ABSTRACT**

The invention relates to a method of treatment for states related to inhibition of angiogenesis and endothelial cell proliferation comprising administering an effective amount of vimentin or its derivatives or its fragments, to a subject in need thereof. Further, the invention relates to a pharmaceutical composition and a medicament comprising vimentin, as well as the use of vimentin in the manufacture of a medicament. Hereby, angiogenesis and endothelial cell proliferation can be controlled, and therapeutic treatment for related states is provided.

**13 Claims, 14 Drawing Sheets**

A

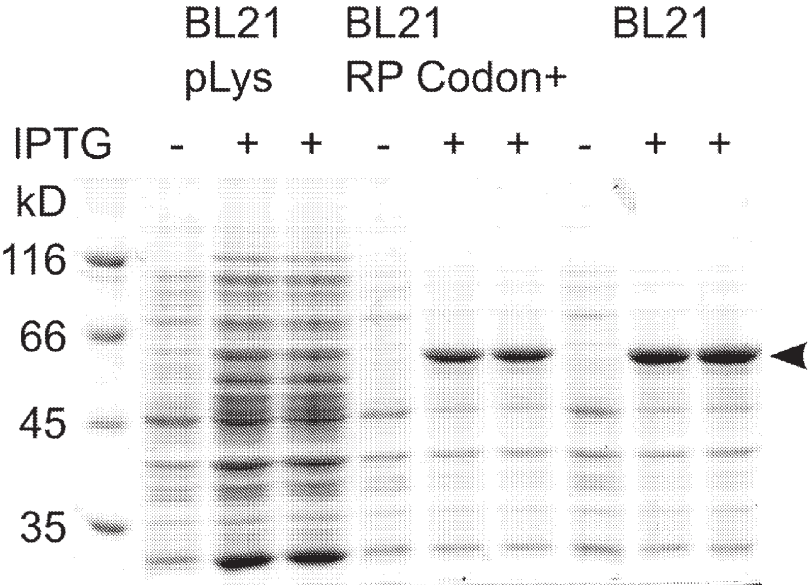


Fig 1a

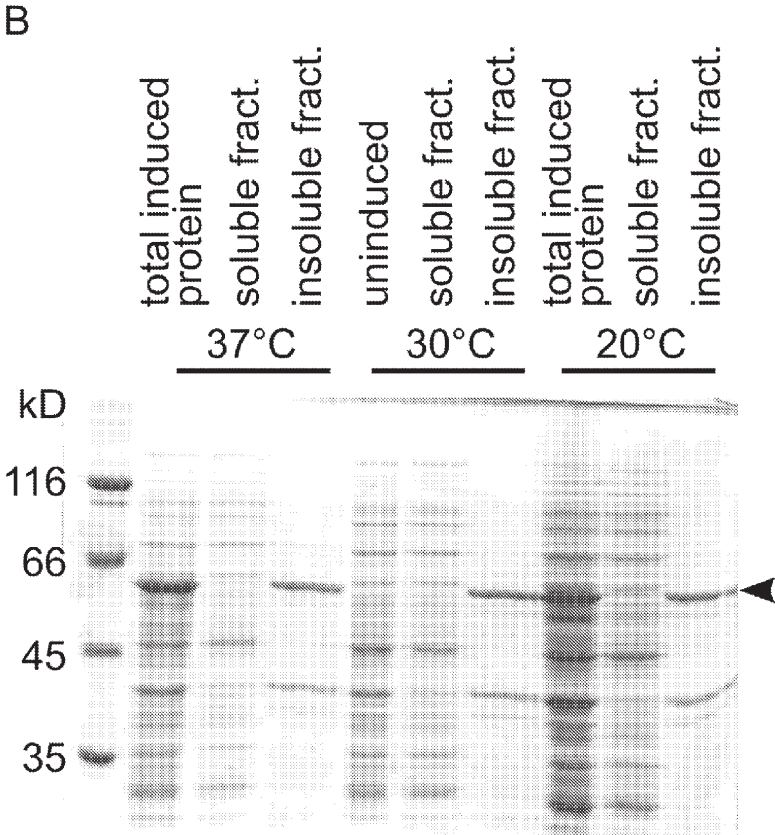


Fig 1b.

C

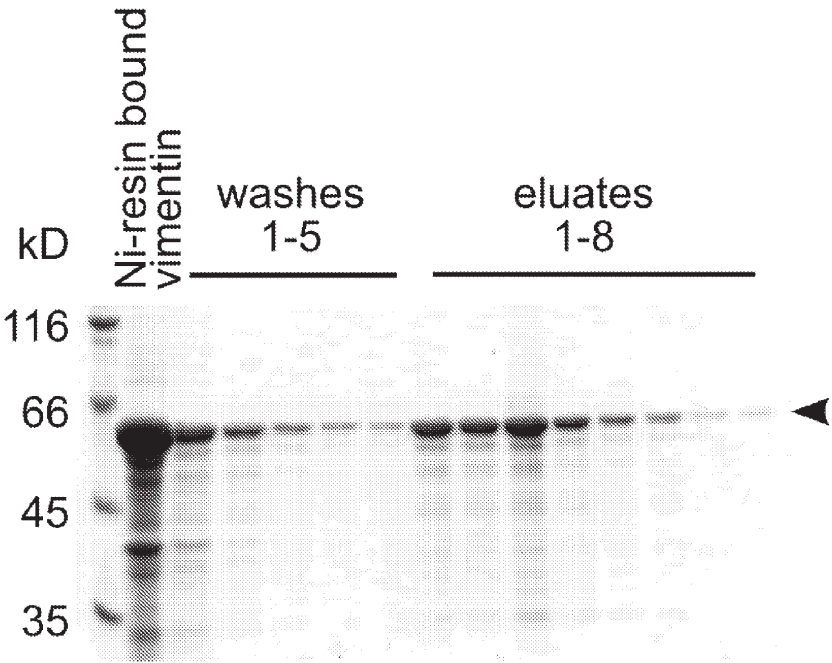


Fig 1c.

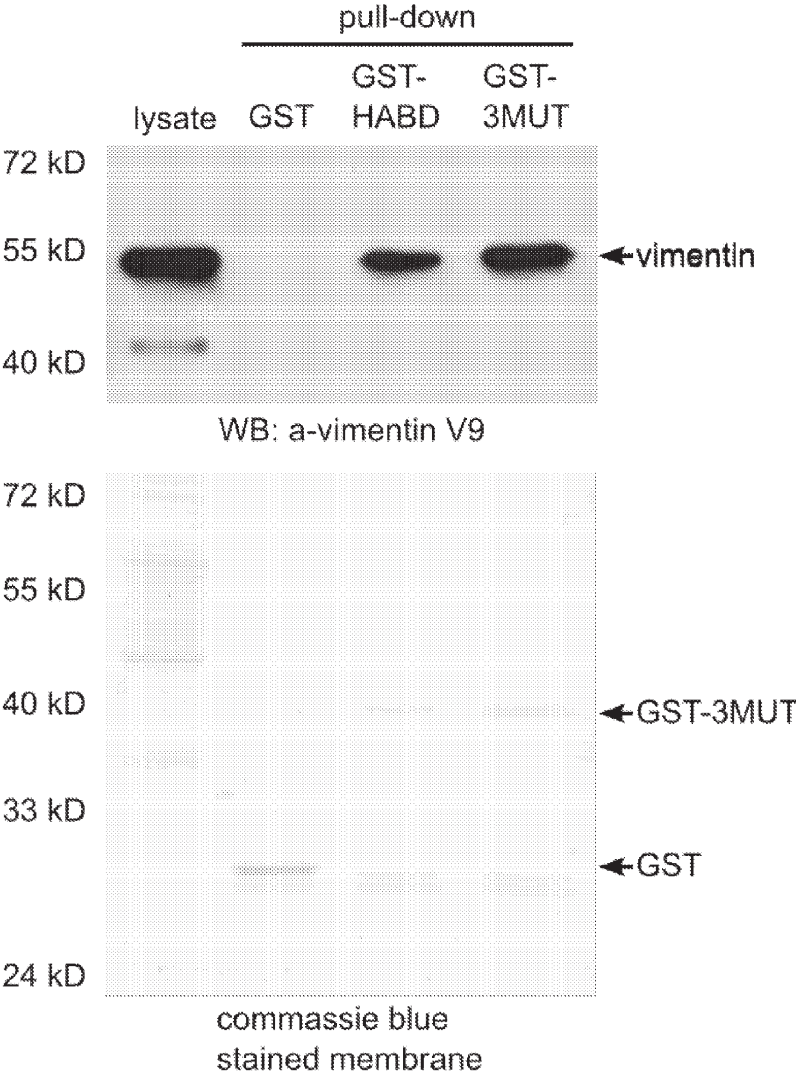


Fig 2a

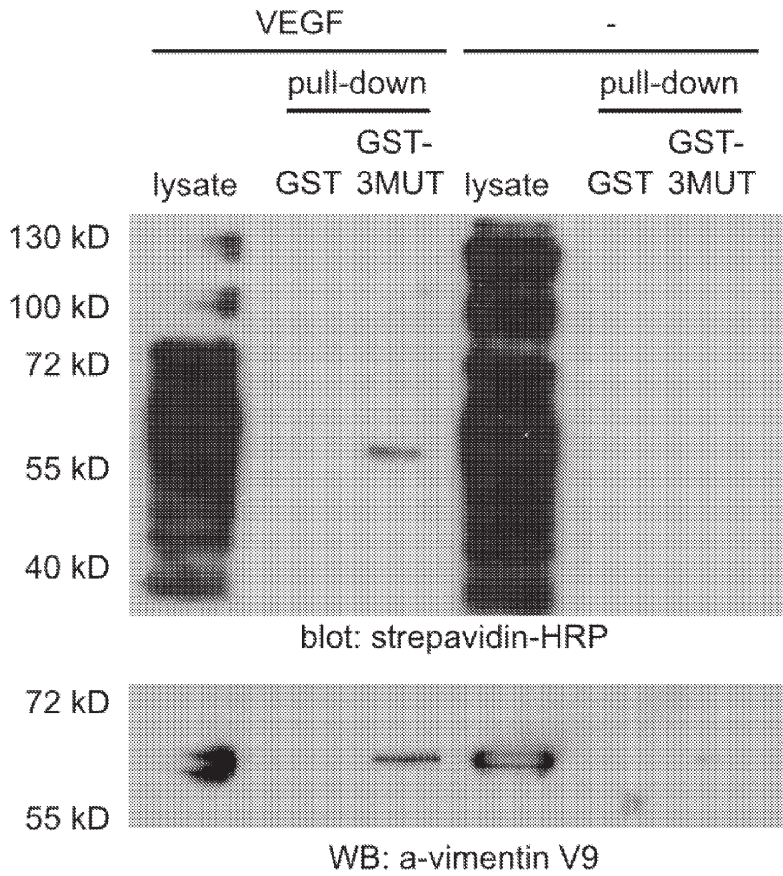


Fig 2b (top) and 2c (bottom).

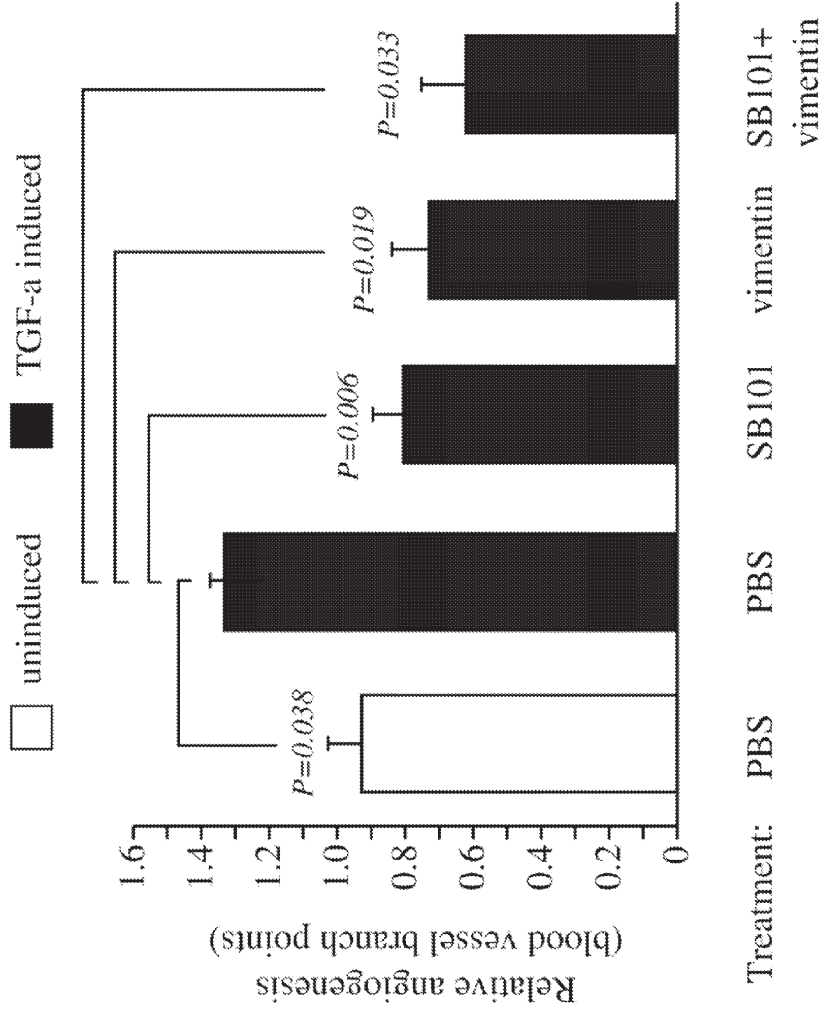


Fig 3.

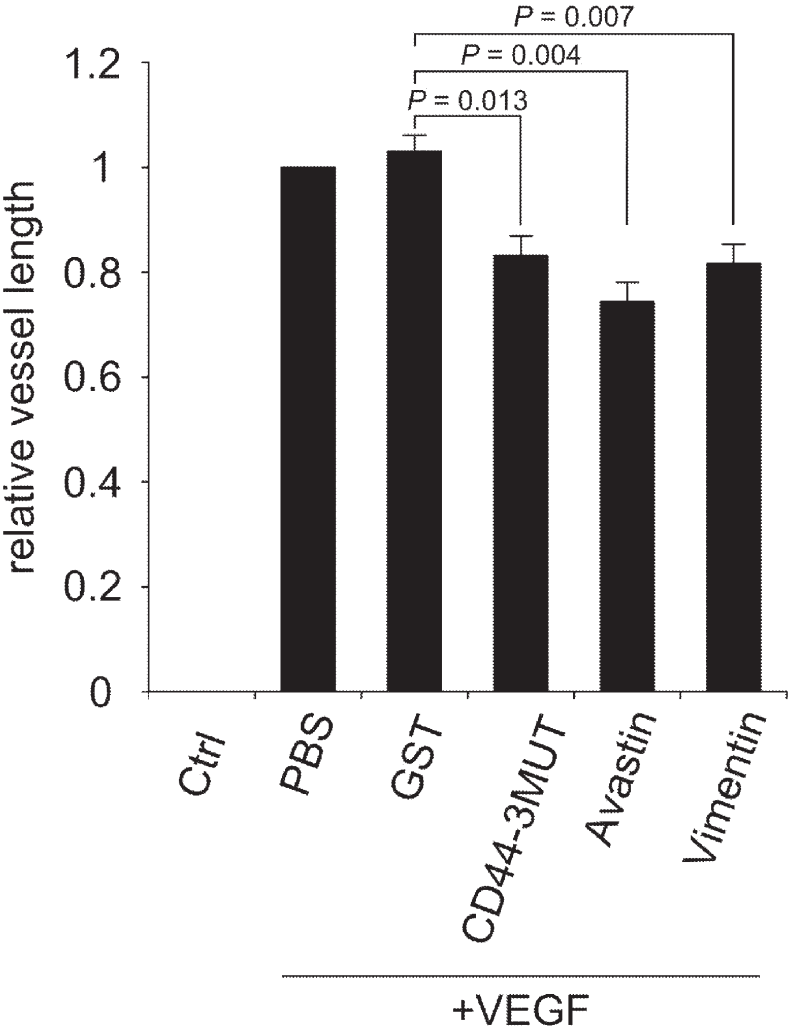


Fig 4.

A

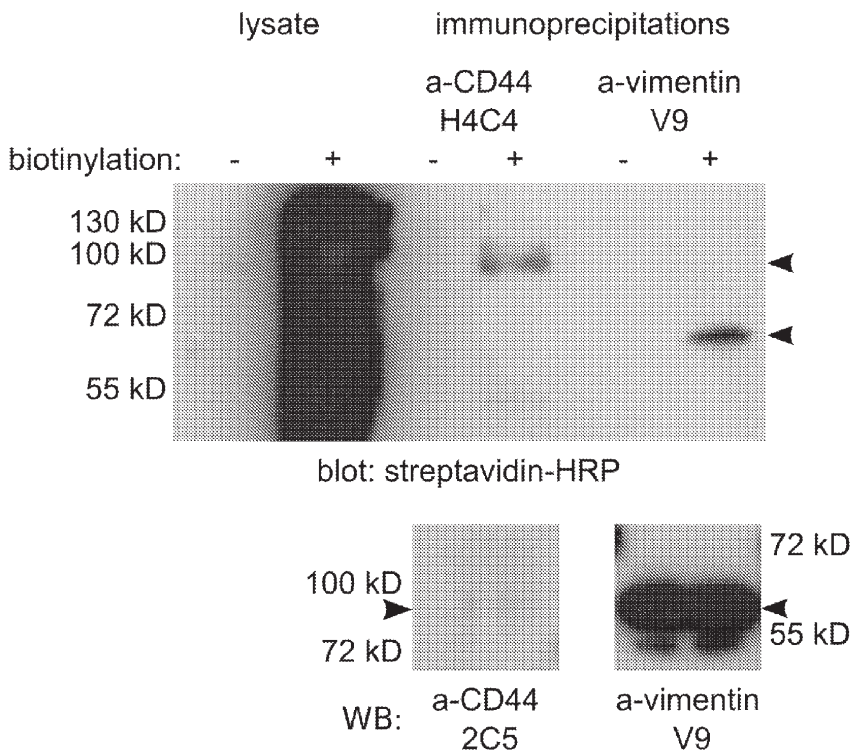
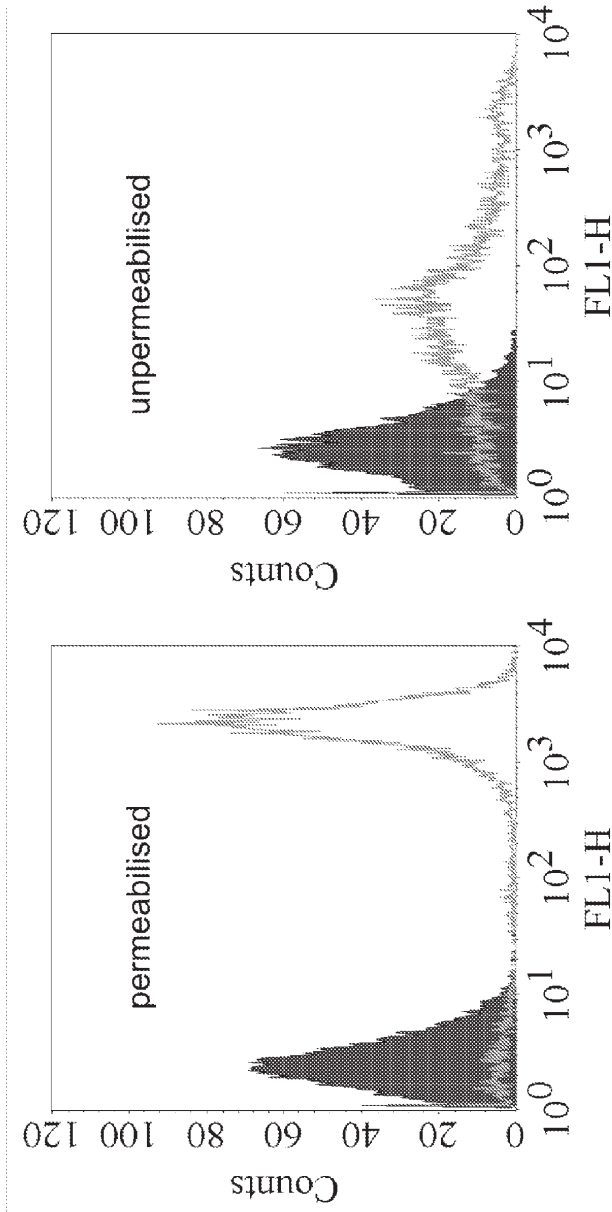


Fig 5a



**B**  
Fig 5b.

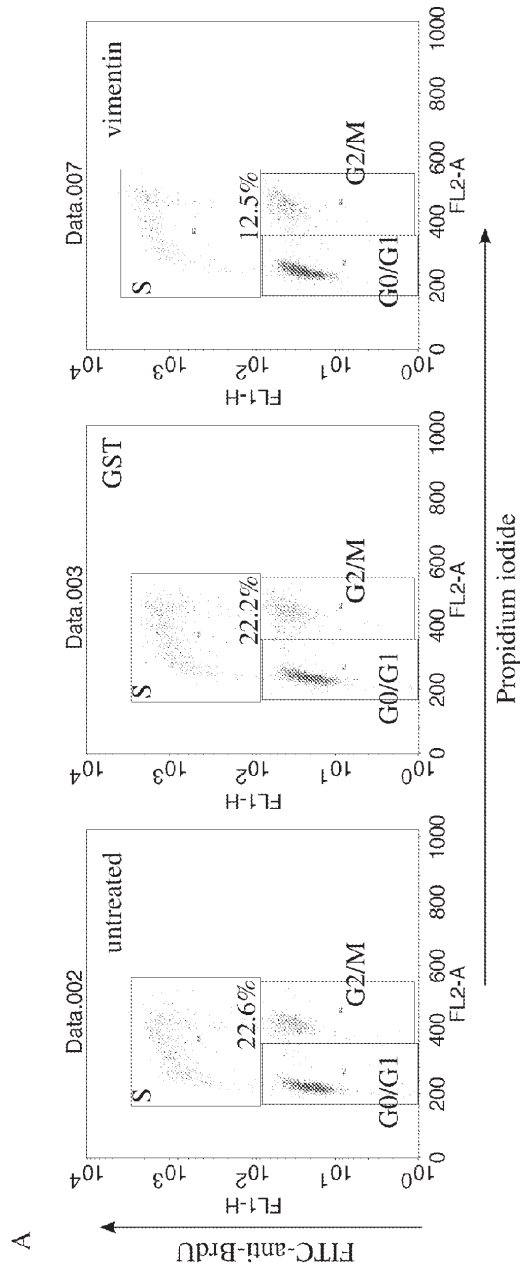


Fig 6a

B

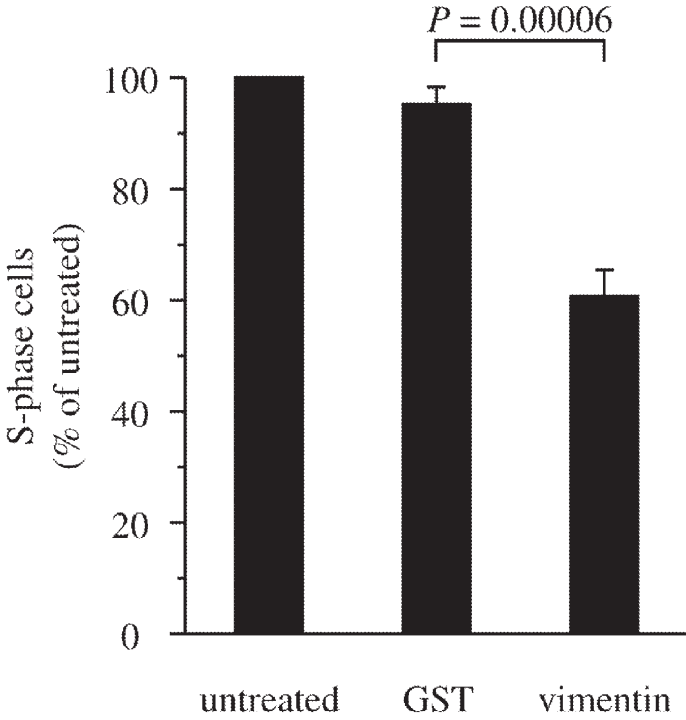


Fig 6b.

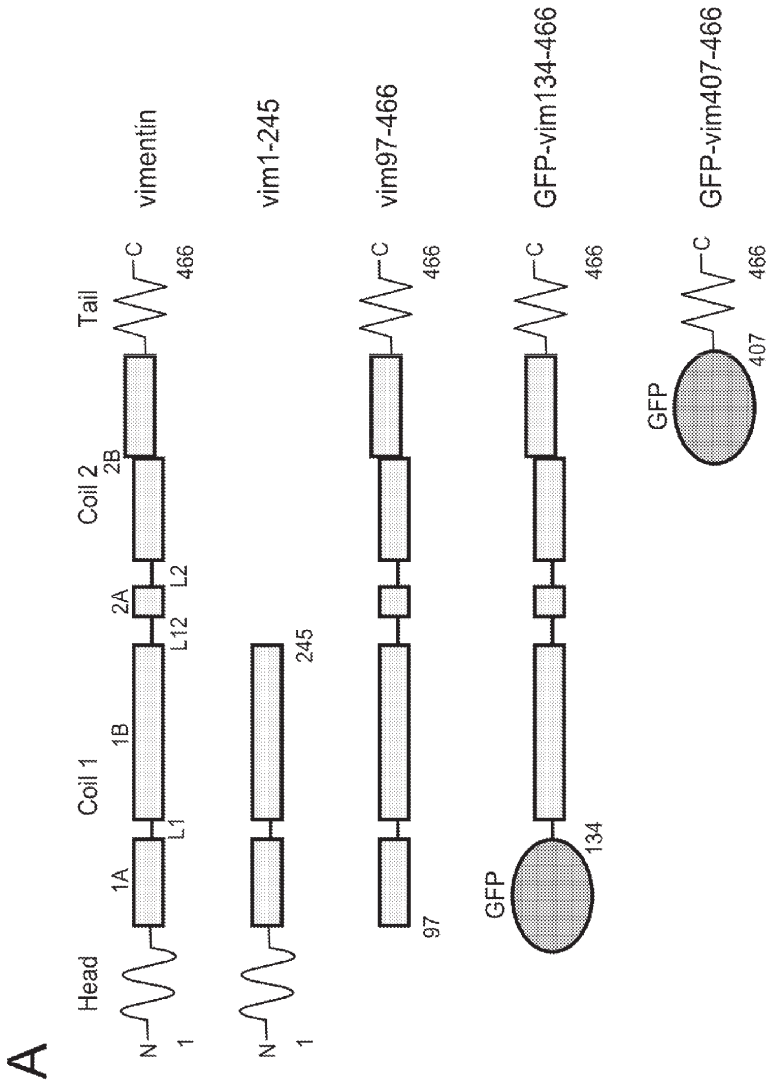


Fig 7A.

B

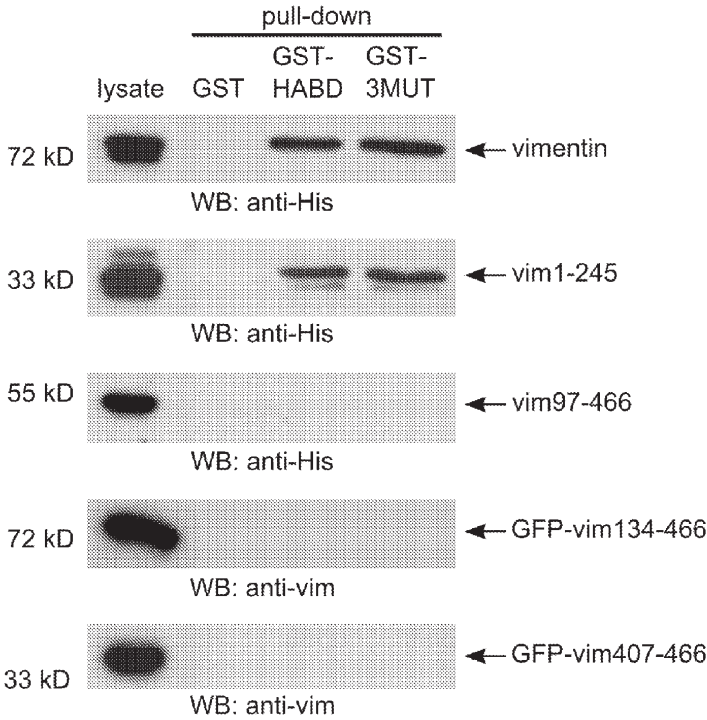


Fig. 7B

Blast alignment of Mesocricetus auratus (Mesau) vimentin aa sequence to Homo sapiens (Hsa) vimentin. For Mesau, mismatches to Hsa sequence are shown.

Score = 867 bits (2239), Expect = 0.0  
 Identities = 452/466 (96%), Positives = 461/466 (98%), Gaps = 1/466 (0%)

Hsa	1	MSTRSVSSSYRRMFGPGGTASRPSSRSVYTTSTRTYSLGSLALRPSTSRSLYASSPGGV	60
Mesau	1	.....SN.Q.N.....-.....S.....A	59
Hsa	61	YATRSSAVRLRSSVPGVRLQLQSDVDFSLADAINTEFKNTRTNEKVELQELNDRFANYIDIK	120
Mesau	60	.V.....M.....	119
Hsa	121	VRFLEQQNKILLAELEQLKGQKSRGLGDLYEEMRELRQVDQLTNDKARVEVERDNLAE	180
Mesau	120	.....	179
Hsa	181	DIMRLREKLQEEMLQREEAENTLQSFQDQVNASLARLDLERKVESLQEEIAFLKHLHEE	240
Mesau	180	.....S.....D.	239
Hsa	241	EIQELQAQIQEQHVQIDVDVSKPDLTAALRDVRRQQYESVAAKNLQEAEEWYKSKFADLSE	300
Mesau	240	.....	299
Hsa	301	AAARNNDALRQAKQESTERYRRQVQSLTCEVDALKGTNESLERQMRMEENFAVEAANYQD	360
Mesau	300	.....N.....L.....	359
Hsa	361	TIGRLQDEIQNMKEEMARHLREYQDLLNVKMLDIEIATYRKLLEGESRISLPLPNFSS	420
Mesau	360	.....	419
Hsa	421	LNLRETNLDSLPLVDTHSKRRTLLIKTVETRDGQVINETSQHDDLE	466
Mesau	420	.....E.....	465

Fig 8.

**METHODS OF USING VIMENTIN TO  
INHIBIT ANGIOGENESIS AND  
ENDOTHELIAL CELL PROLIFERATION**

SEQUENCE LISTING

This application contains nucleotide sequence and amino acid sequence disclosures which are provided in sequence listing.

TECHNICAL FIELD

The invention relates to a method of treatment for states related to inhibition of angiogenesis and endothelial cell proliferation.

TECHNICAL BACKGROUND

CD44 is a transmembrane glycoprotein which functions as cell surface hyaluronic acid (HA) receptor (Aruffo A et al. Cell. 1990 Jun. 29; 61(7):1303-13.). CD44 is involved in cell adhesion on HA, cell migration and HA metabolism.

We have discovered earlier that soluble recombinant CD44 hyaluronic acid binding-domain (CD44-HABD) inhibits angiogenesis in vivo (Päll T et al, Oncogene. 2004 Oct. 14; 23(47):7874-81.). Importantly, CD44-HABD inhibits angiogenesis and endothelial cell proliferation independently of HA-binding (Päll et al, supra). Therefore the inventors hypothesized that CD44 binds to another ligands besides HA on endothelial cells to exert its effects.

Thus, there is a need to find molecules interacting with CD44-HABD, in order to further understanding and control angiogenesis and endothelial cell proliferation, and to provide therapeutic treatment for related states. It is therefore an object of the invention to identify such molecules.

Vimentin is known to be overexpressed in tumor endothelium and targeting vimentin using an antibody has been shown to inhibit angiogenesis both in vivo and in vitro (WO/2007/039255).

SUMMARY OF THE INVENTION

The inventors have now been able to identify one binding partner to CD44, namely vimentin. The inventors have surprisingly found that purified vimentin protein and fragments thereof inhibit endothelial cell proliferation and thereby inhibit angiogenesis.

Thus, in a first aspect, the invention provides a method of treatment for states related to inhibition of angiogenesis and/or endothelial cell proliferation comprising administering an effective amount of vimentin or its derivatives or its fragments, to a subject in need thereof. The vimentin may be in its unmodified and/or phosphorylated form and/or an otherwise modified variant.

In one embodiment, the vimentin has to be at least 95% homologous to human vimentin amino acid sequence, preferably 100% homologous to SEQ ID NO: 1.

In one embodiment, the vimentin fragment comprises at least amino acids 1-97 of a full length vimentin, preferably the amino-acids 1-97 of human vimentin (SEQ ID NO: 12).

In further embodiments the state to be treated is chosen from the following group: ocular diseases causing blindness or impaired vision, states of chronic inflammation, psoriasis, atherosclerosis, restenosis, cancer growth and metastasis, all forms of cancer diseases and tumours, and hemangioma.

In a second aspect of the invention, the invention provides a method for screening for a binding partner for vimentin, comprising the steps of:

providing the molecule comprising the vimentin binding domain;

contacting a potential binding partner to vimentin or its derivative or its fragment; and

determining the effect of said potential binding partner on vimentin.

In one embodiment of the second aspect the potential binding partner is chosen from the group comprising peptides and proteins.

In another embodiment a pharmaceutical composition is provided comprising at least one vimentin binding partner according to the method of the second aspect and/or vimentin in mixture or otherwise together with at least one pharmaceutically acceptable carrier or excipient.

In a further embodiment, a method for the treatment of states chosen from ocular diseases causing blindness or impaired vision, states of chronic inflammation, psoriasis, atherosclerosis, restenosis, cancer growth and metastasis, all forms of cancer diseases and tumours, and hemangioma is provided, comprising administering to the patient a pharmaceutical composition according to the above embodiment.

In a third aspect, a medicament comprising vimentin or its derivatives or its fragments is provided. Preferably the vimentin or the fragment has a sequence that is at least 95% homologous to SEQ ID NO: 1. More preferably the sequence is 100% homologous to SEQ ID NO: 1. In other preferable embodiments of the third aspect, the fragment comprises amino-acids 1-97 of a vimentin. In a further embodiment, the fragment comprises the amino acid sequence of SEQ ID NO: 12.

In a fourth aspect, a use of vimentin or its derivatives or its fragments in the manufacture of a medicament for treating states related to inhibition of angiogenesis and/or endothelial cell proliferation is provided.

DEFINITIONS

By "vimentin or its derivatives or its fragments" is meant any molecule, such as an analogue to vimentin, showing a similar or basically the same effect, or a fragment of vimentin, as well as a fusion protein comprising vimentin, or at least an active fragment of vimentin, showing similar or basically the same effect as vimentin. Examples include fusion proteins of vimentin and a fusion partner such as GST, GFP, FLAG, Fc, etc.

By "analogues and recombinant variants" of a molecule comprising vimentin, are meant molecules, such as fusion proteins, comprising vimentin, thereby at least partly exerting essentially the properties of the vimentin.

By "states related to the inhibition of angiogenesis and/or endothelial cell proliferation" are meant such states and diseases, which may be treated or affected by an inhibition of the angiogenesis and/or endothelial cell proliferation.

By "a binding partner" for a molecule comprising vimentin is meant a molecule having affinity for vimentin or mutants thereof.

By "a receptor molecule, or a part of a receptor molecule" is meant a molecule acting as a receptor, or being part of a receptor.

By "a modified variant" is in the context of the invention meant any modification to a normal wild type-molecule, such as deletions, insertions, substitutions, analogs, fragments or recombinant variants thereof.

DETAILED DESCRIPTION OF THE INVENTION

The inventors set out to search for proteins that can interact with CD44-HABD independently of its hyaluronic acid bind-

ing capability by using GST-tagged CD44-HABD R41AR78SY79S mutant (CD44-3MUT). The inventors used GST pull-down and peptide mass fingerprinting to identify proteins from human endothelial cells interacting with CD44-3MUT. Here the inventors have discovered that CD44-3MUT binds vimentin expressed on endothelial cell surface. The inventors have found that purified recombinant bacterially expressed vimentin inhibits endothelial cell proliferation in vitro and neoangiogenesis in chick chorio allantoic membrane (CAM). This especially surprising since antibodies against vimentin has been reported to block angiogenesis (WO/2007/039255).

It was recently found that vimentin is secreted by macrophages and vimentin secretion is regulated by pro- and anti-inflammatory cytokines (Mor-Vaknin et al. Nat Cell Biol. 2003 January; 5(1):59-63). Vimentin is an intermediate filament protein expressed in cells of mesodermal origin. Vimentin deficient mice develop and reproduce normally (Colucci-Guyon et al. Cell. 1994 Nov. 18; 79(4):679-94). However, it was found that blood vessel integrity is compromised in vimentin knock-out (KO) mice. Kidneys from vimentin KO mice synthesize less vasodilating agent nitric oxide and renal arteries in these mice are more sensitive to vasoconstricting peptide endothelin. Resulting endothelin/nitric oxide imbalance leads to an impairment of flow-induced vasodilation and causes lethality in pathological conditions, such as reduction of renal mass (Terzi et al. Am J. Pathol. 1997 April; 150(4): 1361-7). Nieminen et al. found that vimentin plays role in lymphocyte adhesion to endothelial cells and transendothelial migration (Nieminen et al. Nat Cell Biol. 2006 February; 8(2):156-62).

The anti-angiogenic activity of vimentin was localized to a N-terminal fragment of vimentin comprising amino-acids 1-97 of vimentin (see example 7). In one embodiment, vimentin fragments comprising this fragment are used for the claimed invention. More preferably, the fragment comprises amino-acids 1-97 of human vimentin having the amino acid sequence of SEQ ID NO: 12.

As shown in FIG. 8, the vimentin protein amino-acid sequence is highly conserved. Therefore, it is likely that vimentin protein from one species would have the same function in another species, e.g. rodent vimentin would give the same effect in humans as in rodents. For instance, in the CAM-assay the human vimentin is effective in chick.

The embodiments listed above may be freely combined with one another. Thus, the details and particulars described above and in the claims apply mutatis mutandis to any other embodiments of the invention. While the invention has been described in relation to certain disclosed embodiments, the skilled person may foresee other embodiments, variations, or combinations which are not specifically mentioned but are nonetheless within the scope of the appended claims.

All references cited herein are hereby incorporated by reference in their entirety.

The expression "comprising" as used herein should be understood to include, but not be limited to, the stated items.

#### BRIEF DESCRIPTION OF THE DRAWINGS

FIGS. 1A-1C. Recombinant Vimentin Bacterial Expression and Purification.

Human vimentin (SEQ ID NO: 1) coding sequence was subcloned into N-terminal His-tag containing bacterial expression vector pET15b. Vimentin expression in bacteria was induced by IPTG and majority of recombinant protein was expressed into inclusion bodies. His-tagged vimentin was purified by using Ni affinity-resin under denaturing con-

ditions. Recombinant protein expression and purification steps were analysed by comassie brilliant blue staining of SDS polyacrylamide gel electrophoresis separated proteins. A, induction of vimentin expression in different *E. coli* BL21 strains. B, optimisation of vimentin induction temperature in *E. coli* BL21. Under these conditions vimentin was expressed into inclusion bodies. C, analysis of different purification steps. Arrowhead indicates the position of recombinant vimentin.

FIGS. 2A-2C. CD44-3MUT Binds Endogenous Vimentin. GST pull-down was used to identify CD44-HABD binding proteins in HUVEC. A, CD44-HABD and its HA non-binding CD44-3MUT precipitate vimentin from HUVEC lysate. B, CD44-3MUT precipitates 60 kD protein from cell surface biotinylated HUVEC lysate after VEGF stimulation and this pull-down reaction contains vimentin. C, Sequential streptavidin precipitation from GST pull-down eluates was analysed by western blotting with anti-vimentin specific mAb.

FIG. 3. Vimentin Treatment Blocks Angiogenesis In Vivo in Chick Chorio-Allantoic Membrane.

Angiogenesis was induced in 10-day old chick CAM's under TGF- $\alpha$  soaked paper filter disc, followed by ectopic addition of indicated recombinant proteins or vehicle alone. 72 hours later, filter discs and surrounding CAM was dissected and angiogenesis was quantified by counting blood vessel branch points directly under filter disc. For analysis, normalised data from five independent experiments was pooled. Data show mean  $\pm$  s.e.m. Statistical analysis was performed using unpaired two-tailed Student's t test.

FIG. 4. Vimentin Treatment Inhibits Vessel Growth in Chick Aortic Arch Angiogenesis Assay.

Vessel growth was induced from aortic arch pieces of 14-day old chick embryo by addition of VEGF. Twenty four hours later, organ cultures were fixed and angiogenic response was quantified by measuring the distance of vessel tip from aortic tissue. For statistical analysis, normalised data from three to five experiments were pooled. Data show mean  $\pm$  s.e.m. Statistical analysis was performed using unpaired two-tailed Student's t test.

FIGS. 5A and B. Vimentin is Expressed on Endothelial Cell Surface.

A, exponentially growing HUVEC were cell surface biotinylated and anti-vimentin or -CD44 mAb-s were used for immunoprecipitation. Immunoprecipitated proteins were visualised by streptavidin-HRP staining B, trypsinised HUVEC were methanol permeabilised or formaldehyde fixed and stained with anti-vimentin mAb and analysed by FACS.

FIGS. 6A and B. Recombinant Vimentin Treatment Inhibits Proliferation of Endothelial Cells In Vitro.

Primary HUVEC were either treated 24 h with 10 microg/ml of indicated proteins or left untreated, respectively, and cell cycle profiles were measured. A, cell cycle profiles from anti-BrdU and propidium iodide double staining of HUVEC from representative experiment. B, the proportion of proliferating cells in cell cycle S-phase of recombinant protein treated cells relative to untreated control. Data show mean  $\pm$  s.e.m. Statistical analysis was performed using unpaired two-tailed Student's t test.

FIGS. 7A and B. CD44-HABD Proteins Bind Vimentin Via its N-Terminal Domain.

Full length vimentin or its deletion mutant constructs were transfected into MCF-7 cells. After incubation cells were lysed and lysate was used in pull-down reaction using GST-tagged CD44-HABD proteins immobilised onto glutathione sepharose beads. After pull-down, beads were washed and bound proteins were eluted. Eluates were analysed on western blot. A, vimentin deletion mutants used in pull-down

reactions. B, WB of pull-down reactions from vimentin and its deletion mutant transfected cell lysates.

FIG. 8. BLAST Alignment of Human (SEQ ID NO:1) and Hamster (SEQ ID NO: 14) Vimentin Sequence.

A very high degree of conservation is seen, with 96% identity and 98% similarity with no gaps.

#### EXAMPLES

The invention will now be further illustrated by means of examples which should not be construed to limit the scope of the invention.

##### Example 1

##### Recombinant Vimentin Bacterial Expression and Purification

Full length human vimentin cDNA clone IRATp970E0267D (RZPD, Berlin, Germany) coding for human vimentin (SEQ ID NO: 1) was used to create N-terminal 6xHis containing vimentin bacterial expression construct in pET15b vector. Briefly, two step subcloning was used, first XhoI/BamHI restriction fragment from C-terminal half of original vimentin cDNA clone was inserted into pET15b. Then 400 bp fragment starting from ATG until to unique XhoI site in vimentin cDNA was PCR amplified by using oligos NdeFW 5'GAACATATGTCCACCAGGTC-CGTGTCC 3' (SEQ ID NO: 2) and XhoRev 5' GCGACT-TGCCTTGGCCCTTGAGCTCC 3' (SEQ ID NO: 3) and inserted into NdeI/XhoI site of vimentin C-terminal half containing pET15b vector. The correctness of resulting vimentin expression construct was sequence verified. Vimentin expression was induced in *E. coli* BL21(DE3) strain 3 hours at 30° C. in TB media with 1 mM IPTG at OD<sub>600</sub>=0.7 (FIG. 1A). Bacteria were pelleted by centrifugation 10 min 5000 rpm at 4° C. in Sorvall RC 5C Plus centrifuge GSA rotor and pellet was resuspended in 30 ml PBS per 1 L of culture. After resuspension, bacteria were lysed by using 1 mg/ml lysozyme 30 min at 4° C., followed by three cycles of freezing and thawing. After freeze-thaw cycles lysate was sonicated. Majority of the expressed vimentin resulted in inclusion bodies (FIG. 1B). Inclusion bodies were pelleted by centrifugation 30 min 15000 rpm in Sorvall RC 5C Plus centrifuge in SS-34 rotor. Inclusion body pellet was then washed twice with buffer containing 50 mM Tris pH=8.0, 100 mM NaCl, 1% Triton X-100, 1 M urea, then twice with buffer containing 50 mM Tris pH=8.0, 100 mM NaCl, 1% Triton X-100 and then once with 50 mM Tris pH=8.0, 100 mM NaCl. After washes inclusion bodies were solubilised over-night (ON) with constant shaking in 8 M urea in 50 mM Tris pH=8.0, 100 mM NaCl at room temperature. Ni Cam resin beads (Sigma-Aldrich) were washed according to manufacturers protocol and beads were then incubated with vimentin inclusion bodies solution 1 hour at 4° C. Then beads were washed 5 times in 10 ml vol wash buffer containing 20 mM Tris pH=8.0, 6 M urea, 100 mM NaCl, 20 mM imidazole. Bound proteins were eluted from beads in 0.5 ml vol with elution buffer containing 20 mM Tris pH=6.3, 6 M urea, 100 mM NaCl, 250 mM imidazole (FIG. 1C). Eluates were then pooled and dialysed sequentially against 6 M, 4 M, 2 M, 1 M and 0.5 M urea in 10 mM Tris pH=8 buffer in 100 times volume excess, at least 2 h each step and followed by ON dialysis in 10 mM Tris pH=8.0. Then protein eluates were dialysed 3 times in 10 mM phosphate buffer pH=7.4 with sequential incubation times 2 h, 4 h and ON.

##### Example 2

##### Cell Surface Expressed Vimentin Binds Recombinant CD44-HABD R41AR78SY79S (CD44-3MUT)

To discover endothelial protein targets for previously described angiogenesis inhibiting protein CD44-3MUT (SEQ ID NO: 13) (Päll T et al, Oncogene. 2004 Oct. 14; 23(47):7874-81.), we performed GST pull-down from HUVEC membrane lysates with GST tagged CD44-3MUT (GST-3MUT). For preparation of membrane fractions, adherent cells were washed with ice-cold PBS and lysed in 50 mM Tris pH 8.0, containing protease inhibitor cocktail (Complete, Roche Applied Science, Mannheim, Germany). Insoluble material was pelleted by centrifugation at 14000 rpm 30 min. 4° C. Pellet was then solubilised in buffer containing 2% CHAPS, 50 mM Tris pH 8.0, 50 mM NaCl, protease inhibitor cocktail and centrifuged 14000 rpm 10 min. at 4° C. Resulting lysate was precleared by incubation 2 h with 20 µg glutathione S-transferase immobilised onto 25 µl Glutathione Sepharose 4 Fast Flow beads (Amersham Biosciences, Uppsala, Sweden) at 4° C. After preclearing, lysate was incubated over-night at 4° C. with 10 µg GST, GST-HABD or GST-3MUT proteins immobilised onto 25 µl glutathione sepharose beads. After incubation beads were pelleted in cold centrifuge and washed 4 times with 200 µl buffer containing 50 mM Tris pH 8.0, 150 mM NaCl, protease inhibitor cocktail. Bound proteins were eluted 5 times with 25 µl 20 mM reduced glutathione, 50 mM Tris pH 8.0. Eluates were pooled and eluted proteins were precipitated by addition of 1 vol. 20% TCA and centrifugation at 14000 rpm 30 min 4° C., precipitate was then washed with cold acetone and aspirated dry. For silver staining and subsequent mass spectrometric analysis, protein samples were solubilised in 1xSDS sample buffer containing 50 mM DTT in final concentration instead of 2-mercaptoethanol and alkylated by addition 1/10 vol of freshly prepared 1 M iodoacetamide and incubation 30 min in dark and cold. Silver staining of proteins separated by SDS-PAGE was performed as described in by Shevchenko et al. (Biochem Soc Trans. 1996 August; 24(3):893-6).

Silver staining of pull-down reactions separated by SDS-PAGE revealed that approximately 60 kD size protein band coprecipitated with GST-3MUT compared to GST alone. This protein band was analysed by peptide mass fingerprinting of trypsinolytic fragments and contained vimentin. To confirm that CD44-HABD proteins coprecipitate vimentin, we used vimentin-specific monoclonal antibody V9 to analyse CD44-HABD GST pull-down reactions by western blotting and found that GST-3MUT as well as GST-HABD coprecipitate vimentin from endothelial cell membrane lysates (FIG. 2A).

To study if SB101 (synonymous with CD44-3MUT) binds cell surface expressed vimentin we performed GST pull-down from surface biotinylated HUVEC lysate. HUVEC were serum starved for 6 h in 0.5% FBS containing media and then induced with 10 ng/ml VEGF<sub>165</sub> 1 h at 37° C. or left uninduced. After growth factor induction, cells were surface biotinylated on tissue culture plate with 5 ml EZ Link sulfo-NHS-SS-biotin (Pierce, Rockford, Ill., USA) 1 mM in PBS, 0.1% Na<sub>2</sub>S<sub>2</sub>O<sub>8</sub>. After biotinylation cells were washed 3 times with PBS-100 mM glycine. Then cells were lysed with 2% CHAPS, 50 mM Tris pH 8.0, protease inhibitor cocktail (Complete, Roche Applied Science, Penzberg, Germany) and incubated 15 min on ice, insoluble material was pelleted by centrifugation in microcentrifuge 14000 rpm 10 min at 4° C. After centrifugation supernatant was aspirated and pellet was

redissolved in 2% CHAPS, 50 mM Tris pH 8.0, protease inhibitor cocktail containing buffer, followed by centrifugation in microcentrifuge 14000 rpm 10 min at 4° C. Supernatant was saved for GST pull-down. For pull-down glutathione sepharose 4 fast flow beads (GE Healthcare Bio-Sciences, Uppsala, Sweden) were preincubated with 10 µg GST-SB101 or GST in 0.5 ml vol PBS. The biotinylated membrane lysate was precleared by incubation 2 h at 4° C. with constant end-over-end rotation by using GST-coupled glutathione beads. Precleared lysate (0.3 ml vol per reaction) was used to pull down GST-SB101 binding proteins, GST-bound glutathione beads were used as control, pull-downs were incubated 2 h at 4° C. with rotation. After pull-down reactions, beads were washed 4 times with 0.4 ml vol wash buffer (50 mM Tris pH 8.0, 150 mM NaCl, protease inhibitor cocktail). Bound proteins were eluted with 20 mM reduced glutathione in 50 mM Tris pH 8.0. Eluates were pooled and volume adjusted to 0.5 ml so that solution contained in final concentration 50 mM Tris pH 8.0, 50 mM NaCl, 4 mM reduced glutathione and 1× protease inhibitor cocktail. After SDS PAGE pull-down reactions were analysed by western blotting with HRP-conjugated streptavidin (FIG. 2B). Results show that SB101 pulls down approximately 60 kDa size biotinylated protein. This process is dependent on growth factor stimulation as can be induced by VEGF.

Next, to verify that SB101 precipitated biotinylated protein band contains vimentin we performed sequential streptavidin precipitation from GST pull-down eluates. For this 25 µl of prewashed streptavidin-agarose resin (Sigma, St. Louis, Mo., USA) was added into GST pull-down eluate and incubated 2 h at 4° C. with rotation. After incubation streptavidin beads were washed in sequence 2 times with 50 mM Tris pH 8.0, 150 mM NaCl, 2 times with 0.1 M Na-borate pH 8.5, 2 times with 0.1 M Na-acetate pH 4.5 and finally with 50 mM Tris pH 8.0, 150 mM NaCl. Bound proteins were then eluted from streptavidin beads with 1×SDS sample buffer containing 50 mM DTT instead of 2-mercaptoethanol 30 min at 50° C. followed by 3 min at 95° C. Then samples were analysed by western blotting with anti-vimentin specific mAb V9.

The result shows that SB101 binds in response to VEGF stimulation endogenous cell surface expressed vimentin (FIG. 2C).

#### Example 3

##### Recombinant Vimentin Inhibits Angiogenesis in Chick Chorio-Allantoic Membrane

10-day-old chick embryos were prepared as described in (Brooks et al. *Methods Mol. Biol.* 1999; 129:257-69). For angiogenesis assay, filter discs soaked with 100 ng/ml TGF-α were placed on CAM's, followed by daily ectopical addition of 10 µg of vimentin, CD44-3MUT or PBS as control (n=6-8 per group). After 72 h, filter discs and the surrounding CAM tissue were dissected and angiogenesis quantified in a dissection microscope. Angiogenesis was assessed as the number of blood vessel branch points within the CAM area directly under the filter discs. Vimentin or CD44-3MUT but not GST treatment completely abolished the angiogenic effect of TGF-α (FIG. 3), indicating that soluble vimentin blocks angiogenesis as effectively as previously described angiogenesis inhibitor CD44-3MUT.

#### Example 4

##### Recombinant Vimentin Inhibits Vessel Growth in Chick Aortic Arch Angiogenesis Assay

Aortic arches were dissected from 14-day old chick embryos. Vessels were dissected free from connective tissue

and cut into approximately 1 mm pieces. Then were aortic fragments embedded into collagen type I gel (Upstate, Lake Placid, N.Y., USA) with final concentration 2 mg/ml in M199 media supplemented with 4 mM L-glutamine, 25 mM HEPES, pH of the gel was adjusted to neutral with 10 N NaOH. Angiogenesis was induced by addition of 20 ng/ml VEGF165 into gel. Recombinant proteins in PBS were added at final concentration 10 µg/ml or vehicle alone for control treatment. For experiment, 35 µl premixed gel was pipetted into 96-well and gelled 20 min at 37° C. to form a bed for aortic tissue, then piece aortic arch was put onto gel and covered with 65 µl of premixed gel. Plate was incubated 24 h at 37° C. with 5% CO<sub>2</sub>. At the end of incubation gel was fixed by addition of 100 µl of 10% formaldehyde in PBS and incubated 48 h at room temperature.

For quantitation photomicrographs were taken with Zeiss Axiovert 200M microscope equipped with Zeiss A-Plan 10× objective and AxioCam MRc camera. Quantitation was done on DIC images with AxioVision 4.5 software by measuring the distance of vessel tip from aortic arch tissue fragment.

Results show that in the absence of VEGF there is no neovessel outgrowth from aortic arch tissue in collagen type I gel and only in response to VEGF induction the robust vessel growth occurs (FIG. 4). When recombinant bacterially expressed vimentin was added into gel the average vessel length was significantly reduced compared to GST control treatment. In these assays vimentin effect was comparable to effects of SB101 (synonymous with CD44-3MUT) and avastin.

#### Example 5

##### Vimentin is Expressed on Endothelial Cell Surface

We performed biotinylation of cell-surface proteins on adherent live HUVEC by using EZ-Link sulfo-NHS-LC-biotin reagent and protocol (Pierce, Rockford, Ill., USA), followed by immunoprecipitation of vimentin from cell lysates by using anti-vimentin mouse mAb V9 (Santa Cruz Biotechnology) or CD44 with mouse mAb H4C4 (Developmental Studies Hybridoma Bank) as positive control for cell surface expressed protein. Biotinylated immunoprecipitated proteins were detected in blot by HRP-conjugated streptavidin (Santa Cruz Biotechnology, Santa Cruz, Calif., USA). As shown in FIG. 5A, vimentin antibody V9 immunoprecipitates from HUVEC lysate biotinylated protein in range of approximately 60 kD, whereas anti-CD44 antibody H4C4 immunoprecipitates biotinylated protein in between 72 and 100 kD size range, which corresponds to expected size of endothelial CD44.

Then we used FACS analysis of anti-vimentin stained permeabilised and non-permeabilised HUVEC to characterize vimentin cell surface expression. FACS analysis for cytoplasmic vimentin of HUVEC permeabilised 10 min in -20° C. methanol shows homogeneous high-intensity staining population (FIG. 5B). When nonpermeabilised cells fixed 10 min at room temperature in 4% formaldehyde/PBS were analysed less intensively staining heterogeneous cell population is apparent.

#### Example 6

##### Recombinant Vimentin Inhibits Human Vascular Endothelial Cell (HUVEC) Proliferation In Vitro

Primary human umbilical vein endothelial cells (HUVEC) were maintained in M199 basal media supplemented with

20% FBS, 10 mM HEPES, 4 mM L-glutamine, 50 µg/ml heparin and 30 µg/ml endothelial cell growth supplement (Upstate, Temecula, Calif., USA) and penicillin-streptomycin. Only cells from up to 7<sup>th</sup> passage were used.

For cell cycle analysis, 60-80% confluent cells were incubated in 10% FBS containing media for 24 h in the presence of recombinant proteins at 10 µg/ml concentration. After 24 h, cells were pulsed with 30 µg/ml bromodeoxyuridine for 60 min, harvested and fixed in ice-cold ethanol. Cells were then stained for BrdU with anti-BrdU mAb G3G4 (Developmental Studies Hybridoma Bank, University of Iowa, Iowa, USA) followed by a FITC-conjugated goat anti-mouse antibody (Jackson Immunoresearch, West Grove, Pa., USA) in parallel staining with propidium iodide. The cell cycle distribution was then analysed with a FACS Calibur flow cytometer and Cellquest software (Becton Dickinson, Franklin Lakes, N.J., USA) after plotting FITC-content vs. propidium iodide (FIG. 6a).

The results from cell cycle analysis of untreated HUVEC population show that the proportion of proliferating cells in S-phase is (mean±s.e.m.) 21.5±2.8% (n=10), whereas S-phase population in GST-control treated cells is 21.9±2.6% (n=7). HUVEC treatment with soluble recombinant vimentin reduces the amount of S-phase cells by 33% to 14.5±1.9% (unpaired two-tailed Student's t test, GST vs. vimentin, P=0.00006; n=6). For statistical analysis the proportion of S-phase cells in GST and vimentin treatment groups was normalised within each experiment to untreated control; as shown in FIG. 6b.

#### Example 7

##### Vimentin Binds to CD44-3MUT Via its N-Terminal Filament Head Domain

For creation of full length vimentin mammalian expression construct, human vimentin cDNA was PCR amplified using oligos 5'-CCGAATTCATGTCCAGGTCCTGTGCC-3' (SEQ ID NO: 4) and 5'-GGCCGCGGTTCAAGGT-CATCGTGATG-3' (SEQ ID NO: 5) containing EcoRI or SacII restriction site respectively. Vimentin fragment was inserted into EcoRI/SacII site of pcDNA3.1/MycHisB vector (VIM-pcDNA; Invitrogen).

Vimentin deletion mutant containing aa 1-245 of SEQ ID NO: 1 (VIM\_1-245; FIG. 7A) was PCR amplified from human vimentin cDNA using oligo pair 5'-CCGAATTCATGTCCAGGTCCTGTGCC-3' (SEQ ID NO: 6) and 5'-GTGCGGCGCCAGCTCCTGGATTCCCTC-3' (SEQ ID NO: 7) and deletion mutant containing aa 97-466 of SEQ ID NO: 1 (VIM\_97-466) using oligo pair 5'-CAGAATTCATGAACACCCGCACCAACGAG-3' (SEQ ID NO: 8) 5'-CAGCGGCGCCCTCAAGGTCATCGTGATG-3' (SEQ ID NO: 9), both pairs contain EcoRI restriction site in forward

oligo and NotI site in reverse oligo. PCR fragments were inserted into EcoRI/NotI site of pcDNA3.1/MycHisB vector.

Vimentin deletion mutant containing aa 407-466 of SEQ ID NO: 1 (VIM\_407-466) was PCR amplified from human vimentin cDNA by using oligos 5'-GAGTGGAAITCGAG-GAGAGCAGG-3' (SEQ ID NO: 10) and 5'-GCCGTCGACATTGCTGCACTGAGTGTGTGC-3' (SEQ ID NO: 11), containing EcoRI or Sall site respectively. Vimentin fragment was inserted into EcoRI/Sall site of pEGFP-C2 vector (Clontech). Vimentin deletion mutant containing aa 134-466 of SEQ ID NO: 1 (VIM\_134-466) was created by inserting XhoI/BamHI restriction fragment from full length human vimentin containing pEGFP-C2 vector (VIM-pEGFP) into pEGFP-C3 vector. pEGFP-VIM construct was created by cutting full-length vimentin from VIM-pcDNA with EcoRI and SacII restrictases and inserting it into pEGFP-C2 vector.

CD44-3MUT binding of vimentin deletion mutants was tested using GST pull-down from cell lysates. MCF-7 cells were transfected with vimentin deletion-constructs on 15 cm cell culture plates using 20 µg DNA with polyethyleneimine (PEI; DNA and PEI were used in ratio 1:2). Transfected cells were incubated at 37° C. for 72 h. Thereafter, adherent cells were washed once with cold PBS and lysed in 2 ml of lysis buffer containing 50 mM Tris pH 8.0, 50 mM NaCl, 2% CHAPS and protease inhibitor cocktail (Roche). For removal of insoluble material the lysates were centrifuged 14000 rpm 30 min at 4° C. Resulting lysates were used in GST pull-down. For pull-down 10 µg GST, GST-HABD or GST-3MUT were immobilised onto glutathione sepharose 4 fast flow beads (GE Healthcare) in 0.5 ml of PBS. Cell lysates were precleared by incubating the lysates with GST-coupled glutathione beads for 2 h at 4° C. with continuous rotation. After preclearing, the lysates (0.6 vol per reaction) were incubated over-night at 4° C. with GST, GST-HABD or GST-3MUT proteins immobilised onto 25 µl glutathione sepharose beads. After pull-down reactions, beads were washed 4 times with 0.3 ml vol wash buffer containing 50 mM Tris pH 8.0, 150 mM NaCl and protease inhibitor cocktail. Bound proteins were eluted 3 times with 25 µl volume elution buffer 20 mM reduced glutathione, 50 mM Tris pH 8.0. Eluates were pooled and after SDS PAAG pull-down reactions were analysed by western blotting with anti-His specific pAb (H-15) (Santa Cruz Biotechnology) or anti-vimentin specific pAb (Genway).

WB of pull-down reactions shows that in addition to full length vimentin, GST-HABD and GST-3MUT coprecipitated from cell lysates VIM\_1-245 mutant (FIG. 7B), whereas VIM 97-466, VIM\_134-466 or VIM\_407-466 did not show any coprecipitation with CD44-HABD proteins. Together, these data indicate that CD44-HABD proteins bind vimentin via its N-terminal aa 1-97 (e.g. SEQ ID NO: 12) containing conserved filament head domain.

---

#### SEQUENCE LISTING

<160> NUMBER OF SEQ ID NOS: 14

<210> SEQ ID NO 1

<211> LENGTH: 464

<212> TYPE: PRT

<213> ORGANISM: Homo sapiens

<400> SEQUENCE: 1

-continued

---

Met Ser Thr Arg Ser Val Ser Ser Ser Ser Tyr Arg Arg Asn Phe Gly  
 1 5 10 15

Gly Pro Gly Thr Ala Ser Arg Pro Ser Ser Ser Ala Ser Tyr Val Thr  
 20 25 30

Thr Ser Thr Arg Thr Tyr Ser Leu Gly Ser Ala Leu Arg Pro Ser Thr  
 35 40 45

Ser Arg Ser Leu Tyr Ala Ser Ser Pro Gly Gly Val Tyr Ala Thr Arg  
 50 55 60

Ser Ser Ala Val Arg Leu Arg Ser Ser Val Pro Gly Val Arg Leu Leu  
 65 70 75 80

Gln Asp Ser Val Asp Phe Ser Leu Ala Asp Ala Ile Asn Thr Glu Phe  
 85 90 95

Lys Asn Thr Arg Thr Asn Glu Lys Val Glu Leu Gln Glu Leu Asn Asp  
 100 105 110

Arg Phe Ala Asn Tyr Ile Asp Lys Val Arg Phe Leu Glu Gln Gln Asn  
 115 120 125

Lys Ile Leu Leu Ala Glu Leu Glu Gln Leu Lys Gly Gln Gly Lys Ser  
 130 135 140

Arg Leu Gly Asp Leu Tyr Glu Glu Glu Met Arg Glu Leu Arg Arg Gln  
 145 150 155 160

Val Asp Gln Leu Thr Asn Asp Lys Ala Arg Val Glu Val Glu Arg Asp  
 165 170 175

Asn Leu Ala Glu Asp Ile Met Arg Leu Arg Glu Lys Leu Gln Glu Glu  
 180 185 190

Met Leu Gln Arg Glu Glu Ala Glu Asn Thr Leu Gln Ser Phe Arg Gln  
 195 200 205

Asp Phe Asp Asn Ala Ser Leu Ala Arg Leu Asp Leu Glu Arg Lys Val  
 210 215 220

Glu Ser Leu Gln Glu Glu Ile Ala Phe Leu Lys Lys Leu His Glu Glu  
 225 230 235 240

Glu Ile Gln Glu Leu Gln Ala Gln Ile Gln Glu Gln His Val Gln Ile  
 245 250 255

Asp Val Asp Val Ser Lys Pro Asp Leu Thr Ala Ala Leu Arg Asp Val  
 260 265 270

Arg Gln Gln Tyr Glu Ser Val Ala Ala Lys Asn Leu Gln Glu Ala Glu  
 275 280 285

Glu Trp Tyr Lys Ser Lys Phe Ala Asp Leu Ser Glu Ala Ala Asn Arg  
 290 295 300

Asn Asn Asp Ala Leu Arg Gln Ala Lys Gln Glu Ser Thr Glu Tyr Arg  
 305 310 315 320

Arg Gln Val Gln Ser Leu Thr Cys Glu Val Asp Ala Leu Lys Gly Thr  
 325 330 335

Asp Glu Ser Leu Glu Arg Gln Met Arg Glu Met Glu Glu Asn Phe Ala  
 340 345 350

Val Glu Ala Ala Asp Tyr Gln Asp Thr Ile Gly Arg Leu Gln Asp Glu  
 355 360 365

Ile Gln Asn Met Lys Glu Glu Met Ala Arg His Leu Arg Glu Tyr Gln  
 370 375 380

Asp Leu Leu Asn Val Lys Met Ala Leu Asp Ile Glu Ile Ala Thr Tyr  
 385 390 395 400

Arg Lys Leu Leu Glu Gly Glu Glu Ser Arg Ile Ser Leu Pro Leu Pro  
 405 410 415

Asn Phe Ser Ser Leu Asn Leu Arg Glu Thr Asn Glu Asp Ser Leu Pro  
 420 425 430

-continued

Leu Val Asp Thr His Ser Lys Arg Thr Leu Leu Ile Lys Thr Val Glu  
 435 440 445

Thr Arg Asp Gly Gln Val Ile Asn Glu Thr Ser Glu His His Asp Asp  
 450 455 460

<210> SEQ ID NO 2

<211> LENGTH: 27

<212> TYPE: DNA

<213> ORGANISM: artificial sequence

<220> FEATURE:

<223> OTHER INFORMATION: chemically synthesized

<220> FEATURE:

<221> NAME/KEY: misc\_feature

<222> LOCATION: (1)..(27)

<223> OTHER INFORMATION: primer

<400> SEQUENCE: 2

gaacatatgt ccaccaggtc cgtgtcc

27

<210> SEQ ID NO 3

<211> LENGTH: 26

<212> TYPE: DNA

<213> ORGANISM: artificial sequence

<220> FEATURE:

<223> OTHER INFORMATION: chemically synthesized

<220> FEATURE:

<221> NAME/KEY: misc\_feature

<222> LOCATION: (1)..(26)

<223> OTHER INFORMATION: primer

<400> SEQUENCE: 3

gcgacttgcc ttggccttg agctcc

26

<210> SEQ ID NO 4

<211> LENGTH: 26

<212> TYPE: DNA

<213> ORGANISM: artificial sequence

<220> FEATURE:

<223> OTHER INFORMATION: chemically synthesized

<220> FEATURE:

<221> NAME/KEY: misc\_feature

<222> LOCATION: (1)..(26)

<223> OTHER INFORMATION: primer

<400> SEQUENCE: 4

ccgaattcat gtccaggctc gtgtcc

26

<210> SEQ ID NO 5

<211> LENGTH: 26

<212> TYPE: DNA

<213> ORGANISM: Artificial sequence

<220> FEATURE:

<223> OTHER INFORMATION: chemically synthesized

<220> FEATURE:

<221> NAME/KEY: misc\_feature

<222> LOCATION: (1)..(26)

<223> OTHER INFORMATION: primer

<400> SEQUENCE: 5

ggccgcggtt caaggtcadc gtgatg

26

<210> SEQ ID NO 6

<211> LENGTH: 26

<212> TYPE: DNA

<213> ORGANISM: artificial sequence

<220> FEATURE:

<223> OTHER INFORMATION: chemically synthesized

<220> FEATURE:

<221> NAME/KEY: misc\_feature

<222> LOCATION: (1)..(26)

<223> OTHER INFORMATION: primer

-continued

---

```

<400> SEQUENCE: 6
ccgaattcat gtecagggtcc gtgtcc                               26

<210> SEQ ID NO 7
<211> LENGTH: 29
<212> TYPE: DNA
<213> ORGANISM: artificial sequence
<220> FEATURE:
<223> OTHER INFORMATION: chemically synthesized
<220> FEATURE:
<221> NAME/KEY: misc_feature
<222> LOCATION: (1)..(29)
<223> OTHER INFORMATION: primer

<400> SEQUENCE: 7
gtgcgggcgc ccagctcctg gatttctc                               29

<210> SEQ ID NO 8
<211> LENGTH: 28
<212> TYPE: DNA
<213> ORGANISM: artificial sequence
<220> FEATURE:
<223> OTHER INFORMATION: chemically synthesized
<220> FEATURE:
<221> NAME/KEY: misc_feature
<222> LOCATION: (1)..(28)
<223> OTHER INFORMATION: primer

<400> SEQUENCE: 8
cagaattcat gaacaccgc accaagag                               28

<210> SEQ ID NO 9
<211> LENGTH: 29
<212> TYPE: DNA
<213> ORGANISM: artificial sequence
<220> FEATURE:
<223> OTHER INFORMATION: chemically synthesized
<220> FEATURE:
<221> NAME/KEY: misc_feature
<222> LOCATION: (1)..(29)
<223> OTHER INFORMATION: primer

<400> SEQUENCE: 9
cagcgggcgc cttcaaggtc atcgtgatg                             29

<210> SEQ ID NO 10
<211> LENGTH: 23
<212> TYPE: DNA
<213> ORGANISM: artificial sequence
<220> FEATURE:
<223> OTHER INFORMATION: chemically synthesized
<220> FEATURE:
<221> NAME/KEY: misc_feature
<222> LOCATION: (1)..(23)
<223> OTHER INFORMATION: primer

<400> SEQUENCE: 10
gagtgaatt cgaggagagc agg                                   23

<210> SEQ ID NO 11
<211> LENGTH: 30
<212> TYPE: DNA
<213> ORGANISM: artificial sequence
<220> FEATURE:
<223> OTHER INFORMATION: chemically synthesized
<220> FEATURE:
<221> NAME/KEY: misc_feature
<222> LOCATION: (1)..(30)
<223> OTHER INFORMATION: primer

```

-continued

&lt;400&gt; SEQUENCE: 11

gccgtcgaca ttgctgcaact gagtgtgtgc

30

&lt;210&gt; SEQ ID NO 12

&lt;211&gt; LENGTH: 97

&lt;212&gt; TYPE: PRT

&lt;213&gt; ORGANISM: Homo sapiens

&lt;400&gt; SEQUENCE: 12

Met Ser Thr Arg Ser Val Ser Ser Ser Ser Tyr Arg Arg Asn Phe Gly  
1 5 10 15Gly Pro Gly Thr Ala Ser Arg Pro Ser Ser Ala Ser Tyr Val Thr  
20 25 30Thr Ser Thr Arg Thr Tyr Ser Leu Gly Ser Ala Leu Arg Pro Ser Thr  
35 40 45Ser Arg Ser Leu Tyr Ala Ser Ser Pro Gly Gly Val Tyr Ala Thr Arg  
50 55 60Ser Ser Ala Val Arg Leu Arg Ser Ser Val Pro Gly Val Arg Leu Leu  
65 70 75 80Gln Asp Ser Val Asp Phe Ser Leu Ala Asp Ala Ile Asn Thr Glu Phe  
85 90 95

Lys

&lt;210&gt; SEQ ID NO 13

&lt;211&gt; LENGTH: 112

&lt;212&gt; TYPE: PRT

&lt;213&gt; ORGANISM: Homo sapiens

&lt;400&gt; SEQUENCE: 13

Gln Ile Asp Leu Asn Met Thr Cys Arg Phe Ala Gly Val Phe His Val  
1 5 10 15Glu Lys Asn Gly Ala Tyr Ser Ile Ser Arg Thr Glu Ala Ala Asp Leu  
20 25 30Cys Lys Ala Phe Asn Ser Thr Leu Pro Thr Met Ala Gln Met Glu Lys  
35 40 45Ala Leu Ser Ile Gly Phe Glu Thr Cys Ser Ser Gly Phe Ile Glu Gly  
50 55 60His Val Val Ile Pro Arg Ile His Pro Asn Ser Ile Cys Ala Ala Asn  
65 70 75 80Asn Thr Gly Val Tyr Ile Leu Thr Ser Asn Thr Ser Gln Tyr Asp Thr  
85 90 95Tyr Cys Phe Asn Ala Ser Ala Pro Pro Glu Glu Asp Cys Thr Ser Val  
100 105 110

&lt;210&gt; SEQ ID NO 14

&lt;211&gt; LENGTH: 465

&lt;212&gt; TYPE: PRT

&lt;213&gt; ORGANISM: Mesocricetus auratus

&lt;400&gt; SEQUENCE: 14

Met Ser Thr Arg Ser Val Ser Ser Ser Ser Tyr Arg Arg Met Phe Gly  
1 5 10 15Gly Pro Gly Thr Ser Asn Arg Gln Ser Ser Asn Arg Ser Tyr Val Thr  
20 25 30Thr Ser Thr Arg Thr Tyr Ser Leu Gly Ser Leu Arg Pro Ser Thr Ser  
35 40 45Arg Ser Leu Tyr Ser Ser Ser Pro Gly Gly Ala Tyr Val Thr Arg Ser  
50 55 60

-continued

---

Ser Ala Val Arg Leu Arg Ser Ser Met Pro Gly Val Arg Leu Leu Gln  
 65 70 75 80  
 Asp Ser Val Asp Phe Ser Leu Ala Asp Ala Ile Asn Thr Glu Phe Lys  
 85 90 95  
 Asn Thr Arg Thr Asn Glu Lys Val Glu Leu Gln Glu Leu Asn Asp Arg  
 100 105 110  
 Phe Ala Asn Tyr Ile Asp Lys Val Arg Phe Leu Glu Gln Gln Asn Lys  
 115 120 125  
 Ile Leu Leu Ala Glu Leu Glu Gln Leu Lys Gly Gln Gly Lys Ser Arg  
 130 135 140  
 Leu Gly Asp Leu Tyr Glu Glu Glu Met Arg Glu Leu Arg Arg Gln Val  
 145 150 155 160  
 Asp Gln Leu Thr Asn Asp Lys Ala Arg Val Glu Val Glu Arg Asp Asn  
 165 170 175  
 Leu Ala Glu Asp Ile Met Arg Leu Arg Glu Lys Leu Gln Glu Glu Met  
 180 185 190  
 Leu Gln Arg Glu Glu Ala Glu Ser Thr Leu Gln Ser Phe Arg Gln Asp  
 195 200 205  
 Val Asp Asn Ala Ser Leu Ala Arg Leu Asp Leu Glu Arg Lys Val Glu  
 210 215 220  
 Ser Leu Gln Glu Glu Ile Ala Phe Leu Lys Lys Leu His Asp Glu Glu  
 225 230 235 240  
 Ile Gln Glu Leu Gln Ala Gln Ile Gln Glu Gln His Val Gln Ile Asp  
 245 250 255  
 Val Asp Val Ser Lys Pro Asp Leu Thr Ala Ala Leu Arg Asp Val Arg  
 260 265 270  
 Gln Gln Tyr Glu Ser Val Ala Ala Lys Asn Leu Gln Glu Ala Glu Glu  
 275 280 285  
 Trp Tyr Lys Ser Lys Phe Ala Asp Leu Ser Glu Ala Ala Asn Arg Asn  
 290 295 300  
 Asn Asp Ala Leu Arg Gln Ala Lys Gln Glu Ser Asn Glu Tyr Arg Arg  
 305 310 315 320  
 Gln Val Gln Ser Leu Thr Cys Glu Val Asp Ala Leu Lys Gly Thr Asn  
 325 330 335  
 Glu Ser Leu Glu Arg Gln Met Arg Glu Met Glu Glu Asn Phe Ala Leu  
 340 345 350  
 Glu Ala Ala Asn Tyr Gln Asp Thr Ile Gly Arg Leu Gln Asp Glu Ile  
 355 360 365  
 Gln Asn Met Lys Glu Glu Met Ala Arg His Leu Arg Glu Tyr Gln Asp  
 370 375 380  
 Leu Leu Asn Val Lys Met Ala Leu Asp Ile Glu Ile Ala Thr Tyr Arg  
 385 390 395 400  
 Lys Leu Leu Glu Gly Glu Glu Ser Arg Ile Ser Leu Pro Leu Pro Asn  
 405 410 415  
 Phe Ser Ser Leu Asn Leu Arg Glu Thr Asn Leu Glu Ser Leu Pro Leu  
 420 425 430  
 Val Asp Thr His Ser Lys Arg Thr Leu Leu Ile Lys Thr Val Glu Thr  
 435 440 445  
 Arg Asp Gly Gln Val Ile Asn Glu Thr Ser Gln His His Asp Asp Leu  
 450 455 460  
 Glu  
 465

---

The invention claimed is:

1. A method to manufacture a medicament for inhibition of angiogenesis or endothelial cell proliferation, said method comprising the use of vimentin according to SEQ ID NO:1, or a fragment thereof comprising SEQ ID NO:12 in the medicament.

2. The method of claim 1, wherein the vimentin consists of SEQ ID NO:1.

3. The method of claim 1, wherein the vimentin fragment consists of SEQ ID NO:12.

4. A medicament for inhibition of either angiogenesis or endothelial cell proliferation, said medicament comprising a fragment of vimentin, wherein said fragment comprises SEQ ID NO:12.

5. A pharmaceutical composition for treating states requiring inhibition of either angiogenesis or endothelial cell proliferation in a human, said composition comprising the vimentin of SEQ ID NO:1 or a fragment thereof comprising SEQ ID NO:12, in a mixture or otherwise together with at least one pharmaceutically acceptable carrier or excipient.

6. A method for the treatment of states requiring inhibition of either angiogenesis or endothelial cell proliferation in a

human, the method comprising administering to the patient a pharmaceutical composition according to claim 5.

7. A method of inhibiting angiogenesis and endothelial cell proliferation, said method comprising using the vimentin of SEQ ID NO:1, a fragment thereof comprising SEQ ID NO:12, or a vimentin which is at least 95% identical to SEQ ID NO:1.

8. The method according to claim 7, wherein the vimentin is in its unmodified or phosphorylated form.

9. The method according to claim 7, wherein the amino acid sequence of the vimentin is SEQ ID NO:1.

10. The method according to claim 7, wherein the vimentin fragment is SEQ ID NO:12.

11. The method according to claim 7, wherein the method is used for treating a state requiring inhibition of either angiogenesis or endothelial cell proliferation.

12. The method of claim 11, wherein the state is a tumorous cancer.

13. The method of claim 7, wherein the method is to inhibit angiogenesis and endothelial cell proliferation in vitro.

\* \* \* \* \*

## ABSTRACT

CD44 is the principal receptor for hyaluronan (HA). CD44 functions in a variety of physiological as well as pathological processes, such as HA metabolism, cell adhesion, migration, lymphocyte trafficking, inflammation and cancer progression. CD44 is also involved in angiogenesis, the growth of new blood vessels, but how exactly CD44 regulates angiogenesis is not clear. Angiogenesis is deregulated in cancer, and treatments targeting angiogenesis show clinical benefit in cancer therapy. However, the efficacy of anti-angiogenic treatments in cancer is limited due to eventual acquisition of drug resistance via several mechanisms. A more detailed understanding of the mechanisms and factors regulating angiogenesis is crucial for the development of more effective anti-angiogenic therapies. In this thesis, our findings on the role of CD44 in angiogenesis and endothelial cell (EC) growth are presented.

Angiogenesis was investigated *in vivo* in two mouse models, in *Cd44*-null mice and in immuno-deficient nude mice. In nude mice, we studied the effect of the recombinant, non-HA-binding mutant of CD44 (CD44-3MUT). However, CD44-3MUT displayed very short serum half-life, which may compromise its *in vivo* efficacy. Therefore, we decided to improve the pharmacokinetic properties of CD44-3MUT. We tested two different approaches. First, we used the chemical addition of the polyethylene glycol (PEG) moiety to the N-terminus and, second, we cloned the Fc region of human IgG to the C-terminus of CD44-3MUT. Both resulting fusion proteins, PEG-CD44-3MUT and CD44-3MUT-Fc, exhibited improved pharmacokinetic properties. CD44-3MUT-Fc displayed shorter serum residence time, but better biodistribution and was easier to produce than PEG-CD44-3MUT. Thus, we chose to use CD44-3MUT-Fc for further *in vivo* studies. *In vivo* angiogenesis assays suggested that CD44 functions as an endogenous inhibitor of angiogenesis. We found that angiogenesis was reduced in CD44-3MUT-Fc-treated nude mice, whereas *Cd44*-null mice displayed augmented angiogenic response compared to wild-type controls. To study the effects of CD44 at cellular level, real-time impedance-based monitoring of cell growth as well as end-point cell viability assays were used. These experiments demonstrated that CD44 is involved in the inhibition of EC proliferation and survival. We found that silencing of CD44 enhanced EC proliferation induced by different growth factors, whereas CD44-3MUT-Fc treatment suppressed EC proliferation. CD44 functions as a co-receptor for several receptor tyrosine kinases and is involved in TGF- $\beta$  signalling. However, we found no changes in the activation or protein levels of growth factor receptors in response to CD44-3MUT-Fc treatment or CD44-silencing. These results suggest that CD44 inhibited EC proliferation independently of specific angiogenic growth factor signalling. Finally, we found that intermediate filament protein vimentin interacts with CD44-HABD via its N-terminus and might also contribute to CD44-mediated EC growth inhibition.

In summary, this study suggests a novel role for CD44 as the inhibitor of angiogenesis and endothelial proliferation. This study also provides some data and implications regarding the molecular mechanism behind this function. Our results suggest that CD44 is important for retaining normal levels of angiogenesis and might thus serve as a target for therapeutic angiogenesis or anti-angiogenesis.

## KOKKUVÕTE

Veresooned varustavad organismi kudesid hapniku ja toitainetega. Täiskasvanud organismis on veresooned enamasti vaikeolekus ning uute veresoonte teke olemasolevatest veresoontest väljapungumise teel (angiogenees) toimub ainult vähestel juhtudel. Sellisteks juhtudeks on näiteks haava paranemine ja kudede taastumine. Angiogenees on väga täpselt reguleeritud protsess ning sellest kõrvalekalded on seotud isheemiliste haiguste, põletikukollete ja ka vähkkasvajatega. Angiogeneesi reguleerivatest mehhanismidest ja selles osalevatest faktoritest parem arusaamine võimaldab uute ja efektiivsemate angiogeneesi ravistrateegiate väljatöötamist.

Üheks angiogeneesi reguleerivaks valgukuks on glükovalk CD44. CD44 üheks olulisemaks ligandiks on hüaluroonhape, mida ta seob üle oma aminotermiinaalse hüaluroonhapet siduva domeeni. CD44 osaleb organismis mitmetes erinevates füsioloogilistes ja patoloogilistes protsessides, näiteks hüaluroonhappe metabolismis, rakuadhesioonis ja migratsioonis, lümfotsüütide liikluses, põletikulistes protsessides ning ka vähitekkes. CD44 funktsioon vererakkude liikluses ning vähkkasvaja siirete moodustumises on hästi teada. Samas, CD44 rolli veresoonte tekkes ja veresoonte sisepinnal paiknevate endoteelirakkude jagunemises on vähem uuritud ning paljud aspektid on veel ebaselged. Sellest lähtuvalt oli käesoleva töö eesmärgiks uurida CD44 seotust angiogeneesiga ning täpsustada tema rolli endoteelirakkude kasvus.

CD44 funktsiooni uurimiseks kasutati kahte erinevat lähenemist. Angiogeneesi uuriti nii CD44-knockout hiirtes kui immuunpuudulikes hiirtes. Immuunpuudulikes hiirtes kavatseti kasutada CD44 toime uurimiseks rekombinantset hüaluroonhapet mittesiduvat CD44 mutanti (CD44-3MUT). CD44-3MUT poolestusaeg hiire veres on väga lühike, mis võib põhjustada tema mõju vähenemist. Seetõttu parandati antud töös kahe erineva lähenemise abil ka CD44-3MUT farmakokineetilisi omadusi. Selleks liideti esmalt keemilise reaktsiooni abil CD44-3MUT aminotermiinaalsesse otsa polüetüleenglükool (PEG) ahel. Teise lähenemisena liideti kloonimise teel CD44-3MUT karboksütermiinaalsesse otsa inimese immuunoglobuliini konstantne Fc domeeni. Nii PEG-CD44-3MUT kui ka CD44-3MUT-Fc farmakokineetilised omadused paranesid tunduvalt võrreldes modifitseerimata CD44-3MUT valguga. CD44-3MUT-Fc poolestusaeg oli küll lühem kui PEG-CD44-3MUT valgul, kuid tänu tema paremale jaotusele kudedes ning kergemale tootmisprotsessile, kasutati edasistes funktsiooniuuringutes just CD44-3MUT-Fc versiooni. Angiogeneesikatsed hiirtes viitasid, et CD44 pidurdab organismis uute veresoonte teket. Kui CD44-knockout hiirtes oli angiogenees suurenenud, siis CD44-3MUT-Fc manustamine vastupidiselt vähendas angiogeneesi. Tõenäoliselt pidurdab CD44 uute veresoonte moodustumist, surudes alla endoteelirakkude jagunemist ja elulemust. Rakukasvu katsed näitasid, et CD44 taseme vähendamine RNA vaigistamise teel võimendas endoteelirakkude

jagunemist. Seevastu CD44 hulga suurendamine CD44-3MUT-Fc söötmesse lisamise abil pidurdas endoteelirakkude kasvu. Edasised uuringud näitasid, et raku tsütoplasma valk vimentiin, mis seondub CD44-le läbi oma aminoterminaalse otsa, osaleb CD44 poolt vahendatud endoteelirakkude kasvu pidurdamises.

Kokkuvõttes viitavad käesolevas doktoritöös olevad andmed, et CD44 toimib kui endoteelirakkude jagunemise ja angiogeneesi negatiivne regulaator. Saadud tulemused viitavad, et CD44 funktsioon on oluline normaalse angiogeneesi taseme säilitamiseks, mis annab alust CD44 valku uurida kui uudset sihtmärki terapeutilises angiogeneesis või angiogeneesivastases vähiravis.

# CURRICULUM VITAE

## Personal data

Name Anne Pink  
Date and place of birth 19.08.1982, Kuressaare  
E-mail address anne.pink@ttu.ee

## Education

2007–2016 Tallinn University of Technology, Department of Gene Technology, PhD studies in chemistry and gene technology  
2005–2007 Tallinn University of Technology, Department of Gene Technology, MSc in gene technology  
2001–2005 Tallinn University of Technology, Department of Gene Technology, BSc in gene technology  
1998–2001 Kuressaare Gymnasium, secondary education

## Professional employment

2015–... Tallinn University of Technology, Faculty of Science, Department of Gene Technology, engineer  
2011–2015 Competence Centre for Cancer Research, researcher  
2010–2013 Tallinn University of Technology, Faculty of Science, Department of Gene Technology, engineer  
2007–2008 Celecure AS, researcher  
2005–2010 Competence Centre for Cancer Research, researcher

## Language competence

Estonian native speaker  
English average  
Russian basic

## Honours

2011 "Exploring science and culture", 6th Joint Tartu – Turku - Tallinn Meeting, the prize for best poster  
2010 Grant for attending ESF-EMBO symposium „Molecular Perspectives on Protein-Protein Interactions“

## Special courses

- 2013 Graduate School in Biomedicine and Biotechnology course on immunohistochemistry and histochemistry, Estonian University of Life Sciences, Tartu
- 2011 BD Biosciences BD FACSCalibur™ Training, Sweden
- 2003 Certificate for completing the course „Laboratory Animal Science and Techniques“, Tallinn University of Technology, Tallinn

## Conferences

- 2014 NYAS research conference „Targeting VEGF-mediated Tumour Angiogenesis in Cancer Therapy“, New York, USA. Poster
- 2012 EMBO annual meeting, Nice, France
- 2010 ESF-EMBO research conference "Molecular Perspectives on Protein-Protein Interactions 2010", Saint Feliu de Guixols, Spain. Poster
- 2009 FEBS/EMBO joint lecture course „Spetsai Summer School: Proteins and their Networks- from specific to global analysis“, Spetses, Greece. Poster

## Theses supervised

- 2015 Kristiina Heinoja, bachelor's thesis „The effect of CD44 knockdown on NF-κB pathway activity in different cancer cell lines“, Tallinn University of Technology
- 2014 Kristine Roos, bachelor's thesis „Cloning and Purification of CD44 Hyaluronic Acid Binding Domain Point Mutants“, Tallinn University of Technology

## Publications

1. **Pink, A**, Kallastu, A, Turkina, M, Školnaja, M, Kogerman, P, Päll, T, Valkna, A (2014). Purification, characterization and plasma half-life of PEGylated soluble recombinant non-HA-binding CD44. *BioDrugs*, 28, 4:393-402.
2. Päll, T, **Pink, A**, Kasak, L, Turkina, M, Anderson, W, Valkna, A, Kogerman, P (2011). Soluble CD44 interacts with intermediate filament protein vimentin on endothelial cell surface. *PLoS ONE*, 6, 12:e29305.

## Patents

1. Methods of using vimentin to inhibit angiogenesis and endothelial cell proliferation; Owner: IBCC Holding AS; Authors: Päll, T, Anderson, W, Kasak, L, **Pink, A**, Kogerman, P, Allikas A, Valkna, A; Priority number: US 13/142,541; Priority date: 13.07.2007

# ELULOOKIRJELDUS

## Isikuandmed

Ees- ja perekonnanimi Anne Pink  
Sünniaeg ja -koht 19.08.1982, Kuressaare  
Kodakondsus Eesti  
E-posti aadress anne.pink@ttu.ee

## Hariduskäik

2007–2016 Tallinna Tehnikaülikool, Geenitehnoloogia Instituut, doktoriõpe (keemia-ja geenitehnoloogia)  
2005–2007 Tallinna Tehnikaülikool, Geenitehnoloogia Instituut, magistri teaduskraad, MSc (geenitehnoloogia)  
2001–2005 Tallinna Tehnikaülikool, Geenitehnoloogia Instituut, bakalaureusekraad, BSc (geenitehnoloogia)  
1998–2001 Kuressaare Gümnaasium, keskharidus

## Teenistuskäik

2015–... Tallinna Tehnikaülikool, Matemaatika-loodusteaduskond, Geenitehnoloogia instituut, insener  
2011–2015 Vähiuuringute Tehnoloogia Arenduskeskus AS, teadur  
2010–2013 Tallinna Tehnikaülikool, Matemaatika-loodusteaduskond, Geenitehnoloogia instituut, insener  
2007–2008 Celecure AS, teadur  
2005–2010 Vähiuuringute Tehnoloogia Arenduskeskus AS, teadur

## Keelteoskus

Eesti keel emakeel  
Inglise keel kesktase  
Vene keel algtase

## Tunnustused

2011 "Exploring science and culture", 6th Joint Tartu – Turku - Tallinn Meeting, parima posterit auhind  
2010 ESF-EMBO sümposiumi „Molecular Perspectives on Protein-Protein Interactions“ stipendium

## Täiendusõpe

- 2013 BMBT doktorikooli Immuunohistokeemia ja histokeemia kursus, Eesti Maatülikool, Tartu
- 2011 BD Biosciences BD FACSCalibur™ Training, Stockholm, Rootsi
- 2003 Sertifikaat kursuse „Laboratory Animal Science and Techniques“ läbimise kohta, TTÜ, Tallinn

## Konverentsid

- 2014 NYAS konverents „Targeting VEGF-mediated Tumour Angiogenesis in Cancer Therapy“, New York, USA. Posterettekannet
- 2012 EMBO aastakonverents, Nizza, Prantsusmaa
- 2010 ESF-EMBO konverents "Molecular Perspectives on Protein-Protein Interactions 2010", Saint Felieu de Guixols, Hispaania. Posterettekannet
- 2009 FEBS/EMBO loengukursus „Spetsai Summer School: Protein and their Networks-from specific to global analysis“, Spetsese saar, Kreeka. Posterettekannet

## Juhendatud lõputööd

- 2015 Kristiina Heinoja, bakalaureusetöö, CD44 vaigistamise mõju NF-κB raja aktiivsusele erinevates vähi rakuliinides“, Tallinna Tehnikaülikool
- 2014 Kristine Roos, bakalaureusetöö, „CD44 hüaluroonhapet siduva domääni punktmutantide kloneerimine ja puhastamine“, Tallinna Tehnikaülikool

## Publikatsioonid

1. **Pink, A**, Kallastu, A, Turkina, M, Školnaja, M, Kogerman, P, Päll, T, Valkna, A (2014). Purification, characterization and plasma half-life of PEGylated soluble recombinant non-HA-binding CD44. *BioDrugs*, 28, 4:393-402.
2. Päll, T, **Pink, A**, Kasak, L, Turkina, M, Anderson, W, Valkna, A, Kogerman, P (2011). Soluble CD44 interacts with intermediate filament protein vimentin on endothelial cell surface. *PLoS ONE*, 6, 12:e29305.

## Patentsed leiutised

1. Methods of using vimentin to inhibit angiogenesis and endothelial cell proliferation; Owner: IBCC Holding AS; Authors: Päll, T, Anderson, W, Kasak, L, **Pink, A**, Kogerman, P, Allikas A, Valkna, A; Priority number: US 13/142,541; Priority date: 13.07.2007

**DISSERTATIONS DEFENDED AT  
TALLINN UNIVERSITY OF TECHNOLOGY ON  
NATURAL AND EXACT SCIENCES**

1. **Olav Kongas**. Nonlinear Dynamics in Modeling Cardiac Arrhythmias. 1998.
2. **Kalju Vanatalu**. Optimization of Processes of Microbial Biosynthesis of Isotopically Labeled Biomolecules and Their Complexes. 1999.
3. **Ahto Buldas**. An Algebraic Approach to the Structure of Graphs. 1999.
4. **Monika Drews**. A Metabolic Study of Insect Cells in Batch and Continuous Culture: Application of Chemostat and Turbidostat to the Production of Recombinant Proteins. 1999.
5. **Eola Valdre**. Endothelial-Specific Regulation of Vessel Formation: Role of Receptor Tyrosine Kinases. 2000.
6. **Kalju Lott**. Doping and Defect Thermodynamic Equilibrium in ZnS. 2000.
7. **Reet Koljak**. Novel Fatty Acid Dioxygenases from the Corals *Plexaura homomalla* and *Gersemia fruticosa*. 2001.
8. **Anne Paju**. Asymmetric oxidation of Prochiral and Racemic Ketones by Using Sharpless Catalyt. 2001.
9. **Marko Vendelin**. Cardiac Mechanoenergetics *in silico*. 2001.
10. **Pearu Peterson**. Multi-Soliton Interactions and the Inverse Problem of Wave Crest. 2001.
11. **Anne Menert**. Microcalorimetry of Anaerobic Digestion. 2001.
12. **Toomas Tiivel**. The Role of the Mitochondrial Outer Membrane in *in vivo* Regulation of Respiration in Normal Heart and Skeletal Muscle Cell. 2002.
13. **Olle Hints**. Ordovician Scolecodonts of Estonia and Neighbouring Areas: Taxonomy, Distribution, Palaeoecology, and Application. 2002.
14. **Jaak Nõlvak**. Chitinozoan Biostratigraphy in the Ordovician of Baltoscandia. 2002.
15. **Liivi Kluge**. On Algebraic Structure of Pre-Operad. 2002.
16. **Jaanus Lass**. Biosignal Interpretation: Study of Cardiac Arrhythmias and Electromagnetic Field Effects on Human Nervous System. 2002.
17. **Janek Peterson**. Synthesis, Structural Characterization and Modification of PAMAM Dendrimers. 2002.
18. **Merike Vaher**. Room Temperature Ionic Liquids as Background Electrolyte Additives in Capillary Electrophoresis. 2002.
19. **Valdek Mikli**. Electron Microscopy and Image Analysis Study of Powdered Hardmetal Materials and Optoelectronic Thin Films. 2003.
20. **Mart Viljus**. The Microstructure and Properties of Fine-Grained Cermets. 2003.
21. **Signe Kask**. Identification and Characterization of Dairy-Related *Lactobacillus*. 2003.
22. **Tiiu-Mai Laht**. Influence of Microstructure of the Curd on Enzymatic and Microbiological Processes in Swiss-Type Cheese. 2003.
23. **Anne Kuusksalu**. 2–5A Synthetase in the Marine Sponge *Geodia cydonium*. 2003.
24. **Sergei Bereznev**. Solar Cells Based on Polycrystalline Copper-Indium Chalcogenides and Conductive Polymers. 2003.

25. **Kadri Kriis.** Asymmetric Synthesis of C<sub>2</sub>-Symmetric Bimorpholines and Their Application as Chiral Ligands in the Transfer Hydrogenation of Aromatic Ketones. 2004.
26. **Jekaterina Reut.** Polypyrrole Coatings on Conducting and Insulating Substrates. 2004.
27. **Sven Nõmm.** Realization and Identification of Discrete-Time Nonlinear Systems. 2004.
28. **Olga Kijatkina.** Deposition of Copper Indium Disulphide Films by Chemical Spray Pyrolysis. 2004.
29. **Gert Tamberg.** On Sampling Operators Defined by Rogosinski, Hann and Blackman Windows. 2004.
30. **Monika Übner.** Interaction of Humic Substances with Metal Cations. 2004.
31. **Kaarel Adamberg.** Growth Characteristics of Non-Starter Lactic Acid Bacteria from Cheese. 2004.
32. **Imre Vallikivi.** Lipase-Catalysed Reactions of Prostaglandins. 2004.
33. **Merike Peld.** Substituted Apatites as Sorbents for Heavy Metals. 2005.
34. **Vitali Syritski.** Study of Synthesis and Redox Switching of Polypyrrole and Poly(3,4-ethylenedioxythiophene) by Using *in-situ* Techniques. 2004.
35. **Lee Põllumaa.** Evaluation of Ecotoxicological Effects Related to Oil Shale Industry. 2004.
36. **Riina Aav.** Synthesis of 9,11-Secosterols Intermediates. 2005.
37. **Andres Braunbrück.** Wave Interaction in Weakly Inhomogeneous Materials. 2005.
38. **Robert Kitt.** Generalised Scale-Invariance in Financial Time Series. 2005.
39. **Juss Pavelson.** Mesoscale Physical Processes and the Related Impact on the Summer Nutrient Fields and Phytoplankton Blooms in the Western Gulf of Finland. 2005.
40. **Olari Ilison.** Solitons and Solitary Waves in Media with Higher Order Dispersive and Nonlinear Effects. 2005.
41. **Maksim Säkki.** Intermittency and Long-Range Structurization of Heart Rate. 2005.
42. **Enli Kiipli.** Modelling Seawater Chemistry of the East Baltic Basin in the Late Ordovician–Early Silurian. 2005.
43. **Igor Golovtsov.** Modification of Conductive Properties and Processability of Polyparaphenylene, Polypyrrole and polyaniline. 2005.
44. **Katrin Laos.** Interaction Between Furcellaran and the Globular Proteins (Bovine Serum Albumin  $\beta$ -Lactoglobulin). 2005.
45. **Arvo Mere.** Structural and Electrical Properties of Spray Deposited Copper Indium Disulphide Films for Solar Cells. 2006.
46. **Sille Ehala.** Development and Application of Various On- and Off-Line Analytical Methods for the Analysis of Bioactive Compounds. 2006.
47. **Maria Kulp.** Capillary Electrophoretic Monitoring of Biochemical Reaction Kinetics. 2006.
48. **Anu Aaspõllu.** Proteinases from *Vipera lebetina* Snake Venom Affecting Hemostasis. 2006.

49. **Lyudmila Chekulayeva.** Photosensitized Inactivation of Tumor Cells by Porphyrins and Chlorins. 2006.
50. **Merle Uudsemaa.** Quantum-Chemical Modeling of Solvated First Row Transition Metal Ions. 2006.
51. **Tagli Pitsi.** Nutrition Situation of Pre-School Children in Estonia from 1995 to 2004. 2006.
52. **Angela Ivask.** Luminescent Recombinant Sensor Bacteria for the Analysis of Bioavailable Heavy Metals. 2006.
53. **Tiina Lõugas.** Study on Physico-Chemical Properties and Some Bioactive Compounds of Sea Buckthorn (*Hippophae rhamnoides* L.). 2006.
54. **Kaja Kasemets.** Effect of Changing Environmental Conditions on the Fermentative Growth of *Saccharomyces cerevisiae* S288C: Auxo-accelerostat Study. 2006.
55. **Ildar Nisamedtinov.** Application of  $^{13}\text{C}$  and Fluorescence Labeling in Metabolic Studies of *Saccharomyces* spp. 2006.
56. **Alar Leibak.** On Additive Generalisation of Voronoï's Theory of Perfect Forms over Algebraic Number Fields. 2006.
57. **Andri Jagomägi.** Photoluminescence of Chalcopyrite Tellurides. 2006.
58. **Tõnu Martma.** Application of Carbon Isotopes to the Study of the Ordovician and Silurian of the Baltic. 2006.
59. **Marit Kauk.** Chemical Composition of CuInSe<sub>2</sub> Monograin Powders for Solar Cell Application. 2006.
60. **Julia Kois.** Electrochemical Deposition of CuInSe<sub>2</sub> Thin Films for Photovoltaic Applications. 2006.
61. **Iiona Oja Açıık.** Sol-Gel Deposition of Titanium Dioxide Films. 2007.
62. **Tiia Anmann.** Integrated and Organized Cellular Bioenergetic Systems in Heart and Brain. 2007.
63. **Katrin Trummal.** Purification, Characterization and Specificity Studies of Metalloproteinases from *Vipera lebetina* Snake Venom. 2007.
64. **Gennadi Lessin.** Biochemical Definition of Coastal Zone Using Numerical Modeling and Measurement Data. 2007.
65. **Enno Pais.** Inverse problems to determine non-homogeneous degenerate memory kernels in heat flow. 2007.
66. **Maria Borissova.** Capillary Electrophoresis on Alkylimidazolium Salts. 2007.
67. **Karin Valmsen.** Prostaglandin Synthesis in the Coral *Plexaura homomalla*: Control of Prostaglandin Stereochemistry at Carbon 15 by Cyclooxygenases. 2007.
68. **Kristjan Piirimäe.** Long-Term Changes of Nutrient Fluxes in the Drainage Basin of the Gulf of Finland – Application of the PolFlow Model. 2007.
69. **Tatjana Dedova.** Chemical Spray Pyrolysis Deposition of Zinc Sulfide Thin Films and Zinc Oxide Nanostructured Layers. 2007.
70. **Katrin Tomson.** Production of Labelled Recombinant Proteins in Fed-Batch Systems in *Escherichia coli*. 2007.
71. **Cecilia Sarmiento.** Suppressors of RNA Silencing in Plants. 2008.
72. **Vilja Mardla.** Inhibition of Platelet Aggregation with Combination of Antiplatelet Agents. 2008.

73. **Maie Bachmann.** Effect of Modulated Microwave Radiation on Human Resting Electroencephalographic Signal. 2008.
74. **Dan Huvonen.** Terahertz Spectroscopy of Low-Dimensional Spin Systems. 2008.
75. **Ly Villo.** Stereoselective Chemoenzymatic Synthesis of Deoxy Sugar Esters Involving *Candida antarctica* Lipase B. 2008.
76. **Johan Anton.** Technology of Integrated Photoelasticity for Residual Stress Measurement in Glass Articles of Axisymmetric Shape. 2008.
77. **Olga Volobujeva.** SEM Study of Selenization of Different Thin Metallic Films. 2008.
78. **Artur Jogi.** Synthesis of 4'-Substituted 2,3'-dideoxynucleoside Analogues. 2008.
79. **Mario Kadastik.** Doubly Charged Higgs Boson Decays and Implications on Neutrino Physics. 2008.
80. **Fernando Perez-Caballero.** Carbon Aerogels from 5-Methylresorcinol-Formaldehyde Gels. 2008.
81. **Sirje Vaask.** The Comparability, Reproducibility and Validity of Estonian Food Consumption Surveys. 2008.
82. **Anna Menaker.** Electrosynthesized Conducting Polymers, Polypyrrole and Poly(3,4-ethylenedioxythiophene), for Molecular Imprinting. 2009.
83. **Lauri Ilison.** Solitons and Solitary Waves in Hierarchical Korteweg-de Vries Type Systems. 2009.
84. **Kaia Ernits.** Study of In<sub>2</sub>S<sub>3</sub> and ZnS Thin Films Deposited by Ultrasonic Spray Pyrolysis and Chemical Deposition. 2009.
85. **Veljo Sinivee.** Portable Spectrometer for Ionizing Radiation "Gammamapper". 2009.
86. **Juri Virkepu.** On Lagrange Formalism for Lie Theory and Operadic Harmonic Oscillator in Low Dimensions. 2009.
87. **Marko Piirsoo.** Deciphering Molecular Basis of Schwann Cell Development. 2009.
88. **Kati Helmja.** Determination of Phenolic Compounds and Their Antioxidative Capability in Plant Extracts. 2010.
89. **Merike Sõmera.** Sobemoviruses: Genomic Organization, Potential for Recombination and Necessity of P1 in Systemic Infection. 2010.
90. **Kristjan Laes.** Preparation and Impedance Spectroscopy of Hybrid Structures Based on CuIn<sub>3</sub>Se<sub>5</sub> Photoabsorber. 2010.
91. **Kristin Lippur.** Asymmetric Synthesis of 2,2'-Bimorpholine and its 5,5'-Substituted Derivatives. 2010.
92. **Merike Luman.** Dialysis Dose and Nutrition Assessment by an Optical Method. 2010.
93. **Mihhail Berezovski.** Numerical Simulation of Wave Propagation in Heterogeneous and Microstructured Materials. 2010.
94. **Tamara Aid-Pavlidis.** Structure and Regulation of BDNF Gene. 2010.
95. **Olga Bragina.** The Role of Sonic Hedgehog Pathway in Neuro- and Tumorigenesis. 2010.

96. **Merle Randrüüt.** Wave Propagation in Microstructured Solids: Solitary and Periodic Waves. 2010.
97. **Marju Laars.** Asymmetric Organocatalytic Michael and Aldol Reactions Mediated by Cyclic Amines. 2010.
98. **Maarja Grossberg.** Optical Properties of Multinary Semiconductor Compounds for Photovoltaic Applications. 2010.
99. **Alla Maloverjan.** Vertebrate Homologues of Drosophila Fused Kinase and Their Role in Sonic Hedgehog Signalling Pathway. 2010.
100. **Priit Pruunsild.** Neuronal Activity-Dependent Transcription Factors and Regulation of Human *BDNF* Gene. 2010.
101. **Tatjana Knjazeva.** New Approaches in Capillary Electrophoresis for Separation and Study of Proteins. 2011.
102. **Atanas Katerski.** Chemical Composition of Sprayed Copper Indium Disulfide Films for Nanostructured Solar Cells. 2011.
103. **Kristi Timmo.** Formation of Properties of  $\text{CuInSe}_2$  and  $\text{Cu}_2\text{ZnSn}(\text{S,Se})_4$  Monograin Powders Synthesized in Molten KI. 2011.
104. **Kert Tamm.** Wave Propagation and Interaction in Mindlin-Type Microstructured Solids: Numerical Simulation. 2011.
105. **Adrian Popp.** Ordovician Proetid Trilobites in Baltoscandia and Germany. 2011.
106. **Ove Pärn.** Sea Ice Deformation Events in the Gulf of Finland and This Impact on Shipping. 2011.
107. **Germo Väli.** Numerical Experiments on Matter Transport in the Baltic Sea. 2011.
108. **Andrus Seiman.** Point-of-Care Analyser Based on Capillary Electrophoresis. 2011.
109. **Olga Katargina.** Tick-Borne Pathogens Circulating in Estonia (Tick-Borne Encephalitis Virus, *Anaplasma phagocytophilum*, *Babesia* Species): Their Prevalence and Genetic Characterization. 2011.
110. **Ingrid Sumeri.** The Study of Probiotic Bacteria in Human Gastrointestinal Tract Simulator. 2011.
111. **Kairit Zovo.** Functional Characterization of Cellular Copper Proteome. 2011.
112. **Natalja Makarytsheva.** Analysis of Organic Species in Sediments and Soil by High Performance Separation Methods. 2011.
113. **Monika Mortimer.** Evaluation of the Biological Effects of Engineered Nanoparticles on Unicellular Pro- and Eukaryotic Organisms. 2011.
114. **Kersti Tepp.** Molecular System Bioenergetics of Cardiac Cells: Quantitative Analysis of Structure-Function Relationship. 2011.
115. **Anna-Liisa Peikolainen.** Organic Aerogels Based on 5-Methylresorcinol. 2011.
116. **Leeli Amon.** Palaeoecological Reconstruction of Late-Glacial Vegetation Dynamics in Eastern Baltic Area: A View Based on Plant Macrofossil Analysis. 2011.
117. **Tanel Peets.** Dispersion Analysis of Wave Motion in Microstructured Solids. 2011.

118. **Liina Kaupmees**. Selenization of Molybdenum as Contact Material in Solar Cells. 2011.
119. **Allan Olsper**. Properties of VPg and Coat Protein of Sobemoviruses. 2011.
120. **Kadri Koppel**. Food Category Appraisal Using Sensory Methods. 2011.
121. **Jelena Gorbatšova**. Development of Methods for CE Analysis of Plant Phenolics and Vitamins. 2011.
122. **Karin Viipsi**. Impact of EDTA and Humic Substances on the Removal of Cd and Zn from Aqueous Solutions by Apatite. 2012.
123. **David Schryer**. Metabolic Flux Analysis of Compartmentalized Systems Using Dynamic Isotopologue Modeling. 2012.
124. **Ardo Illaste**. Analysis of Molecular Movements in Cardiac Myocytes. 2012.
125. **Indrek Reile**. 3-Alkylcyclopentane-1,2-Diones in Asymmetric Oxidation and Alkylation Reactions. 2012.
126. **Tatjana Tamberg**. Some Classes of Finite 2-Groups and Their Endomorphism Semigroups. 2012.
127. **Taavi Liblik**. Variability of Thermohaline Structure in the Gulf of Finland in Summer. 2012.
128. **Priidik Lagemaa**. Operational Forecasting in Estonian Marine Waters. 2012.
129. **Andrei Errapart**. Photoelastic Tomography in Linear and Non-linear Approximation. 2012.
130. **Külliki Krabbi**. Biochemical Diagnosis of Classical Galactosemia and Mucopolysaccharidoses in Estonia. 2012.
131. **Kristel Kaseleht**. Identification of Aroma Compounds in Food using SPME-GC/MS and GC-Olfactometry. 2012.
132. **Kristel Kodar**. Immunoglobulin G Glycosylation Profiling in Patients with Gastric Cancer. 2012.
133. **Kai Rosin**. Solar Radiation and Wind as Agents of the Formation of the Radiation Regime in Water Bodies. 2012.
134. **Ann Tiiman**. Interactions of Alzheimer's Amyloid-Beta Peptides with Zn(II) and Cu(II) Ions. 2012.
135. **Olga Gavrilova**. Application and Elaboration of Accounting Approaches for Sustainable Development. 2012.
136. **Olesja Bondarenko**. Development of Bacterial Biosensors and Human Stem Cell-Based *In Vitro* Assays for the Toxicological Profiling of Synthetic Nanoparticles. 2012.
137. **Katri Muska**. Study of Composition and Thermal Treatments of Quaternary Compounds for Monograin Layer Solar Cells. 2012.
138. **Ranno Nahku**. Validation of Critical Factors for the Quantitative Characterization of Bacterial Physiology in Accelerostat Cultures. 2012.
139. **Petri-Jaan Lahtvee**. Quantitative Omics-level Analysis of Growth Rate Dependent Energy Metabolism in *Lactococcus lactis*. 2012.
140. **Kerti Orumets**. Molecular Mechanisms Controlling Intracellular Glutathione Levels in Baker's Yeast *Saccharomyces cerevisiae* and its Random Mutagenized Glutathione Over-Accumulating Isolate. 2012.
141. **Loreida Timberg**. Spice-Cured Sprats Ripening, Sensory Parameters Development, and Quality Indicators. 2012.

142. **Anna Mihhalevski.** Rye Sourdough Fermentation and Bread Stability. 2012.
143. **Liisa Arike.** Quantitative Proteomics of *Escherichia coli*: From Relative to Absolute Scale. 2012.
144. **Kairi Otto.** Deposition of In<sub>2</sub>S<sub>3</sub> Thin Films by Chemical Spray Pyrolysis. 2012.
145. **Mari Sepp.** Functions of the Basic Helix-Loop-Helix Transcription Factor TCF4 in Health and Disease. 2012.
146. **Anna Suhhova.** Detection of the Effect of Weak Stressors on Human Resting Electroencephalographic Signal. 2012.
147. **Aram Kazarjan.** Development and Production of Extruded Food and Feed Products Containing Probiotic Microorganisms. 2012.
148. **Rivo Uiboupin.** Application of Remote Sensing Methods for the Investigation of Spatio-Temporal Variability of Sea Surface Temperature and Chlorophyll Fields in the Gulf of Finland. 2013.
149. **Tiina Kriščiunaite.** A Study of Milk Coagulability. 2013.
150. **Tuuli Levandi.** Comparative Study of Cereal Varieties by Analytical Separation Methods and Chemometrics. 2013.
151. **Natalja Kabanova.** Development of a Microcalorimetric Method for the Study of Fermentation Processes. 2013.
152. **Himani Khanduri.** Magnetic Properties of Functional Oxides. 2013.
153. **Julia Smirnova.** Investigation of Properties and Reaction Mechanisms of Redox-Active Proteins by ESI MS. 2013.
154. **Mervi Sepp.** Estimation of Diffusion Restrictions in Cardiomyocytes Using Kinetic Measurements. 2013.
155. **Kersti Jääger.** Differentiation and Heterogeneity of Mesenchymal Stem Cells. 2013.
156. **Victor Alari.** Multi-Scale Wind Wave Modeling in the Baltic Sea. 2013.
157. **Taavi Päll.** Studies of CD44 Hyaluronan Binding Domain as Novel Angiogenesis Inhibitor. 2013.
158. **Allan Niidu.** Synthesis of Cyclopentane and Tetrahydrofuran Derivatives. 2013.
159. **Julia Geller.** Detection and Genetic Characterization of *Borrelia* Species Circulating in Tick Population in Estonia. 2013.
160. **Irina Stulova.** The Effects of Milk Composition and Treatment on the Growth of Lactic Acid Bacteria. 2013.
161. **Jana Holmar.** Optical Method for Uric Acid Removal Assessment During Dialysis. 2013.
162. **Kerti Ausmees.** Synthesis of Heterobicyclo[3.2.0]heptane Derivatives *via* Multicomponent Cascade Reaction. 2013.
163. **Minna Varikmaa.** Structural and Functional Studies of Mitochondrial Respiration Regulation in Muscle Cells. 2013.
164. **Indrek Koppel.** Transcriptional Mechanisms of BDNF Gene Regulation. 2014.
165. **Kristjan Pilt.** Optical Pulse Wave Signal Analysis for Determination of Early Arterial Ageing in Diabetic Patients. 2014.
166. **Andres Anier.** Estimation of the Complexity of the Electroencephalogram for Brain Monitoring in Intensive Care. 2014.

167. **Toivo Kallaste**. Pyroclastic Sanidine in the Lower Palaeozoic Bentonites – A Tool for Regional Geological Correlations. 2014.
168. **Erki Kärber**. Properties of ZnO-nanorod/In<sub>2</sub>S<sub>3</sub>/CuInS<sub>2</sub> Solar Cell and the Constituent Layers Deposited by Chemical Spray Method. 2014.
169. **Julia Lehner**. Formation of Cu<sub>2</sub>ZnSnS<sub>4</sub> and Cu<sub>2</sub>ZnSnSe<sub>4</sub> by Chalcogenisation of Electrochemically Deposited Precursor Layers. 2014.
170. **Peep Pitk**. Protein- and Lipid-rich Solid Slaughterhouse Waste Anaerobic Co-digestion: Resource Analysis and Process Optimization. 2014.
171. **Kaspar Valgepea**. Absolute Quantitative Multi-omics Characterization of Specific Growth Rate-dependent Metabolism of *Escherichia coli*. 2014.
172. **Artur Noole**. Asymmetric Organocatalytic Synthesis of 3,3'-Disubstituted Oxindoles. 2014.
173. **Robert Tsanev**. Identification and Structure-Functional Characterisation of the Gene Transcriptional Repressor Domain of Human Gli Proteins. 2014.
174. **Dmitri Kartofelev**. Nonlinear Sound Generation Mechanisms in Musical Acoustic. 2014.
175. **Sigrid Hade**. GIS Applications in the Studies of the Palaeozoic Graptolite Argillite and Landscape Change. 2014.
176. **Agne Velthut-Meikas**. Ovarian Follicle as the Environment of Oocyte Maturation: The Role of Granulosa Cells and Follicular Fluid at Pre-Ovulatory Development. 2014.
177. **Kristel Hälvin**. Determination of B-group Vitamins in Food Using an LC-MS Stable Isotope Dilution Assay. 2014.
178. **Mailis Päre**. Characterization of the Oligoadenylate Synthetase Subgroup from Phylum Porifera. 2014.
179. **Jekaterina Kazantseva**. Alternative Splicing of *TAF4*: A Dynamic Switch between Distinct Cell Functions. 2014.
180. **Jaanus Suurväli**. Regulator of G Protein Signalling 16 (RGS16): Functions in Immunity and Genomic Location in an Ancient MHC-Related Evolutionarily Conserved Synteny Group. 2014.
181. **Ene Viiard**. Diversity and Stability of Lactic Acid Bacteria During Rye Sourdough Propagation. 2014.
182. **Kristella Hansen**. Prostaglandin Synthesis in Marine Arthropods and Red Algae. 2014.
183. **Helike Lõhelaid**. Allene Oxide Synthase-lipoxygenase Pathway in Coral Stress Response. 2015.
184. **Normunds Stivriņš**. Postglacial Environmental Conditions, Vegetation Succession and Human Impact in Latvia. 2015.
185. **Mary-Liis Kütt**. Identification and Characterization of Bioactive Peptides with Antimicrobial and Immunoregulating Properties Derived from Bovine Colostrum and Milk. 2015.
186. **Kazbulat Šogenov**. Petrophysical Models of the CO<sub>2</sub> Plume at Prospective Storage Sites in the Baltic Basin. 2015.
187. **Taavi Raadik**. Application of Modulation Spectroscopy Methods in Photovoltaic Materials Research. 2015.

188. **Reio Pöder.** Study of Oxygen Vacancy Dynamics in Sc-doped Ceria with NMR Techniques. 2015.
189. **Sven Siir.** Internal Geochemical Stratification of Bentonites (Altered Volcanic Ash Beds) and its Interpretation. 2015.
190. **Kaur Jaanson.** Novel Transgenic Models Based on Bacterial Artificial Chromosomes for Studying BDNF Gene Regulation. 2015.
191. **Niina Karro.** Analysis of ADP Compartmentation in Cardiomyocytes and Its Role in Protection Against Mitochondrial Permeability Transition Pore Opening. 2015.
192. **Piret Laht.** B-plexins Regulate the Maturation of Neurons Through Microtubule Dynamics. 2015.
193. **Sergei Žari.** Organocatalytic Asymmetric Addition to Unsaturated 1,4-Dicarbonyl Compounds. 2015.
194. **Natalja Buhhalko.** Processes Influencing the Spatio-temporal Dynamics of Nutrients and Phytoplankton in Summer in the Gulf of Finland, Baltic Sea. 2015.
195. **Natalia Maticiuć.** Mechanism of Changes in the Properties of Chemically Deposited CdS Thin Films Induced by Thermal Annealing. 2015.
196. **Mario Öeren.** Computational Study of Cyclohexylhemicucurbiturils. 2015.
197. **Mari Kalda.** Mechanoenergetics of a Single Cardiomyocyte. 2015.
198. **Ieva Grudzinska.** Diatom Stratigraphy and Relative Sea Level Changes of the Eastern Baltic Sea over the Holocene. 2015.
199. **Anna Kazantseva.** Alternative Splicing in Health and Disease. 2015.
200. **Jana Kazarjan.** Investigation of Endogenous Antioxidants and Their Synthetic Analogues by Capillary Electrophoresis. 2016.
201. **Maria Safonova.** SnS Thin Films Deposition by Chemical Solution Method and Characterization. 2016.
202. **Jekaterina Mazina.** Detection of Psycho- and Bioactive Drugs in Different Sample Matrices by Fluorescence Spectroscopy and Capillary Electrophoresis. 2016.
203. **Karin Rosenstein.** Genes Regulated by Estrogen and Progesterone in Human Endometrium. 2016.
204. **Aleksei Tretjakov.** A Macromolecular Imprinting Approach to Design Synthetic Receptors for Label-Free Biosensing Applications. 2016.
205. **Mati Danilson.** Temperature Dependent Electrical Properties of Kesterite Monograin Layer Solar Cells. 2016.
206. **Kaspar Kevvai.** Applications of <sup>15</sup>N-labeled Yeast Hydrolysates in Metabolic Studies of *Lactococcus lactis* and *Saccharomyces Cerevisiae*. 2016.
207. **Kadri Aller.** Development and Applications of Chemically Defined Media for Lactic Acid Bacteria. 2016.
208. **Gert Preegel.** Cyclopentane-1,2-dione and Cyclopent-2-en-1-one in Asymmetric Organocatalytic Reactions. 2016.
209. **Jekaterina Služenikina.** Applications of Marine Scatterometer Winds and Quality Aspects of their Assimilation into Numerical Weather Prediction Model HIRLAM. 2016.
210. **Erkki Kask.** Study of Kesterite Solar Cell Absorbers by Capacitance Spectroscopy Methods. 2016.

211. **Jürgen Arund**. Major Chromophores and Fluorophores in the Spent Dialysate as Cornerstones for Optical Monitoring of Kidney Replacement Therapy. 2016.
212. **Andrei Šamarin**. Hybrid PET/MR Imaging of Bone Metabolism and Morphology. 2016.
213. **Kairi Kasemets**. Inverse Problems for Parabolic Integro-Differential Equations with Instant and Integral Conditions. 2016.
214. **Edith Soosaar**. An Evolution of Freshwater Bulge in Laboratory Scale Experiments and Natural Conditions. 2016.
215. **Peeter Laas**. Spatiotemporal Niche-Partitioning of Bacterioplankton Community across Environmental Gradients in the Baltic Sea. 2016.
216. **Margus Voolma**. Geochemistry of Organic-Rich Metalliferous Oil Shale/Black Shale of Jordan and Estonia. 2016.
217. **Karin Ojamäe**. The Ecology and Photobiology of Mixotrophic Alveolates in the Baltic Sea. 2016.